

**UNIVERSIDAD AUTÓNOMA DE MADRID**

Facultad de Medicina

Departamento de Bioquímica



**Doctoral Thesis**

**Mechanistic characterization of p62 as a driver of  
melanoma metastasis**

**PANAGIOTIS KARRAS**

Madrid, 2017

**UNIVERSIDAD AUTÓNOMA DE MADRID**

Facultad de Medicina

Departamento de Bioquímica



**Doctoral Thesis**

**Mechanistic characterization of p62 as a driver of  
melanoma metastasis**

**PANAGIOTIS KARRAS**

Thesis Director

**Dr. María S. Soengas**



**Spanish National Cancer Research Center**

Madrid, 2017

**Dr. María S. Soengas**, Head of the Melanoma Group at Molecular Oncology program of the Spanish National Cancer Research Center (CNIO)

CERTIFIES:

That the study “**Mechanistic characterization of p62 as a driver of melanoma metastasis**” developed by **Panagiotis Karras** meets the necessary requirements to obtain the **PhD Degree** and, to this purpose, will be presented at the Universidad Autónoma de Madrid. This work has been carried out under my direction and hereby I authorize its defense to a specific PhD Committee assembled for this purpose.

I hereby issue this certification in Madrid on May 22<sup>nd</sup> 2017.

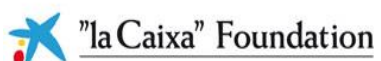
María S. Soengas

PhD, Thesis Director

The work in this doctoral thesis was carried out in the Melanoma Group at the Spanish National Cancer Research Centre (CNIO) from November 2011 to June 2017 under the supervision of María S. Soengas.

This work has been supported by the following fellowship and grant:

- "La caixa" International PhD Programme (November 2011- November 2015)
- Retos-colaboracion-2014 EC-I
- FUNDACIÓN La maratón de TV3



*Dedicated to my father*

*Αφιερωμένη στον πατέρα μου*

***ACKNOWLEDGMENTS /  
AGRADECIMIENTOS***

This is the part of the thesis that you realize that nothing will be possible without the participation, the effort and the advice of many people to make this happen. After five and a half years of continuous and intense working I have reached to the end of my PhD. These years were very challenging but truly productive at scientific and personal level helping me to progress and develop my personality. During this PhD I had to face many challenges and count my limits but these were the moments that you have to stand up and face them, and without the help of all the people involved I wouldn't have managed it.

First of all, I would like to thank you **Marisol** for the great opportunity that you gave me to become part of this wonderful lab. I am really thankful and lucky collaborating with you conducting my PhD to your lab. These years were highly productive for me and your support, your advice and the supervision helped me the most to progress and become better scientist and person. I appreciate a lot all your effort and your help to develop the project and I wish all the best to you and to the lab in the future.

I would like to thank also my tutor **Amparo Cano** for being a part of my thesis and being available when I needed her. It was great to meet her and discuss with her. Besides my tutor, I would like to give my gratitude to all the members of my thesis committee: **Dr. Jose L. Rodríguez-Peralto**, **Dr. Hector Peinado**, **Dr. Guillermo Velasco**, **Dr. Encarnación Martínez Salas** and **Dr. Raúl Mendez**. Thank you all, it's an honor to have you in my thesis committee.

This PhD thesis would never be carried out without the support and the help of the **Melanoma Group**. I would like to express my sincere and special thanks to all the current and past members of the lab. No words can express my gratitude and my feelings for all of you guys that you were my travelling companion to this unexplored journey. I have so many memories from all these years, all the trips and the nights out and all the fun moments that we lived together. This is something that makes this lab special and it's really hard to find nowadays. KEEP GOING MELANOMA GROUP!

This is a team work effort that everyone has contributed and hopefully, all the effort will soon be rewarded! This team work effort does not only include the melanoma group, it includes the invaluable contributions of the CNIO Units that made their best and always were here to contribute and solve all the pending questions and problems that I had to face. Thanks a lot to all the people from **Confocal Unit**, **Proteomics Unit**, **Histopathology Unit**, **Bionformatic Unit** and many special thanks to the **animal facility** for the huge work that they did to maintain the mouse colonies all these years.

I would like to thank all the members of **Epithelial and Carcinogenesis** and **Microenvironment and Metastasis Groups** for the fruitful joint meetings and the constructive conversations. Their inputs and their critical suggestions were important for the

development of the projects and for my personal progress. Special thanks to **Paco Real** for his suggestions, advice and the very productive conversations during these years.

Additionally I would like to give my gratitude to all the collaborators from **Hospital 12 de Octubre**, especially to **Dr. Pablo L. Ortiz-Romero** and **Dr. Jose L. Rodríguez-Peralto** for providing all the human biopsies. Moreover all the people in the hospital that were responsible for performing the experimental procedures and analyzing all the histological data.

Finally, everything would be impossible if I did not have my **family**, my **relatives** and my **friends** surrounding me with support and love during all these years. Everything that I have achieved comes from the continuous support and the unconditional love of my parents and my brother. Thank you for standing by me and trusting me to all my decisions. **THANK YOU SO MUCH FROM THE BOTTOM OF MY HEART.**

# ***CONTENTS***

CONTENTS.....	1
I.ABBREVIATIONS.....	9
II.SUMMARY/RESUMEN.....	17
Summary.....	19
Resumen.....	21
III.INTRODUCTION.....	25
3.1 Melanocyte: the cell of origin of melanoma.....	27
3.2 Classification of melanocytic lesions.....	28
3.2.1 Bening melanocytic nevi.....	28
3.2.2 Malignant melanoma.....	29
<i>Classification by anatomical site</i> .....	29
<i>Classification by clinicopathological criteria (Clark model-linear evolution)</i> .....	30
<i>Classification by clinicopathological criteria (AJCC-non linear evolution)</i> .....	32
<i>Classification by genetic alterations</i> .....	32
3.4 “Classical” versus “Lineage-Specific” oncogenes in melanoma.....	34
3.5 Non-Oncogene Addiction in melanoma.....	34
3.5.1 Autophagy.....	35
3.5.2 Autophagy: A “double-edged” sword in cancer.....	36
<i>Autophagy as a tumor suppressor</i> .....	37
<i>Autophagy as a tumor promoter</i> .....	38
3.5.3 Autophagy in melanoma.....	40
3.6 Cargo receptors in autophagy.....	41
3.7 p62 as an autophagy adaptor and a signaling hub.....	42
3.7.1 Structure of p62.....	42

3.7.2 Transcriptional regulation of p62 .....	44
3.7.3 p62 in cancer progression and metastasis .....	44
<i>p62 autophagy dependent roles in cancer</i> .....	44
<i>p62 as a signaling hub in cancer</i> .....	45
IV.OBJECTIVES .....	49
V.MATERIALS AND METHODS .....	53
5.1 Cell Culture.....	55
5.2 Protein Immunoblotting.....	55
5.3 RNA extraction, PCR and qPCR.....	57
5.4 Cloning of genes into lentiviral constructs .....	57
5.5 Gene Silencing and ectopic expression via lentiviral transduction of shRNAs.....	58
5.6 siRNA-mediated transient genetic inactivation of p62 .....	59
5.7 p62 gene targeting in cells using CRISPR/Cas9 .....	59
5.8 Clonogenic capacity of cells (Colony Formation) .....	59
5.9 Matrigel invasion assays.....	60
5.10 Drug treatments in vitro .....	60
5.11 RNA stability assay (Actinomycin D treatment) .....	60
5.12 Isobaric Tag for Relative and Absolute Quantitation (ITRAQ) .....	61
(I) Sample Preparation .....	61
(II) Protein Digestion and labeling with ITRAQ reagents.....	61
(III) OFFGEL Fractionation.....	62
(IV) Peptide analysis by nanoLC-MS/MS .....	62
(V) Data analysis .....	63
5.13 Co-Immunoprecipitation assay followed by Mass Spectrometry .....	63

5.13.1 Subcellular Fractionation followed by Co-Immunoprecipitation assay .....	63
5.13.2 Mass Spectrometry .....	64
(I) Sample Preparation.....	64
(II) LC-MS/MS analysis .....	65
(III) Data analysis.....	65
5.14 RNA Immunoprecipitation (RIP) followed by qPCR.....	66
5.15 Immunofluorescence in fixed cells .....	67
5.16 Tissue Immunostaining.....	67
(I) Immunofluorescence .....	67
(II) Immunohistochemistry in human and mouse biopsies .....	68
a. Tissue microarrays (TMAs) and immunohistochemistry (human samples) .....	68
b. Immunohistochemistry (mouse samples) .....	68
5.17 Mitochondrial Respiration .....	69
5.18 Mice breedings and activation of Tyr::CreER transgene .....	69
5.19 Subcutaneous inoculation of B16-F10 cells into p62 deficient mice .....	70
5.20 Genotyping .....	70
5.21 GO terms, Networks, Heatmaps and Venn Diagrams .....	71
5.22 Statistical Analyses.....	71
<b>VI. RESULTS.....</b>	<b>73</b>
6.1 Expression and prognostic studies support pro-metastatic roles of p62 in human melanomas.....	75
6.2 Tumor-, but not stromal-driven p62 favors melanoma progression in GEMM.....	77
6.3 p62 controls key proliferative and metastatic signatures in melanoma cells.....	81
6.4 p62-deficient melanoma cells support new protumorigenic activities of this protein .	83

6.5 Quantitative proteomics (iTRAQ) for the identification of downstream effectors of p62 .....	87
6.6 FERMT2 is a novel risk factor for poor prognosis in melanoma acting downstream of p62 .....	90
6.7 The p62 interactome identifies RNA binding proteins as novel binding partners in melanoma.....	94
6.8 p62-IGF2BP1 interaction controls the mRNA stability of multiple pro-metastatic factors.....	99
<i>VII.DISCUSSION</i> .....	105
7.1 Expression and prognostic studies of p62 in human melanomas.....	108
7.2 Pathophysiological roles of p62 <i>in vivo</i> .....	109
7.3 p62 known functions are not altered in melanoma .....	110
7.4 Novel roles of p62 in melanoma progression and metastasis .....	112
7.5 p62 interactors in the regulation of mRNA stability.....	113
<i>VIII.CONCLUSIONS/CONCLUSIONES</i> .....	117
Conclusions.....	119
Conclusiones.....	122
<i>IX.REFERENCES</i> .....	125
<i>X.APPENDIX</i> .....	147
10.1 Supplementary tables and figures .....	149
10.2 Publications .....	166
10.3 Presentations .....	166
10.4 Fellowships/Awards.....	167
10.5 Certificates .....	167

## ***I . ABBREVIATIONS***

<b>4-HT</b>	4-hydroxytamoxifen
<b>ActD</b>	Actinomycin D
<b>AJCC</b>	American Joint Committee on Cancer Melanoma Staging
<b>ALM</b>	Acral Lentiginous Melanoma
<b>AMBRA1</b>	Autophagy And Beclin 1 Regulator 1
<b>aPKC</b>	atypical protein kinase C
<b>ASH</b>	Alcoholic SteatoHepatitis
<b>ATCC</b>	American Type Culture Collection
<b>ATG5</b>	Autophagy protein 5
<b>ATGs</b>	AuTophagy-related genes
<b>BAP1</b>	BRCA1 associated protein 1
<b>BECN1</b>	Beclin 1
<b>BRAF</b>	v-raf murine sarcoma viral oncogene homolog B
<b>BRCA1</b>	BReast CAncer 1
<b>BSA</b>	Bovine serum albumin
<b>CAFs</b>	Cancer-Associated Fibroblasts
<b>CCLE</b>	Cancer Cell Line Encyclopedia
<b>CCND1</b>	CyCliN D1
<b>CDK1</b>	Cyclin-Dependent Kinase 1
<b>CDK4</b>	Cyclin-Dependent Kinase 4
<b>CDKN2A</b>	Cyclin Dependent Kinase Inhibitor 2A
<b>cDNA</b>	complementary DNA
<b>CNIO</b>	Centro Nacional de Investigaciones Oncológicas
<b>CNS</b>	Central Nervous System
<b>CREB</b>	cAMP Response Element-Binding protein
<b>CSCs</b>	Cancer Stem Cells
<b>DAPI</b>	4,6-diamidino-2-phenylindole
<b>DCT</b>	DopaChrome Tautomerase
<b>DFCP1</b>	Double FYVE-Containing Protein 1
<b>DMEM</b>	Dulbecco's Modified Eagle's Medium
<b>ECAR</b>	Extra-Cellular Acidification Rate
<b>eCLIP</b>	enhanced UV CrossLinking and Immunoprecipitation
<b>EDTA</b>	Ethylenediaminetetra-acetic acid
<b>EMT</b>	Epithelial to Mesenchymal Transition
<b>ESCRT</b>	Endosomal Sorting Complex Required for Transport
<b>FBS</b>	Fetal Bovine Serum

<b>FDA</b>	Food and Drug Administration
<b>FDR</b>	False Discovery Ratio
<b>FERMT2</b>	Fermitin family homolog 2
<b>GABARAP</b>	GABA(A) Receptor-Associated Protein
<b>GEMM</b>	Genetically Engineered Mouse Model
<b>GNAQ</b>	guanine nucleotide binding protein $\alpha$ q polypeptide
<b>GO</b>	Gene Ontology
<b>GSEA</b>	Gene Set Enrichment Analysis
<b>HCC</b>	hepatocellular carcinoma
<b>HDACis</b>	Histone DeAcetylase inhibitors
<b>HES1</b>	Hairy/Enhancer of Split
<b>HKGF</b>	Human Keratinocyte Growth Factors
<b>HRAS</b>	v-Ha-ras harvey rat sarcoma viral oncogene homolog
<b>HRP</b>	HorseRadish Peroxidase
<b>IGF2BP</b>	Insulin-like Growth Factor 2 mRNA-Binding Proteins
<b>IgG</b>	Immunoglobulin G
<b>IHC</b>	ImmunoHistoChemistry
<b>IPA</b>	Ingenuity Pathway Analysis
<b>iTRAQ</b>	isobaric Tag for Relative and Absolute Quantitation
<b>JNK</b>	c-Jun N-terminal kinases
<b>KEAP1</b>	Kelch Like ECH Associated Protein 1
<b>KIR</b>	Keap1-Interacting Region
<b>KO</b>	knock out
<b>LC3</b>	Microtubule-associated proteins 1A/1B light chain 3B
<b>LC-MS/MS</b>	Liquid Chromatography tandem-Mass Spectrometry
<b>LIR</b>	LC3-Interacting Region
<b>LMM</b>	Lentigo Malignant Melanoma
<b>MAPK</b>	Mitogen-Activated Protein Kinase
<b>MC1R</b>	melanocortin 1 receptor
<b>MEFs</b>	Mouse Embryonic Fibroblasts
<b>MITF</b>	microphthalmia-associated transcription factor
<b>MM</b>	Mucosal Melanoma
<b>mRNA</b>	messenger RNA
<b>mTOR</b>	mechanistic Target Of Rapamycin
<b>mTORC1</b>	mechanistic Target Of Rapamycin Complex 1
<b>MVB</b>	MultiVesicular Body

<b>MYC</b>	V-Myc Avian Myelocytomatosis Viral Oncogene Homolog
<b>NASH</b>	Non Alcoholic SteatoHepatitis
<b>NBR1</b>	Neighbor of BRCA1 gene 1
<b>NDP52</b>	Nuclear Dot Protein 52
<b>NF1</b>	NeuroFibromin 1
<b>NF-<math>\kappa</math>B</b>	Nuclear factor of kappa light polypeptide gene enhancer in B-cells 1
<b>NM</b>	Nodular Melanoma
<b>NQO1</b>	NAD(P)H Quinone dehydrogenase 1
<b>NRAS</b>	Neuroblastoma RAS viral oncogene homolog
<b>NRF2</b>	NFE2-Related Factor 2
<b>OCR</b>	Oxygen Consumption Rate
<b>OIS</b>	Oncogene-Induced Senescence
<b>PanIN</b>	Pancreatic Intraepithelial Neoplasia
<b>PAX3</b>	Paired box gene 3
<b>PB1</b>	Phox1 and Bem1p
<b>PCR</b>	Polymerase Chain Reaction
<b>PE</b>	PhosphatidylEthanolamine
<b>PI(3)K</b>	Phosphatidylinositol-4,5-bisphosphate 3-Kinase
<b>PKA</b>	protein kinase A
<b>PtdIns3P</b>	Phosphatidylinositol-3-Phosphate
<b>PTEN</b>	Phosphatase and TEnsiN homologue
<b>PyMT</b>	Polyoma Middle T antigen
<b>qPCR</b>	quantitative Polymerase Chain Reaction
<b>RB1</b>	RetinoBlastoma 1
<b>RBP</b>	RNA Binding Protein
<b>RGP</b>	Radial-Growth Phase
<b>RIP</b>	RNA ImmunoPrecipitation
<b>ROS</b>	Reactive Oxygen Species
<b>RT- qPCR</b>	Reverse transcription- quantitative polymerase chain reaction
<b>RT-PCR</b>	Real time Polymerase Chain Reaction
<b>RXR</b>	Retinoid X Receptor
<b>S6K1</b>	Ribosomal protein S6 Kinase beta-1
<b>SDS-PAGE</b>	Sodium dodecyl sulfate-polyacrylamide gel electrophoresis
<b>SEM</b>	Standard error of estimate of mean
<b>SF3B1</b>	Splicing Factor 3B subunit 1
<b>sgRNA</b>	short guide RNA

<b>shRNA</b>	short haipin RNA
<b>siRNA</b>	small (or short) interfering RNA
<b>SMG</b>	Significantly Mutated Genes
<b>SOX10</b>	SRY-box-containing gene 10
<b>SQSTM1</b>	Sequestosome-1
<b>SRY</b>	Sex-determining Region Y
<b>SSM</b>	Superficial Spreading Melanoma
<b>STRING</b>	Search Tool for the Retrieval of Interacting Genes/Proteins
<b>SWI/SNF</b>	SWItch/Sucrose Non-Fermentable
<b>TB</b>	TRAF6 Binding
<b>TCGA</b>	The Cancer Genome Atlas
<b>TMA</b>	Tissue MicroArray
<b>TNM</b>	Tumor Node Metastasis
<b>TP53</b>	Tumor protein 53
<b>TRAF6</b>	TNF Receptor-Associated Factor 6
<b>TYRP1</b>	tyrosinase-related protein-1
<b>UBA</b>	UBiquitin-Associated
<b>ULK1</b>	Unc-51-Like Kinase 1
<b>UM</b>	Uveal Melanoma
<b>UTR</b>	UnTranslated Region
<b>UV</b>	UltraViolet
<b>UVRAG</b>	UV irradiation Resistance-Associated Gene
<b>VDR</b>	Vitamin D Receptor
<b>VGP</b>	Vertical-Growth Phase
<b>Vps34</b>	Vacuolar protein sorting-associated protein 34
<b>WHO</b>	World Health Organisation
<b><math>\alpha</math>MSH</b>	$\alpha$ -melanocyte stimulating hormone

## ***II . SUMMARY / RESUMEN***

## Summary

Cutaneous melanoma is the most aggressive form of skin cancer. The aggressive nature of this disease is manifested by the fact that lesions of barely 2 mm in depth already bear a high potential for metastasis. High throughput analyses have identified recurrent alterations in oncogenic pathways (i.e involving BRAF, NRAS, PI3K>AKT, NF1 or NOTCH, among others) that have paved the way for the development of molecularly-targeted therapies. However, melanoma is also a prime example of how a complex (epi)genome can activate compensatory protective responses (also against recently-approved immune checkpoint blockers). A rather unexplored strategy to search for putative tumor drivers is to focus on lineage-specific oncogenic dependencies rather on common cancer hallmarks conserved with other malignancies. In melanoma, these lineage-specific oncogenes have been traditionally linked to melanosome and pigmentation pathways. However, our group has recently identified new signalling cascades distinctively enriched in melanoma cells. These include specific RNA binding proteins (CPEB4, UNR), as well as over 30 endolysosomal factors. Analysis of autophagy, another lysosomal-associated process also revealed selective heterozygous losses in ATG5 as a feature favouring poor patient prognosis.

p62/SQSTM1 (sequestosome 1) was an attractive candidate to pursue for its known links in autophagy and as a signaling hub for multiple protein-protein complexes. Importantly, although p62 has been found accumulated in a broad spectrum of tumor types, there is no clear consensus on whether it acts as a tumor promoting or tumor suppressive agent, particularly in the context of metastasis.

Here we present a comprehensive analysis of p62 expression and functional requirement in melanoma cells, clinical biopsies and newly generated genetically engineered mouse models. This strategy was used to assess key pending questions in this field such as: (i) what is the relative impact of p62 copy number in the stroma vs benign and malignant melanocytic lesions, particularly in the context of metastasis; (ii) does p62 share autophagy and non-autophagy roles with other tumor types, or (iii) does it act in a tumor-specific manner?, and if so, (iv) what are the underlying mechanisms. To this end, particular attention was dedicated to genome-wide analyses of the p62 interactome and its global impact on the transcriptome and proteome of melanoma cells. Computational analyses, studies in GEMM and proteomic analyses were also performed in comparison to ATG5. In addition, targeted gene depletion was exploited to assess best known functions of p62 as a signaling hub. Together, this integrated approach revealed a distinct impact of p62 in the control of melanoma-enriched gene networks. Finding an unexpected role of p62 opposing mRNA decay of *FERMT2* and other pro-metastatic factors, our data ultimately revealed a new function of p62 as a hub of RNA binding proteins. Together, the results of this PhD thesis offer a platform for tumor-type specific functions of p62 in cancer.

## Resumen

El melanoma cutáneo es la forma más agresiva y letal de cáncer de piel, tanto es así, que lesiones de menos de 2 mm de grosor ya poseen una gran capacidad metastásica. A través del desarrollo de múltiples análisis a gran escala se han podido identificar una serie de alteraciones recurrentes en diversas rutas de señalización oncogénicas (BRAF, NRAS, PI3K >AKT, NF1 y/o NOTCH entre otros), lo que ha facilitado el desarrollo de terapias genéticamente dirigidas. A pesar de ello, el melanoma es uno de los mejores ejemplos de cómo un (epi) genoma tan complejo y con tal número de alteraciones, puede resultar en la activación de mecanismos compensatorios de adaptación y protección frente a los tratamientos vigentes. Una estrategia aún poco explorada en la identificación de nuevas dianas pro-oncogénicas es el estudio restringido de las dependencias oncogénicas asociadas a linaje, en lugar de perseguir alteraciones comunes a otros tipos de tumores. En melanoma estos oncogenes específicos de linaje se han asociado clásicamente a rutas de pigmentación y producción de melanosomas. Sin embargo nuestro grupo ha identificado nuevas rutas de señalización selectivamente enriquecidas en melanoma. Entre sus componentes se han encontrado proteínas de unión a RNA (CPEB4, UNR) y más de 30 proteínas endolisosomales. Por otro lado, estudios previos de nuestro grupo sobre autofagia, un proceso asociado a los lisosomas, muestran que la pérdida selectiva de una copia del gen que codifica para la proteína ATG5 se encuentra asociada a un pronóstico desfavorable en pacientes. Por todo lo anteriormente mencionado, p62/SQSTM1 (sequestosoma 1) se presenta como un candidato atractivo en melanoma, tanto por su relevante función en autofagia, como por funcionar como plataforma de señalización en numerosos tipos tumorales. Sin embargo, aunque se ha observado que p62 se encuentra sobre-expresado en múltiples tipos de cáncer, aún no existe un consenso sobre su papel como promotor o supresor tumoral, particularmente en metástasis. Por todo ello, esta tesis se planteó con los siguientes objetivos: (i) determinar del impacto en el número de copias de p62, tanto en el estroma tumoral como en lesiones melanocíticas (benignas y malignas), y particularmente en melanoma metastásico; (ii) definir si las funciones de p62, en autofagia y otros procesos celulares, son específicos en melanoma o comunes a otros tumores (iii), y por último, (iv) caracterizar el mecanismo de acción específico en melanoma. Para responder a estas cuestiones se ha realizado un exhaustivo análisis de la función de p62 en líneas celulares de melanoma, biopsias clínicas y modelos animales modificados genéticamente. A su vez, se ha dedicado especial énfasis al interactoma de p62 y al impacto que esta proteína tiene en el transcriptoma y proteoma celular. En paralelo, se ha analizado mediante estudios de proteómica y computacionales el papel de p62 y ATG5 en animales modificados genéticamente para ambos genes. Y por último, mediante ensayos de pérdida de función, se ha caracterizado la función de p62 como plataforma de señalización.

Integrando las aproximaciones anteriormente descritas, se ha descubierto que p62 tiene un papel protector en la estabilidad del mRNA de FERMT2 y otros factores pro-metastásicos, por lo que se describe por primera vez la función de p62 como plataforma de señalización a través de proteínas de unión a RNA (RBPs). En conjunto, estos resultados revelan nuevas funciones de p62 y determinan su especificidad en melanoma.

### ***III . INTRODUCTION***

### 3.1 Melanocyte: the cell of origin of melanoma

Melanocytic neoplasms range from benign lesions (melanocytic nevi), to malignant ones, termed melanomas. All originate from melanocytes, which are neural crest-derived cells<sup>1</sup>. Although melanocytes are located in mucosas, leptomeninges and uveal sites, these cells reside primarily in the skin<sup>2-5</sup>. Consequently, most melanomas are of cutaneous origin, accounting for ~90% of deaths from skin cancer<sup>6</sup> due to the high aggressive capacity to metastasize<sup>7-10</sup>.

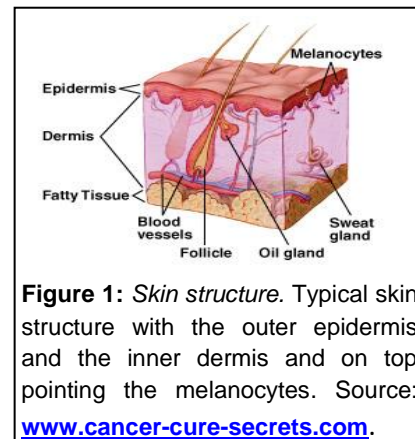


**Figure 1:** Skin structure. Typical skin structure with the outer epidermis and the inner dermis and on top pointing the melanocytes. Source: [www.cancer-cure-secrets.com](http://www.cancer-cure-secrets.com).

The melanocyte lineage is derived from the neural crest, which has its origins in the neural tube. Following its formation, neural crest cells delaminate from the dorsal-most aspect of the neural tube by a process of epithelial-to-mesenchymal transition. These cells are highly migratory and form many specialised structures in the developing embryo by migration, proliferation and differentiation<sup>11</sup>. **Melanoblasts**, the melanocytes precursors, migrate during embryonic development mostly to the basal layer of the skin (**Figure 1**), where melanocyte:keratinocyte number ratio is typically of 1:10<sup>12,13</sup>. Keratinocytes, together with surrounding cells like dermal fibroblasts sustain melanocyte function and survival in response to environmental signals such as UV radiation<sup>14</sup>. There are approximately 1,500 melanocytes per square millimetre of human epidermis, corresponding to nearly 3 billion cutaneous melanocytes in the skin of an average human<sup>15</sup>. Melanocytes represent a minority cell population within the basal epidermis, and divide infrequently, less than twice a year<sup>16</sup> and mainly provide melanin pigment to their neighbouring keratinocytes<sup>17</sup>. Melanin is a complex macromolecule that scatters and absorbs UV radiation, and epidermal keratinocytes use it to protect their nucleus from UV radiation-induced DNA damage<sup>18</sup>. The pigments are synthesized within specialized organelles called **melanosomes**. Mechanistically, the proliferation and pigment production of melanocytes is stimulated by UV radiation-induced DNA damage to keratinocytes, which subsequently secrete  $\alpha$ -melanocyte stimulating hormone ( $\alpha$ MSH) in a p53-dependent manner<sup>19</sup>.  $\alpha$ MSH binds to the melanocortin 1 receptor (MC1R), which is expressed on melanocytes activates the cAMP/protein kinase A (PKA)/CREB signaling pathway and enhances the level of the microphthalmia-associated transcription factor (MITF). MITF promotes the synthesis of melanin, which melanocytes deliver to keratinocytes<sup>20</sup>. A reduction in its activity is coupled to reduce melanin synthesis and pigmentation<sup>21</sup>. MITF also regulates melanosome biogenesis<sup>22,23</sup> and trafficking<sup>24</sup>.

In addition to MITF, during embryogenesis, the survival and migration of melanocytes rely on other signaling pathways such as Wingless signaling (Wnt)/ $\beta$ -catenin, the endothelin B

receptor and its ligand endothelin-3, the receptor tyrosine kinase KIT and its ligand KIT-ligand/SCF (stem cell factor), NOTCH<sup>25,26</sup>, paired box gene 3 (PAX3), SRY-box10 (SOX10), hairy/enhancer of split (HES1)<sup>27-31</sup>. Outside the skin, melanocytes are present in considerable numbers in the uveal tract of the eye and at lower densities in other tissues, such as the meninges and the anogenital tract. However, the melanocytic neoplasms that originate from these melanocytes are distinctly different in their histopathological and genetic status from cutaneous melanomas<sup>5,32-34</sup>.

The treatment landscape for advanced-stage, unresectable or metastatic melanoma has shifted dramatically over a short period of time. From a devastating disease with poor survival (~9 months) the discovery of FDA approved targeted agents and immunotherapeutic antibodies (**Table S1**, appendix) has led to a tremendous improvement of the response rates and the increase in overall survival with the simultaneous reduction of the adverse effects<sup>35</sup>.

## 3.2 Classification of melanocytic lesions

---

### 3.2.1 Bening melanocytic nevi

Melanocytic nevi are benign proliferations of melanocytes with theoretically a low likelihood of progressing to melanoma. Nevertheless, their high prevalence makes them contributors to a considerable portion of melanomas<sup>36-38</sup>. **Congenital nevi** are presented at birth or shortly after, while **acquired nevi** tend to appear with more than six months of age and are accumulated during life time<sup>32</sup>. Acquired nevi can exhibit a *lentiginous growth pattern* or a *congenital growth pattern*. The latter category does not necessarily imply that the nevi was present at birth as in bona fide congenital nevi, but indicates that it has a similar growth pattern. Lentiginous and congenital pattern nevi can be stratified as **i. junctional**, in which melanocytes appear at the dermo-epidermal junction; **ii. dermal**, depending on whether melanocytes appear on the dermis; and **iii. compound**, when melanocytes appear in both places, respectively<sup>39-41</sup>. **Spitz nevi** are another type of melanocytic neoplasm characterized by a predominance of large polygonal (epithelioid) or spindled melanocytes with enlarged nuclei and often multinucleated cells<sup>42,43</sup>. **Blue nevi** are characterized by the proliferation of dendritic, spindled, ovoid, or epithelioid melanocytes in tissues without any significant epithelial involvement. While the majority involve the skin, they can be encountered in many other organs<sup>39,44</sup>. A long-standing debate and controversial category of benign lesions is termed as **intermediate melanocytic neoplasm**. This grey zone of neoplasms contains lesions with overlapping benign and malignant histopathological features. The overall mutation burden is higher than those of unequivocally benign lesions. This category also contains the contentious category of lesions known as **dysplastic nevi**<sup>45-</sup>

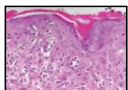
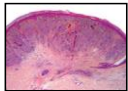
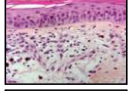
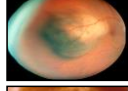
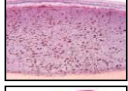
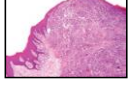
<sup>47</sup>. There is clear evidence that individuals with multiple dysplastic nevi are at increased risk of developing melanoma over their lifetime<sup>48,49</sup>.

The mutational status of oncogenes in benign nevi such as **NRAS** in congenital nevi<sup>50</sup>, **HRAS** in spitz nevi<sup>43</sup>, and later **BRAF** in acquired nevi<sup>51</sup>, **GNAQ** or **GNA11** in blue nevi<sup>34,52</sup> came as a surprise as many of them are common in melanomas. After acquiring an initiating mutation, a melanocyte will undergo limited proliferation to form a nevus, before entering a state that has been described as “senescence-like”<sup>53,54</sup>. However, several observations indicate that at least some melanocytes within a nevus retain the ability to proliferate<sup>55,56</sup>.

### 3.2.2 Malignant melanoma

#### *Classification by anatomical site*

Melanoma has been classified in several ways taking into account various variables such as histopathological type, vertical growth, whether it has spread to nearby lymph nodes or any other organ, among other factors. The traditional clinical and pathological classification scheme for melanoma includes four subtypes based on the pioneering work of Wallace Clark, more than forty years ago<sup>60</sup>, and has been included to the current World Health Organisation (WHO) classification<sup>61</sup>. The 4 categories are briefly described below with representative images and the most common mutated genes depicted in **Figure 2**<sup>57-59</sup>.

	Image	Histology	Common Mutated Genes	
Melanoma Subtypes	SSM			<b>BRAF 59-78%</b> NRAS 3-22%
	NM			<b>BRAF 43-68%</b> NRAS 12-31%
	ALM			<b>BRAF 12-23%</b> NRAS 8-15% <b>KIT 9-36%</b>
	LMM			<b>BRAF 40-60%</b> NRAS 15-29% KIT 16-28%
	UM			<b>GNAQ 46-50%</b> KIT 1-76%
	MM			<b>BRAF 3-11%</b> NRAS 5-13% <b>KIT 15-39%</b>

**Figure 2:** Traditional melanoma subtypes and their most frequently mutated oncogenes. Source: Refs.<sup>57-59</sup>.

- I. **Superficial Spreading Melanoma (SSM)** is the most common subtype, comprising approximately 75% of all malignant melanomas. A quarter of this type of melanoma are originate from with a pre-existing nevi, while most develop de novo<sup>62</sup>. **SSM** is usually flat with an intra-epidermal component and is linked to episodes of severe sunburn<sup>63-65</sup>.
- II. **Nodular Melanoma (NM)** represents 15 to 30% of all melanomas. They progress to invasiveness more quickly than any other type of melanoma. Although it is an aggressive lesion, the prognosis for a patient with a NM is the same as for any other subtype<sup>65,66</sup>.
- III. **Acral Lentiginous Melanoma (ALM)** is the least common variant, representing 2% to 8% of all melanomas in white people and 29% to 72% in dark skin population. ALM commonly develops in palmar regions, plantar regions, and occasionally subungual surfaces<sup>65,67</sup>.

**IV. Lentigo Malignant Melanoma (LMM)** accounts for 4% to 15% of melanomas. LMM represents *in situ* melanoma that 5% to 8% of the cases may progress to invasive lentigo malignant melanoma. Transformation is slow and the lesion can be present for 10 to 50 years before undergoing vertical growth<sup>68,69</sup>.

Furthermore, other rare forms of melanoma such as **uveal melanoma (UM)** and **mucosal melanoma (MM)** belong to the category of **non-cutaneous melanoma**. UM, account for approximately 5% of all melanomas in the US with a 10-year survival rates at 50% and is among the most lethal presentations of melanoma<sup>70,71</sup>. MM, account for 1% of all melanomas and primarily involves the mucosa of the anogenital region, nasal cavity, and paranasal sinuses, but can occur in all mucosal sites<sup>72</sup>.

*Classification by clinicopathological criteria (Clark model-linear evolution)*

Cancer progression has been conceptualized as a multistep process whereby normal cells accumulate genetic alterations that enable tumor growth and metastatic dissemination<sup>73</sup>. Classically, the different steps of melanoma progression are characterized by different histologic lesions according to the Clark model<sup>8,74,75</sup>. Melanoma is thought to arise in one of two ways: (1) with no visible precursor lesion or (2) in association with a benign melanocytic proliferation (nevus or mole). Five distinct stages have been proposed in the evolution of melanoma on the basis of such histological criteria (**Figure 3**):

**I. Benign nevi.** This first step refers to the proliferation of structurally normal melanocytes leading to the benign nevi. The absence of progression is probably due to **Oncogene-Induced Senescence (OIS)**, in which growth that is stimulated by the activation of oncogenic pathways is limited<sup>76</sup>. Hotspot mutations in **BRAF** (up-to 82% of acquired nevi<sup>51</sup>) or **NRAS** genes (up-to 81% of congenital nevi<sup>77</sup>) lead to the MAPK pathway activation which triggers a stress response leading to permanent G1 arrest<sup>78,79</sup>. However, these features cannot be used as markers of benign melanocytic tumors since malignant melanoma cells may also display similar phenotypic and molecular signatures<sup>80-84</sup>. It has been reported that senescence-like phenotypes can be induced genetically in metastatic melanoma cells suggesting that induction of senescence could be a novel therapeutic approach to treat melanoma<sup>85-87</sup>.

**II. Dysplastic nevi.** They may arise from pre-existing benign nevi or as new lesions. Genetically, in 25-40% of cases of familial melanoma, a genetic defect inactivates **CDKN2A**, a single gene that encodes two tumor suppressor proteins, p16<sup>INK4A</sup> and p19<sup>ARF88-90</sup>; in 25-50% of non-familial melanoma, a different tumor-suppressor gene, phosphatase and tensin homologue (**PTEN**), is inactivated by mutation<sup>91-93</sup>. **CDKN2A** or **PTEN** mutations are not

enough to the development of melanoma, but it is unclear precisely when such mutations occur<sup>8</sup>.

**III. Radial Growth Phase (RGP).** RGP consist in the intraepidermal proliferation of melanoma cells, which can be confined to the epidermis forming an *in situ melanoma* or penetrate the papillary dermis growing as small nests<sup>94</sup>. Multiple pathogenic alterations are accumulated over a considerable period of time, as reflected by their relatively late age of onset and slow development. This is more notable for neurofibromin 1 (**NF1**) mutant neoplasms, which affect older patients<sup>95-98</sup>. Melanoma *in situ* lesions are more common on chronically sun-exposed anatomical sites and tend to have a high mutation<sup>39,95,99</sup>.

**IV. Vertical Growth Phase (VGP).** The invasiveness begins once the melanoma cells leave the epithelium of the epidermis and enter the subjacent mesenchymal tissue<sup>100</sup>. In the **VGP** melanoma cells inherit driver mutations that activate the **MAPK** pathway, as well as **TERT** and members of the **SWI/SNF** chromatin-remodelling complex<sup>45</sup>. A small fraction of melanomas appear suddenly as nodular growths indicating that either accumulating mutations were in rapid succession, or perhaps more likely, they come directly from melanocytes that already harboured the secondary and/or the tertiary genetic alterations<sup>39,45</sup>. There seems to be no further substantial increase in the burden of point mutations from **RGP** to **VGP**<sup>45,101,102</sup>. In the molecular level, secretion of soluble factors and extracellular matrix proteins enable melanoma cells to communicate with their microenvironment cells<sup>103-106</sup>.

**V. Metastatic Melanoma.** Once melanoma cells have disseminated beyond the local site they are termed as **metastatic**, which generally appear first in the lymph nodes of the draining area of the primary tumour. Apart from lymph nodes; brain, liver, bone and intestine are the sites that are most frequently colonized by metastatic melanoma cells<sup>107</sup>. Sentinel lymph node resection does not experience an extension of life expectancy in patients<sup>108,109</sup>. Moreover, circulating tumour cells are commonly found in patients who present with only regional metastasis, or even no metastases at all<sup>110-112</sup>. Metastatic melanoma tends to have the highest proliferative index of all stages of melanoma. Mutations that confer resistance to targeted therapies can also lead to simultaneous emergence of resistant clones at many separate body sites<sup>113</sup>. The last decade, studies showed that melanoma cells secrete signals (**exovesicles**) from the very early stages of progression; and these signals “**educate**” the organs and prepare the so-called “**pre-metastatic niche**” to be metastasized for the colonization of melanoma cells to come<sup>114-117</sup>.

### Classification by clinicopathological criteria (AJCC-non linear evolution)

For years, Clark classification has been known to have prognostic significance, and has served as a criterion in several melanoma staging systems. However, only 20–30% of melanomas arise in association with a nevus precursor<sup>119,120</sup>. Several investigators have demonstrated that the level of invasion is less reproducible among pathologists, and is less accurate in providing prognostic information compared to tumor thickness<sup>121,122</sup>. As there are many routes to primary tumor formation, there are likely also many routes to the establishment of clinically meaningful metastatic disease (Figure 3). This prompted

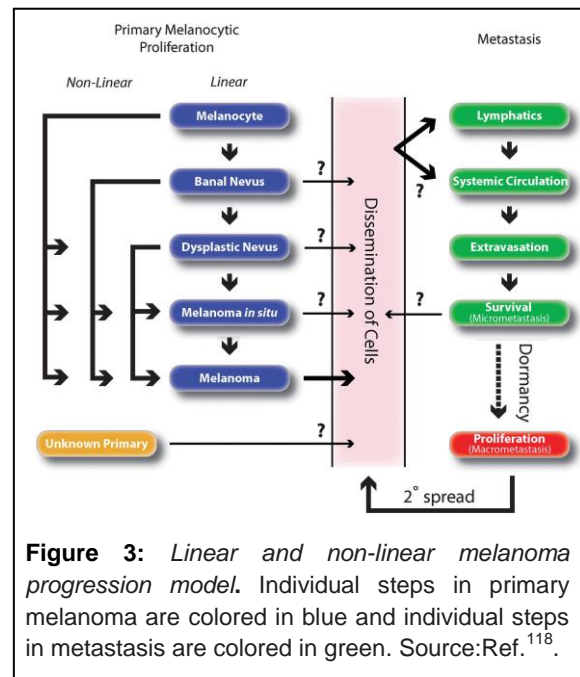


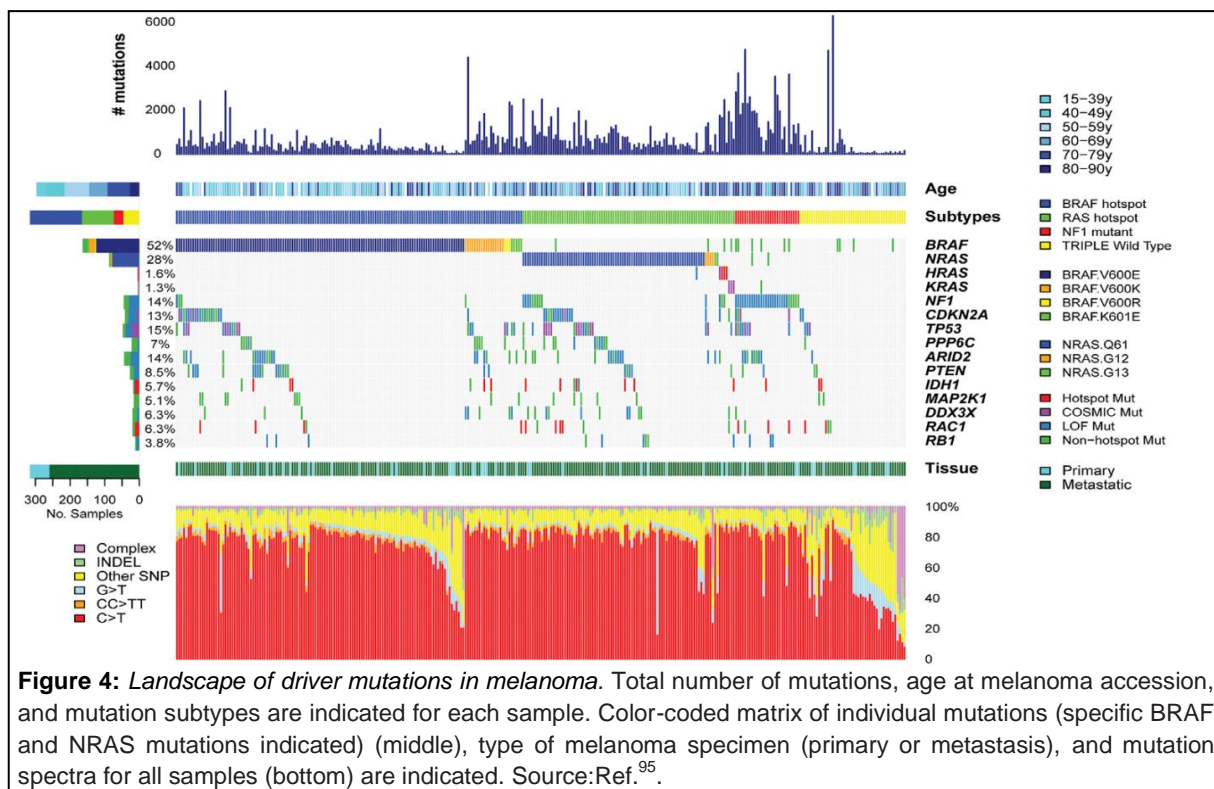
**Figure 3:** Linear and non-linear melanoma progression model. Individual steps in primary melanoma are colored in blue and individual steps in metastasis are colored in green. Source:Ref.<sup>118</sup>.

the definition of a revised model for melanoma progression which also theorizes melanoma as developing *de novo*. In the new staging system, Clark's level has far less importance. The **TNM** (Tumor, Node, Metastasis) classification and stage grouping of melanoma patients is based on clinical and histopathological prognostic factors, endorsed by AJCC database (American Joint Committee on Cancer Melanoma Staging)<sup>100</sup>. The **T** category is based on the thickness (or depth) of the primary melanoma and is further subcategorized to include the presence or absence of ulceration and mitotic rate- two very important prognostic features of a primary melanoma. The **N** category is determined by the presence and extent of regional lymph node involvement, and is further subcategorized according to number of involved lymph nodes and whether the metastases were macroscopic or microscopic (palpable or determined by sentinel-node evaluation, respectively). In-transit and satellite metastases are also included in the N staging. The **M** category is determined by the presence or absence of distant metastases (including skin), by site of disease, and serum LDH level<sup>100</sup>. The new revised AJCC (8<sup>th</sup>) classification includes molecular markers and newly acquired insights into the molecular underpinnings of cancer. This edition features 12 entirely new staging systems and a refined emphasis on a personalized-medicine approach<sup>123</sup>.

### Classification by genetic alterations

Due to melanoma complexity, integration of molecular data with relevant clinical and histopathological information are likely to be an important interim step before research

advances to a level permitting a mechanism-based classification. Detailed genetic studies using massively parallel sequencing have clarified the prevalence of driver oncogenes and have identified unique genetically-defined subpopulations of melanoma. Melanoma exhibits the highest rate of genetic alterations among cancer type<sup>124</sup> and whole-genome sequencing studies have confirmed that 80% of those changes are related with UV mutagenesis<sup>125</sup>. However, the above (and additional) studies have either focused on single high-throughput platforms of large sample sets or multi-platform analyses of fewer samples<sup>126,127</sup>. The Cancer Genome Atlas (TCGA) is the largest systematic multi-platform characterization of 333 cutaneous melanomas at the DNA, RNA, and protein levels to create a catalogue of somatic alterations and describe their potential biological and clinical significance (Figure 4)<sup>95</sup>.



From this study a framework for genomic classification into four subtypes based on the pattern of the most prevalent significantly mutated genes (SMGs) was established: i. **BRAF mutant**, ii. **RAS mutant**, iii. **NF1 mutant**, iv. and **Triple-WT (wild-type)**. The largest genomic subtype was defined by the presence of **BRAF hot-spot mutations**. Of the 318, 52% (n=166) harboured **BRAF somatic mutations**. Of those, 145 targeted the well documented V600 amino acid residue: **V600E** (n=124), **V600K** (n=18), and **V600R** (n=3). The second major subtype is defined by the presence of **RAS hot-spot mutations**, including known amino acid changes with functional consequences, in all three RAS family members (N-, K- and H-RAS). Overall, 28% had **NRAS** somatic mutations. The third most frequently observed SMG in the MAPK pathway was **NF1**, which was mutated in 14% of samples. More than half of its mutations were predicted to be loss-of-function (LoF) events

(as an alternative way to activate the canonical MAPK pathway). The **Triple-WT subtype** (n=46) was defined as a heterogeneous subgroup characterized by a lack of hot-spot BRAF, N/H/KRAS, or NF1 mutations<sup>95</sup>. The above **SMGs**, and additional that were found mutated in lower fraction samples, are components of the **MAPK** and the **PI(3)K** (Phosphatidylinositol-4,5-bisphosphate 3-Kinase) pathways and were also confirmed to be activated.

### 3.4 “Classical” versus “Lineage-Specific” oncogenes in melanoma

---

As shown in **Figure 4** and in **Table S2** (Appendix) the majority of melanoma oncogenes signal through the **MAPK** and/or **PI3K** pathways. Other examples of initiating oncogenic events are the amplification of the cell cycle regulators CCND1 or CDK4<sup>128</sup>. These oncogenic mutations are accompanied by alterations in tumor suppressor genes such as CDKN2A<sup>129,130</sup>, PTEN<sup>128,129</sup>, TP53<sup>131</sup> and RB1<sup>132</sup>, among others. These factors suffer activating genetic aberrations which are frequently shared among different tumor types and have been termed “**classical oncogenes**”<sup>133</sup>.

Besides these aberrantly activated/deactivated genes which are shared among different types of cancer, there seems to be a **lineage-specific element** to certain pathways that are able to transform melanocytes and that contribute to the robust metastatic potential of melanoma. The best characterized lineage specific gene in melanoma is **MITF**<sup>134</sup>. MITF has been defined as the master regulator of melanocyte development, differentiation and pigmentation<sup>135</sup>. Amplification of MITF has been identified in approximately 15% of melanomas<sup>134</sup>. Loss-of-function mutations of MITF result in the complete absence of the melanocytic lineage<sup>136</sup>. Loss of MITF expression is lethal to most melanoma cell lines *in vitro* (by inducing cell cycle arrest<sup>136</sup> or DNA damage<sup>137</sup>). Intriguingly, MITF depleted melanoma cells are also highly invasive<sup>138</sup>. These contradictions have led to a proposed **rheostat model** where low MITF is a hallmark of stem-like cells (invasive phenotype), whereas MITF-positive cells either proliferate or differentiate depending on the expression levels or post-translational modifications. As MITF levels and activity are strongly influenced by the microenvironment, the effect of MITF expression on melanoma cell identity is dynamic<sup>139-141</sup>. Importantly, our group recently identified the endolysosomal GTPase RAB7 as an MITF-independent mechanism of lineage-regulation in melanoma<sup>142</sup>.

### 3.5 Non-Oncogene Addiction in melanoma

---

Cancer cells are addicted to “**classical**” or to “**Lineage-Specific**” oncogenes in order to sustain hyper-activated signaling pathways and progress. However, there are many genes

that are unable to directly promote tumor formation but whose reduction in activity can become rate-limiting to the pathway. By this rationale, cancer cells are addicted to both oncogenes and non-oncogenes. To describe this addiction of cancer cells to the functions of non-oncogenes, this phenomenon was termed as “**non-oncogene addiction**”<sup>143,144</sup>. One cellular process in melanoma proposed to be mediated by oncogenic and non-oncogenic mediators is **autophagy**.

### 3.5.1 Autophagy

Autophagy is the major intracellular degradation process by which cytoplasmic materials are delivered to and degraded in the lysosome. However, the purpose of autophagy is not the simple elimination of materials; but instead, serves as a dynamic recycling system that produces new building blocks and energy for cellular renovation and homeostasis. The term was introduced in 1966 by de Duve, derived from the Greek words

“*auto*” and “*phagy*” meaning “*self*” and “*eating*”, to describe the occurrence of distinct intracellular, membranous vesicles that contained degraded cytoplasmic material<sup>146</sup>.

Autophagy is classified as **microautophagy**, **chaperone-mediated autophagy** and **macroautophagy**<sup>147</sup>. In microautophagy, the lysosome itself engulfs small components of the cytoplasm by inward invagination of the lysosomal membrane. Membrane dynamics during microautophagy may be quite similar to that of endosomal sorting complex required for transport (ESCRT)-dependent multivesicular body (MVB) formation, which occurs in the late endosome<sup>148</sup>. The chaperone-mediated autophagy does not involve membrane reorganization; instead, proteins directly translocate across the lysosomal membrane during chaperone-mediated autophagy<sup>149</sup>. Macroautophagy (herein will be referred as “**autophagy**”) is thought to be the major type of autophagy, and it has been studied most extensively compared to other categories. Although autophagy was initially considered a non selective cellular process, the specific catabolism of cellular organelles like mitochondria,

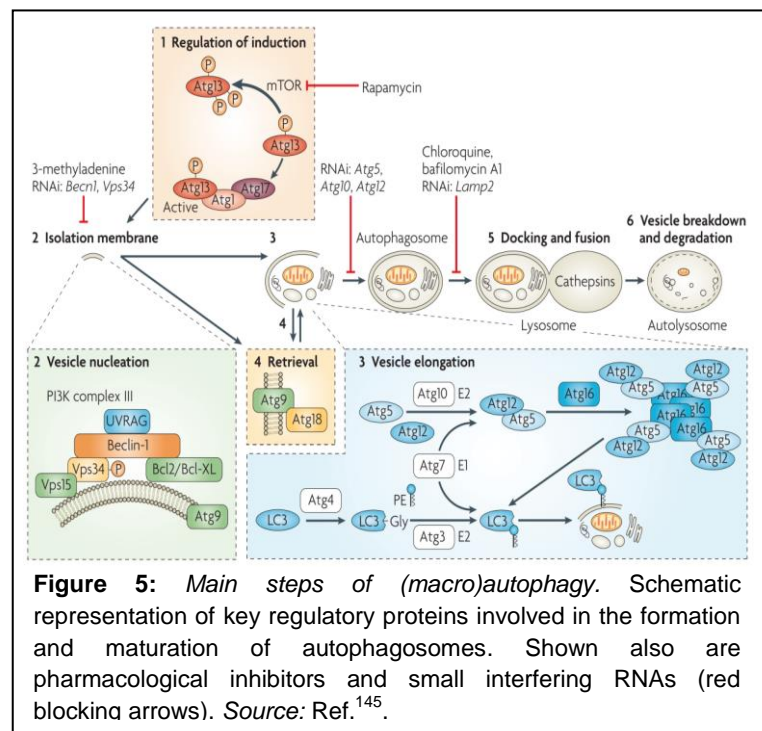


**Figure 5:** Main steps of (macro)autophagy. Schematic representation of key regulatory proteins involved in the formation and maturation of autophagosomes. Shown also are pharmacological inhibitors and small interfering RNAs (red blocking arrows). Source: Ref.<sup>145</sup>.

peroxisomes, endoplasmic reticulum, and ribosomes has been discovered and is termed “mitophagy”<sup>150,151</sup>, “pexophagy”<sup>152,153</sup>, “ERphagy/reticulophagy”<sup>154</sup>, and “ribophagy”<sup>155</sup>, respectively. In general, the role of autophagy to maintain cellular homeostasis requires the versatility to recognize a diverse range of substrates and stimuli<sup>156</sup>. Autophagy is orchestrated by a number of highly conserved AuTophagy-related genes (**ATGs**), which were originally identified in yeast, with many of these genes having orthologues in mammalian cells<sup>157,158</sup>. The main steps and the core components of this process are highlighted in **Figure 5** and in **Table S3** in the Appendix. Briefly, double-membrane-bound **autophagosomes** develop in a multi-step process starting by the engulfment of cytoplasmic material by the **phagophore**<sup>159</sup>. This process involves the de-repression of the mTOR Ser/Thr kinase which inhibits autophagy by phosphorylating the Atg13 (*step 1*). This leads to the dissociation of Atg13 from a protein complex that contains Atg1 kinase (the fly orthologue of ULK1) and Atg17. When mTOR is inhibited, re-association of Atg13 with Atg1 induces autophagy<sup>160,161</sup>. Among the initial steps of vesicle nucleation is the activation of mammalian Vps34 (a class III PI3K) to generate phosphatidylinositol-3-phosphate (PtdIns3P) (*step 2*). Activation of Vps34 depends on the formation of a complex in which beclin-1 (Becn1; the mammalian orthologue of Atg6), UVRAG (UV irradiation resistance-associated tumour suppressor gene) and a myristylated kinase (Vps15, or p150 in humans) participate. Two ubiquitin-like conjugation systems are part of the vesicle elongation process (*step 3*). One pathway involves the covalent conjugation of Atg12 to Atg5, with the help of the E1-like enzyme Atg7 and the E2-like enzyme Atg10. The second involves the conjugation of phosphatidylethanolamine (PE) to LC3/Atg8 (LC3 is one of the mammalian homologues of Atg8). Lipid conjugation leads to the conversion of the soluble form of LC3 (named **LC3-I**) to the autophagic vesicle-associated form (**LC3-II**)<sup>162,163</sup>. LC3-II is used as a marker of autophagy because its lipidation and specific recruitment to autophagosomes provides a shift from diffuse to punctate staining of the protein<sup>164</sup>. The mechanism of retrieval in which the Atg9 complex participates is poorly studied (*step 4*). Autophagosomes undergo maturation by fusion with lysosomes to create **autolysosomes** (*steps 5 and 6*). In the autolysosomes, the inner membrane and the cargo are degraded by lysosomal enzymes that act optimally within this acidic compartment<sup>145,165-167</sup>. In the phagosome formation, autophagy related proteins participate in the orchestrated fusion of Golgi-, endosome- and plasma-membrane-derived membranes<sup>168-171</sup>.

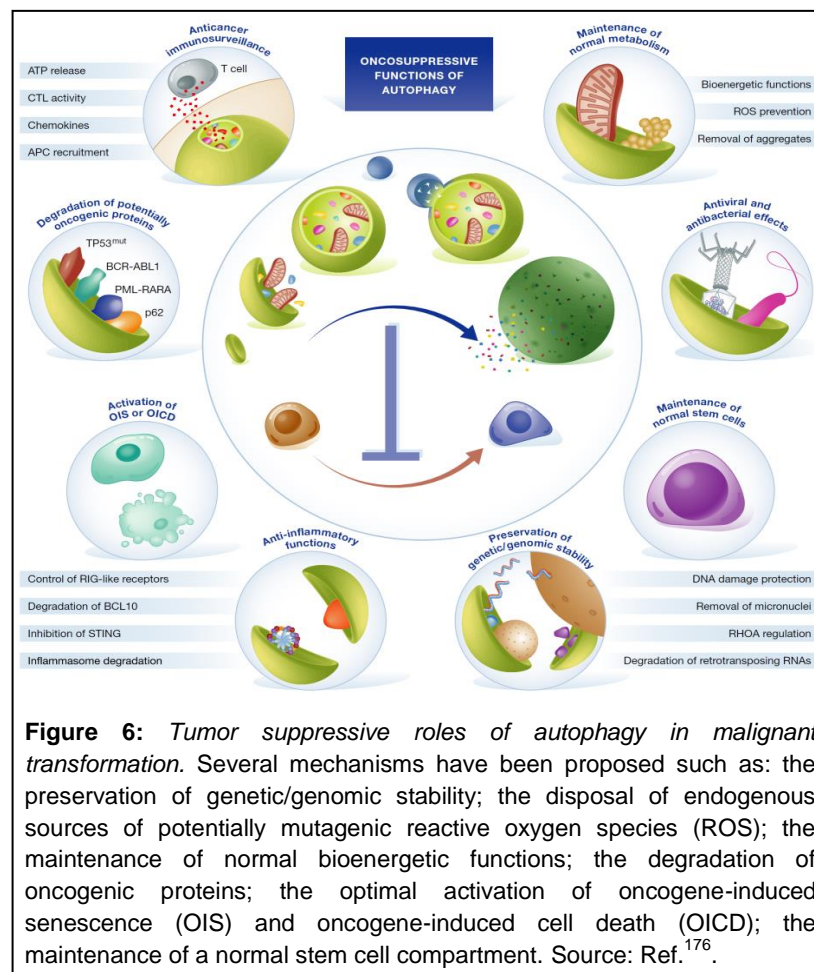
### 3.5.2 Autophagy: A “double-edged” sword in cancer

Autophagy plays a key role in the maintenance of cellular homeostasis. In healthy cells, such a homeostatic activity constitutes a robust barrier against malignant transformation. In

cancer, autophagy can be **tumor-suppressive**<sup>172,173</sup> or **tumor promoting**<sup>174,175</sup> in different contexts<sup>176</sup>. Large-scale analyses from **TCGA** indicate that the core autophagy machinery largely escapes genomic mutation in human cancers<sup>177</sup>. Autophagy impacts cellular metabolism, the proteome, and organelle numbers and quality, which alter cell functions in diverse ways. Additionally, autophagy can promote a cross-talk between the tumor and the stroma, which can support tumor growth. Thus, the role of autophagy is determined by nutrient availability, microenvironment stress, and the presence of an immune system<sup>178</sup>.

### *Autophagy as a tumor suppressor*

Autophagy was initially thought to be a tumor-suppression mechanism. This concept derived from early reports that the essential autophagy gene **ATG6/BECN1** (part of the class III PI3K complex) was monoallelically lost in 40% to 75% in various cancer types. *Becn1*<sup>+/-</sup> mice (*Becn1*<sup>-/-</sup> are not viable) spontaneously develop various malignancies, including lymphomas as well as lung and liver carcinomas<sup>179-183</sup>. However, in human tumors, to assess the possibility that **BECN1** is acting as a tumour



suppressor is complicated because of the close proximity of the **BECN1** gene and the potent tumor suppressor **BRCA1**<sup>184</sup>. Mutations in BRCA1 are known drivers in human breast and ovarian cancers. This makes difficult to rule out the possibility that in human tumors, it is loss of BRCA1 rather than BECN1 that is important. Indeed, TCGA data shows there is no significant loss of BECN1 independent of BRCA1 loss<sup>185</sup>.

The mosaic deletion of **Atg5** in mice or **Atg7** in mouse livers produces only benign hepatomas, suggesting that complete and specific autophagy deficiency promotes liver

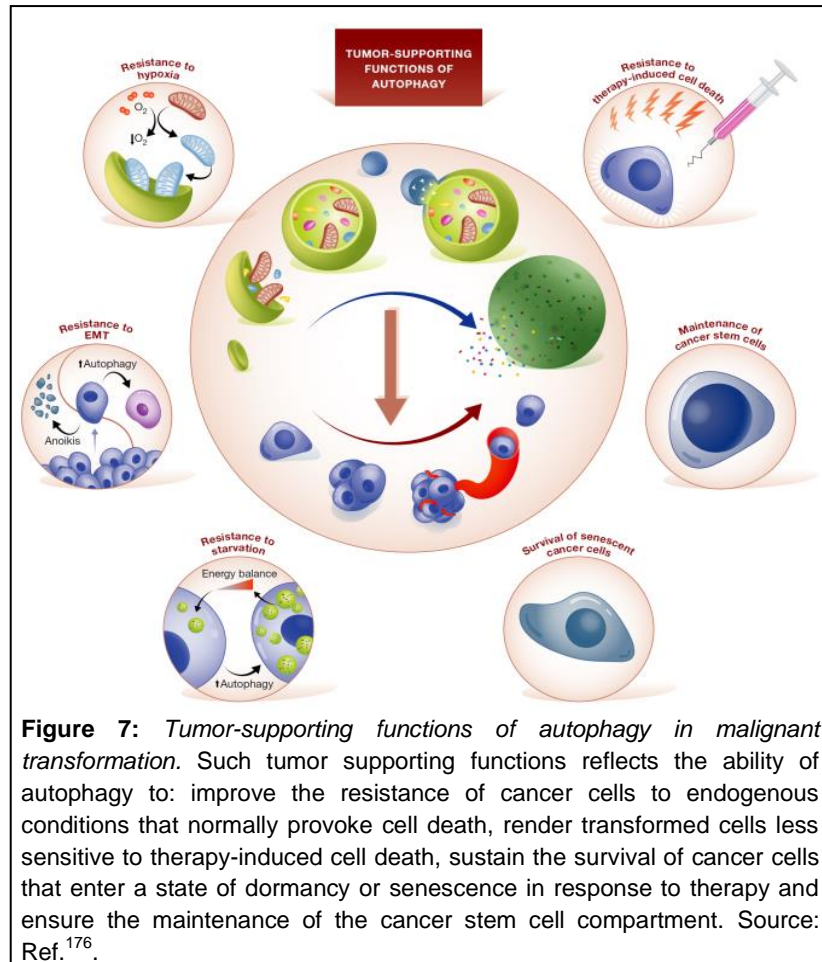
tumor initiation but restricts progression to malignant disease<sup>186</sup>. Similarly, loss of *Atg5* or *Atg7* in the mouse pancreas promotes benign pancreatic intraepithelial neoplasia (**PanIN**) formation but prevents progression to malignant disease<sup>187,188</sup>. Autophagy loss in the liver and pancreas causes oxidative stress, chronic tissue damage, and inflammation, all factors that are well known to promote tumor initiation<sup>189</sup>. This chronic state of tissue damage, cell death, and inflammation promotes compensatory proliferation, producing cells vulnerable to mutation and oncogenic transformation. **Atg7** deletion increased oxidative stress and enhanced tumor growth at early stages, but promoted abnormal mitochondria accumulation, proliferation defects, a decrease in tumor burden, and increased survival of animals in more advanced stages of tumorigenesis<sup>190</sup>. Similarly, deletion of **Atg7** in mice expressing an activating mutation of B-Raf (*Braf*<sup>+V600E</sup>) promotes early tumor development in the lung but also inhibits the progression to a more malignant phenotype and increases mouse survival<sup>191</sup>. An additional autophagy-promoting factor that has tumor suppressor functions is **Atg4C**, where its deletion in mice leads to the development of fibrosarcomas<sup>192</sup>. Finally, it has been proposed that autophagy contributes to oncogene induced cell death or oncogene-induced senescence, two oncosuppressive mechanisms. The activation of various oncogenes imposes a significant stress on healthy cells, a situation that is normally aborted through the execution of a cell death program<sup>193,194</sup>, or cell senescence<sup>195</sup>.

The above studies, and other, have shown that autophagy deficiency causes oxidative stress, mitochondrial defects, activation of the DNA damage response, genome instability and other features that are highlighted in **Figure 6**. It remains unclear if these premalignant tumors in autophagy-deficient mice are in a “benign” state that requires additional genetic alterations to promote malignant transformation (e.g. p53 mutation), or if autophagy inhibition can only promote premalignant/benign tumor formation but somehow protects cells from advancing to malignant cancers<sup>189,196-199</sup>.

#### *Autophagy as a tumor promoter*

In established tumor cells, autophagy is hijacked to serve as a cell survival mechanism that plays a vital role in facilitating tumor cell growth. Several potential mechanisms in cancer have been suggested and are depicted in **Figure 7**. The notion that autophagy represents a mechanism that promotes tumor growth is based on the need of tumor cells to adapt to an environment that is hypoxic, as well as growth factor and nutrient deprived. Furthermore, tumor cells generally have high proliferation rates, which translate into higher bioenergetic and biosynthetic needs compared to non-transformed cells. These requirements can be fulfilled by increasing autophagy as a mechanism that permits obtaining both ATP and metabolic intermediates<sup>190</sup>. Importantly, for tumor cells in which the oncogene **Ras** is activated, high levels of basal autophagy and dependence on this mechanism for survival

are observed. For these reasons, autophagy is thought to promote tumor cell survival by increasing stress tolerance and providing a pathway that permits obtaining the nutrients necessary to meet the enhanced energetic requirements of these cells<sup>187,200</sup>. A first indication that autophagy may promote cancer came from the observations that autophagy is up-regulated in hypoxic tumor regions, suppresses tumor-induced inflammation, and promotes tumor cell survival<sup>201</sup>.



In GEMM for lung cancer, sporadic activation of an oncogenic allele of Kras (**Kras<sup>G12D</sup>**) results in tumor initiation and gradual progression to adenomas and adenocarcinomas upon acquisition of TP53 mutations. Deletion of *Atg7* dramatically alters the progression of these tumors, producing the accumulation of defective mitochondria, accelerated induction of p53, and proliferative arrest. *ATG7* loss promotes the formation of oncocytomas instead of adenomas and carcinomas, proliferation is suppressed, and tumor burden is reduced. Surprisingly, mice with *Atg7<sup>+/+</sup>* tumors die from cancer, whereas mice with *Atg7<sup>-/-</sup>* tumors die from inflammatory pneumonia, demonstrating that *Atg7*-deficient lung tumors trigger an immune response<sup>202</sup>.

In pancreatic adenocarcinoma, **KRAS<sup>G12D</sup>**-driven cells enter a state of dormancy in response to oncogene ablation and exhibit activated autophagy to efficiently counteract metabolic stress. Interestingly, these cells (characterized as cancer stem cells) have the ability to efficiently form tumors *in vivo*, and this relies on autophagy<sup>203-205</sup>.

**FIP200** (key component of autophagosome) deficiency in mammary cancer suppresses tumor growth and prolongs mouse survival via the disruption of autophagy machinery<sup>206,207</sup>. FIP200 loss in mammary tumors activates an immune response and T-cell depletion partly restores the growth of FIP200-deficient tumors. This suggests that targeting FIP200 or other

components of the autophagy initiation complex may suppress breast cancer by activating innate and adaptive anti-tumor immune responses<sup>208</sup>.

In glioblastoma it is demonstrated that autophagy is crucial for both glioma initiation and sustained growth in a Kras-driven mouse model where shRNAs against Ulk1, Atg7, or Atg13 promote senescence and extended mouse survival<sup>209</sup>.

Epithelial to Mesenchymal Transition (**EMT**) is one of the leading biological processes of metastasis during cancer<sup>210,211</sup>. Several works show that EMT requires autophagy to support viability of potentially metastatic cancer cells<sup>174,212-214</sup>.

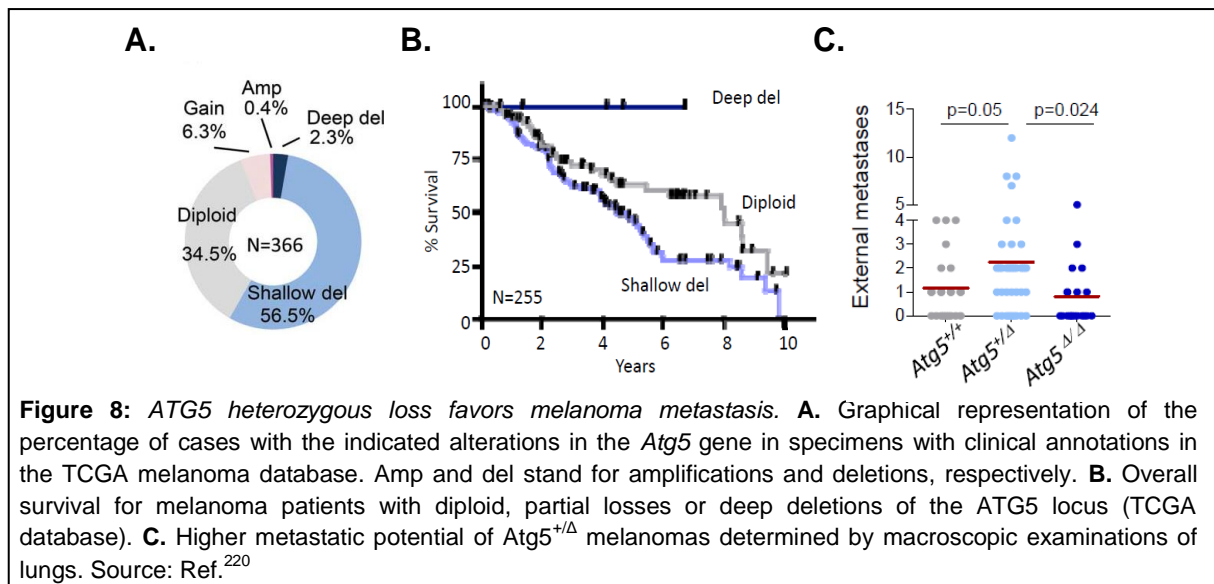
Autophagy is an evolutionarily conserved mechanism and its role in cancer depends on many factors like tissue type, tumor stage, and the type of oncogenic mutation involved<sup>215</sup>.

### 3.5.3 Autophagy in melanoma

Melanomas have a high level of basal autophagosomes suggestive of increased autophagy. Melanoma patients with higher levels of autophagosomes have decreased survival<sup>216</sup>. BRAF targeted therapy results in a transient response in some patients with BRAF mutant melanoma, only to relapse shortly thereafter. In a GEMM of melanoma (*Braf*<sup>V600E</sup>/*Pten*<sup>-/-</sup>), *Atg7* deficiency prevents melanoma initiation and proliferation and prolongs survival. Although the mechanism is not firmly established, *Atg7* prevents oxidative stress, apoptosis, fibrosis, and, notably, senescence, a known barrier to melanoma growth and progression<sup>217</sup>. Moreover, autophagy in *Braf*-resistant melanoma cells either by *ATG5* knockdown or pharmaceutically was not sufficient in restoring sensitivity to Vemurafenib (*Braf*<sup>V600E</sup> inhibitor) treatment; however, combinational treatment increased melanoma cell death<sup>218</sup>.

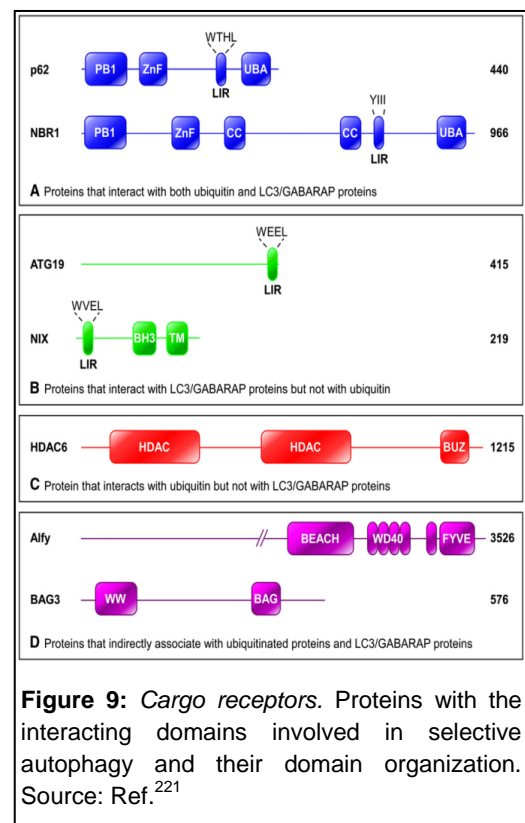
On the other hand, two autophagy markers, *ATG5* and *LC3*, were found significantly decreased in patients with early-stage cutaneous melanoma as compared with those with benign nevi<sup>219</sup>. Importantly, studies in our lab using GEMM, *in vitro* studies and data from TCGA database revealed that specific heterozygous loss of *ATG5* favors melanoma metastasis and it's a poor indicator of survival (**Figure 8**). Of note, the tumors in the *ATG5* heterozygous mice were more resistant to targeted therapy with a *Braf*<sup>V600E</sup> inhibitor (Dabrafenib)<sup>220</sup>. Although mechanistically was not characterized how the specific loss triggers metastasis, it is speculated that the expression levels of autophagy proteins should be fine tuned in order to regulate downstream factors that favor invasion.

Whether other proteins of autophagy machinery behave in the same manner is poorly characterized.



### 3.6 Cargo receptors in autophagy

As was mentioned above, the turnover of damaged organelles, removal of protein aggregates, and elimination of intracellular pathogens, are highly selective and tightly regulated processes that require selective sequestration of the specific cargo into autophagosomal membranes<sup>221,222</sup>. An autophagy receptor is defined by its ability to bridge cargo and autophagosomal membrane, leading to the engulfment of cargo by the autophagic vesicle. Selectivity is achieved through autophagy receptors. The interaction of cargo receptors with **LC3/GABARAP** relies on the formation of an intermolecular  $\beta$ -sheet to which the cargo receptor contributes a single strand, the so-called LC3-interacting region (**LIR**). LIR motifs in general interact with autophagy modifier proteins of the LC3/GABARAP family<sup>223</sup>. In mammalian cells, more than two dozen autophagy receptors were identified by the yeast two-hybrid system and proteomic approaches<sup>224</sup>. There is an additional class of proteins **autophagy adaptors** that also bind to members of the LC3/GABARAP family (**Figure 9**). However, they do not facilitate engulfment and



subsequent degradation of cargo, but serve as anchor points for the autophagy machinery and regulate initiation, conjugation, transport and fusion of autophagosomes<sup>225</sup>.

One of the most characterized cargo receptors in the higher organisms is **p62** also known as **Sequestosome-1 (SQSTM1)**. Unexpectedly, p62 localizes to the phagophore even in the absence of LC3 interaction<sup>226</sup>. Self-oligomerization of p62 rather than binding to LC3 is critical for the translocation of p62 to the autophagosomal membrane<sup>227</sup>.

### 3.7 p62 as an autophagy adaptor and a signaling hub

---

**p62** was first identified as a 62 kDa protein which binds lymphocyte-specific protein tyrosine kinase (Lck), a Src family member<sup>228</sup>. Later, p62 was also reported to be a binding partner of atypical protein kinase C (aPKC)<sup>229,230</sup>. Since its initial discovery, p62 through the well-defined structural elements has been characterized to act as an **autophagy adaptor** and also as a **signaling hub** due to its ability to interact with key signaling proteins.

#### 3.7.1 Structure of p62

p62 is ubiquitously expressed in various cell types, mainly in the cytoplasm, and is also present in the nucleus, autophagosomes, and lysosomes<sup>231-233</sup>. It contains multiple major domains (**Figure 9**) such as the **PB1** (Phox1 and Bem1p regions, aa 20–102), the **ZZ** (ZZ-type zinc finger, aa 122-166), the **TB** (TRAF6 binding, aa 225-250) and the **KIR** (Keap1-interacting region, aa 346–359) that confer the ability to interact with key components involved in essential signaling pathways<sup>234,235</sup>. Two other domains, **UBA** (Ubiquitin-associated domain, aa 391–436) and the **LIR** (LC3-interacting region, aa 337-343) domains, cause p62 to function as an adaptor between autophagy and ubiquitinated proteins<sup>236</sup>.

The **UBA** domain of p62 can bind both K48-linked and K63-linked Ub chains<sup>237-239</sup>. Exposure to proteasome inhibitors or expression of polyglutamine-expanded huntingtin, UBA is phosphorylated in Ser407 by ULK1 kinase, which is required during the early steps of autophagosome biogenesis. This phosphorylation destabilizes the UBA dimer interface. Subsequently, Ser403 of the UBA domain is phosphorylated by casein kinase 2 or TANK-binding kinase 1 to increase the binding affinity of p62 for ubiquitin chains<sup>240</sup>. The UBA is frequently mutated in Paget's disease. This pathology is characterized by an increase in the number and the activity of osteoclasts, leading to bone architecture abnormalities<sup>241,242</sup>.

The **LIR** domain, via an 11 amino-acid portion located in the 332-343 region, is responsible for the association of p62 with all isoforms of the LC3 protein and consequently the targeting in the autophagic machinery<sup>243</sup>. There are a series of salt bridges and hydrogen bonds between p62 and LC3. The hydrophobic (Trp340–Leu343) and acidic cluster

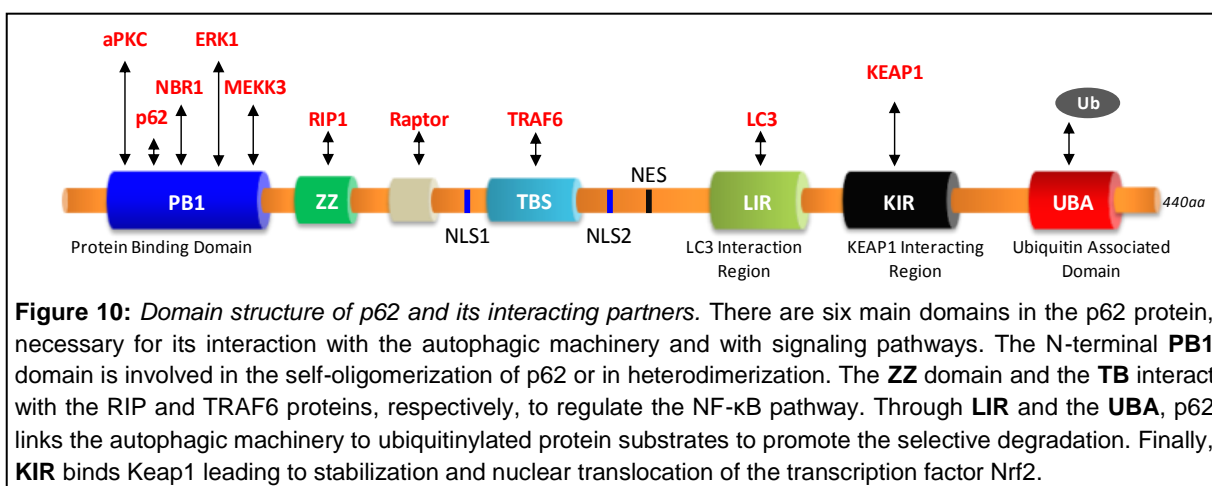
(Asp337–Asp339) of p62 are very important for LC3 binding, and these motifs are conserved across species. Disruption of the interaction is sufficient to impair the degradation of p62, resulting in the formation of ubiquitin- and p62-positive inclusions<sup>244</sup>.

The **KIR** domain interacts with Keap1, a Cullin3-ubiquitin E3 ligase complex adaptor protein. In turn, Keap1-promoted polyubiquitinylation and subsequent proteasomal degradation of the transcription factor Nrf2 are inhibited. As a consequence, the expression of cytoprotective, antioxidant Nrf2 target genes is increased<sup>199,245</sup>. Moreover, the p62 gene itself is a target for Nrf2; thus, the appropriate oxidative stress response is supported by a positive feedback regulation between p62 and Nrf2<sup>246</sup>. Autophagy has a strong impact on Nrf2 activation, since p62 not only disrupts Keap1-Nrf2 interaction but also removes Keap1 from the cytosol via selective autophagy<sup>247</sup>.

The **ZZ** domain is related to NF- $\kappa$ B signaling and glucose regulation. This domain could associate with RIPK1. Recently, some studies reveal that the ZZ domain of SQSTM1 may links autophagy to N-end rule pathway<sup>248,249</sup>.

The **TB** domain of p62 interacts with TRAF6, an E3 ubiquitin ligase that regulates mTORC1 activity by K63-ubiquitination in a p62-interaction dependent manner. Through this TB domain, p62 could function as a crucial mediator for mTORC1 activity regulation<sup>233</sup>.

The **PB1** domain was characterized initially by its ability to bind atypical protein kinase C (PKC  $\zeta$  and  $\iota$ )<sup>229,250</sup>. Heterodimerization of p62 with atypical PKC is crucial for the regulation of the NF $\kappa$ B pathway. Indeed, following binding of the RANK ligand to its cognate receptor RANK in osteoclasts, the association of p62 with either atypical PKC (or with TRAF6 via TB domain) contributes to the activation of IKK (Ik-B Kinase) and to the nuclear translocation of NF $\kappa$ B. p62 binds and inhibits ERK1, which is crucial for the negative regulation of adipogenesis and obesity and the ensuing inflammation<sup>251</sup>. The PB1 domain plays a role in p62 self and hetero-oligomerization with other PB1 domain containing proteins, such as NBR1<sup>252</sup>. Finally, PB1-mediated p62 self-oligomerization is essential for its localization to the autophagosome formation site, a process that is independent of LC3 localization<sup>227</sup>.



### 3.7.2 Transcriptional regulation of p62

One of the main modes of transcriptional regulation of p62 is dependent on the **NRF2** transcription factor<sup>245</sup>. NRF2 binds to the antioxidant-responsive element (ARE motif) located in the p62 promoter to promote the expression of *p62 mRNA*. In the absence of oxidative stress, NRF2 is maintained as an inactive protein in the cytoplasm through its interaction with the KEAP1. In addition to its specific regulation by NRF2, p62 can interact directly with KEAP1 via its KIR domain and is able to dissociate NRF2 from KEAP1, thus promoting the activation and nuclear translocation of NRF2<sup>199,253</sup>. Additionally, the constitutive activity of the **Ras/MEK/ERK1/2**<sup>3,254</sup> and the **JNK/c-Jun**<sup>255,256</sup> pathways regulates p62 at transcriptional level in different systems. Finally, other stimuli including phorbol 12-myristate 13- acetate (PMA), calcium and IL-3, drastically increase the expression of p62 mRNA in a very short time<sup>257</sup>.

### 3.7.3 p62 in cancer progression and metastasis

As mentioned above, p62 expression is elevated in response to a variety of cellular stresses, especially those that result in impaired autophagic flux. p62 is overexpressed in many human cancers. Studies have shown that p62 is overexpressed in hepatocellular carcinoma (HCC)<sup>189,258-263</sup>, intrahepatic cholangiocarcinoma<sup>264</sup>, pancreatic cancer<sup>265</sup>, lung cancer<sup>262,266,267</sup>, oral, head and neck cancer<sup>268,269</sup>, esophageal cancer<sup>270</sup>, gastric cancer<sup>265,271</sup>, colon cancer<sup>262,272</sup>, breast cancer<sup>273-278</sup>, prostate cancer<sup>278-284</sup>, melanoma<sup>285</sup>, endometrial cancer<sup>286</sup>, ovarian cancer<sup>287</sup>, glioblastoma multiforme<sup>288</sup> and kidney cancer<sup>289</sup>, as well as chronic liver diseases, such as alcoholic and non-alcoholic steatohepatitis (ASH, NASH) that increase HCC risk<sup>259,290-293</sup>. In the **Table S4** (Appendix) are listed the main functions of p62 in different pathological diseases and mainly in different types of cancer.

#### *p62 autophagy dependent roles in cancer*

p62 has been identified as one of the many autophagy receptors and may promote autophagic degradation of cargos through at least three mechanisms. First, p62 is directly associated with early autophagosome formation by recruiting Atg proteins to the autophagosome formation site through its PB1 domain independent of its LIR<sup>227</sup>. Second, p62 binds to ubiquitinated proteins to form protein aggregates via its UBA domain. Third, p62 also directly interacts with LC3 via its LIR motif (**Figure 10**)<sup>236,243</sup>. Along with its PB1 partner, NBR1 (Neighbor of BRCA1 gene 1), it has been proposed to regulate the packing and delivery of polyubiquitinated, misfolded, aggregated proteins and dysfunctional organelles for their clearance through autophagy in mammalian cells and in the fruit fly *Drosophila*<sup>243,294,295</sup>.

Defects in autophagy promote a failure of protein and organelle quality control in cells, which leads to p62 accumulation, resulting in perturbation of gene expression, increased genome damage and tumorigenesis<sup>189</sup>. Importantly, in autophagy deficient and apoptosis-incompetent tumor cells, metabolic stress leads to the accumulation of p62, elevated expression of endoplasmic reticulum (ER) chaperones, damaged mitochondria, and reactive oxygen species (ROS). This increase in p62 levels is critical for tumorigenesis, as overexpression of p62 in this cell model leads to increased tumor volume in mouse xenograft experiments<sup>189,296</sup>.

A relevant *in vivo* study described that complete inhibition of autophagy in hepatocytes; induced by deletion of the essential autophagy genes, *Atg5* or *Atg7*; causes spontaneous liver injury, hepatomegaly, and appearance of liver tumors<sup>186</sup>. These tumors, however, are benign adenomas<sup>297</sup>. Liver adenomas in liver-specific *Atg7*<sup>-/-</sup> mice show strong accumulation of p62 and subsequent NRF2 activation due to autophagy inhibition, and both tumor growth and liver injury are markedly suppressed by p62 loss<sup>186,298</sup>. Liver injury is alleviated by NRF2 ablation and exacerbated by Keap1 deletion in liver-specific *Atg7*<sup>-/-</sup> mice<sup>199</sup>. This indicates that p62 may also be a central element in a quality-control mechanism for the disposal of toxic aggregates.

p62 has been proposed as a critical regulator of the EMT factor, Twist1. Insufficient autophagy causes accumulation of p62 and promotes cell proliferation and migration through stabilization of the oncogenic transcription factor Twist1<sup>299</sup>.

In established breast tumors **FIP200**-mediated autophagy is required for maintaining tumor growth *in vivo* and the accumulated p62 upon autophagy blockage stimulated the growth of autophagy-deficient tumors. These results revealed a rather synergistic mechanism of p62 signaling and autophagy in the promotion of cancer growth<sup>207</sup>. Of note, recent studies found that p62 is not only required for the proper elimination of ubiquitinated proteins but also participates in the autophagic clearance of non-ubiquitinated substrates<sup>300</sup>.

Several studies highlight that although p62 usually recruits ubiquitinated cargos, loss of p62 has little effect on selective autophagy. This lack of phenotypic impact might be explained by the presence of other autophagy receptors including **NBR1**, **NDP52** (Nuclear Dot Protein 52 kDa) and **Optineurin**<sup>236,301,302</sup>.

### *p62 as a signaling hub in cancer*

Unlike other autophagy adaptors, with the exception of NBR1, p62 is also a central hub due to its ability to interact with key signaling proteins through well-defined structural elements. Therefore, it is possible that autophagy only intervenes as a facilitator or an inhibitor of the prooncogenic action of p62<sup>296,303</sup>.

In ductal pancreatic adenocarcinoma, the constitutive activation of Ras activates the NF- $\kappa$ B pathway to trigger increased p62 synthesis, and this newly synthesized p62, in turn, interacts with **TRAF6** to amplify Ras signaling in a positive feedback loop<sup>304</sup>. The same observations arise from studies on lung cancer in which Ras activation stimulates the TRAF6-p62-NF- $\kappa$ B complex that is necessary to inhibit deleterious ROS production<sup>253</sup>. In glioblastoma multiforme, p62 is strongly overexpressed harboring a mesenchymal oncogenic signature and this overexpression is concomitant with **MAPK** activation<sup>288</sup>.

**mTORC1** is sensitive to inhibition by rapamycin and senses multiple cellular and environmental cues including nutrient availability, energy levels, protein misfolding and growth signals. p62 can promote mTORC1 activation by directly interacting with **Raptor**, a key component of mTORC1. In response to stimulation with amino acids, deletion of p62 results in reduced mTORC1 activity. Conversely, overexpression of p62 enhanced mTORC1 activation. Moreover, p62 serves as a docking site and is required for mTORC1 localization to the lysosomal membrane in response to amino acid stimulation. Therefore, **p62-mTORC1** signaling may also establish another line of feedback regulating p62 levels.<sup>282</sup>.

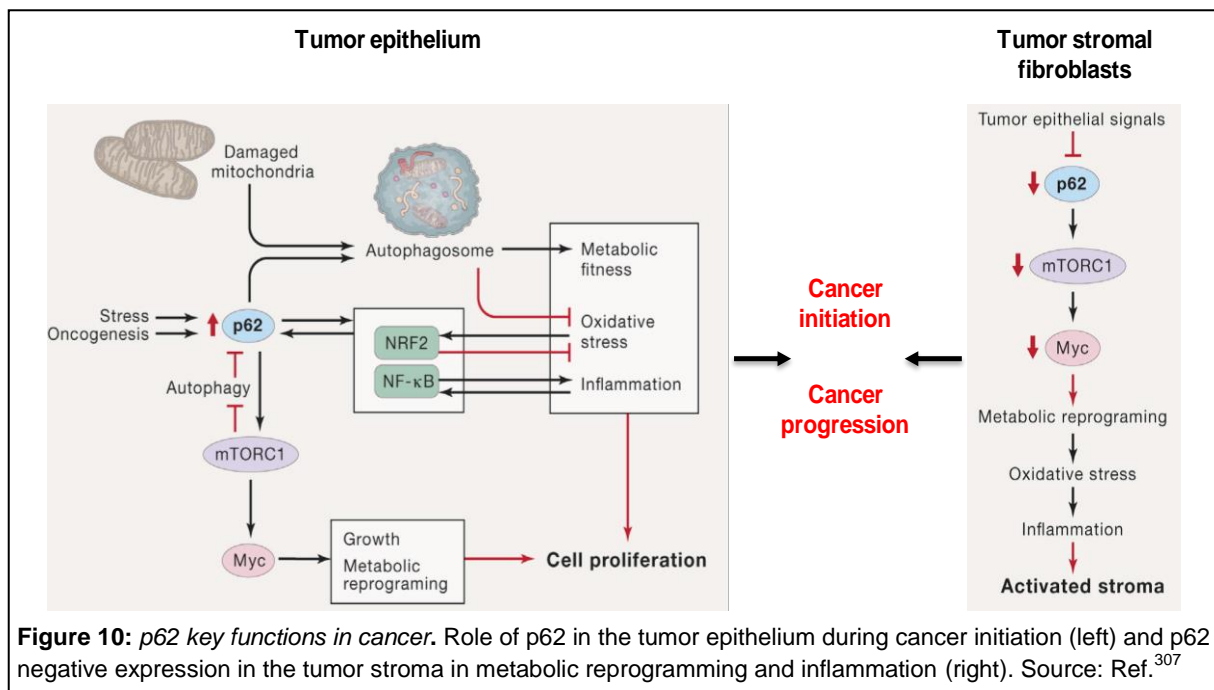
The positive regulation of p62 and c-Myc was also addressed in breast cancer stem cells by delaying the degradation of *MYC mRNA* through the repression of let-7a and let-7b, thus promoting *MYC mRNA* stabilization at the post-transcriptional level<sup>277</sup>.

Interestingly, chronic p62 accumulation occurs in human pancreatitis and most liver degenerative diseases<sup>305</sup>. High p62 levels promote the activation of NRF2 that results in the transcriptional activation of the p62 gene making a feed-forward loop that promotes cancer initiation<sup>199,245,306</sup>. Although p62 inactivation in liver parenchymal cells abrogates the expression of the NRF2-dependent anti-oxidant response, it also results in the disappearance of hepatocytes that accumulate ROS, which presumably serve as HCC-initiating cells. The loss of these cells is most likely due to inactivation of the NRF2-mediated protective response as well as inhibition of **mTORC1** activation and **c-Myc** expression (**Figure 11**). These studies demonstrate that p62 accumulation in a chronically damaged liver is one of the most important factors that lead to HCC development. The proof of principle that p62 is an oncogenic protein is that its overexpression *in vivo* is sufficient to induce HCC. This effect of p62 is independent of autophagy because overexpression of a p62 variant lacking the UBA domain, and therefore stripped of its autophagy adaptor function, was also sufficient to drive HCC<sup>260,307</sup>. In contrast, a recent study revealed that p62 is downregulated in stellate cells (another type of cells in the liver) acting as a suppressor of HCC development. More specifically, it was shown that p62 is a negative regulator of liver inflammation and fibrosis through its ability to promote Vitamin D Receptor signaling (i.e. **VDR:RXR** heterodimerization) in HSCs, whose activation supports HCC<sup>308</sup>. The high

complexity of the liver clearly demonstrates that p62 may exert different levels of expression and opposing roles in cell populations even in the same cancer type.

Tumor-suppressive functions of p62 were also found during mitosis. During the early mitotic phase p62 is phosphorylated by **CDK1** allowing the cells to properly progress through mitosis. Cancer cells expressing a non phosphorylatable p62 mutant display higher tumorigenic properties *in vivo* and *in vitro*<sup>309</sup>.

Apart from cancer cells, many tumors display reduced levels of p62 in their stroma, especially in cancer-associated fibroblasts (CAFs) (**Figure 11**). p62-deficient stromal fibroblasts exhibit increased production of IL-6, which is critical for **TGF- $\beta$**  synthesis that converts CAFs into activated myfibroblasts that promote tumor progression. This downregulation of p62 in CAFs is needed for acquiring their tumor-promoting function. Decreased **mTORC1** activity due to the downregulation of p62 results in reduced **c-Myc** levels and the concomitant increase in **ROS** levels under conditions of autophagy competence. Interestingly, the increased oxidative stress in these stromal cells translated into higher levels of IL-6 that promoted TGF- $\beta$  synthesis, being both required for CAF activation in p62-deficient prostate cancer stroma<sup>278</sup>.



The above results can explain why genetic inactivation of p62 at an organism level is associated with increased tumor progression<sup>278</sup>, whereas the selective inactivation of p62 in cancer epithelial cells restrains cancer initiation<sup>260,307</sup>.

## ***IV. OBJECTIVES***

This PhD thesis stemmed from our interest in the identification of melanoma drivers, with a particular interest in lineage-specific or lineage-enriched metastatic pathways that may represent new prognostic factors and putative targets for drug development.

The adaptor protein p62/SQSTM1 (sequestosome 1) was selected for its previously reported functions at the crossroads of autophagy<sup>189,300</sup> and lysosomal-associated pathways, both with melanoma-selective features. Moreover, p62 can also function as a signaling hub<sup>260,282</sup>, although there is no clear consensus on whether it acts as a tumor promoting<sup>253,260</sup> or tumor suppressive agent<sup>278,308</sup>. For example, while p62 is an indisputable autolysosome cargo<sup>186,227,236</sup>, other roles as a hub for multiple protein-protein complexes can be highly cell type dependent (mTOR, KEAP1-NRF2 pathway, MYC metabolism)<sup>260,282,299,308</sup>. These pleiotropic functions of p62 illustrate the need for integrated expression and functional studies in physiologically-relevant systems.

The main goal of this PhD thesis was to dissect the expression and functional contribution of p62 to melanoma progression. To this end, we integrated a comprehensive analysis in melanoma cell lines, tissue specimens and newly-generated mouse models. In addition an integrated –omic strategy (transcriptome/proteome/interactome studies) was performed.

Therefore, the main goal was pursued in the following **specific objectives**:

1. **THE CHARACTERIZATION OF THE PATHOPHYSIOLOGICAL ROLES OF P62 IN VIVO BY GENERATING MELANOMA MOUSE MODELS HARBOURING ALLELIC LOSS FOR P62.**
2. **THE FUNCTIONAL CHARACTERIZATION OF P62 IN MELANOMA BY AN -OMIC COMPREHENSIVE ANALYSES.**
3. **THE DISSECTION OF THE MOLECULAR MECHANISMS OF P62 IN MELANOMA.**

***V. MATERIALS AND  
METHODS***

## 5.1 Cell Culture

The human melanoma cell lines SK-Mel-5, SK-Mel-19, SK-Mel-28, SK-Mel-103, UACC-62, WM-115, WM-164, WM-209 and LU-1205, were selected for their genetic background, recapitulating the most frequent genetic alterations in this disease (see **Table 1**). B16-F10 (ATCC) mouse melanoma cells were used for subcutaneous injections in mice. All these cells were cultured in Dulbecco's modified Eagle's medium (DMEM, Lonza, cat. No. BE12-604F/U1) supplemented with 10% fetal bovine serum (FBS, Lonza, cat. No. DE14-801F) and 100 µg/mL Penicillin/Streptomycin (Invitrogen, cat. No. 15070-063). Primary human melanocytes, keratinocytes and fibroblasts were isolated as described before<sup>310</sup> from neonatal foreskins obtained from the Hospital Niño Jesús, Madrid, Spain. Melanocytes were cultured in Medium 254 (Invitrogen, cat. No. M-254CF-500) supplemented with 1% melanocyte growth factors (HMGS, Invitrogen, cat. No. S-002-5), 0.2 mM CaCl<sub>2</sub> and 100 µg/mL Penicillin/Streptomycin; keratinocytes were cultured in Epilife Medium (Invitrogen, cat. no. M-Epi-500) supplemented with 1% human keratinocyte growth factors (HKGS, Invitrogen, cat. No. S-001-5), 0.2 mM CaCl<sub>2</sub> and 100 µg/mL Penicillin/Streptomycin and fibroblasts were cultured in DMEM, supplemented with 10% FBS, and 100 µg/mL Penicillin/Streptomycin.

**Table 1:** Human melanoma cell lines used in this PhD thesis study.

CELL LINE	STAGE	BRAF	NRAS	PTEN*	p62*
SK-Mel-5	LN met	V600E	WT	+	++
SK-Mel-19	Primary Melanoma	V600E	WT	+	++
SK-Mel-28	LN met	V600E	WT	+	+++
SK-Mel-103	Primary Melanoma	WT	Q61R	+	+
UACC-62	Primary Melanoma	V600E	WT	-	+++
WM-115	Primary Melanoma	V600E	ND	-	++
WM-164	LN met	V600E	WT	+	++
WM-209	met	WT	G12A	ND	+
LU-1205	Lung met	V600E	WT	-	++

\*: protein levels; **WT**: wild type; **ND**: not determined

## 5.2 Protein Immunoblotting

Cells were harvested and total cell lysates were obtained using 1x **Laemmli buffer** (62.5 mM Tris-HCl pH 6.8, 2% SDS, 10% glycerol and 5% β-mercaptoethanol) and boiled at 95°C for 5 minutes or **RIPA buffer** [50mM Tris-HCl pH 8, 150 mM NaCl, 1% Nonidet P-40 (NP-40), 0.5 % Sodium Deoxycholate, 0.1% SDS, 1mM EDTA pH 7.4 and supplemented

protease (Roche Diagnostics, cat. No. 11836170001) and phosphatase inhibitors (Santa Cruz, cat. No. sc-45045). Protein concentrations were determined using the Bio-Rad Protein Assay (Bio-Rad Laboratories) according to manufacturer's protocol. Protein immunoblots were performed by standard SDS-PAGE electrophoresis in polyacrylamide gels and subsequently transferred to Immobilon-P membranes (Millipore, cat. No. IPVH00010) using Mini Trans-Blot Cell system (Bio-Rad Laboratories). Transfer was performed at 100V during 1 hour at 4°C. Membranes were blocked with 5% milk in tris-buffered saline with 0.05% Tween-20 (TBS-T) for 1 hour at RT. Primary antibodies (**Table 2**) were diluted in 5% milk or 5% BSA in TBS-T and incubated overnight at 4°C or 1 hour at RT. Secondary antibodies were diluted in 5% milk TBS-T or in PBS and incubated for 1 hour at RT (**Table 3**).

**Table 2:** Primary Antibodies used in this PhD thesis.

Primary antibody	Company	Cat. Number	Isotype
Atg5	Cell Signaling Technology	2630	Rabbit
Atg7	Cell Signaling Technology	2631	Rabbit
Beta-Actin (AC-15)	Sigma-Aldrich	A5441	Mouse
GAPDH	Monoclonal core unit (CNIO)	-	Mouse
Histone 3	Abcam	ab1791	Rabbit
HMG2	Cell Signaling Technology	8179	Rabbit
IgG	Sigma-Aldrich	I5006	Rabbit
IGF2BP1 /IGF2BP1	MBL Ribonomics	RN007P	Rabbit
KEAP1	Proteintech Group	10503-2-AP	Rabbit
Kindlin-2/FERMT2	Millipore	MAB2617	Mouse
Kindlin-2/FERMT2	Abcam	ab74030	Rabbit
LC3B	Cell Signaling Technology	2775	Rabbit
Myc	Millipore	06-340	Rabbit
NBR1	Abnova	H00004077-M01	Mouse
NQO1	Abcam	ab28947	Mouse
p62	BD Biosciences	610832	Mouse
p62	Abcam	ab101266	Rabbit
p62	Novus Biologicals	NBP1-49956	Rabbit
p65	Santa Cruz Biotechnology, Inc.	sc-372	Rabbit
phospho-NF-kB p65	Cell Signaling Technology	3037	Rabbit
phospho-S6 (Ser240/244)	Cell Signaling Technology	2215	Rabbit
S6 (5G10)	Cell Signaling Technology	2217	Rabbit
Tubulin	Sigma-Aldrich	T 9026	Mouse

**Table 3:** Secondary Antibodies used in this PhD thesis.

Secondary antibody	Company	Cat. Number	Isotype
TrueBlot Rabbit IgG-HRP	Rockland antibodies	18-8816-31	mouse
TrueBlot Mouse IgG-HRP	Rockland antibodies	18-8817-33	rat monoclonal

Secondary antibody	Company	Cat. Number	Isotype
Rabbit IgG-HRP	GE Healthcare	NA934	donkey
Mouse IgG-HRP	GE Healthcare	NA9310	donkey

### 5.3 RNA extraction, PCR and qPCR

Total RNA was extracted and purified from cell pellets using RNeasy Mini-Kit (QIAGEN, cat. No. 74104) following the manufacturer's instructions. RNA concentration was determined by NanoDrop Spectrophotometer ND-100 (NanoDrop Biotechnologies). 1-2µg total RNA was reverse-transcribed into cDNA using the high capacity cDNA reverse transcriptase kit (Applied Biosystems, cat. No. 4368814), according to manufacturer's protocol. 20ng of the total cDNA were subjected to real-time quantitative polymerase chain reaction (RT-qPCR - 60°C annealing temperature) using Power SYBR® Green PCR Master Mix (Applied Biosystems, cat. No. 4367659). Assays were run in triplicates on the 7900HT Fast Real-Time PCR system (Applied Biosystems) or QuantStudio™ 6 Flex Real-Time PCR System (Applied Biosystems). The primer sequences and annealing temperatures listed on **Table 4**. GAPDH and β-actin were used as loading control to normalize mRNA expression.

**Table 4:** Primers used in this PhD thesis.

Gene	Forward Primer (5' – 3')	Reverse Primer (5' – 3')	°C
CD2AP	GGTGGCTGGAAGGAGAACTA	GTTTGATGGGCAAAGTGTCA	60
EHMT2	GGAGGAAGCTGAACTCAGGAGG	GACTGAAATCATCACCACCAC	60
FERMT2	GATGCTAAGCTTCAGTTCACC	GGGTGTCTGATATTTAAAGTCTTAC	60
FLOT1	CCCATCTCAGTCACTGGCATT	CCGCCAACAT CTCCTTGTTT	60
GAPDH	GAAGGCTGGGGCTCATTGTC	CCAGGGGTGCTAAGCAGTTG	60
HMGA2	GAAGCAGCAGCAAGAACCAAC	GCTTCTGCTTTCTTTTGAGCTG	60
NCEH1	TGGACAACAGTTTACTCAAGA	GATCATTGCCTGCACAAAGT	60
OGFOD1	CCCTGGACCTGTACAGCATT	GACCATGAAACCAGCCACTT	60
p62	TAGCGCTACCGGTCGCCA	CCGGAATTTTCGAGCGGCCAA	60
TOP2A	ACAAGACATCAAAGTGAAGTAAAGCC	GCAGACTCAAACACAGACAAAGC	60
β-actin	GGCACCACACCTTCTACAATG	GTGGTGGTGAAGCTGTAGCC	60

### 5.4 Cloning of genes into lentiviral constructs

The primers that were used in the cloning of p62 and FERMT2 are indicated in the **Table 5**. A Kozak sequence was added in the forward sequence. For p62 cloning amplified fragments and empty FG12-CMV-GFP-Puro vector were digested by NheI (NEB Inc, cat. no. R0131S) and XhoI (NEB Inc, cat. No. R0146S). For FERMT2 cloning amplified fragments

and empty pLV-CMV-SV40-Puro vector were digested by XhoI (NEB Inc, cat. No. R0146S) and NheI (NEB Inc, cat. no. R0131S). The products were digested at 37°C for 3 hours in the presence of NEBuffer Cutsmart (NEB Inc, cat. No. B7204S) and BSA (NEB Inc, cat. No. B9001). Digested PCR products were purified by PCR purification kit following manufacturer instructions (QIAquick PCR Purification Kit, cat. No. 28104). Ligation was performed (3:1, insert:vector molar ratio) with T4 DNA Ligase (NEB Inc, cat. No. M0202). For bacterial transformation Stbl3 cells were used (Thermo Scientific, cat. No. C737303). Plasmid isolation was performed following manufacturer instructions (QIAGEN-tip 500, cat. No. 10063). Insertion was checked by DNA sequencing.

**Table 5:** Primers for cloning used in this PhD thesis.

Gene	Forward Primer (5' – 3')	Reverse Primer (5' – 3')	°C
p62	TTAACGCTAGCGGAGCCATGGCGTCGCTCAC CGTG	GTAACTCGAGTCACAACGGCGGGGGATG C	62
FERMT2	TTAACCTCGAGGGAGCCATGGCTCTGGACGG GATAA	GTAAAGCTAGCTCACACCCAACCACTGGT AAGTT	59

## 5.5 Gene Silencing and ectopic expression via lentiviral transduction of shRNAs

Lentiviral supernatants were generated using HEK 293FT cells transfected via standard protocols of calcium phosphate precipitation: 500µL of HBS solution (280 mM NaCl, 10 mM KCl, 1.5 mM Na<sub>2</sub>HPO<sub>4</sub>·2H<sub>2</sub>O, 12 mM dextrose and 50 mM HEPES), 250 nM of CaCl<sub>2</sub>, 4 µg of vector plasmid, and 4 µg of each of the lentiviral packaging constructs (pRSV-REV, pMDLg/pRRE and the VSV-G expression plasmid pHCMVG). Media was changed 8 hours after transfection and the viral supernatants were collected 24 hours later. Cells were infected with the viral supernatants and 4 µg/mL of Polybreen (Sigma-Aldrich). Infected cells were selected with 1 µg/mL of Puromycin (Sigma-Aldrich).

For genetic inactivation of p62, FERMT2 and NBR1, melanoma cells were infected with short hairpin RNAs purchased from Sigma-Aldrich (**Table 6**).

For ectopic expression of p62 and FERMT2, melanoma cells were stably infected with the lentiviral constructs, pLV-CMV-p62-mcherry-Puro and pLV-CMV-FERMT2-SV40-Puro in parallel with the corresponding empty vectors.

**Table 6:** short hairpin RNAs used in this PhD thesis

Gene	TRC number	Sequence	region
shcon	SHC001	CAACAAGATGAAGAGCACCAA	-
p62	TRCN0000007237	CCGGCCTCTGGGCATTGAAGTTGATCTCGAGATCAACTTCAATGCC AGAGGTTTTT	CDS
FERMT2	TRCN0000128058	CCGGGCGGACAGTTCTTACAACCTACTCGAGTAAGTTGTAAGAACTG TCCGCTTTTTTG	CDS
FERMT2	TRCN0000128511	CCGGCCGAAGAACTTTCTCTCTTAACTCGAGTTAAGAGAGAAAGTTCT TCGGTTTTTTG	CDS
NBR1	TRCN0000123159	CCGGGCTTCATAGTTATTTGGCATTCTCGAGAATGCCAAATAACTATG AAGCTTTTTG	3-UTR
NBR1	TRCN0000123160	CCGGGCAGCATTGTGGATGAGAATCTCGAGATTCTCATCCACAAAT GCTGCTTTTTG	CDS

## 5.6 siRNA-mediated transient genetic inactivation of p62

Cells were transfected with specific short interfering RNA (siRNA) molecules using Lipofectamine 2000 Transfection Reagent (Invitrogen, cat. No. 11668027) according to manufacturer's protocol. Specifically, for genetic silencing of p62 pool of siRNAs (Dharmacon, cat. No. L-010230-00-0005) was used at a final concentration of 100nM. Expression analyses were performed at 72h post-transfection, by protein immunoblotting and/or RT-PCR.

## 5.7 p62 gene targeting in cells using CRISPR/Cas9.

Gene-specific sgRNA oligos were cloned into the lentiCRISPR\_v2 expression vector (Addgene, cat. No. 52961), which bicistronically expresses sgRNA and Cas9 nuclease. The sgRNA sequence was determined by the CRISPR Design Tool (<http://crispr.mit.edu/>) targeting the first exon of all p62 isoforms. The designed sgRNAs were **sgp62\_1**: CACCGCACCGTGAAGGCCTACCTTC and **sgp62\_2**: CACCGCGCTACACAAGTCGTAGTCT. Lentiviruses were produced in 293FT cells and infections were performed as previously described<sup>31</sup>. Gene silencing efficiency was determined by immunoblotting.

## 5.8 Clonogenic capacity of cells (Colony Formation)

Low confluency colony formation assays were performed by seeding  $1 \times 10^3$  (SK-Mel-103) or  $5 \times 10^3$  (SK-Mel-28, UACC-62) cells per well onto 6-well plates. Cells were allowed to grow for 10-14 days, followed by fixation with cold methanol for 10 minutes. Colonies were stained

with 0.4g/L crystal violet (Sigma). The number of colonies was quantified from micrographs of the plates using the ImageJ software.

## **5.9 Matrigel invasion assays**

---

The invasive activity of melanoma cells was determined by matrigel transwell invasion assays using Boyden chambers (0.8  $\mu$ m BD BioCoat™ Matrigel™ Invasion Chambers; from BD Biosciences, cat. No. 354480), according to the manufacturer's guidelines. Briefly,  $10^5$  cells were serum-starved overnight and were seeded in serum-free DMEM onto the upper chamber. DMEM containing 10% FBS was placed in the lower chamber. After incubation for the indicated time intervals, invading and non-invading cells were first fixed with 4% paraformaldehyde and then stained with DAPI. Single cells were visualized by confocal detection of DAPI-stained nuclei through the 40x objective of a TCS-SP5-WLL (AOBS-UV) spectral microscope (Leica Microsystems, Wetzlar, Germany). The transwell membrane was also visualized by laser reflection. LAS AF Matrix screening Software was used for an automated high-throughput acquisition across the total width of the matrigel membrane in 9 different fields per experimental condition. IMARIS 6.3 Software was used to quantify the % of invading cells (normalized to the total cell number per field). Data are presented as means  $\pm$  SEMs of three independent experiments performed in triplicates.

## **5.10 Drug treatments in vitro**

---

To assess the autophagic flux in melanoma, cells were treated with autophagy activator Rapamycin at 25nM (Selleckchem, cat. No S1039) and autophagosome-lysosome inhibitor Chloroquine used at 20 $\mu$ M (Sigma Aldrich, cat. No. C6628) at indicated times. Cells were fixed or collected for further Immunofluorescence and Immunoblotting assays.

## **5.11 RNA stability assay (Actinomycin D treatment)**

---

p62 genetic silenced cells and cells with non-targeting shRNA were seeded on day 4 after infection (250000 cells/6cm plate). Cells were treated with Actinomycin D (Sigma Aldrich, cat. No. A9415) at 5  $\mu$ g/ml concentration. After treatment, cells were washed with ice cold PBS and collected via scraping at indicated time points (0, 1, 2, 4 and 6 hours). RNA extraction, quantification, reverse transcription and qPCR were performed as described above.

## 5.12 Isobaric Tag for Relative and Absolute Quantitation (ITRAQ)

Melanoma cell pellets from two melanoma cell lines (SK-Mel-103 and UACC62) were extracted 3 days upon p62 or ATG5 genetic inactivation and proteins were subjected to proteome analysis by iTRAQ.

### (I) Sample Preparation

Cell pellets were washed 3 times with cold PBS containing protease inhibitors (Mini Complete, Roche) and then resuspended in 500  $\mu$ L of ice-cold RIPA lysis buffer (150 mM NaCl, 1.0% NP-40, 0.5% sodium deoxycholate, 0.1% SDS, 1 mM EDTA, 1 mM EGTA, 50 mM Tris, pH 8.0 plus protease inhibitors) and 0.1% Benzonase Nuclease (Novagen, Darmstadt, Germany). Samples were vortexed, sonicated and clarified by centrifugation at 4 °C and 16,100  $\times$  g for 15 min. The supernatants containing the protein fraction were collected and cleaned up by acetone precipitation with 6 volumes of ice-cold acetone. Pellets were dissolved in 7M urea 2M thiourea. The protein concentration of the samples was determined according to the Bradford assay using BSA as standard (Protein Assay Kit, Bio-Rad, Hercules, CA).

### (II) Protein Digestion and labeling with ITRAQ reagents

Samples were digested using the filter aided sample preparation (FASP) method as described above. Briefly, 100  $\mu$ g of each sample dissolved in 7M urea 2M thiourea was loaded on the filter, reduced with 10 mM DTT 1 h at 37°C and alkylated using 50 mM iodoacetamide for 20 min in the dark. The excess of reduction and alkylation reagents was washed. The proteins were digested overnight using endoproteinase Lys-C from *Acromobacter lyticus* M497-1 (Wako Pure Chemical Industries, Osaka, Japan) with 1:50 enzyme to protein ratio. Finally, trypsin (Promega, Madison, WI) was added and samples were subjected to a second digestion for 6 h. Each tryptic digest was labeled according to the manufacturer's instructions (AB Sciex, Framingham, MA) with one isobaric amine-reactive tag as follows: Tag114; Tag116; Tag115; Tag117. After one hour incubation, labeled samples were pooled, and evaporated to dryness in a vacuum centrifuge. The iTRAQ sample was cleaned up using a Sep-Pak C18 cartridge for SPE (Waters Corp., Milford, MA)<sup>312</sup>. Eluted peptides were vacuum-dried and reconstituted in OFFGEL solution (5% glycerol, 1% ampholytes pH 3-10) prior to electrofocusing.

### **(III) OFFGEL Fractionation**

For pI-based peptide separation, we used the 3100 OFFGEL Fractionator system (Agilent Technologies, Böblingen, Germany) with a 24-well set-up. The IPG gel strips of 24 cm-long (GE Healthcare, München, Germany) with a 3–10 linear pH range were rehydrated for 15 min with the Peptide IPG Strip Rehydration Solution according to the protocol of the manufacturer. Subsequently, 150  $\mu$ L of sample was loaded in each well. Electrofocusing of the peptides was performed at 20°C and 50  $\mu$ A until the 50 kVh level was reached. After focusing, the 24 peptide fractions were withdrawn and the wells rinsed with 100  $\mu$ L of a solution of 0.1%TFA. Rinsing solutions were pooled with their corresponding peptide fraction. All fractions were evaporated by centrifugation under vacuum. Solid phase extraction and salt removal was performed with home-made columns based on Stage Tips with C8 Empore Disks (3M, Minneapolis, MN)<sup>313</sup> filled with Poros Oligo R3 resin (Life Technologies). Eluates were evaporated to dryness and maintained at 4°C. Just prior nano-LC, the fractions were resuspended in H<sub>2</sub>O with 0.1% (v/v) formic acid (FA).

### **(IV) Peptide analysis by nanoLC-MS/MS**

Digested samples were separated by on-line reversed-phase nanoscale capillary LC and analyzed by electrospray MS/MS. The experiments were performed on an Eksigent nano LC system (Eksigent) coupled to an LTQ Orbitrap Velos mass spectrometer (Thermo Scientific, Bremen, Germany) equipped with a nanoelectrospray ion source (Proxeon Biosystems, Odense, Denmark). Peptides were resuspended in 0.1% FA and loaded from a cooled nanoLC AS-2 autosampler (Eksigent). In order to pre-concentrate and desalt the samples before switching the pre-column in line with the separation column, 5  $\mu$ L from each sample was loaded onto a reversed-phase ReproSil Pur C18-Aq 5  $\mu$ m 0.3 x 10 mm trapping cartridge (SGE Analytical, Australia), and washed for 15 min at 2.5  $\mu$ L/min with loading buffer (0.1% FA). The peptides were eluted from a RP ReproSil Pur C18-AQ 3  $\mu$ m 200 x 0.075 mm (Dr. Maisch GmbH, Ammerbuch-Entringen, Germany) by application of a binary gradient consisting of 2% ACN in 0.1% FA (buffer A) and 100% ACN in 0.1%FA (buffer B), with a flow rate of 300 nL/min. Peptides were separated using the following gradient: 0-5 min 2% B, 5-150 min 40% B and 150-165 min 98% B. The column was operated at a constant temperature of 30°C. The LTQ Orbitrap Velos was operated in positive ionization mode. The MS survey scan was performed in the FT analyzer scanning a window between 250 and 1750 m/z. The resolution was set to 60 000 FWHM at m/z 400. The m/z values triggering MS/MS with a repeat count of 1 were put on an exclusion list for 60 s. The minimum MS signal for triggering MS/MS was set to 1000 counts. In all cases, one microscan was recorded. The lock mass option was enabled for both MS and MS/MS mode and the

polydimethylcyclosiloxane ions (PDMS, protonated (Si(CH<sub>3</sub>)<sub>2</sub>O))<sub>6</sub>; m/z 445.120025) were used for internal recalibration of the mass spectra<sup>314</sup>. For the HCD, up to the 15 most abundant isotope patterns with charge  $\geq 2$  from the survey scan were selected with an isolation window of 2 m/z fragmented in the C-trap collision cell. Normalized collision energy was set to 42%, the Q value to 0.25 and an activation time to 0.10 ms. Waveform filter was activated. The resulting fragments were detected in the Orbitrap system with a resolution of 7500 FWHM at m/z 400. The maximum ion injection times for the survey scan and the MS/MS scans were 500 ms and 250 ms respectively and the ion target values were set to 1E6 and 2E4, respectively for each scan mode.

## **(V) Data analysis**

The raw files were processed using the Proteome Discoverer 1.3.0.339 software suite (Thermo Scientific). The fragmentation spectra were searched against the concatenated SwissProt Human database (release date: March 21, 2012; 20329 entries) using MASCOT<sup>315</sup> as the search engine (v 2.2) with the precursor and fragment mass tolerances set to 10 ppm and 0.075 Da, respectively, and with up to two missed cleavages. Lysine and peptide N-termini labeling with iTRAQ-4plex reagent as well as carbamidomethylation of cysteine were considered as fixed modifications, while oxidation of methionine was chosen as variable modification for database searching. Minimal peptide length was set to 6 amino acids and Mascot ion score  $> 20$ . Peptide identification false discovery rate (FDR) was less than 1%. In case that identified peptides were shared by two or more proteins (homologs or isoforms), they were reported by Proteome Discoverer as one protein group. The results were then exported into Excel for manual data interpretation. Although relative quantification and some statistical data were provided by the Proteome Discoverer software, an additional 1.3-fold change cutoff for all iTRAQ ratios (ratio  $< 0.77$  or  $> 1.3$ ) was selected to classify proteins as up- or down-regulated<sup>316-318</sup>. Proteins with iTRAQ ratios below the low range (0.77) were considered to be under-expressed, while those above the high range (1.3) were considered overexpressed. Protein classification (biological process and protein class) was performed by Ingenuity Pathway Analysis (IPA) software, using the entire list of identified proteins as the reference data set to analyze the regulated proteins.

## **5.13 Co-Immunoprecipitation assay followed by Mass Spectrometry**

---

### **5.13.1 Subcellular Fractionation followed by Co-Immunoprecipitation assay**

Cells at 80% confluency were washed twice with ice cold PBS and collected by scraping with PBS. Cells were lysed first on ice for 5min in cytoplasmic extraction buffer (Tris/HCl

pH=8 50mM, EDTA pH=8 2mM, NP-40 0.1%, Glycerol 10%). Samples were centrifuged at 3000 rpm for 5min. Pellets were washed once with cytoplasmic extract buffer then resuspended in high-salt NP-40 buffer (50 mM Tris pH=8, 150 mM NaCl, 5mM EDTA, 1% nonionic detergent NP40). The buffers were supplemented with protease (Applied Biosystems, cat. No. 88266) and RNase inhibitors (Applied Biosystems, cat. No. N8080119). Extracts were incubated for 20 minutes at 4°C under rotation and sonicated in a Bioruptor Standard (Diagenode) for 10 minutes at medium amplitude. The extracts were centrifuged at maximum speed and the supernatant was collected. After preclearing by protein A Dynabeads (Invitrogen, cat No. 10001D) for 30 minutes at 4°C, protein concentrations were determined and 2mg of total protein extract per condition was subjected to immunoprecipitation using p62 antibody (Abcam, ab101266) or rabbit IgG (Sigma-Aldrich, I5006) as a negative control coupled to protein A Dynabeads for 3h at 4°C. Immunoprecipitates were washed extensively, 4-6 times with the corresponding lysis buffers. For Mass Spectrometry Analysis two sequential elutions with 100µl of urea 8M each step (Tris-HCl 0,1M + protease inhibitor) at 37°C for 15 min under high agitation. The two elution products were combined for Mass Spectrometry injection. For validation of protein-protein interactions independent co-IP experiments were performed and the immunoprecipitates were eluted in NP-40 buffer mixed with loading dye, boiled at 95°C for 5 minutes and supernatant were collected for immunoblotting assays.

### **5.13.2 Mass Spectrometry**

#### **(I) Sample Preparation**

Eluted proteins were subjected to label free proteome analysis. Samples were digested by means of the standard FASP protocol<sup>319</sup>. Briefly, samples were eluted with UT buffer (8M urea in 100 Mm Tris-HCl, pH=8.01) with continuous mixing at 37°C and transfer to a filter unit. Proteins were then reduced with 10 mM DTT, alkylated using 50 mM iodoacetamide for 20 min in the dark and the excess of reagents was washed out with UA twice. Proteins were digested with endoproteinase Lys-C (Wako) during 6 hours in a wet chamber (1:50 enzyme to substrate ratio). Finally, samples were diluted in 50 mM ammonium bicarbonate to reduce the urea concentration to 1M and subsequently digested with Trypsin Gold (Promega) overnight at 37 °C. Resulting peptides were further desalted and concentrated using homemade reversed phase micro-columns filled with Poros Oligo R3 beads (Life Technologies). The samples were dried using the Speed-Vac and dissolved in 30 µL of 0.1% formic acid (FA).

## (II) LC-MS/MS analysis

Desalted peptides were separated by reversed-phase chromatography using a nanoLC Ultra system (Eksigent), directly coupled with a LTQ-Orbitrap Velos instrument (Thermo Fisher Scientific) via nanoelectrospray source (ProxeonBiosystem). Peptides were loaded onto the column (Dr. Maisch, Reprosil-Pur C18 GmbH 3  $\mu\text{m}$ , 200x0.075 mm), with a previous trapping column step (Prot Trap Column 0.3 x 10 mm, ReproSil C18-AQ, 5  $\mu\text{m}$ , 120 $\text{\AA}$ , SGE), during 10 min with a flow rate of 2.5  $\mu\text{l}/\text{min}$  of loading buffer (0.1% FA). Elution from the column was made with a 90 min linear gradient (buffer A: 2% ACN, 0.1%FA; buffer B: 100% ACN, 0.1%FA) at 300 nL/min. The peptides were directly electrosprayed into the mass spectrometer using a PicoTip emitter (360/20 OD/ID  $\mu\text{m}$  tip ID 10  $\mu\text{m}$ , New Objective) a 1.4 kV spray voltage with a heated capillary temperature of 325°C and S-Lens of 60%. Mass spectra were acquired in a data-dependent manner, with an automatic switch between MS and MS/MS scans using a top 20 method with a threshold signal of 800 counts. MS spectra were acquired with a resolution of 60000 (FWHM) at 400  $m/z$  in the Orbitrap, scanning a mass range between 350 and 1500  $m/z$ . Peptide fragmentation was performed using collision induced dissociation (CID/CAD) and fragment ions were detected in the linear ion trap. The normalized collision energy was set to 35%, the Q value to 0.25 and the activation time to 10 ms. The maximum ion injection times for the survey scan and the MS/MS scans were 500 ms and 100 ms respectively and the ion target values were set to 1E6 and 5000, respectively for each scan mode. Samples were run in duplicates.

## (III) Data analysis

Raw files were analyzed by Proteome Discoverer (version 1.4.1.14) against a forward-reverse concatenated human database (UniProtKB/Swiss-Prot, 88354 sequences, 26/03/2013 release). Oxidation of methionines was set as variable modification whereas carbamidomethylation of cysteines was considered as fixed modification in the SequestHT search engine. Minimal peptide length was set to 6 amino acids, a maximum of two missed-cleavages were allowed. Peptides were filtered at 1% FDR using Percolator. In case that identified peptides were shared by two or more proteins (homologs or isoforms), they were reported by Proteome Discoverer as one protein group. As stated above, each sample was run in triplicate. Label-free analysis was performed with Proteome Discoverer using the spectral count values determined by the software. Further analysis was done using Excel and MultiExperiment Viewer software (version 4.8.1). The changes in protein abundance between the different samples were measured via a direct comparison of the spectral count values. Protein classification (molecular function, biological process and protein class) was performed by STRING<sup>320</sup> software. Raw files from the eluted samples were also analyzed by

MaxQuant<sup>321</sup> (version 1.4.1.2) (UniProtKB/Swiss-Prot human database, canonical and isoform sequences, 39748 sequences, 01/22/2014 release), including phosphorylation on serine, threonine and tyrosine residues as variable modification. The rest of search parameters were set as above. For protein assessment, at least two unique peptides provided by Andromeda search engine<sup>322</sup> with a FDR = 1% were required. Results at peptide label were exported to excel for further analysis.

#### **5.14 RNA Immunoprecipitation (RIP) followed by qPCR**

---

p62 infected cells or control cells (non targeting shRNA) at 80% confluence were fixed in 1% formaldehyde for 10 minutes at room temperature (RT), and fixation was stopped by adding 1M Glycine for 5 minutes at room temperature. After washing with ice cold PBS, cells were collected by scraping and lysed with in NT2 buffer (50 mM Tris–HCl pH 7.5, 150 mM NaCl, 1mM MgCl<sub>2</sub>, 0.5% Nonidet P-40 and 1 mM EDTA) supplemented with protease and RNase inhibitors. For the solubilization of crosslinked complexes, lysates were sonicated for 10 minutes at medium intensity. The lysates were centrifuged at maximum speed and the supernatant was collected. After preclearing by protein A Dynabeads for 30 minutes at 4°C, samples were immunoprecipitated using IGF2BP1 antibody (MBL Ribonomics, cat. No. RN007P) or rabbit IgG (Sigma, cat. No. I5006) as a negative control coupled to protein A Dynabeads for 3h at 4°C. Immunoprecipitates were washed extensively, 4-6 times and resuspended in NT2 buffer containing 50µg proteinase K (Roche Applied Science, cat. No. 03115836001), 1% SDS, 200mM NaCl and 10mM EDTA. Samples were split into two (1:4 for protein, 3:4 for RNA extraction). The protein fraction was mixed with loading dye, boiled at 95°C for 5 minutes and supernatant was collected. RNA elution was done by consecutive incubations at 55°C for 30 minutes and at 65°C for 45 minutes. Supernatants were collected and digested with DNase I for 10 minutes at RT. RNA was extracted with the TRI Reagent (Sigma, cat No. T9424) following manufacturer's protocol. The total amount of RNA immunoprecipitated and 1µg of RNA extracted from inputs were retrotranscribed using cDNA reverse transcriptase Superscript III (ThermoScientific, cat No. 18080044) and qPCR were performed as described before. Fold binding enrichment of target mRNAs in the immunoprecipitated fraction was calculated after normalization with the gene expression from the inputs or with the negative controls. All the experiments were performed in three biological replicates. The primers used for RIP-qPCR are listed in **Table 7**.

---

## 5.15 Immunofluorescence in fixed cells

---

Cells were cultured on cover slips and were fixed with 4% paraformaldehyde in PBS at room temperature or with ice cold methanol for 20 min. Cells were then washed twice with 0.1M glycine in PBS for 10min each, permeabilized with 0.2% Triton X-100 in PBS for 5 min, washed twice with PBS and incubated with 1% BSA in PBS at room temperature for 30 min. Fixed cells were incubated with primary antibody diluted in blocking buffer (1% BSA in PBS) at room temperature for 1 h. Cells were then washed three times with PBS and incubated with Invitrogen's Alexa-conjugated secondary antibodies at room temperature for 1h. Cells were washed 3 times with PBS and counterstaining of nuclei with 4,6-diamidino-2-phenylindole (DAPI) and mounting of the cover slips were done with Prolong Gold (Invitrogen, cat. No. P36930) 20 minutes before imaging. Negative controls were obtained by omitting the primary antibody. The following primary antibodies were used: p62 (Novus Biosciences, cat No. 610832); IGF2BP1 (Cell Signaling Technology, cat. No. 8482); LC3B (Cell Signaling Technology, cat. No. 2775). Alexa Fluor 555 anti-rabbit IgG (Invitrogen, cat. No. A-31572) and Alexa Fluor 488 anti-mouse IgG (Invitrogen, cat. No. A-21202) were used as secondary antibodies.

---

## 5.16 Tissue Immunostaining

---

### (I) Immunofluorescence

Paraffin-embedded tumor samples were stained for p62 (Novus Biologicals, cat. No. NBP1-49956), LC3B (Cell Signaling Technology, cat. No. 2775d), phospho-p65 (Cell Signaling Technology, cat. No. 3037). After deparaffinization and antigen retrieval (10 mmol/L sodium citrate buffer at pH 6) the samples were incubated overnight with primary antibodies at 4 °C in a humidified chamber. Mouse IgG (M.O.M.) Blocking Reagent (Vector Laboratories; MKB-2213); and Image-iT FX signal enhancer (Invitrogen; cat. No. I36933) were used before the primary antibody incubation according to manufacturer's protocols for mouse samples. Then rinsed and incubated with fluorescent secondary antibodies for 1 hour at room temperature. For detection, Alexa Fluor 555 anti-rabbit IgG (Invitrogen, cat. No. A-31572) and Alexa Fluor 488 anti-mouse IgG (Invitrogen, cat. No. A-21202) were used. Nuclei were counterstained with DAPI and mounted with Prolong Gold (Invitrogen, cat. No. P36930) 20 minutes before imaging. The fluorescence emission was acquired using a confocal TCSSP5-WLL (AOBS-UV) spectral microscope (Leica Microsystems, Wetzlar, Germany).

## (II) Immunohistochemistry in human and mouse biopsies

### a. Tissue microarrays (TMAs) and immunohistochemistry (human samples)

For p62, melanocytic tumors including dermal nevi (n=31), dysplastic nevi (n=29), primary radial growth phase (RGP) malignant melanoma (n=16), primary vertical growth phase (VGP) melanoma (n=105), cutaneous metastasis (n=30), lymph node (n=28) and visceral (n=22) melanoma metastases were used for immunohistochemistry (IHC) and TMAs construction as previously described<sup>323</sup>. FERMT2 staining was performed using anti-FERMT2 antibody, clone 3A3 (Merck Millipore). For FERMT2, melanocytic tumors including dermal nevi (n=34), primary vertical growth phase (VGP) melanoma (n=82), cutaneous (n=33), lymph node (n=28) and visceral (n=22) melanoma metastases were used. p62-specific staining was scored blinded and considered positive for p62 taking into account both the percentage of positive cells and the intensity of its expression. It was blinded scored as follows: negative (no expression), low (weak intensity or <50% of the cells with strong intensity of expression) and high ( $\geq$ 50% of the cells with strong intensity of expression). For FERMT2 the scoring system was as follows: negative (no expression), low (weak intensity or <50% of the cells with strong intensity of expression) and high ( $\geq$ 50% of the cells with strong intensity of expression).

IHC was performed on 4- $\mu$ m-thick sections of formalin-fixed, paraffin-embedded samples. p62 (anti-p62 Ick ligand BD Biosystem) and FERMT2 (anti-Kindlin-2 antibody, clone 3A3 Merck Millipore) staining were performed on a Bond<sup>TM</sup> Automated System (Leica Microsystems)<sup>323</sup>. The IHCs were performed in the Dermatology and Pathology Department at the Hospital 12 de Octubre Medical School and the scoring was blinded by the Drs. Erica Riveiro-Falkenback, Pablo Ortiz-Romero and Jose L Rodríguez-Peralto.

### b. Immunohistochemistry (mouse samples)

Tissue samples were fixed in 10% neutral buffered formalin (4% formaldehyde in solution), paraffin-embedded and cut at 3  $\mu$ m, mounted in superfrost<sup>®</sup> plus slides and dried overnight. For different staining methods slides were deparaffinized in xylene and re-hydrated through a series of graded ethanol until water. Consecutive sections were stained with hematoxylin and eosin (H&E) and for immunohistochemistry an automated immunostaining platform was used (Ventana Discovery XT, Roche). Antigen retrieval was first performed with high or low pH buffer, depending on the primary antibody (CC1m, Roche or RiboCC, Roche); endogenous peroxidase was blocked (peroxide hydrogen at 3%) and slides were then incubated with the appropriate primary antibody as detailed: rabbit monoclonal anti-ATG5 (EPR1755 (2); 1:600; Abcam ab108327), rabbit polyclonal anti-p62 (SQSTM1; 1:150; Novus Biologicals NBP1-49956), rabbit polyclonal anti-S100 (1:500;

Dako, Z0311), and goat polyclonal anti-Sox10 (1/300; Santa Cruz sc-17342. After the primary antibody, for Sox10, slides were incubated with the corresponding secondary antibodies (rabbit anti goat biotinylated, Dako) and visualization systems when needed (OmniRabbit, Ventana, Roche) conjugated with horseradish peroxidase. The rest of the antibodies were incubated with UltraMap Rabbit (Ventana, Roche) conjugated with alkaline phosphatase. Immunohistochemical reaction was developed using 3,30-diaminobenzidine tetrahydrochloride (DAB) (Chromomap DAB, Ventana, Roche) and Naphtol with Fast Red (FR) (Chromomap RED, Ventana, Roche) as a chromogen . Nuclei were counter stained with Carazzi's hematoxylin. Finally, the slides was dehydrated, cleared and mounted with a permanent mounting medium for microscopic evaluation.

### 5.17 Mitochondrial Respiration

$5 \times 10^3$  cells of p62 deficient SK-Mel-103 and UACC-62 cells with the corresponding shcon cells were plated per well in XF 96-well microplates and incubated for 24 hr at 37 °C in 5% CO<sub>2</sub>. Respiration was measured under basal conditions, and in response to Oligomycin (ATP synthase inhibitor; 0.5 μM; Sigma Aldrich, cat. no. 75351) and the electron transport chain accelerator ionophore FCCP (Trifluorocarbonyl cyanide Phenylhydrazone; 0.5 μM; Quimigen S.L., cat. no. SC-203578). Finally, respiration was stopped by adding the electron transport chain inhibitors Rotenone and Antimycin A (1 μM each; Sigma Aldrich, cat. no. R8875 and A8674, respectively). Oxygen consumption rate (OCR) and extra-cellular acidification rate (ECAR) were measured with a XF96 Extracellular Flux Analyzer (Seahorse Biosciences) as per the manufacturer's recommended protocol. OCR and ECAR values were normalized to cell number. Four technical replicates were used per condition in three independent experiments.

### 5.18 Mice breedings and activation of Tyr::CreER transgene

The following strains were used in this study: Tyr::CreERT2<sup>/1Lru</sup><sup>324</sup>, p62-deficient mice<sup>325</sup>, Atg5<sup>tm1Myok</sup><sup>326</sup>, Braf<sup>tm1Mmcm</sup> (Braf<sup>CA/CA</sup>)<sup>327</sup>, Pten<sup>tm2Mak</sup><sup>328</sup>. For simplicity these lines are herein referred as to Tyr:CreERT2, p62KO, Atg5<sup>flox/flox</sup>, Braf<sup>CA/CA</sup>, and Pten<sup>flox/flox</sup>, respectively. For the analysis of melanomas, breedings were set to generate Tyr:CreERT2; Braf<sup>CA/CA</sup> Pten<sup>flox/flox</sup> background with different p62 or/and Atg5 copy number (herein referred to as Atg5<sup>+/+</sup>, Atg5<sup>-/+</sup>, Atg5<sup>-/-</sup> or p62<sup>+/+</sup>, p62<sup>-/+</sup>, p62<sup>-/-</sup>, respectively).

Topical administration was performed by applying 2μl (2mg/ml) of (Z)-4-Hydroxytamoxifen (Sigma Aldrich, cat. No.H7904) in ethanol on the skin back at postnatal days 2, 3 and 4. For systemic administration, 8 week-old mice were induced by 100 ml intraperitoneal injection of

tamoxifen (Sigma, T5648; stock 8 mg/ml) for 3 consecutive days. Tumor growth was measured every 5 days blinded to the experimental conditions at the indicated time intervals after post-mortem depilation. Tumor volume was estimated using a calliper and calculated as  $V = \frac{a \times b^2 \times \pi}{6}$ , where “a” stand for the bigger and “b” for the smaller diameter of the tumor. Studies for tumor growth and survival were performed. Mice were sacrificed 8 weeks upon 4-hydroxytamoxifen administration or when total tumor volume was exceed  $2\text{cm}^3$ . Necropsy was performed collecting tumor samples and mouse tissues for histopathological and protein detection studies.

### 5.19 Subcutaneous inoculation of B16-F10 cells into p62 deficient mice

$5 \times 10^5$  B16-F10 (ATCC), resuspended in PBS, mouse melanoma cells were inoculated subcutaneously in the back of 8 week old mice expressing different copies of p62. Development of subcutaneous tumor was monitored every week, blinded to the experimental conditions at the indicated time intervals, and measured by caliper, as described above. The mice were sacrificed 3 weeks after injection and tumors were collected for histopathological and protein detection studies. All experiments with mice met the Animal Welfare guidelines and were performed in accordance with protocols approved by the Institutional Ethics Committee of CNIO.

### 5.20 Genotyping

Genotyping of every strain was obtained by DNA extraction from the tails of each mouse after the weaning. Briefly, mouse tails were digested overnight with DNA digestion buffer (50mM Tris-HCl with pH 8, 100mM EDTA with pH 8, 100mM NaCl, 1% SDS and 20mg/ml proteinase K (Roche, cat. No. 03115852001) at  $55^\circ\text{C}$ . Then, saturated NaCl was added and after full speed centrifugation the supernatant was collected equal volume of ice cold isopropanol was added. Precipitated DNA was washed with 70% ethanol and then resuspended in TE buffer (10mM Tris, pH 8 and 1mM EDTA). PCRs were performed for target gene amplification. The samples were loaded into agarose gels. Primers that were used for genotyping are indicated in the **Table 7**.

**Table 7:** Primers for genotyping used in this PhD thesis.

Gene	Forward Primer (5' – 3')	Reverse Primer (5' – 3')	°C
p62-WT	CTTACGGGTCCTTTTCCCAAC	TCCTCCTTGCCCAGAAGATAG	57
p62-KO	CTGCATGTCTTCTCCCATGAC	TAGATACCTAGGTGAGCTCTG	57
Pten	CTCCTCTACTCCATTCTTCCC	ACTCCCACCAATGAACAAAC	57
Cre	GGCTGGACCAATGTAATATTG	CATCATCGAAGCTTCACTG	55

Gene	Forward Primer (5' – 3')	Reverse Primer (5' – 3')	°C
m-Actin	TCATCAGGTAGTCAGTGAGGTCGC	CACCACACCTTCTACAATGAGCTG	55
Braf	TGAGTATTTTTGTGGCAACTGC	CTCTGCTGGGAAAGCGGC	55
Atg5-WT	ACAACGTCGAGCACAGCTGCGCAAGG	GAATATGAAGGCACACCCCTGAAATG	60
Atg5-KO	CAGGGAATGGTGTCTCCAC	GTACTGCATAATGGTTAACTCTTGC	60

## 5.21 GO terms, Networks, Heatmaps and Venn Diagrams

GSEA was applied to previously reported data sets from the Cancer Cell Line Encyclopedia evaluating gene lists as described before<sup>329</sup>. Gene sets showing FDR<0.25 after Kolmogorov-Smirnoff testing were considered enriched between classes under comparison. Significantly enriched (p≤0.05) GO biological processes and functions for differentially expressed proteins upon p62 genetic inactivation and p62 interactome were identified by using Ingenuity Pathway Analysis (IPA) software and String database<sup>330</sup>. Heatmap and correlation graphs for RNA and protein levels were created by Perseus v1.5.1.6. Venn diagrams were created by using online tools Venny v2.0<sup>331</sup> and jvenn<sup>332</sup>.

## 5.22 Statistical Analyses

Unless otherwise indicated, statistical analyses were performed using Graphpad Prism software with unpaired two-tailed t-test. p62 and FERMT2 *in vivo* correlation was analyzed by Chi-square test. For microarray hybridization and gene expression analyses, gene sets showing FDR<0.25 after Kolmogorov-Smirnoff testing were considered enriched between classes under comparison. For survival analysis, clinical data and immunohistochemical scoring were performed blind, and data were compiled only after all analyses were completed. p62 and FERMT2 IHC stainings were quantified by two independent investigators. The distribution of the patients according to p62 and FERMT2 expression was analyzed by Chi-square test (sex, ulceration and clinical staging) and Student's t test (age and Breslow). Disease Free Survival (DFS) curves were estimated with Kaplan-Meier product-limit method and survival curves were compared using logrank test. DFS was defined as the time interval between diagnosis (made by histopathological study of primary melanoma) and the development of the first metastasis. It was considered censored for patients who did not present metastasis at last follow-up. The hazard ratio was calculated using Cox regression and adjusted with univariate and multivariate models adjusting by Breslow, Clinical Stage and T3 category.

## ***VI . RESULTS***

## 6.1 Expression and prognostic studies support pro-metastatic roles of p62 in human melanomas

Databases such as The Cancer Genome Atlas (TCGA) are being consolidated as a versatile platform to screen for oncogenic drivers and tumor suppressors across large cohorts of clinically-annotated biopsies<sup>333</sup>. For example, TCGA served as the starting point of selective dose-dependent downregulation of ATG5 and multiple lysosomal-associated factors we have reported in aggressive melanomas<sup>142,220</sup>.

Therefore, we interrogated the TCGA for genomic alterations and expression changes that could guide in subsequent functional studies of p62 in this

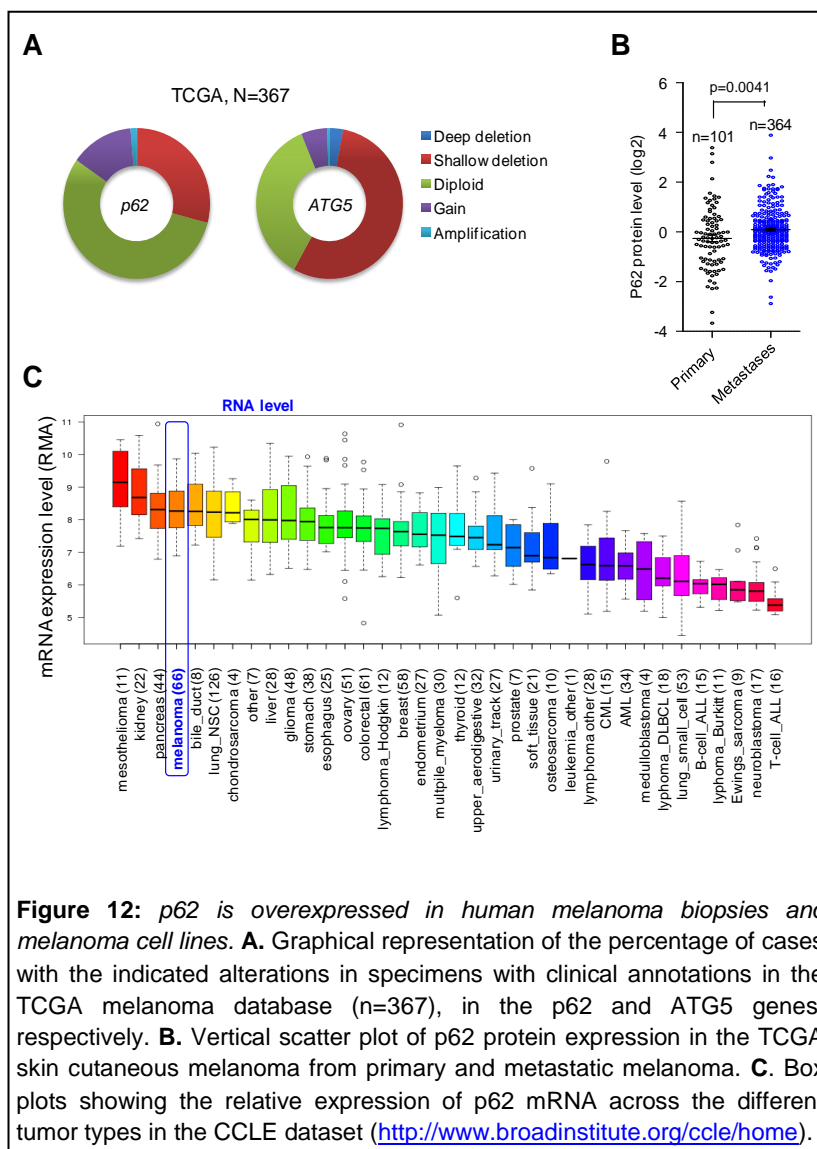
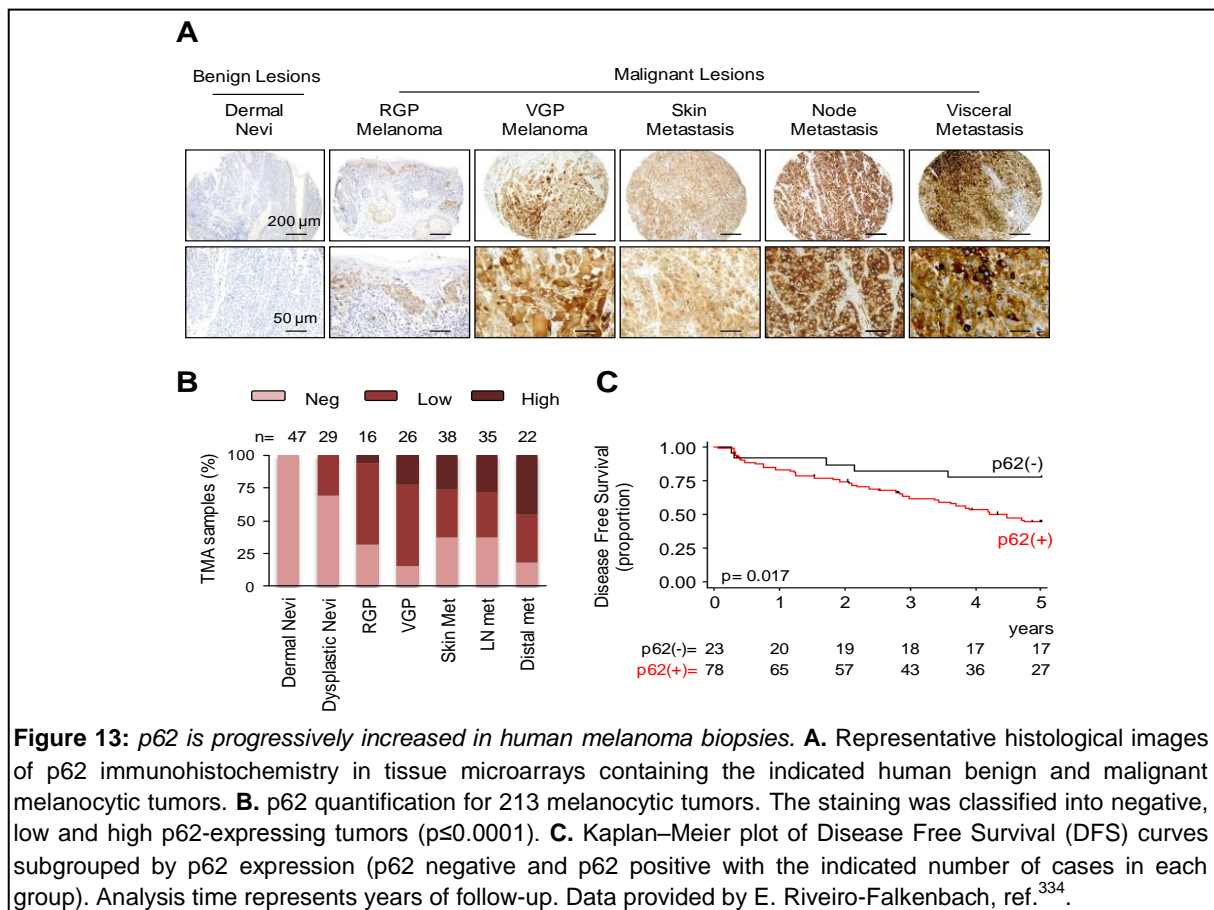


**Figure 12:** p62 is overexpressed in human melanoma biopsies and melanoma cell lines. **A.** Graphical representation of the percentage of cases with the indicated alterations in specimens with clinical annotations in the TCGA melanoma database (n=367), in the p62 and ATG5 genes, respectively. **B.** Vertical scatter plot of p62 protein expression in the TCGA skin cutaneous melanoma from primary and metastatic melanoma. **C.** Box plots showing the relative expression of p62 mRNA across the different tumor types in the CCLE dataset (<http://www.broadinstitute.org/ccle/home>).

disease. Interestingly, allelic losses of the p62 locus were notably less frequent than for ATG5 in the TCGA melanomas (<28% vs 56%; **Figure 12A**) indicating distinct roles of these two proteins in melanoma. Additionally, TCGA revealed a significant upregulation of p62 protein expression at metastatic sites (skin in transit, regional lymph nodes and distal visceral organs), when compared to primary melanomas (see number of specimens analyzed and the corresponding *p*-values in **Figure 12B**). Of note, the relatively high expression of p62 in melanoma was supported by Cancer Cell Line Encyclopedia database (**Figure 12C**; CCLE, encompassing over 700 cell lines of 25 different cancer types).

The above data were independently validated by immunohistochemical staining of p62 in high density tissue microarrays (TMAs; n=213 samples) covering a broad spectrum of melanocytic lesions at different stages of progression (provided by E. Riveiro-Falkenbach)<sup>334</sup>. These included common and dysplastic nevi, primary melanomas at radial and vertical growth phase of expansion (RGP and VGP, respectively), as well as metastases from skin, lymph node and visceral sites. All acquired human dermal nevi analyzed were found with a largely undetectable p62 staining (see representative examples in **Figure 13A** and quantification in **Figure 13B**). These data therefore, support the concept that this protein is not involved in suppressor mechanisms that maintain common nevi in a benign state<sup>285</sup>. Interestingly, a retrospective 5-year follow-up study in an independent cohort of 101 clinically-annotated melanoma specimens showed that patients with positive p62 expression presented an increased risk for the development of metastasis with respect to negative cases (hazard ratio 2.96 and p=0.022; **Figure 13C**).

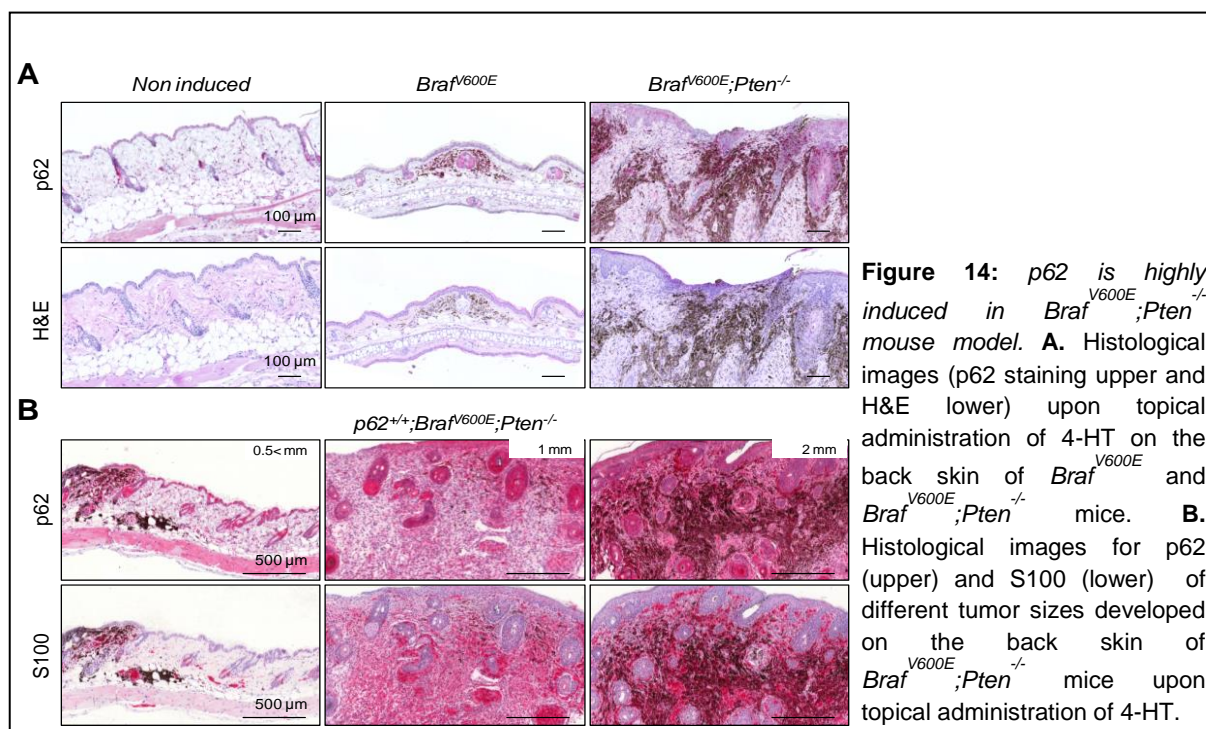


Altogether, these data suggest that p62 may be involved not only in cutaneous melanomas<sup>285</sup>, but also, at advanced and metastatic stages of this disease.

## 6.2 Tumor-, but not stromal-driven p62 favors melanoma progression in GEMM

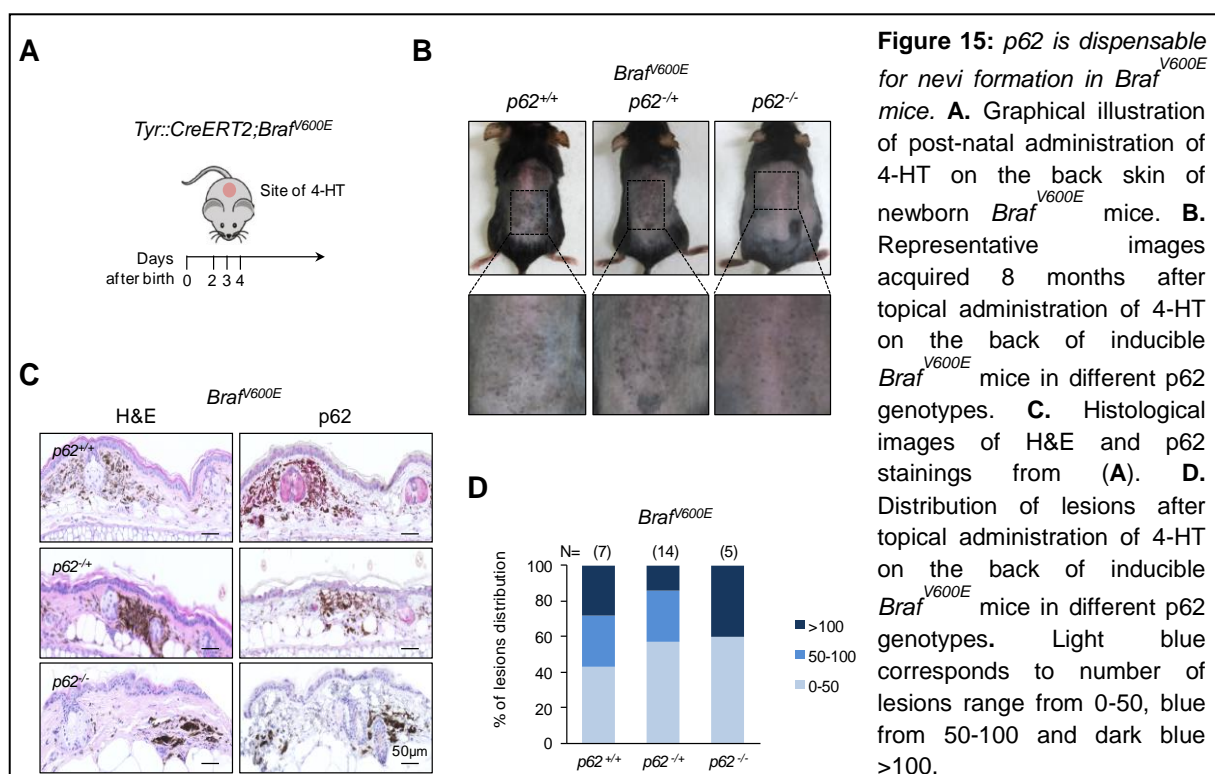
p62 has been found overexpressed in multiple neoplasias<sup>189,258-263,265-267</sup>. However, high p62 levels are not an unequivocal indicator of functional requirement, as pro- and antitumoral roles of this protein have been reported depending on the system analyzed. In particular, genetically-engineered mouse models (GEMM) reported in the context of cancer for prostate and hepatocellular carcinomas<sup>260,282</sup> have revealed distinct roles of p62 in tumor and stromal cells; in the latter with suppressive function<sup>278,308</sup>. Therefore, we generated new GEMM to dissect the contribution of p62 to melanoma progression. To mimic benign nevi, p62-deficient mice<sup>325</sup> were crossed into the *Tyr::CreERT2;Braf<sup>V600E</sup>* strain, where constitutively active Braf (Braf<sup>V600E</sup>) is induced by means of a tamoxifen-inducible Cre-recombinase restricted to the melanocytic compartment<sup>327</sup>. In turn, crosses into *Tyr::CreERT2;Braf<sup>V600E</sup>;Pten<sup>-/-</sup>* animals were used to assess the impact of p62 in the context of the characteristic BRAF<sup>V600E</sup> and PTEN loss of human cutaneous melanomas<sup>327</sup>. Pigmented lesions were optically and histopathologically monitored at different time points after topical application of 4-hydroxytamoxifen (4-HT).

In the normal (uninduced) skin, histological analyses revealed p62 mostly confined to the hair bulge expressing low levels (**Figure 14A**, pink staining). Consistent with dysplastic human nevi shown in **Figure 13A**, hyperplastic lesions in *Tyr::CreERT2;Braf<sup>V600E</sup>* animals (herein referred to as *Braf<sup>V600E</sup>* for simplicity) showed a modest induction of p62 staining (pink signal in pigmented-brown-melanocytic cells in middle panels of **Figure 14A**).



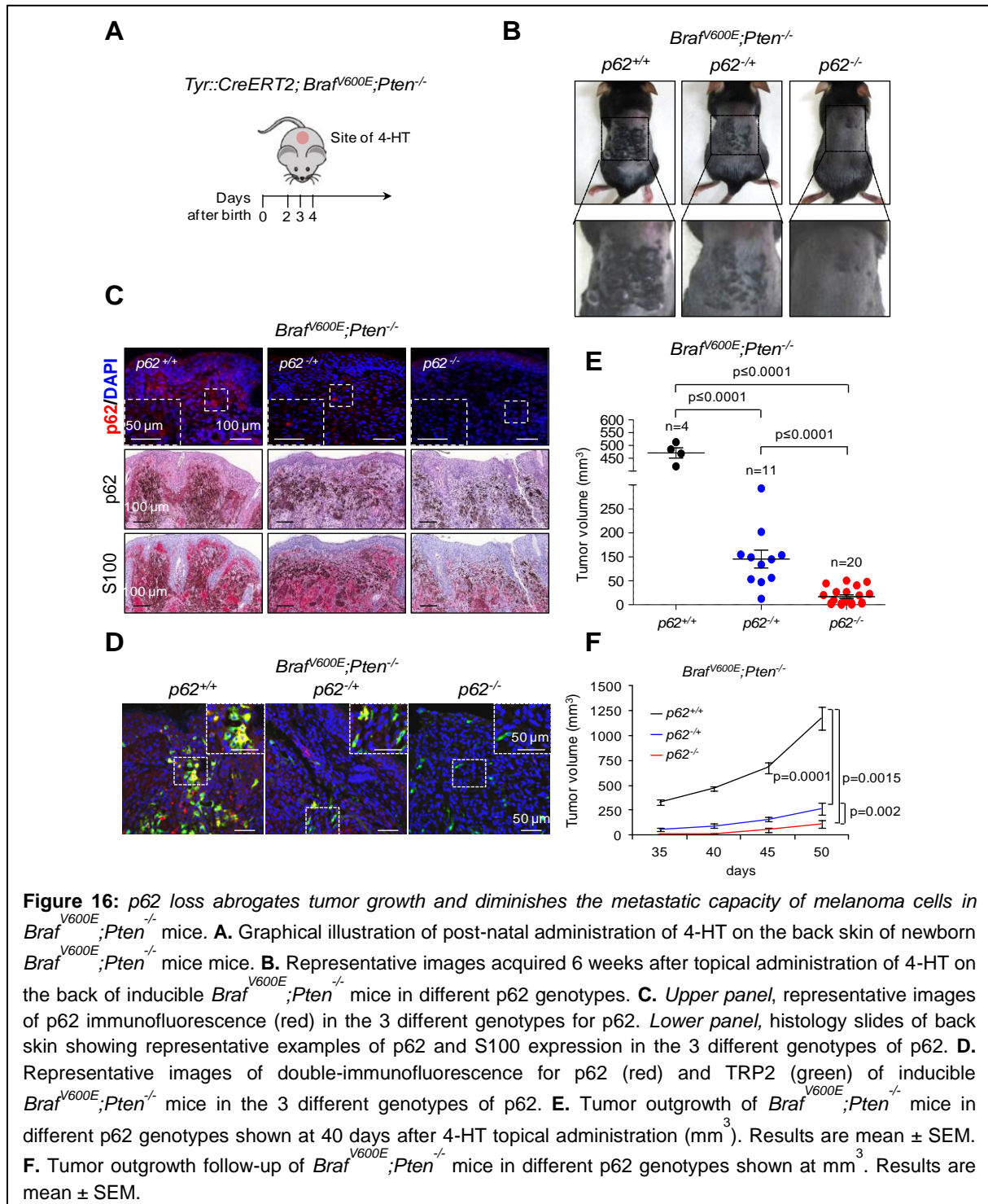
In contrast,  $Braf^{V600E};Pten^{-/-}$  melanomas showed a marked increased p62 staining in histological sections (**Figure 14A**, right panel). Interestingly, p62 accumulation was particularly evident as melanomas progressed and became invasive (**Figure 14B**).

To determine the contribution of p62 in benign nevi, mice with monoallelic and biallelic loss of p62 were crossed into  $Tyr::CreERT2;Braf^{V600E}$  strain. Nevus formation was followed by visual inspection after 4-HT administration (**Figure 15A**). As summarized in **Figures 15B-C** p62 was largely dispensable for the generation of benign melanocytic lesions, as neither their onset, number nor progression were significantly affected by heterozygous or homozygous loss of this gene (see the corresponding quantifications in **Figure 15D**). In this  $Tyr::CreERT2;Braf^{V600E}$  background, melanomas were not developed, independently on the presence or absence of p62.



We then questioned the effect of allelic loss of p62 in melanoma, with particular emphasis in the transition from radial to vertical/metastatic growth (e.g. under similar settings that have revealed protumorigenic roles of  $Atg5$  heterozygous loss<sup>220</sup>). This was performed by topical administration of 4-HT on the back of the skin of  $Braf^{V600E};Pten^{-/-}$  strains with different allelic status of p62 (**Figure 16A**). In these animals, heterozygous p62 deletion led to a visibly compromised melanoma development, which was further inhibited in  $p62^{-/-}$  background (see representative macrographs of **Figure 16B**). The relevance of p62 in the  $Braf^{V600E};Pten^{-/-}$  melanomas was confirmed histologically (IHC or IF) by staining for the melanocytic markers S100 or TRP2 (**Figures 16C-D**, respectively). Quantitative analyses of tumor volume

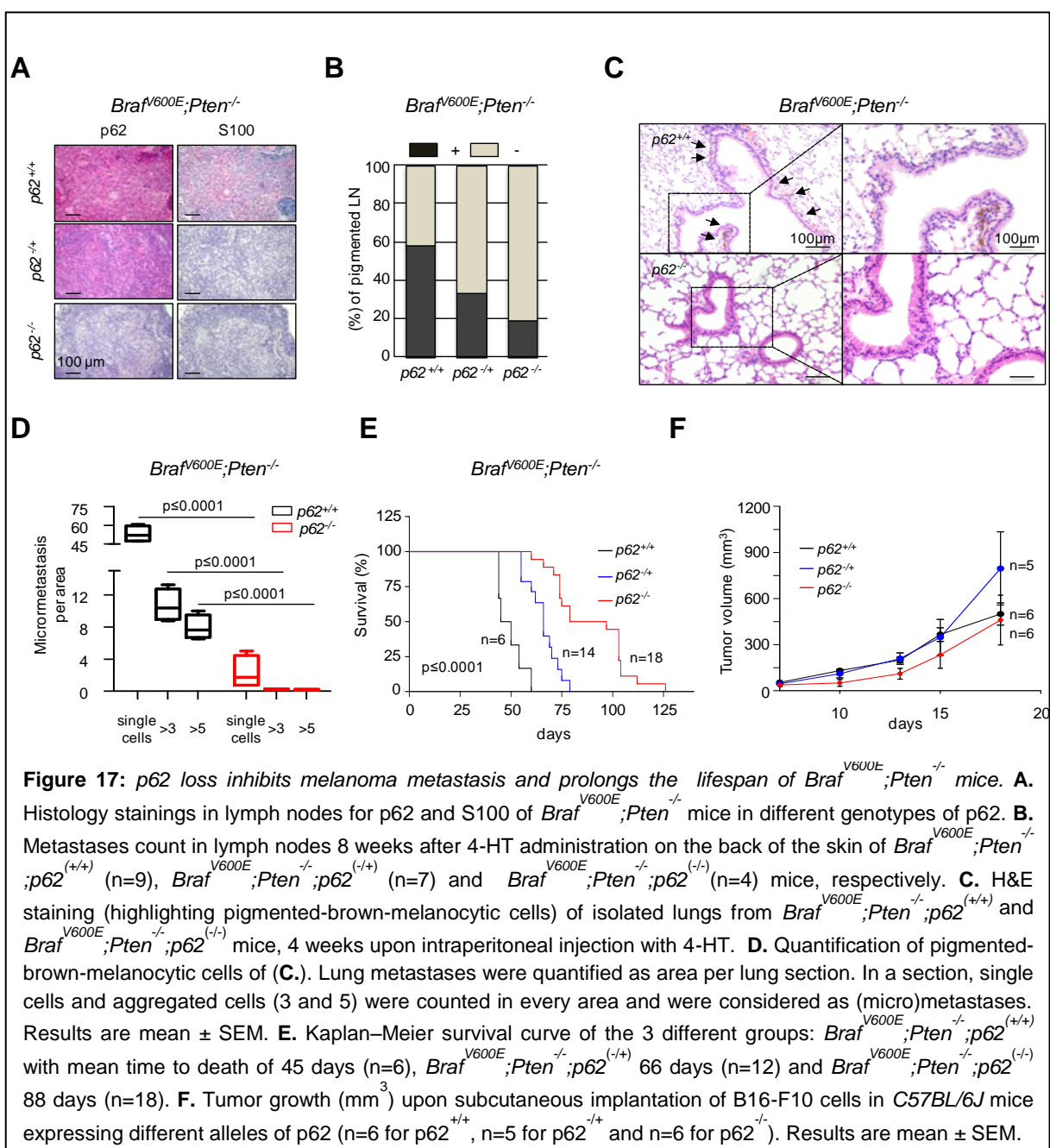
emphasized deleterious effects of mono and bi-allelic deletions of *p62* in the *Braf<sup>V600E</sup>;Pten<sup>-/-</sup>* background (Figures 16E-F) ;  $p \leq 0.0001$ ).



*p62* loss not only reduced tumor growth of cutaneous melanomas (Figures 16E-F), but also led to a markedly decreased metastatic efficiency to proximal (inguinal) and distal (axillar) lymph nodes (Figures 17A-B). To address the relevance of *p62* in the metastatic potential a to distal organs (i.e. lungs), *Braf<sup>V600E</sup>;Pten<sup>-/-</sup>* adult mice were induced systemically

by 4-HT (intraperitoneal injections, see Materials and methods, 5.18). The enhanced lung (micro)metastases that were observed in  $p62^{+/+}$  background were diminished in mice with bi-allelic deletion of  $p62$ , four weeks upon induction (**Figures 17C-D**). Consequently, follow-up studies revealed a dose-dependent impact of  $p62$  loss on the survival of melanoma-bearing  $Braf^{V600E};Pten^{-/-}$  mice (**Figure 17E**). The results above support a key role of melanoma-expressed  $p62$  in tumor progression and metastasis.

To rule out possible effects on the stroma<sup>278</sup>, a separate set of  $p62^{+/+}$ ,  $p62^{+/-}$  and  $p62^{-/-}$  mice were used as hosts for implantation of syngenic B16 melanoma cells. Interestingly, the allelic status of  $p62$  in this system had no significant impact on these B16-tumors (**Figures 17F**).



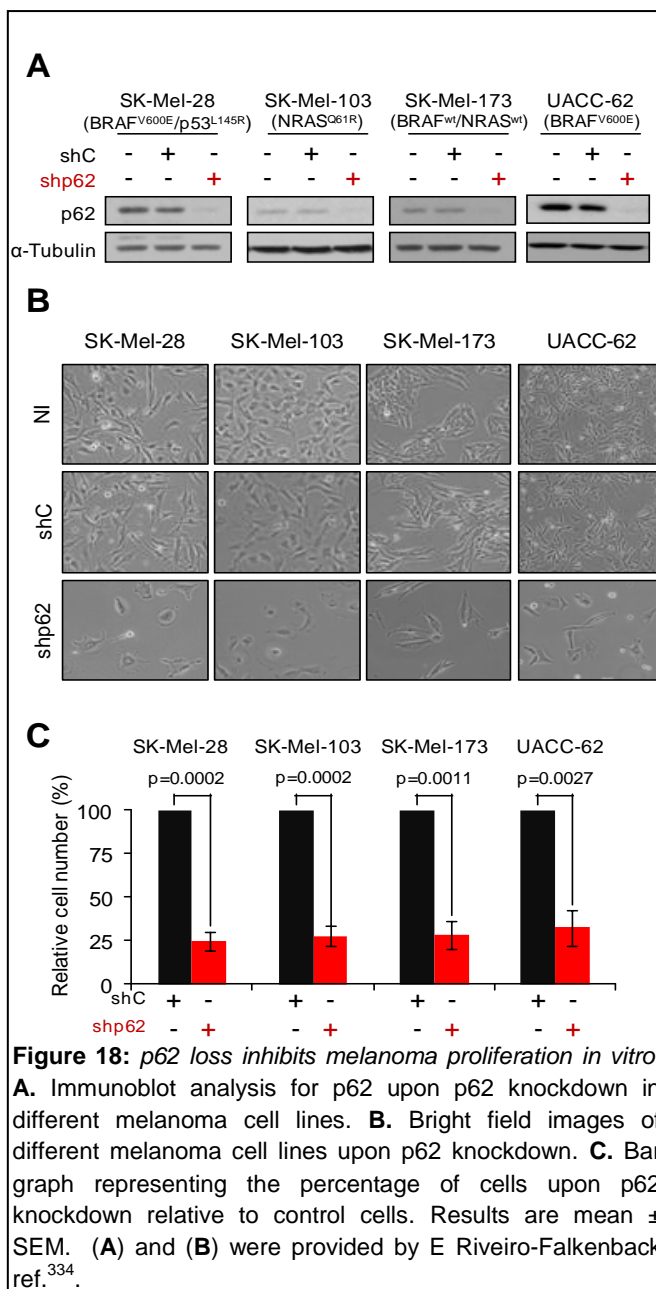
Together, these data: (i) provide physiological relevance of dose-dependent roles of p62 in melanoma progression; and importantly, (ii) separate melanomas from other tumor types where p62 has a more dominant suppressive role in the stromal compartments.

### 6.3 p62 controls key proliferative and metastatic signatures in melanoma cells

As indicated above, the roles of p62 in cancer cells are highly dependent on the tumor type. Ultimately, these can range from proper entry and exit through mitosis<sup>309,335</sup> to dispensable effects on cell cycle, but a key role in the control of cell viability<sup>253</sup>.

Previous studies in our laboratory have demonstrated the functional role of p62 in human melanoma cells by means of lentiviral-driven transduction of short hairpin interfering RNAs (shRNAs)<sup>334</sup>. In short, sustained p62 depletion (**Figure 18A**) resulted in phenotypic changes visualized by cell flattening and reduced growth capacity in human melanoma cell lines (**Figure 18B**). This effect is independent of the main genetic alterations in melanoma such as *BRAF* and *NRAS* mutations. p62 shRNA effectively reduced p62 protein expression in all the cell lines tested (**Figure 18A**), with the concomitant inhibition of their proliferative capacity in cell monolayers (see quantifications in **Figure 18C**).

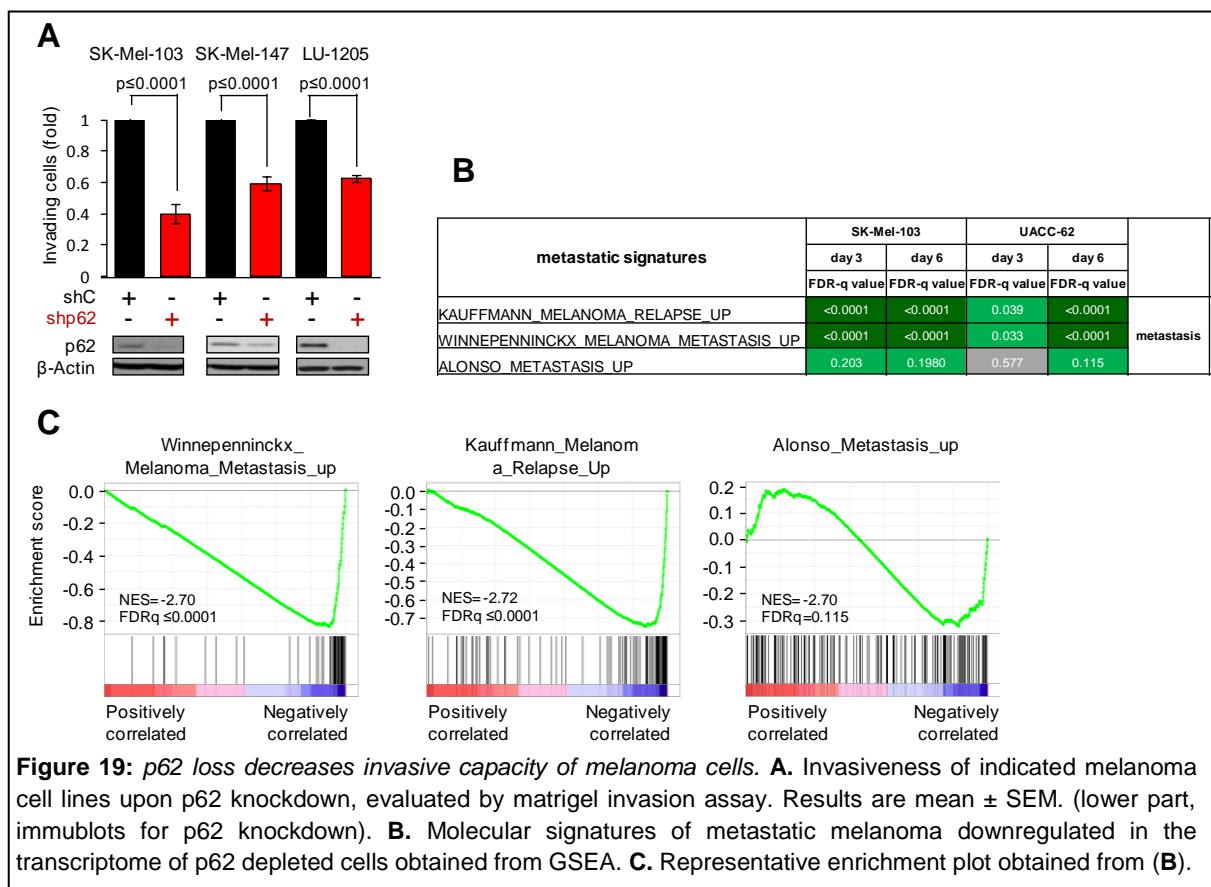
The inhibited proliferative capacity was found translated into a marked decreased tumorigenic growth in mouse xenograft models<sup>334</sup>. Moreover, p62 depleted cells revealed that the compromised proliferation was associated to reduced entry in S-phase<sup>334</sup>. Finally, transcriptomic profiles at early time points after p62 depletion in SK-Mel-103 and UACC-62,



as representative examples of NRAS and BRAF-mutated melanomas, identified cellular pathways (**Table S5**, appendix) related to vesicular trafficking (upregulated) and to cell cycle (downregulated)<sup>334</sup>. These results provide therefore, a mechanistic explanation for the association between p62 and proliferation that we had found in aggressive human melanomas and the inhibited tumor development in genetically engineered melanoma mouse models.

Functions of p62 in metastasis, as indicated above, are less understood. To study this process in human melanoma cells, matrigel-based assays were used upon p62 depletion in different metastatic cell lines. As shown in **Figures 19A**, melanoma cells showed a decreased invasive capacity upon p62 depletion compared with the control cells. Together, these results reinforce the concept of p62 as modulator of poor prognosis in melanoma patients and the aggressive and metastatic potential of the newly generated p62-GEMM. By text mining and guided searches via the Molecular Signatures Database (MSigDB) from GSEA platform we identified 3 comprehensive transcriptomic molecular signatures to be selectively upregulated in metastatic melanomas<sup>336-338</sup>. Interestingly, these melanoma-metastasis signatures were significantly downregulated in the transcriptome of p62-depleted SK-Mel-103 and UACC-62 cells (**Figures 19B-C**).

Therefore, these data support a coordinated effect of p62 on multiple signaling cascades, with new insight on signatures specifically linked to metastasis.



## 6.4 p62-deficient melanoma cells support new protumorigenic activities of this protein

Next, we set to study the molecular basis underlying the dependency of melanoma cells on p62. To this end, we tested main known roles of this protein (e.g., modulation of autophagy, mTOR, NF- $\kappa$ B, MYC signaling, oxidative stress and mitochondrial function) that have been described in other systems<sup>253,260,282,339,340</sup>. It is likely that these functions may be differentially regulated under endogenous or exogenous stress inducers (i.e. nutrient deprivation or therapeutic agents). However, here we selected to study basal conditions, where p62 was found essential to maintain malignant features of melanoma cells as described above. First, to define whether p62 is a substrate of autophagy, histological stainings were performed in generated autophagy-deficient melanomas, using GEMM models we have reported before for conditional depletion of *Atg5* (*TyrCre::ERT2;Braf<sup>V600E</sup>;Pten<sup>-/-</sup>;Atg5<sup>fl/fl</sup>*)<sup>220</sup>. As shown in **Figure 20A**, *Atg5* deficiency lead to the accumulation of p62 foci, reminiscent of autophagosome defects in these cells. Accumulation of p62 was also observed in human melanoma cells (UACC-62) blocking lysosomal degradation with chloroquine (**Figure 20B**). Interestingly, in p62 depleted cells, activation (Rapamycin) or inhibition (Chloroquine) of autophagy did not affect the levels of the autophagosomal marker LC3 (**Figure 20C**). However, only a fraction of p62 foci colocalized with the LC3 in CQ-treated cells (**Figure 20B**) suggesting the participation of p62 in additional complexes. In fact, no obvious differences were found in the focal staining of LC3, and in the amount of the autophagosome-lipidated LC3-II form when p62 was depleted *in vivo* -murine *Braf<sup>V600E</sup>;Pten<sup>-/-</sup>* melanomas (see immunomicrographs in **Figure 20D**; and representative immunoblots for LC3-II and ATG5 in **Figure 20E**). Similarly, neither p62 overexpression nor p62 depletion in human cultured melanoma cells significantly altered basal LC3-II and ATG5 levels (**Figure 20F**).

To further characterize the p62 dependency in autophagy, newly generated GEMM *TyrCre::ERT2;Braf<sup>V600E</sup>;Pten<sup>-/-</sup>;Atg5<sup>fl/fl</sup>;p62KO* were induced by topical administration of 4-HT and were followed for 8 weeks. From the **Figure 20G** (results in double compound mice) it was observed that the inhibitory effect of p62 allelic loss in the development of *Braf<sup>V600E</sup>;Pten<sup>-/-</sup>* melanomas was not affected by the genomic status of *Atg5*.

All together, these data conclusively demonstrate that p62 is a target of autophagy in melanoma, but not an essential driver of the process.

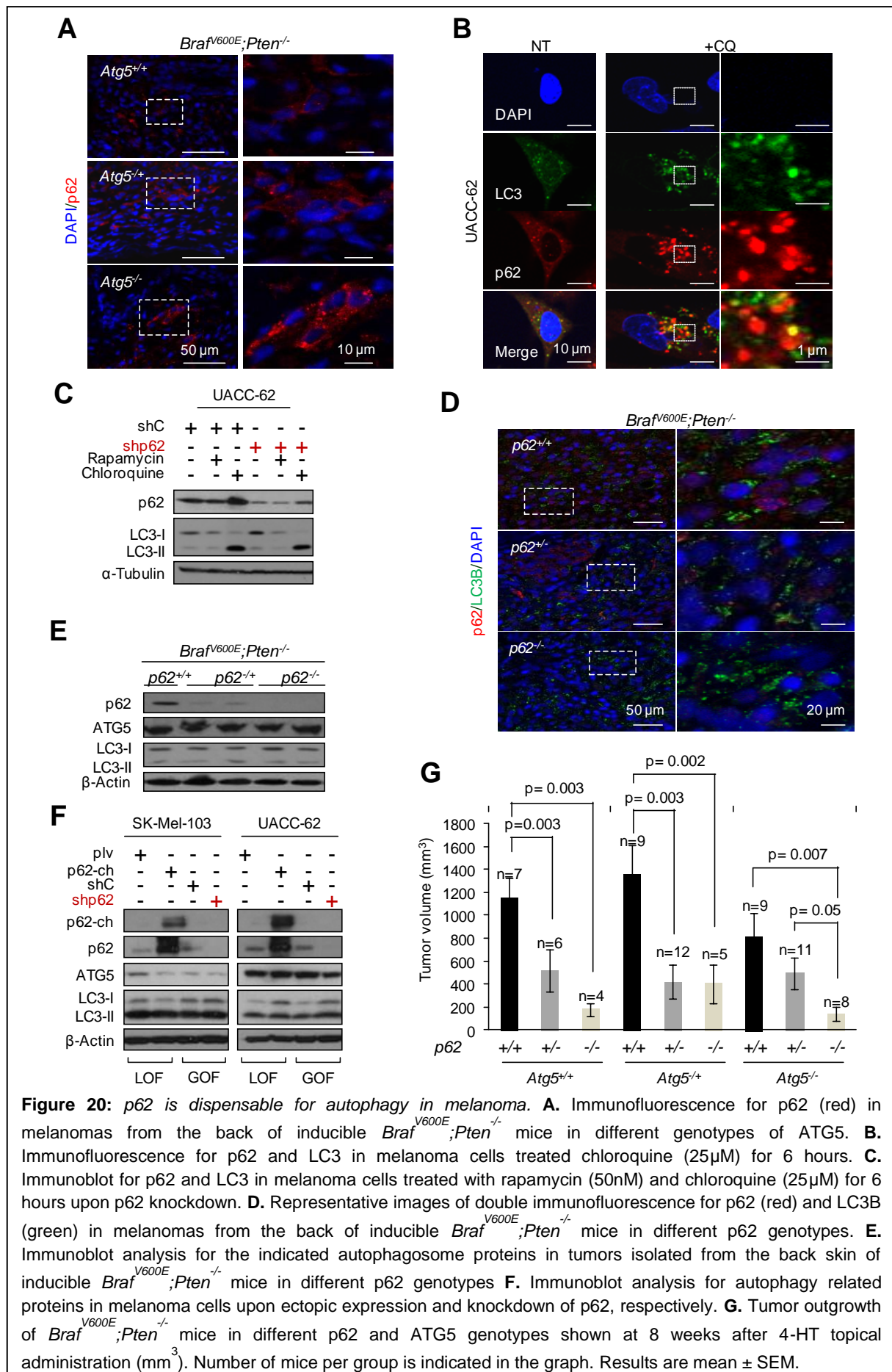
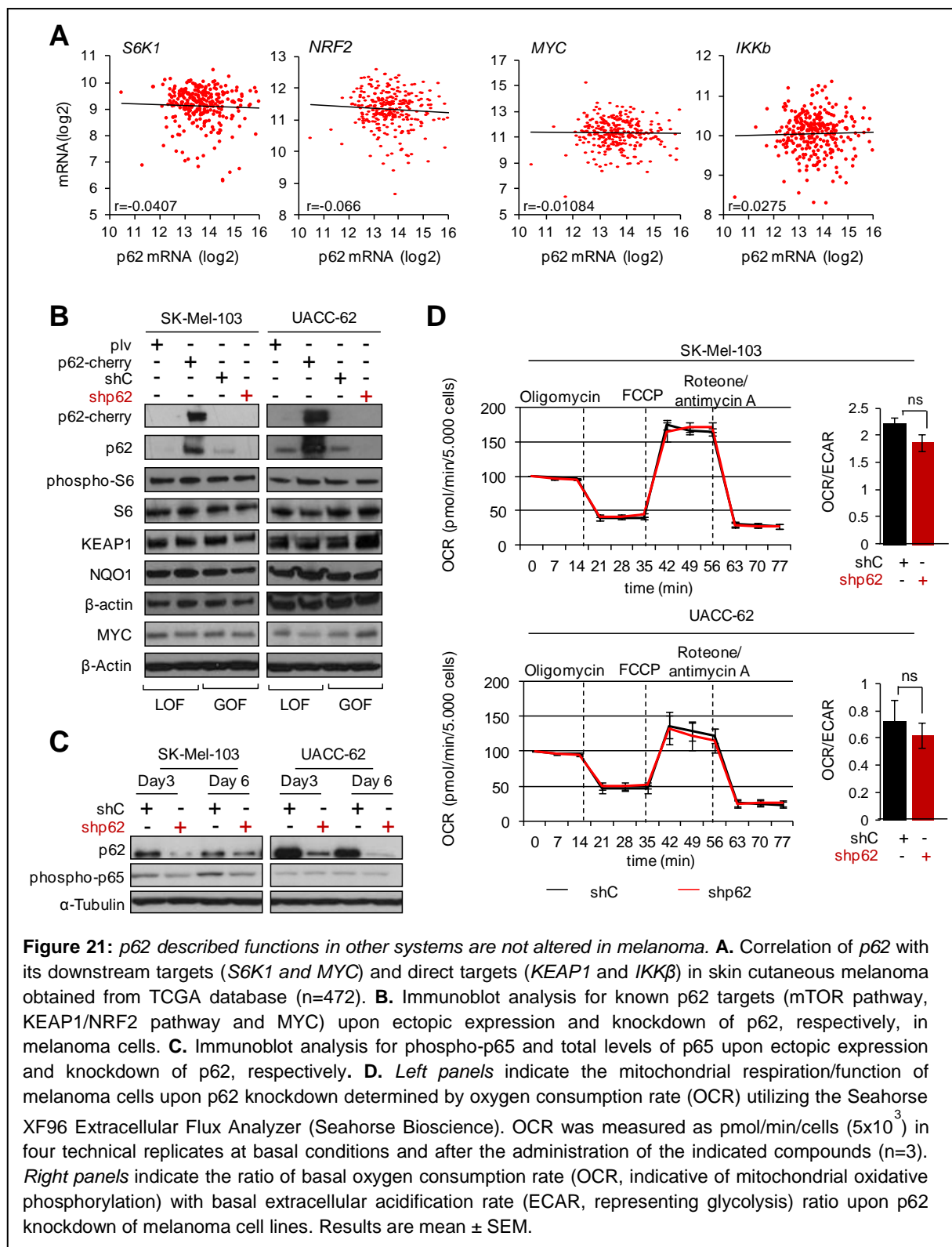


**Figure 20:** *p62* is dispensable for autophagy in melanoma. **A.** Immunofluorescence for p62 (red) in melanomas from the back of inducible *Braf<sup>V600E</sup>;Pten<sup>-/-</sup>* mice in different genotypes of ATG5. **B.** Immunofluorescence for p62 and LC3 in melanoma cells treated chloroquine (25μM) for 6 hours. **C.** Immunoblot for p62 and LC3 in melanoma cells treated with rapamycin (50nM) and chloroquine (25μM) for 6 hours upon p62 knockdown. **D.** Representative images of double immunofluorescence for p62 (red) and LC3B (green) in melanomas from the back of inducible *Braf<sup>V600E</sup>;Pten<sup>-/-</sup>* mice in different p62 genotypes. **E.** Immunoblot analysis for the indicated autophagosome proteins in tumors isolated from the back skin of inducible *Braf<sup>V600E</sup>;Pten<sup>-/-</sup>* mice in different p62 genotypes. **F.** Immunoblot analysis for autophagy related proteins in melanoma cells upon ectopic expression and knockdown of p62, respectively. **G.** Tumor outgrowth of *Braf<sup>V600E</sup>;Pten<sup>-/-</sup>* mice in different p62 and ATG5 genotypes shown at 8 weeks after 4-HT topical administration (mm<sup>3</sup>). Number of mice per group is indicated in the graph. Results are mean ± SEM.

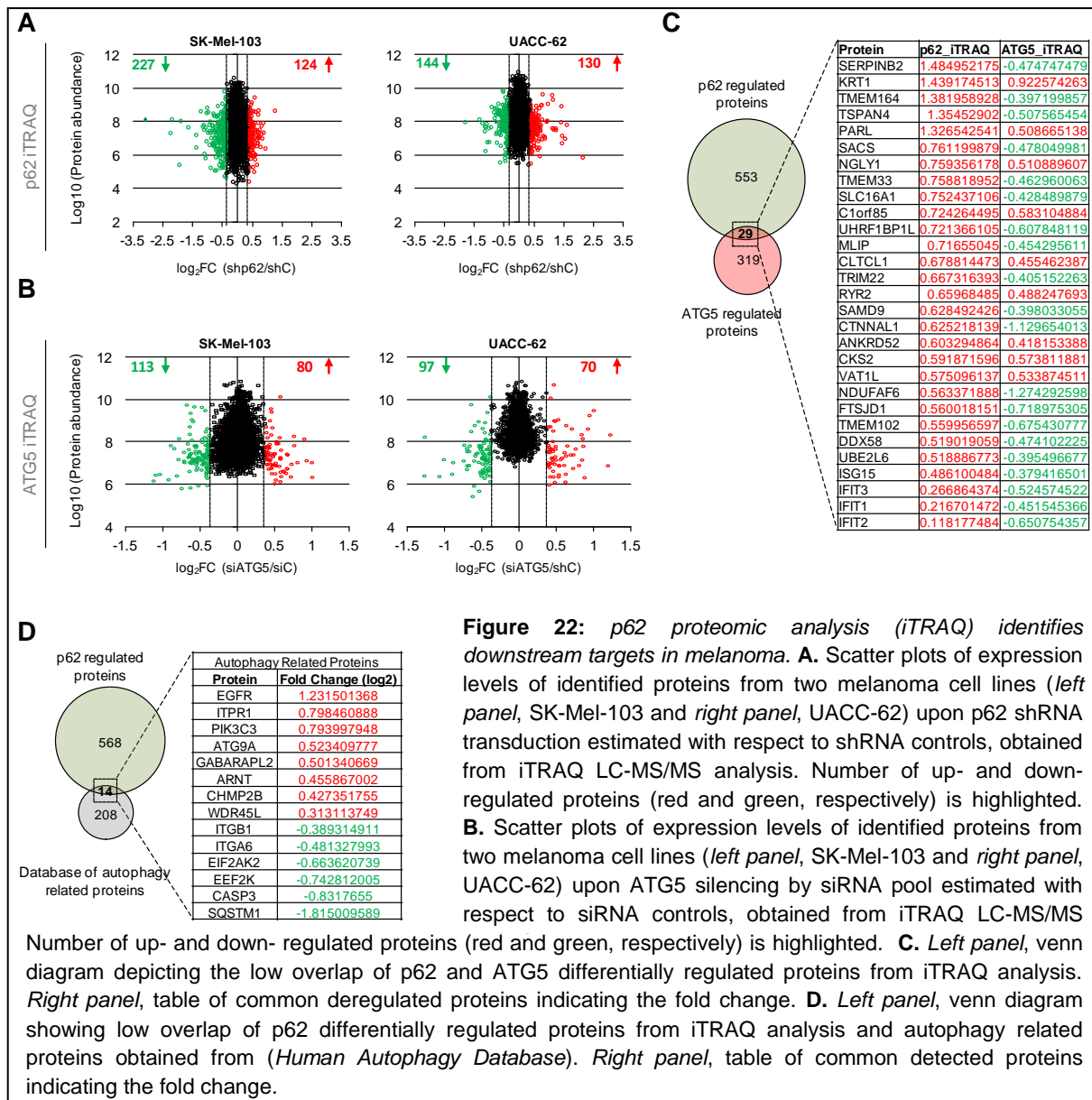
We then tested the mTOR pathway using three approaches: (i) mining TCGA for a correlation between the effector *S6K1* and *p62 mRNA* in clinical biopsies as described before<sup>282</sup> and performing (ii) gain and loss of function studies in two independent melanoma cell lines (i.e. overexpressing and depleting p62). Results from patient specimens revealed no correlation of *S6K1* with *p62* expression (**Figure 21A**). Consistent with these negative results, neither upregulation nor depletion of p62 had detectable effects on the phosphorylation of S6, another classical reporter of mTOR function (**Figure 21B**). Similar studies failed to reveal significant correlations between *p62* and the cytoprotector *NRF2* and its downstream target *NQO1* (**Figures 21A-B**). This was also the case for *MYC*, an oncogene that may be regulated by p62 under oxidative stress (**Figures 21A-B**). Regarding NF- $\kappa$ B, p62-IKK $\beta$  levels were not correlated in TCGA, and no changes in the phosphorylation of p65 were observed upon p62 loss (**Figure 21C**). Finally, the mitochondrial function of melanoma cells was not impaired by p62 loss as defined by monitoring oxygen consumption rate (OCR) in two melanoma cell lines (**Figure 21D, left panels**). This study revealed also that the ratio of oxidative phosphorylation and the glycolysis was not altered suggesting that the mitochondrial respiration of p62 depleted cells was functional (**Figure 21D, right panels**). Altogether, these results separate melanomas from other tumor types, suggesting yet additional roles of p62 in malignancy.



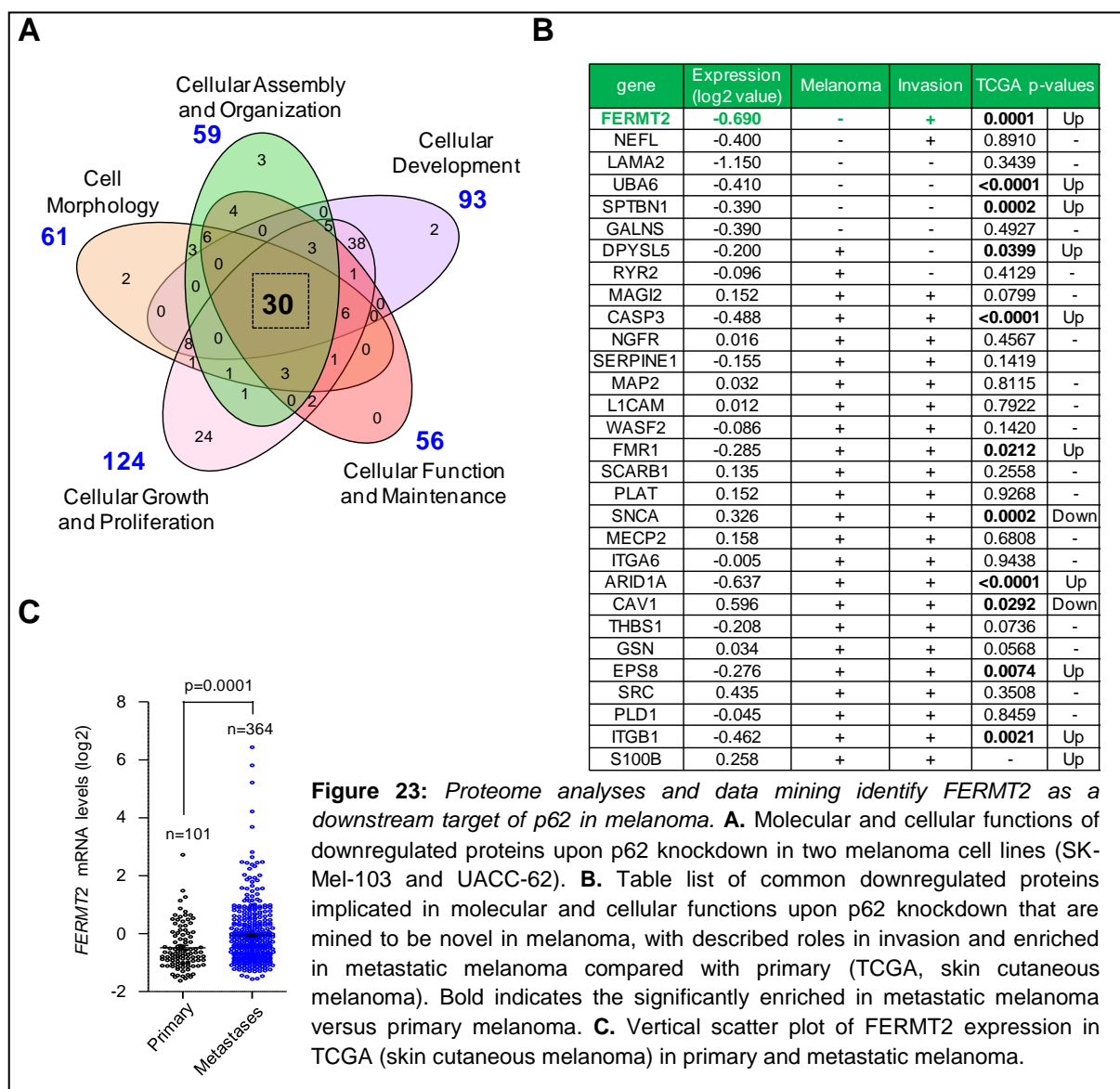
## 6.5 Quantitative proteomics (iTRAQ) for the identification of downstream effectors of p62

---

While high throughput proteomics have been reported to identify interactor networks in autophagy pathways<sup>341</sup>, no similar studies have been described for p62 in cancer cells. Therefore, multiplexed isobaric Tags for Relative and Absolute Quantification (**iTRAQ**) and subsequent LC-MS/MS (liquid chromatography tandem-mass spectrometry) were performed for parallel comparisons of control and p62-shRNA melanoma cells (SK-Mel-103 and UACC-62, in triplicates). In addition, proteomic analyses were run in both cell lines for ATG5 depletion as a reference for autophagy-associated changes in gene expression. Filters and cut off parameters for the identification of significantly deregulated proteins followed standards in the field<sup>317</sup> (as indicated in the Materials and Methods, 5.12). Interestingly, the fraction of significantly downregulated proteins after depletion of p62 and ATG5 was surprisingly low in both, SK-Mel-103 and UACC-62 cells (6.4 and 6.6% affected proteins for p62 shRNA cells, respectively; and 3.2% and 2.5% for ATG5 siRNA cells; respectively), as summarized in scatter plots of **Figures 22A-B** (see legends for the specific number of affected proteins per cell line and **Tables S6-9** in the appendix). Therefore, we concluded that although p62 and ATG5 (autophagy) may have pleiotropic roles; these ultimately affect a rather restricted sets of proteins. However, the p62- and ATG5-associated iTRAQ changes were unexpectedly divergent (i.e. proteins upregulated upon p62 depletion, were downregulated for the ATG5 counterparts; see venn diagram and the specific list of affected proteins in **Figure 22C**). Furthermore, we found the p62-iTRAQ data in melanoma displaying also a minor overlap with proteins annotated in the *Human Autophagy Database* (**Figure 22D**). These results confirm p62 acting primarily beyond autophagy in melanoma cells.



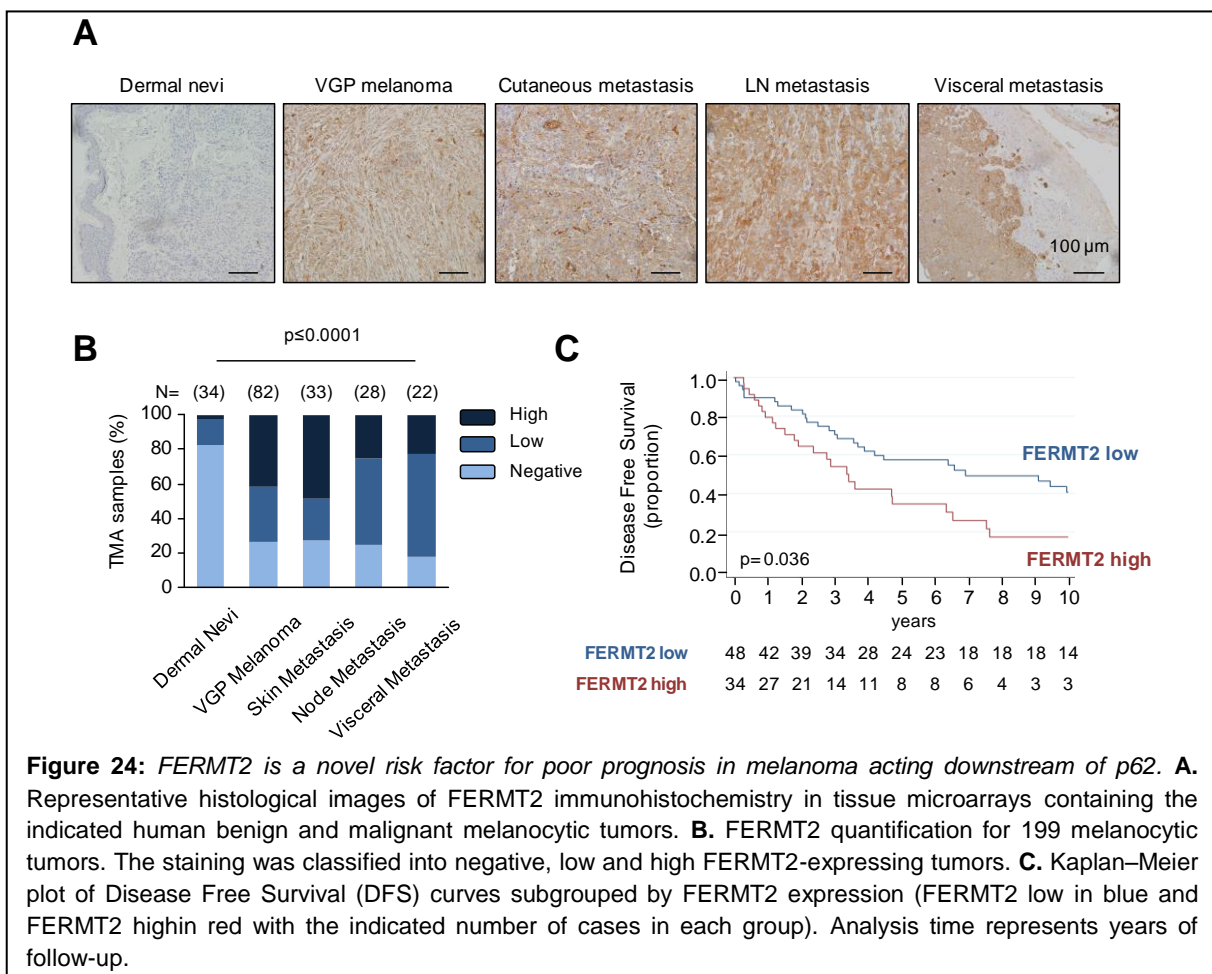
Ingenuity Pathway Analysis (IPA) was then performed on iTRAQ-p62 data, aggregating proteomic data from SK-Mel-103 and UACC-62 cells. For this study, we focused on downregulated factors after p62 depletion (adjusted p-values<0.05), under the hypothesis that those may reflect tumor drivers controlled by p62. Enriched signaling cascades found in this IPA analysis corresponded to (i) Cell Morphology, (ii) Cellular Assembly and Organization, (iii) Cellular Development, (iv) Cellular Function and Maintenance, and (v) Cellular Growth and Proliferation (**Figure 23A**). These 5 functional categories shared 30 proteins (**Figure 23A**), which were then ranked using two criteria: (i) novelty, namely, no reported links to melanoma, and (ii) annotated roles in invasion and metastasis -as these are the least understood functions of p62. To further narrow down these candidates to those with a higher likelihood of physiological relevance, we mined the TCGA database for differential expression in metastatic vs primary melanomas.



RNA sequencing-based information from TCGA database was mined for our candidates in  $n=101$  primary melanomas and in  $n=364$  metastatic cases (see p-values in **Figure 23B**). From this analysis and the applied selection criteria, we identified 6 proteins (FERMT2, NEFL, LAMA2, UBA6, SPTBN1, GALNS) not previously annotated in melanoma and no direct links with p62. Two of the identified proteins (FERMT2, NEFL) have been linked with roles in metastasis (**Figures 23B**). However, *FERMT2* was the putative target that was significantly enriched in metastatic biopsies compared with primary in TCGA database and downregulated in both melanoma cell lines (**Figures 23C**). *FERMT2* (Fermitin Family Member 2/KINDLIN-2) is a scaffold protein involved in cell adhesion and migration<sup>342</sup>, with well-reported links to metastasis in different cancer types, although regulatory mechanisms are not well understood<sup>343-345</sup>. Together, these results pointed to *FERMT2* as a key driver of malignant features of melanoma cells, acting downstream of p62.

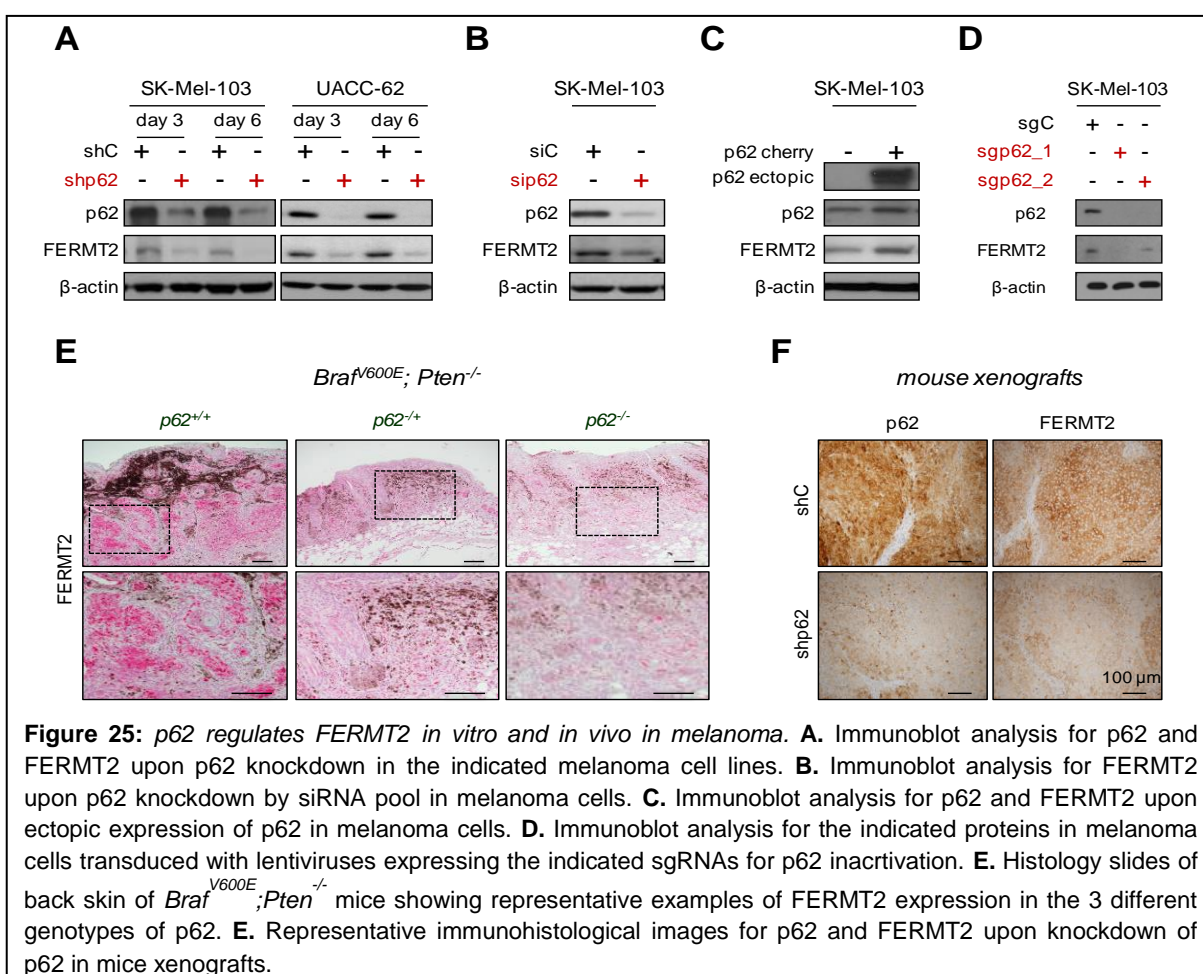
## 6.6 FERMT2 is a novel risk factor for poor prognosis in melanoma acting downstream of p62

Before proceeding to functional analyses, histological analyses were performed to confirm a melanoma-associated accumulation of FERMT2 at the protein level. These were performed on TMAs containing melanocytic benign and malignant lesions at different stages of the disease (see **Table S10** in the appendix for detail on the specimens analyzed,  $n=199$  in total). Interestingly, and as the case for p62, FERMT2 was undetectable (or very low) in the dermal nevi studied. Vertically invading melanomas (VGPs) and metastases (particularly at the skin) were found highly positive by immunohistochemistry (**Figures 24A-B**). In an independent validation cohort of 82 VGPs with annotated 10-year follow up, high FERMT2 expression showed a significant correlation to poor disease free survival (**Figure 24C**, **Tables S10-12** in the appendix; double analyses for p62 and FERMT2 expression are discussed below).



To demonstrate the relevance of FERMT2 as a downstream effector of p62, loss and gain of function studies were performed. Specifically, p62 was depleted (shRNA or siRNA pool) or

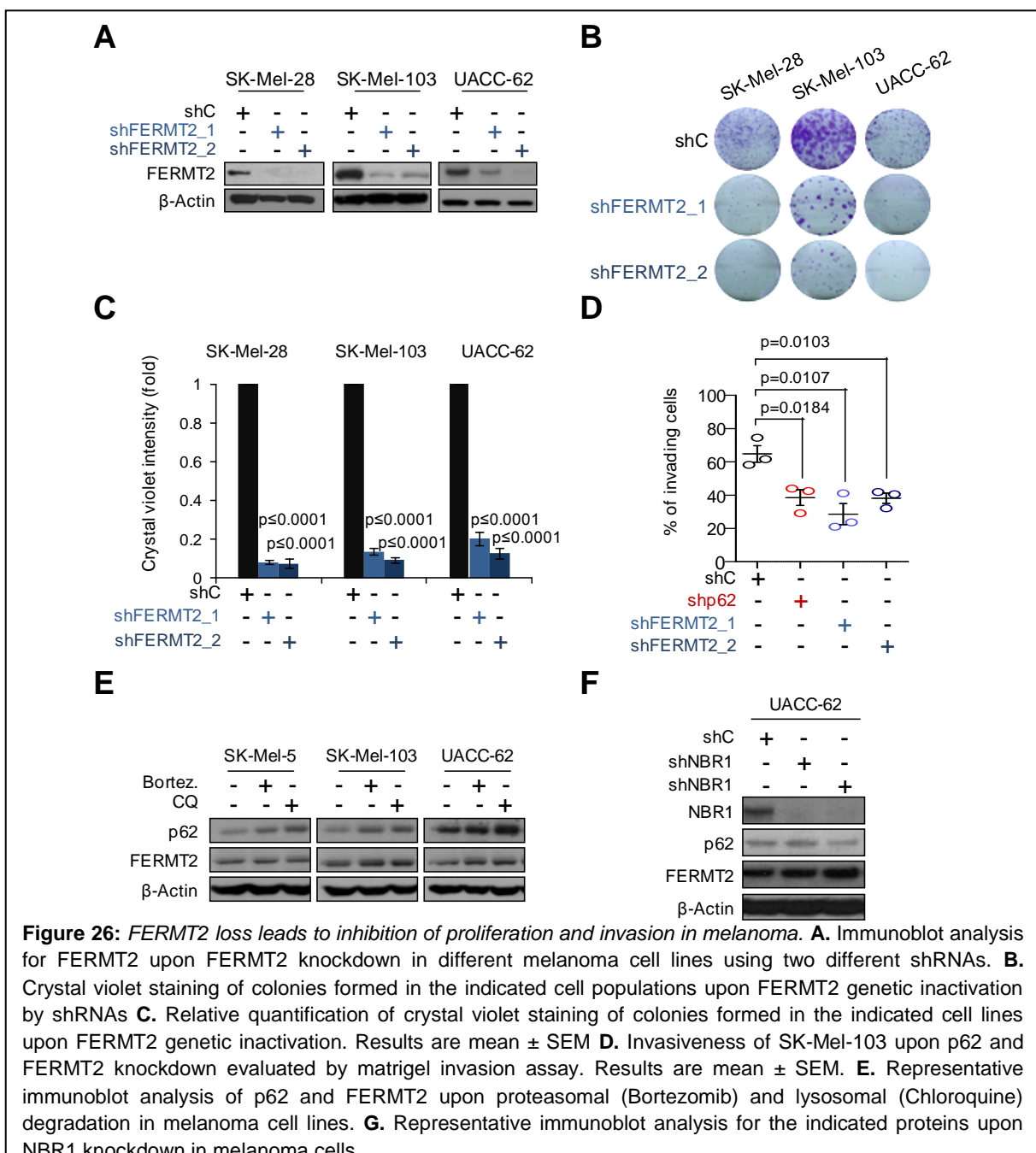
overexpressed by means of lentiviral transfer. The effect on FERMT2 protein expression by these strategies was consistent: downregulation upon p62 depletion, and increase through ectopic p62 expression (**Figures 25A-C**). To independently validate FERMT2 as bona fide target of p62, two short guide RNAs (sgp62\_1 and sgp62\_2) were generated for CRISPR/Cas9-mediated gene depletion. As shown in **Figure 25D**, sgRNAs effectively eliminated p62 expression and consequently the levels of FERMT2 (versus scrambled sgRNA). *In vivo*, FERMT2 levels were decreased in *Braf<sup>V600E</sup>;Pten<sup>-/-</sup>* GEMM melanomas as a function of p62 allelic loss (see the differential staining in *p62<sup>+/+</sup>* with respect to *p62<sup>+/-</sup>* and *p62<sup>-/-</sup>* in **Figure 25E**). Similar results were found for xenografts of human melanoma cells (SK-Mel-103) expressing p62 shRNA and implanted in mice compared to the corresponding control (**Figure 25F**).



Next, we determined whether depletion of FERMT2 phenocopied p62 loss. Two independent shRNAs were identified to provide a sustained and efficient downregulation of FERMT2 (see immunoblots in **Figure 26A** for three melanoma cell lines). FERMT2-deficient melanoma cells showed a markedly reduced proliferative capacity in long term colony formation assays (**Figure 26B-C**). Moreover, depletion of FERMT2 (as the case for p62)

resulted in a significant reduction in invasive potential of otherwise aggressive melanoma cells (**Figure 26D**).

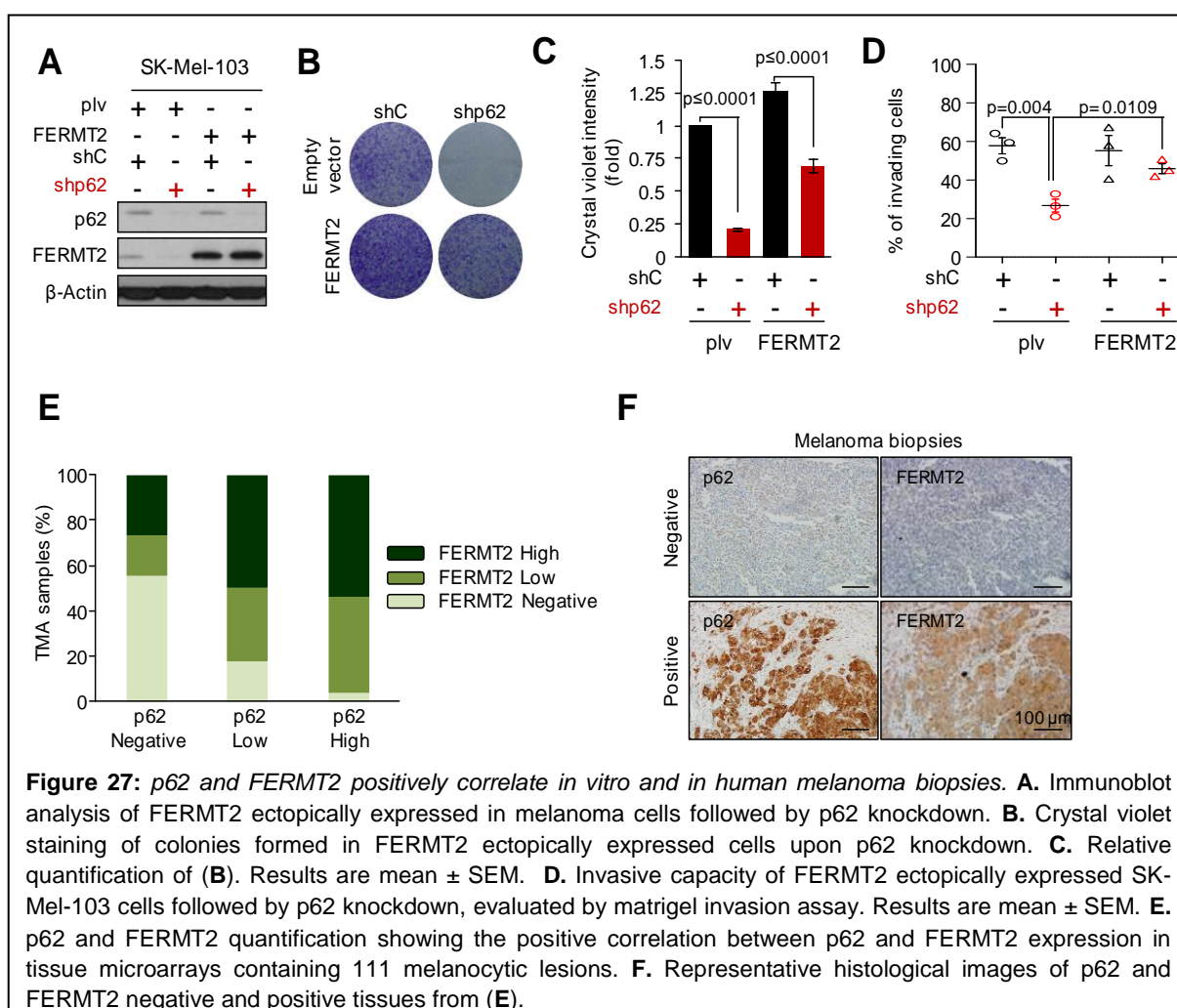
To determine if FERMT2 levels are regulated by p62 through degradation (main function of p62), melanoma cells were treated with inhibitors of the proteasome (Bortezomib) and lysosome (Chloroquine). While p62 was accumulated (especially in CQ-treated cells), FERMT2 levels were not affected. Additionally, another main cargo receptor protein, NBR1, was depleted in melanoma cells. NBR1 exhibits similar domain architecture to p62 and it has been reported that these two proteins cooperate in autophagy<sup>294</sup>. NBR1 depletion did not affect the expression levels of FERMT2 (**Figure 26F**), strengthening the concept that p62 acts on FERMT2 expression in a manner beyond autophagy.



Importantly, to demonstrate that FERMT2 is indeed a physiologically-relevant p62 target, rescue experiments were performed. To this end, melanoma cells were infected with lentiviruses expressing ectopic FERMT2, or an empty vector control. Each of these subpopulations was then depleted for p62 (**Figure 27A**). As shown in **Figures 27B-D**, this ectopic FERMT2 expression diminished the effect of p62 depletion in the proliferative and invasive features of melanoma cells. Therefore, while p62 may certainly impinge on multiple signaling cascades (**Figure 23A**), main roles in proliferation and invasion largely depend on FERMT2.

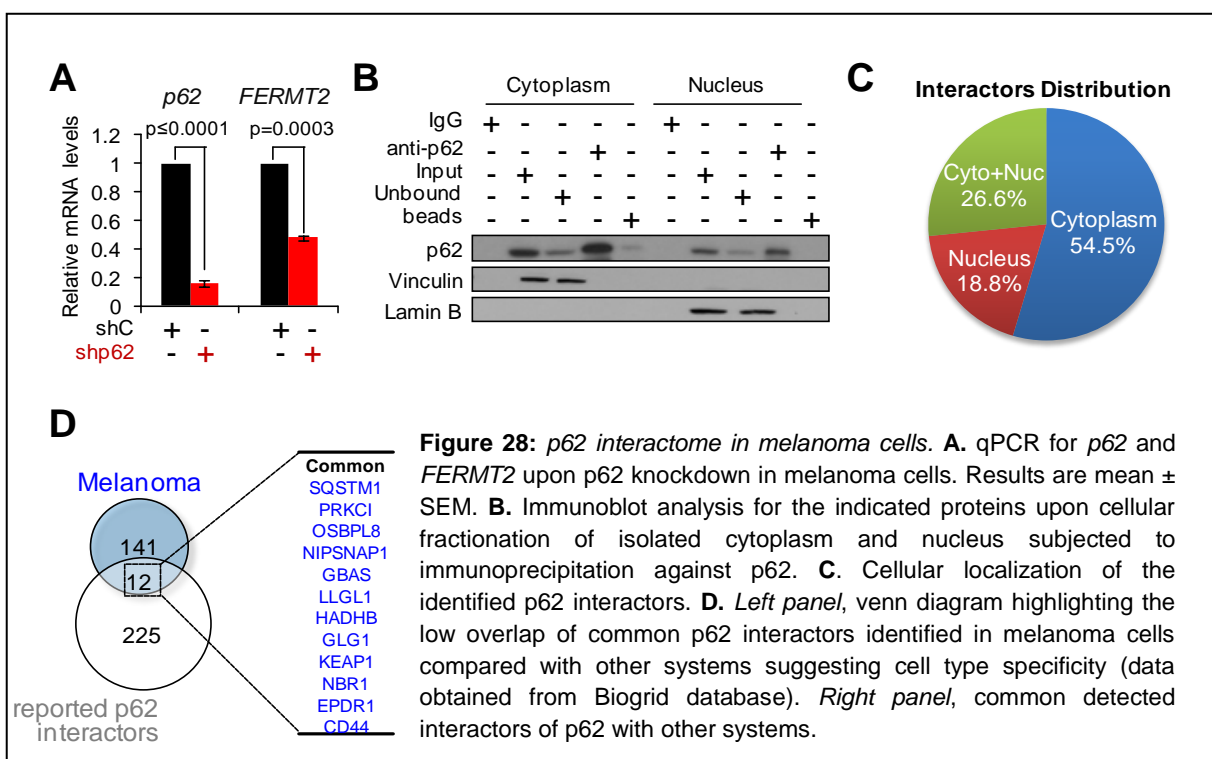
The corollary of the data above is that FERMT2 and p62 expression should be correlated in patient biopsies. To this end, we constructed a TMA containing 111 melanocytic lesions, and stainings for p62 and FERMT2 were performed in consecutive sections. As illustrated in **Figure 27E**, 20% of p62 negative melanomas still expressed high FERMT2, but overall, Chi-squared test indicated a positive correlation between the two proteins ( $p=0.001$ ; see representative examples in **Figure 27F**).

Altogether, these results identify FERMT2 as a physiologically-relevant novel indicator of poor prognosis in melanoma, acting downstream of p62.



## 6.7 The p62 interactome identifies RNA binding proteins as novel binding partners in melanoma

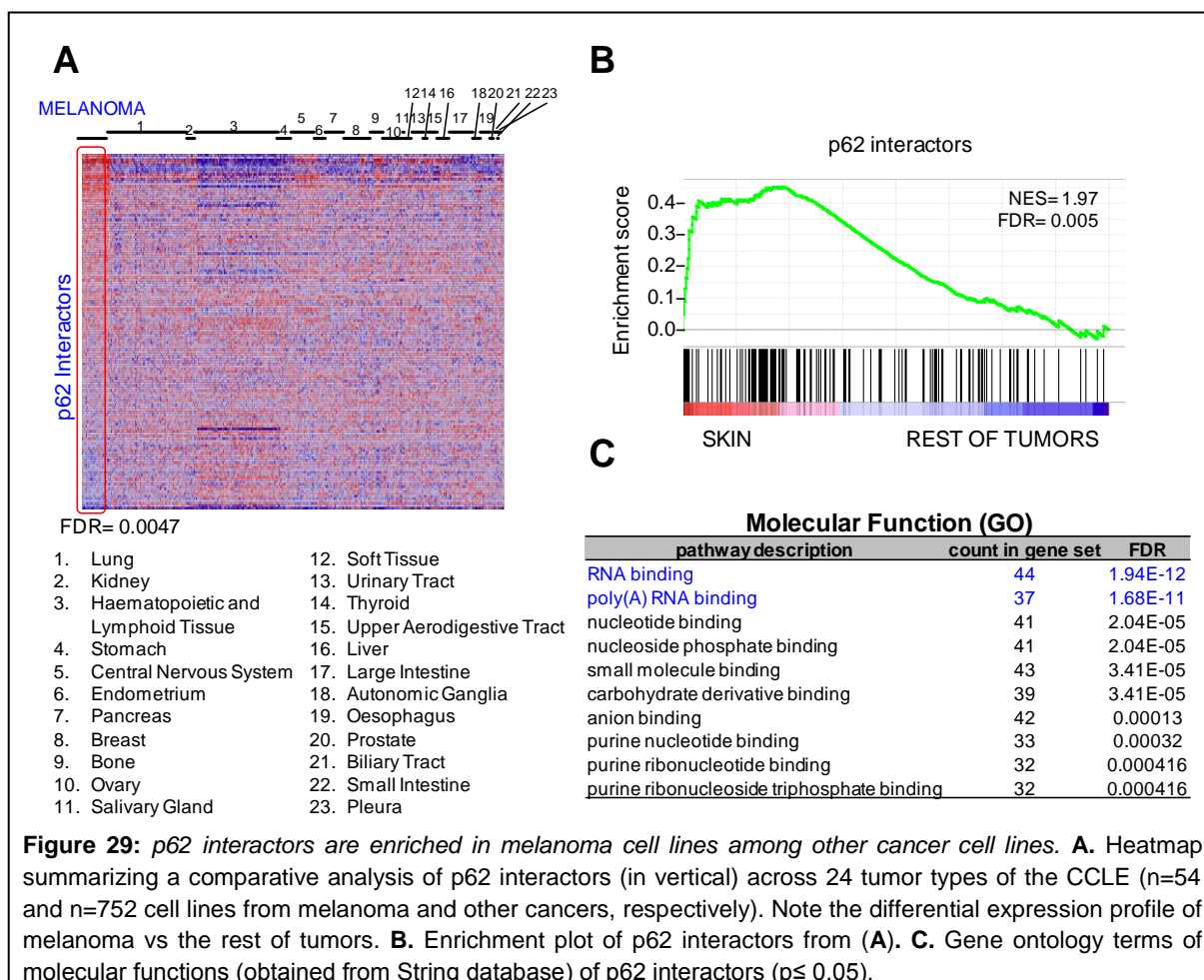
Next, we investigated the mechanism by which p62 regulates *FERMT2*. As p62 has been reported to act as a hub to define the localization and stability of other proteins, we questioned whether this was the case for *FERMT2*. However, no interaction between these two proteins was found by immunoprecipitation assays (data not shown). Interestingly, quantitative RT-PCR revealed a 50% reduction *FERMT2* RNA in p62 depleted melanoma cells (**Figure 28A**). Therefore, we set to study roles of p62 in RNA regulation. As p62 does not have RNA binding domains<sup>277</sup>, we hypothesized that the regulation of *FERMT2* could be indirect, perhaps via transcription factors or RNA binding proteins.



No genome-wide proteomic information is available for p62 interactors in cancer which we could use as a guideline. However, mining the *Biological General Repository for Interaction Datasets (BioGRID)*<sup>346</sup> 256 unique p62 interactors were identified (extracted from low and high throughput analyses in various systems). A global inspection of these known p62 interactors did not reveal reported regulators of *FERMT2*. Therefore, affinity purification followed by LC-MS/MS were performed to dissect interactors of endogenous p62 in melanoma cells. More specifically, these analyses were performed on UACC-62 cells using a highly efficient p62-immunoprecipitating antibody upon subcellular fractionation of the cytoplasm and the nucleus (**Figure 28B**; see Materials and methods, 5.13). The eluted samples were analyzed with MaxQuant bioinformatic tools, using Andromeda as a peptide

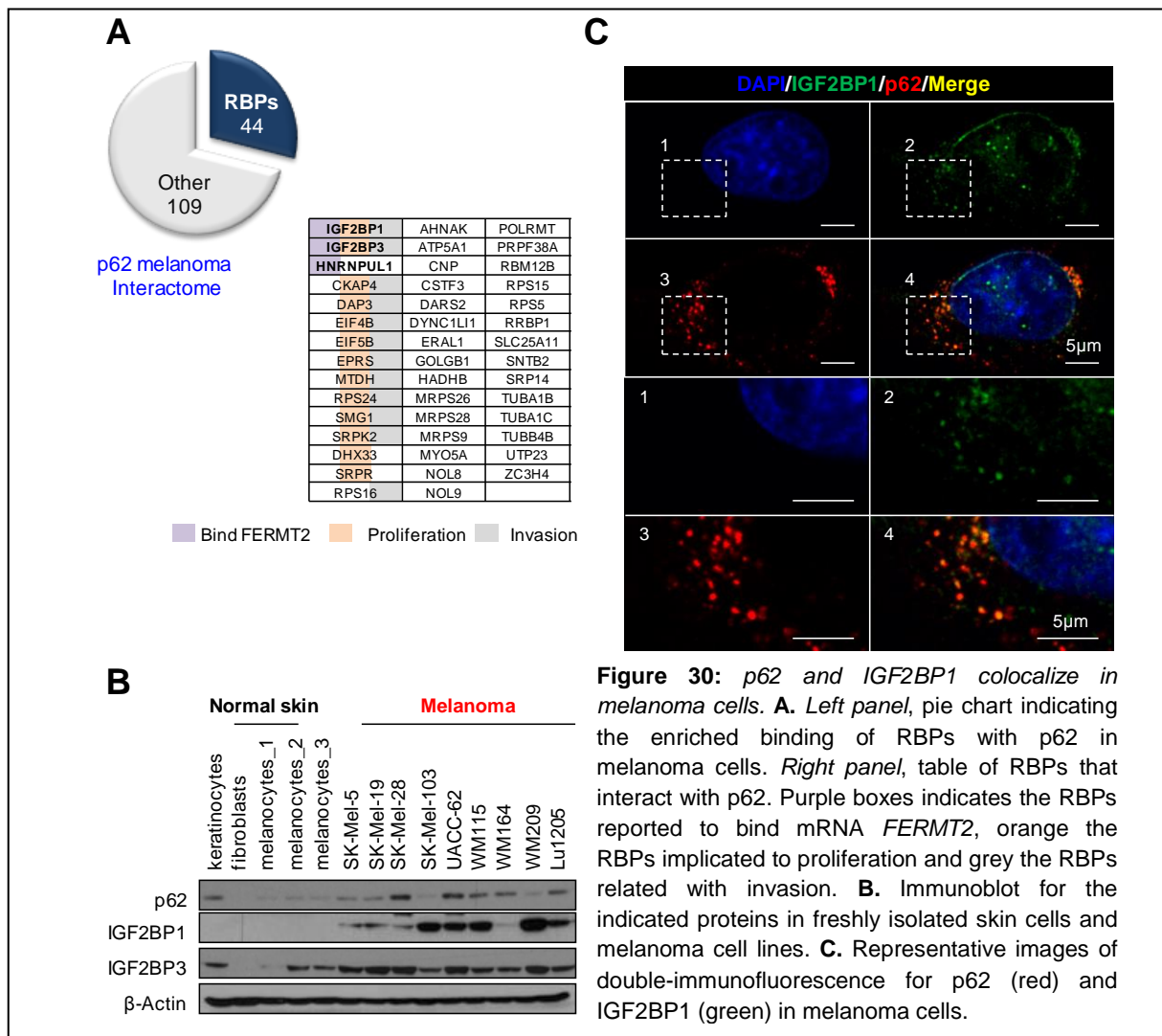
search engine for probabilistic scoring<sup>321,322</sup>. Using an FDR = 1%, this strategy identified 153 proteins as putative interactors of p62 in melanoma cells (**Table S13**, appendix). 54.5% of p62 interactors were found to localize in the cytoplasm; 18.8% in the nucleus; and 26.6% in both compartments (**Figure 28C**) supporting the dynamic role of p62 mainly in the cytoplasm, but also as a shuttling protein from the cytoplasm to the nucleus<sup>232,308</sup>. Surprisingly, the overlap between p62-melanoma interactome and the p62-BioGRID data was rather low, with only 12 proteins in common (**Figure 28D**). These results therefore, suggest a melanoma-specific nature of the p62 bound proteins. This hypothesis was indeed confirmed by GSEA using as a reference the Cancer Cell Line Encyclopedia (CCLE), which contains information from 752 cell lines, 54 of which are from melanomas (see heatmap plots of this comparative analysis in **Figures 29A-B**; FDR=0.0047).

STRING<sup>330</sup> (Search Tool for the Retrieval of Interacting Genes/Proteins) was then used to explore the molecular functions of the p62-affinity precipitated proteins in melanoma cells. Surprisingly, the most enriched GO terms found were related to a particular enrichment in RNA binding processes (see highly significant FDR values in **Figure 28C**). Therefore, these results support the attractive scenario of p62 having new cellular roles as a hub for RNA binding proteins (RBPs).

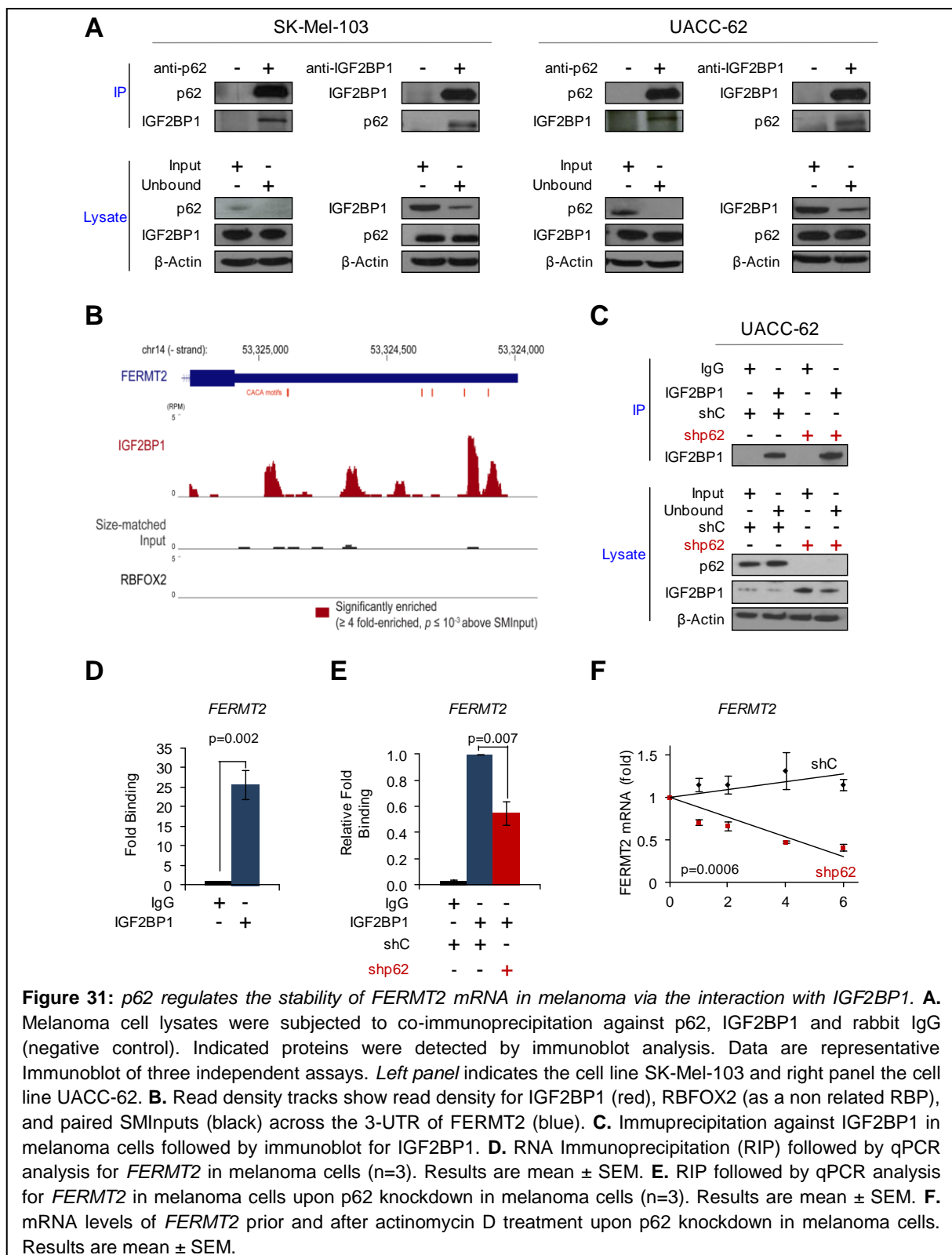


The data above open new avenues of research in the p62 and RBP fields that could be explored in future studies. Here, we focused on the possibility of a “p62-RBP axis” as a modulator of *FERMT2*. From the interactome analyses of **Figures 28-29**, we found 44 RBPs as putative p62 interactors. It was not practical to assess in detail each of these proteins. Therefore, candidates for functional characterization were selected in two steps: first, the 44 p62-interactors were screened through the CLIPdb 2:POSTAR<sup>347</sup> database for binding to *FERMT2 mRNA*. Specifically, CLIPdb 2:POSTAR was selected as it represents the largest collection of experimentally probed and computationally predicted RBP binding sites in the human and mouse transcriptomes<sup>347</sup>. Secondly, for a more guided analyses, text mining was performed on the 44 p62-precipitated RBPs for functions related with cancer cell proliferation and invasion. As summarized in **Figures 30A**, this approach yielded 2 RBPs (IGF2BP1 and IGF2BP3) that fitted the three criteria: (i) p62 interaction, (ii) binding to *FERMT2 mRNA* in other settings, (iii) and functions that could account for roles of p62 in tumor progression and metastasis.

IGF2BP1 and IGF2BP3 are homologues of the insulin-like growth factor 2 (IGF2) messenger RNA (mRNA)-binding proteins<sup>348,349</sup>. Both are highly conserved oncofetal RBPs that regulate RNA processing at several levels, including localization, translation, and stability<sup>349</sup>. Importantly, IGF2BP1 and IGF2BP3 have been previously shown to be upregulated during melanoma progression, with key roles in tumor cell invasion<sup>350,351</sup>, although with no links to p62. The overexpression of IGF2BP1 and IGF2BP3 was validated by immunoblot analysis in freshly isolated normal skin cells and in a panel of melanoma cells (**Figure 30B**). Using double immunofluorescence analyses we found a visible colocalization of p62 with IGF2BP1 but not with IGF2BP3 (**Figures 30C** and data not shown). Therefore, we centered on IGF2BP1 for further characterization. This selection was further reinforced by finding that large scale analyses of IGF2BP1 binding sites in human pluripotent stem cells included *FERMT2* as a direct target<sup>352</sup>.



From the results above, the hypothesis we set to demonstrate is that p62 by binding IGF2BP1 may favor the ability of this RBP to bind and stabilize *FERMT2* mRNA. First, p62-IGF2BP1 interaction was confirmed in different melanoma cell lines by reciprocal co-immunoprecipitations assays (see immunoblots in **Figures 31A**). Secondly, data obtained from enhanced UV crosslinking and immunoprecipitation fort IGF2BP1<sup>352</sup> to analyze the binding to *FERMT2* mRNA. From the data analyzed it was observed that IGF2BP1 binds to the 3'UTR of *FERMT2* (**Figure 31B**). Independent RNA Immunoprecipitation (RIP) with anti-IGFBP1 antibodies followed by qPCR proved that IGF2BP1 indeed binds *FERMT2* mRNA (immunoblot for IGF2BP1 immunoprecipitation in **Figure 31C**; see 25-fold difference in binding with respect to IgG control in **Figure 31D**). Thirdly, RIP-qPCR was performed in melanoma cells depleted for p62, finding a reduced IGF2BP1 binding to *FERMT2* by 50% (**Figures 31E**).

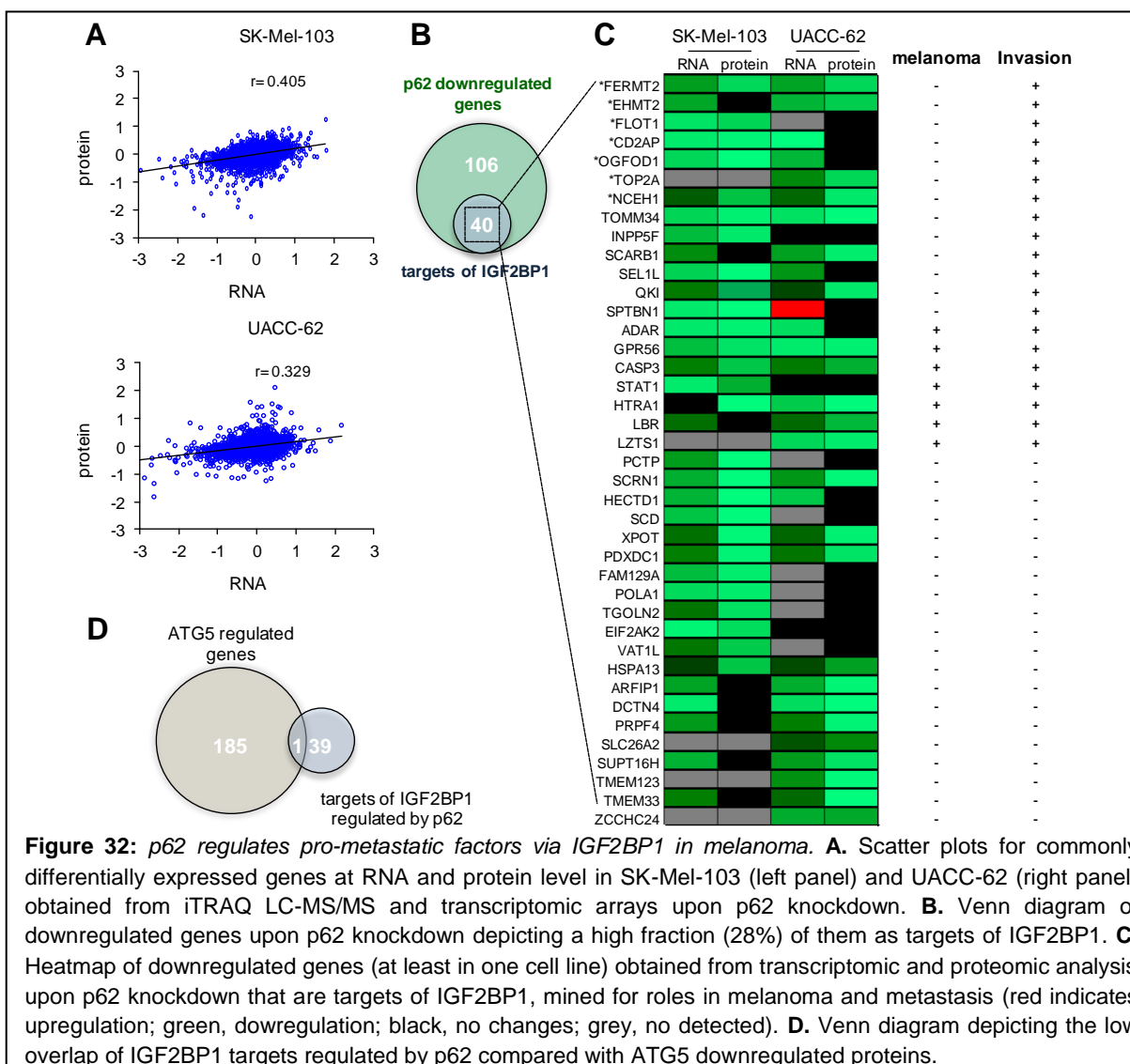


Finally, *FERMT2* mRNA half life was assessed in the presence or absence of p62 (through actinomycin D treatments to prevent new transcription). Melanoma cells depleted for p62 exhibited a significant acceleration of *FERMT2* mRNA decay (**Figures 31F**,  $p=0.006$ ).

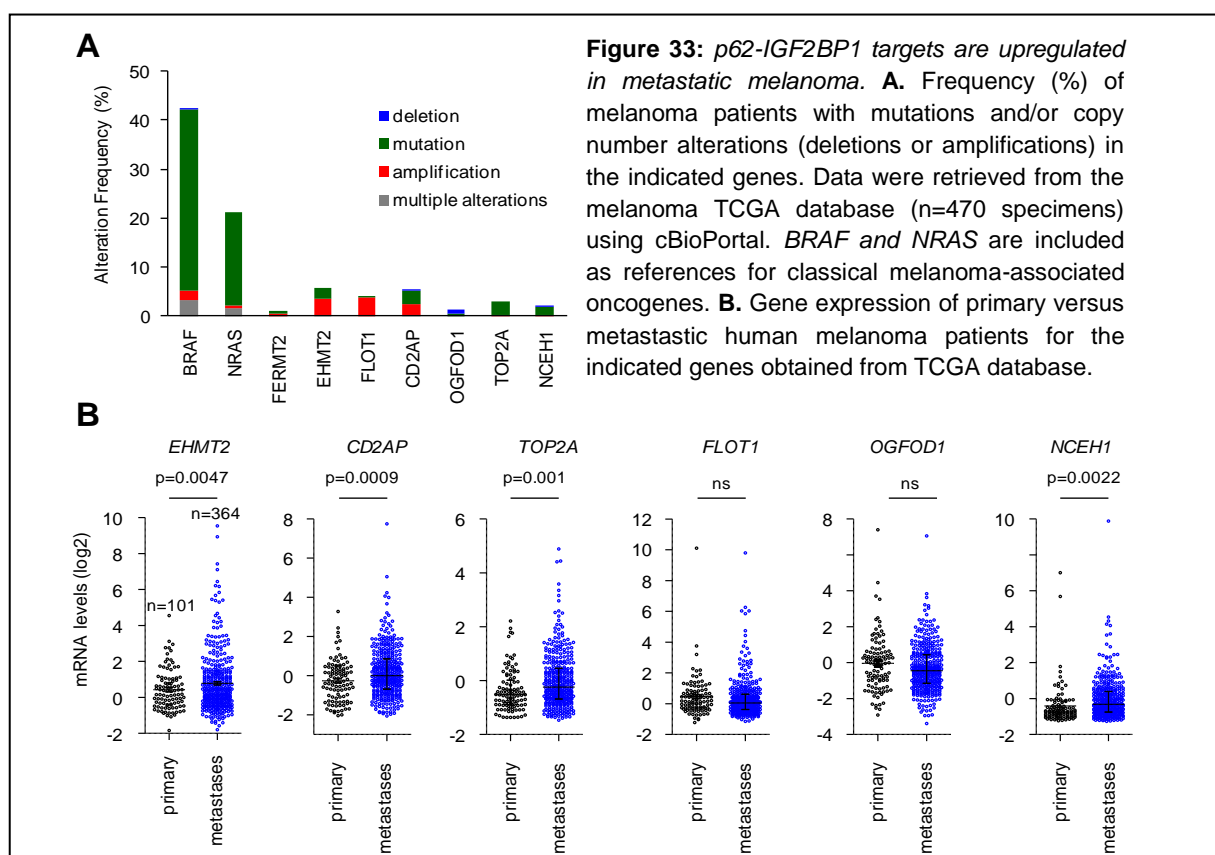
In conclusion, this comprehensive -omic approach (transcriptomic, proteomic and interactomic analyses) revealed a p62>IGF2BP1>FERMT2 axis embedded within a newly-identified function of p62 as binding partner for RBPs.

## 6.8 p62-IGF2BP1 interaction controls the mRNA stability of multiple pro-metastatic factors

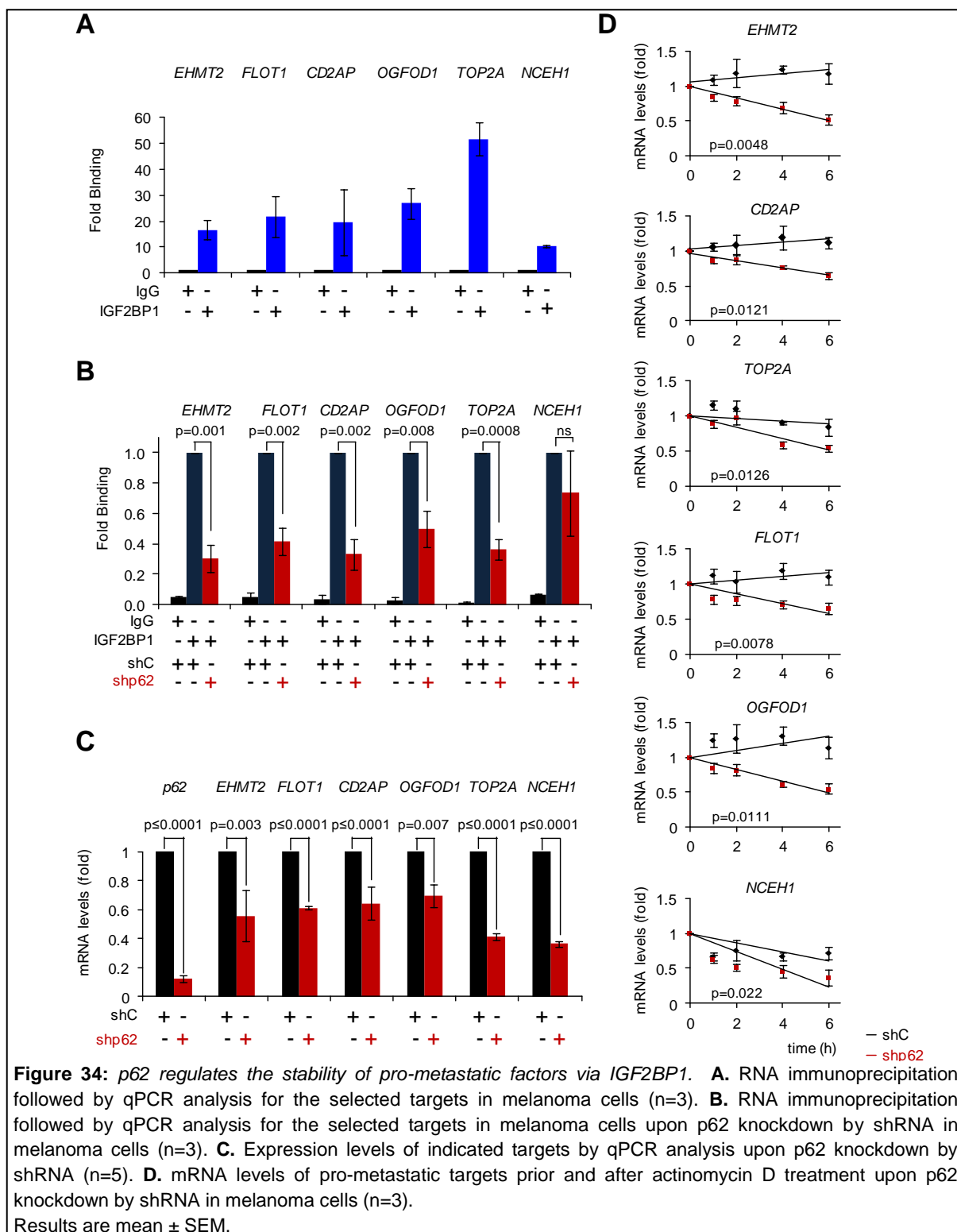
IGF2BP family members are highly pleiotropic RBPs<sup>348,349,353</sup>. Therefore, we considered unlikely that FERMT2 would be the only pro-metastatic factor regulated by the p62-IGF2BP1 interaction. In particular, we questioned whether indeed IGF2BP1 could contribute to a broader impact of p62-related functions. The transcriptomic and proteomic analyses of p62 showed mild positive correlation in the detected genes (**Figure 32A**) and we therefore focused on genes positively controlled by p62 where changes at RNA levels had a significant impact on protein expression.



This gene set, found to include 146 genes, was obtained by merging aggregated transcriptomic and proteomic data in SK-Mel-103 and UACC-62 (**Figure 32B**). These 146 p62-regulated genes were crossed with IGF2BP1-binding targets described by eCLIP (enhanced UV CrossLinking and Immunoprecipitation) in other cell types (human stem cells)<sup>352</sup>. This approach revealed a highly significant set of p62-modulated genes (40/146; i.e. 27%) with the potential to be under the control of IGF2BP1 in melanoma (**Figure 32C**). Of note, these identified genes were not overlapping in ATG5-regulated genes from iTRAQ analysis gene list (**Figure 32D**) suggesting that these factors are not regulated by p62 via the autophagy machinery. These results therefore, further support a key role of this RBP in melanoma progression. For validation, representative genes considered attractive for not being linked to melanoma, but reported with pro-metastatic functions were selected (**Figure 32C**). We thus chose different gene categories: (i) *EHMT2* and *TOP2A* as examples for transcriptional regulators<sup>354,355</sup>; (ii) modulators of vesicular trafficking (*FLOT1* and *CD2AP*), that favored progression in different types of cancer<sup>356-358</sup>; (iii) and pro-metastatic genes with roles in metabolism (*NCEH1* and *OGFOD1*)<sup>359,360</sup>. Intriguingly, the selected factors neither exhibit high mutational status nor copy number alterations (deletions or amplifications) in human melanoma biopsies (**Figure 33A**; data extracted from TCGA, n=470 specimens). However, the levels of expression are increased in metastatic compared with primary melanoma biopsies (**Figure 33B**).



As IGF2BP1 was found to bind the 3' UTR of these factors in other systems<sup>352</sup> we set to determine whether these candidates were also IGF2BP1 targets in melanoma. RIP followed by qPCR demonstrated that this was the case (see the differential binding of the IGF2BP1 antibody with respect to IgG control in **Figure 34A**). Moreover, this binding was significantly decreased in p62 deficient cells (**Figure 34B**), ultimately resulting in reduced mRNA expression of all the candidates studied (**Figure 34C**).



To determine whether this inhibited mRNA levels were a consequence of accelerated degradation, cells were treated with actinomycin D to blunt new mRNA synthesis and thus define the half-life of these transcripts. Results showing the requirement of p62 to sustain the stability of all these factors (*EHMT2*, *TOP2A*, *FLOT1*, *CD2AP*, *NCEH1* and *OGFOD1*) are summarized in **Figure 34D**.

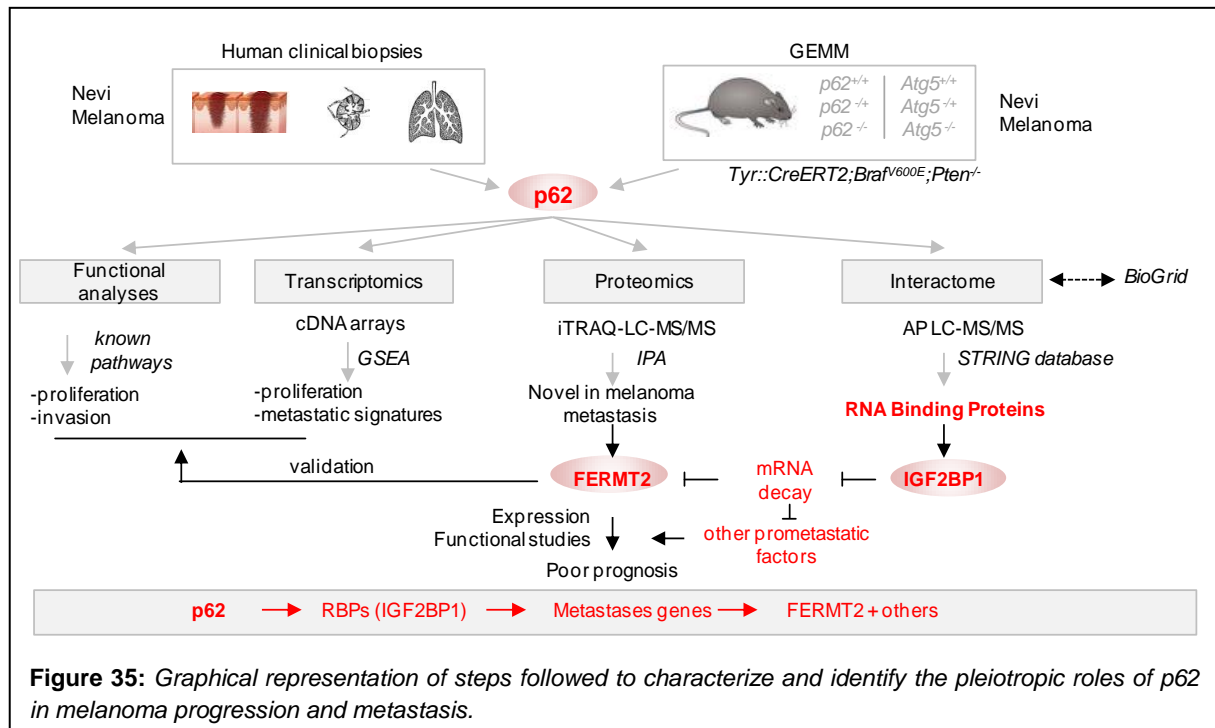
Collectively, these results strongly illustrate that p62 regulates the stability of a broad range of pro-metastatic factors, and described the RNA binding factor IGF2BP1 as a key mediator in this newly identified function.

## ***VII . DISCUSSION***

Melanomas are prime examples of aggressive tumors that proceed with a plethora of changes in the transcriptome and proteome<sup>95,361-364</sup>. Characterization and identification of oncogenes provides new features and traits in melanoma progression, especially at the metastatic stages of the disease. However, the oncogenic factors rarely act via single targets. This complexity is particularly notorious for proteins such as Sequestosome 1/p62, which function by pleiotropic protein-protein interactions.

In this PhD thesis we performed a global analysis of p62 expression and mechanism of action in melanoma cells, clinical biopsies and newly-generated mouse models. The selection of p62 as a putative new modulator of selective gene sets enriched in melanoma was prompted by previously described roles of this protein in lysosomal-associated functions, primarily autophagy<sup>186,298</sup>, which we had found with a distinct lineage-selective regulation in this disease<sup>220</sup>. Therefore, we questioned whether p62 (like the autophagy effector ATG5) may be tuned down in invasive or metastatic stages of melanoma progression. In parallel, we also set to define to which extent p62 was required for autophagosome formation. These studies were combined with a comprehensive characterization of the p62-modulated transcriptome, proteome and interactome. Briefly, it was found that (i) the *p62* locus does not suffer frequent heterozygous losses we had reported for *ATG5*<sup>220</sup>; moreover, p62 protein was found overexpressed in TCGA-metastatic melanomas, a feature we confirmed by (ii) histological analyses in independent patient cohorts (in collaboration with Hospital 12 de Octubre), where positive expression was associated with poor prognosis in melanoma patients<sup>334</sup>. (iii) The new GEMM confirmed that p62 is required for the progression and the metastasis of malignant melanoma, and more interestingly the loss of p62 prolongs the survival of the mice. (iv) Genetic silencing of p62 abrogated the proliferation and invasion capabilities of cultured melanoma cells. (v) At molecular level, it was found that known roles of p62 in the modulation of mTOR, NF-κB, KEAP1-NRF2, MYC and mitochondrial respiration were not affected. (vi) More interestingly, it was found that p62 exhibits distinct roles and does not impair the autophagic machinery. (viii) Additionally, from a comprehensive -omics analyses in melanoma cells we identified metastatic signatures significantly downregulated upon p62 depletion. The downstream effector of p62, FERMT2 was identified and proposed as a novel risk factor for poor prognosis in melanoma. (ix) Surprisingly, a large set of RBPs was identified to interact with p62. Among them, IGF2BP1 (via the interaction with p62) was found to regulate the stability of the pro-metastatic factor FERMT2 (and others). Together, these results provide new insights in the role of p62 in melanoma and ultimately separate this disease from other pathologies, where this protein is also overexpressed.

The **Figure 34** illustrates the findings of this PhD thesis highlighting the main steps that were followed to characterize and identify the new role of p62 in melanoma progression and metastasis.



## 7.1 Expression and prognostic studies of p62 in human melanomas

Publicly available databases are being consolidated as a versatile platform to screen for oncogenic drivers and tumor suppressors across large cohorts of clinically-annotated biopsies (TCGA)<sup>333</sup> and cell lines (CCLE)<sup>329</sup>. Of high importance, the TCGA platform has performed a systematic multi-platform characterization of cutaneous melanomas (~300 biopsies) at the DNA, RNA, and protein levels to create a catalogue of somatic alterations and describe their potential biological and clinical significance. These analyses established a genomic/transcriptomic framework of classification that has potential implications for prognosis and therapy<sup>95</sup>. Moreover, it provides evidence for exploring how additional molecular alterations may explain observed biological and clinical differences among the subtypes. It also provides signposts for identification of druggable targets and predictive biomarkers, as well as potentially useful guidance for decisions about therapy. p62 overexpression has been addressed in various cancers types (see introduction and **Table S4** in the appendix) but still its expression pattern during tumor progression and metastasis is not well characterized. Intriguingly, there is no clear consensus on whether it acts as a tumor promoting<sup>253,260</sup> or tumor suppressive agent<sup>278,308</sup> (i.e. liver cancer). In melanoma, a

recent study characterized the expression of p62 in primary tumors<sup>285</sup>; however the contribution of the protein at later stages was not addressed.

In this PhD thesis, mining TCGA database we found a significant upregulation of p62 protein expression at metastatic sites (skin in transit, regional lymph nodes and distal visceral organs), when compared to primary melanomas. The relatively high expression of p62 in melanoma was supported by CCLE (encompassing over 700 cell lines of 25 different cancer types). These findings were independently validated by immunohistochemical studies for p62 in high density tissue microarrays covering a broad spectrum of melanocytic lesions at different stages of progression<sup>334</sup>. The significant upregulation of the protein at the later stages of the disease raise the possibility that during metastasis p62 levels are tune up to maintain the tumorigenic features of the cells. Furthermore, from a retrospective 5 year-follow up analysis of p62 expression in clinically-annotated primary melanomas it was demonstrated that p62 can be an independent prognostic indicator of patient outcome<sup>334</sup>.

Collectively, results obtained from databases and independent validation support the oncogenic roles of p62 in melanoma, especially in metastasis.

## 7.2 Pathophysiological roles of p62 *in vivo*

Genetically-modified mouse models (GEMM) have been instrumental in defining cell-type dependent roles of p62 in cancer development. For example, in GEMM of hepatocellular carcinoma (HCC), p62 was found to act as a sufficient and necessary oncogene in stressed cancer initiating cells (hepatocytes)<sup>260</sup>, but as a tumor suppressor in hepatic stellate cells<sup>308</sup>. Prostate cancer models have revealed also tumor suppressive functions of p62 exerted by rewiring the metabolism of stromal fibroblasts<sup>278</sup>. In this PhD thesis two GEMM were generated to dissect the contribution of p62 to melanoma progression. For the benign nevi, the *Tyr::CreERT2;Braf<sup>V600E</sup>* strain was crossed with *p62* mice (*p62<sup>+/+</sup>*, *p62<sup>-/+</sup>*, *p62<sup>-/-</sup>*). From these studies it was observed that the allelic loss of p62 (monoallelic and biallelic) was dispensable for the generation of benign melanocytic lesions. Moreover, melanomas were not developed in the presence or absence of p62. These findings (i) recapitulate our clinical data where the different types of nevi exhibit negative or very low levels of p62. (ii) Moreover, support that p62 is dispensable for the transformation of the benign nevi to melanomas in the context of these individual oncogenic changes *in vivo*. However, when *p62* mice (*p62<sup>+/+</sup>*, *p62<sup>-/+</sup>*, *p62<sup>-/-</sup>*) were crossed to *Tyr::CreERT2;Braf<sup>V600E</sup>;Pten<sup>-/-</sup>* strain, to recapitulate melanoma progression, the effect was different. Allelic loss of *p62* in these mice led to a significantly (i) compromised melanoma development, (ii) nodular and lung metastasis were diminished (iii) and the survival was extended. (iv) Interestingly, we observed that the p62-deficient microenvironment does not override the requirement for p62

in the melanoma tumors. Indeed, the contribution of stroma cells (where p62 levels are low) did not result in increased melanomagenesis when B16 melanoma cells were implanted in *p62 KO* mice. This is different as in the case of prostate cancer where the p62 negative expression of stromal fibroblasts led to epithelial cell proliferation<sup>278</sup>. These findings support the cell type specific roles of p62 in the contribution of tumor progression and also shed light to devising therapeutic strategies depending on the cancer type.

Autophagy has been shown to play complex roles in the regulation of cancer development and progression where p62 functions as a cargo receptor<sup>236</sup>. We and other, have shown that GEMM with defective autophagy lead to the accumulation of p62<sup>186,217,220,236</sup>. An important finding of this study was that p62 has distinct roles from autophagy in melanoma. Using GEMM and functional studies *in vitro* we found that p62 is not essential for autophagosome formation and the autophagic machinery. Classical autophagy markers did not change *in vitro* and *in vivo* upon p62 loss. Interestingly, *Atg5* defective melanoma mice (*TyrCre::ERT2;Braf<sup>V600E</sup>;Pten<sup>-/-</sup>;Atg5<sup>fl/fl</sup>*) with accumulated p62 aggregates display no synergistic effect in tumor progression when the mice were crossed with *p62 KO* mice. Thus p62 may be essential (clearance of ubiquitinated proteins) but it is not necessary for autophagy machinery during tumor progression. These results are supported from the fact that other cargo receptors including NBR1 (neighbor of BRCA1 gene 1) and NDP52 (nuclear dot protein 52), OPTN (optineurin), and TAX1BP1 (Tax1-binding protein 1)<sup>365,366</sup> can compensate the loss of p62 and act in the degradation process of autophagy. Of note, ablation of p62 in hepatocytes or pancreatic acinar cells does not result in any obvious autophagy defects<sup>260,302</sup>, suggesting that its function is redundant with that of other cargo receptors. Finally, the findings from proteomic studies strengthen our data that p62 acts beyond autophagy.

### **7.3 p62 known functions are not altered in melanoma**

---

The data obtained from human biopsies and the GEMM reinforced the concept of p62 as modulator of aggressive and metastatic potential. These data were supported by the significantly decreased melanoma metastatic signatures (obtained from GSEA) from the transcriptomic arrays in p62 depleted cells. Considering the pleiotropic effects of p62 in different cancer types our studies failed to characterize an active role of the protein to any of the known pathways described.

One well described role of p62 is the hyperactivation of mTOR pathway by tethering proteins to endo/lysosomes (e.g. Raptor and RAGs; TRAF6; MEKK3)<sup>282,283,339</sup> in prostate cancer. However, (i) through data mining in TCGA (ii) and functional studies *in vitro* it was found no dependency with *p62* expression. These data were supported from the

transcriptomic and proteomic studies where no enrichment of mTOR pathway was observed. Accordingly, the interactome analysis failed to identify mTOR related proteins as interactors of p62. The findings that p62 is not involved in mTOR activation, first support the hypothesis that p62 acts in a cell type specific manner. Secondly, it raises the possibility that this pathway can be regulated by other lysosomal genes where melanoma exploits a lineage-specific wiring of the endolysosomal pathway<sup>142</sup>. Thirdly, these studies were performed at basal conditions, where p62 was found essential to maintain malignant features of melanoma cells. It would be of high interest to explore the possible role of p62 under situations of cellular stress and nutrient availability where mTOR has been found to be hyperactivated by p62<sup>282,339</sup>.

In the same manner, studies for KEAP1-NRF2 pathway (antioxidant response) failed to show positive correlation with p62. Keap1 binds NRF2 and promotes its degradation in a p62-dependent manner<sup>247,367</sup>, whereas Keap1 itself is degraded through autophagy on p62 binding<sup>27</sup>. In cancer, NRF2 is stabilized by p62 via degradation of Keap1 resulting in the induction of antioxidant response elements<sup>199,306</sup>. Although p62 was found to interact with KEAP1 in the interactome arrays, our studies revealed no changes of both proteins (and downstream targets, such as NQO1) in melanoma. Various studies have shown that KEAP1-NRF2 pathway plays important role in cancer progression<sup>260,261,368,369</sup> through p62; however there are studies supporting that this pathway can be regulated in a p62 independent manner<sup>370,371</sup>. Thus, this suggests that in melanoma this pathway can be regulated independently of p62 or under stress conditions (ROS-inducers or chemotherapeutic agents) that need to be addressed in future studies.

NF- $\kappa$ B is considered to be a central player in linking inflammation and cancer<sup>372</sup> where previous studies have shown that p62 induces its activation in different diseases<sup>207,253,304,373,374</sup>. Following the same strategy, NF- $\kappa$ B downstream targets (phospho-p65, IKK $\beta$ ) were not correlated with p62 in melanoma cells. Moreover, NF- $\kappa$ B players were not found to interact with p62 in the interactome arrays.

p62 positively regulates MYC oncogene via (i) mTORC1<sup>260</sup>, (ii) KEAP1-NRF2<sup>260</sup> or by repressing the expression of the microRNAs let-7a/b<sup>277</sup>. In our study, neither correlation was observed (TCGA, *in vitro*) nor the stability of MYC was affected in p62 depleted cells (data not shown). A possible explanation comes from the fact that the above pathways were not affected by p62, consequently MYC levels remained stable.

Finally, the mitochondrial bioenergetics that p62 alters in other systems<sup>340</sup> remain stable in p62 depleted cells raising the possibility that other mitophagy related proteins (Parkin<sup>375</sup>, Optineurin<sup>376</sup>) act in a compensatory way in the absence of p62 in melanoma.

Overall, the above data indicated that the basal levels of p62 that are sufficient to maintain tumorigenesis in melanoma are not altering described pathways in other systems supporting the hypothesis of cell type specific roles of this protein.

#### **7.4 Novel roles of p62 in melanoma progression and metastasis**

---

Our initial studies to assess mechanistically how p62 maintains tumorigenesis and promotes metastasis indicated that this protein with the pleiotropic effects does not alter known pathways described in other systems. In the light of the above results, we decided to proceed to an unbiased transcriptomic, proteomic and interactome analyses in melanoma cells. Gene Set Enrichment Analyses (GSEA) in p62 shRNA-associated transcriptomic profiles identified a large variety of pro-tumorigenic factors in melanoma cells that included expected modulators of cell cycle and mitosis<sup>309,334</sup>. However, these studies also revealed mRNA-regulated factors not previously assigned to p62. Importantly, these included the gene signatures we and others had reported to be enriched in metastatic melanomas, as well as a large set of pro-metastatic factors with no reported links to this disease.

The proteomic analyses provides a useful platform for downstream targets that p62 regulates in melanoma. From this study the first observation was that the percentage of the affected proteins by p62 depletion was rather low (6.5% for SK-Mel-103 and 7% for UACC-62) indicating that p62 ultimately affects a rather restricted sets of proteins. Ingenuity Pathway Analysis (IPA) in p62 depleted cells identified molecular and cellular functions altered that are essential for the oncogenic features of the protein. Setting selection criteria to the identified proteins and combining data with RNA sequencing-based information from TCGA revealed that 24 of these proteins have been linked to melanoma with roles in invasion and metastasis; 9 of these proteins were found enriched in metastatic biopsies (**Figure 23**). However these proteins have not previously linked with p62 indicating it as an upstream regulator in melanoma. It will be interesting in future studies to characterize the connection of p62 with these proteins and shed light to new pathways that the protein is implicated.

Of interest, 6 proteins were identified with no previous link to melanoma (FERMT2, NEFL, LAMA2, UBA6, SPTBN1, GALNS) and two of them were found with positive roles in metastasis in other systems (FERMT2<sup>377,378</sup>, NEFL<sup>379,380</sup>). FERMT2 was more significantly enriched in metastatic melanoma (TCGA) and was found to be downregulated in both melanoma cell lines. FERMT2 is itself a signaling hub, best known for its roles in the binding and recycling of integrins<sup>381,382</sup>, and the activation of multiple signaling cascades involved in cell adhesion, cell motility and invasion<sup>342,383</sup>. To date, FERMT2 regulation has been reported primarily by post-transcriptional mechanisms, involving phosphorylation<sup>384,385</sup> and

integrin-dependent conformational changes<sup>386,387</sup>. We demonstrated the positive regulation of p62-FERMT2 (i) performing functional studies, (ii) using GEMM and (iii) a large cohort of human melanocytic lesions. Our studies identified FERMT2 as a physiologically-relevant novel indicator of poor prognosis in melanoma, acting downstream of p62. Although, the oncogenic potential of FERMT2 has been reported in other systems<sup>344,388-390</sup>, this is the first study that shows the clinical relevance of the protein in melanoma. In this context, the data suggested that these two proteins may have a clinical relevance in melanoma and can be used as potential biomarkers.

## 7.5 p62 interactors in the regulation of mRNA stability

---

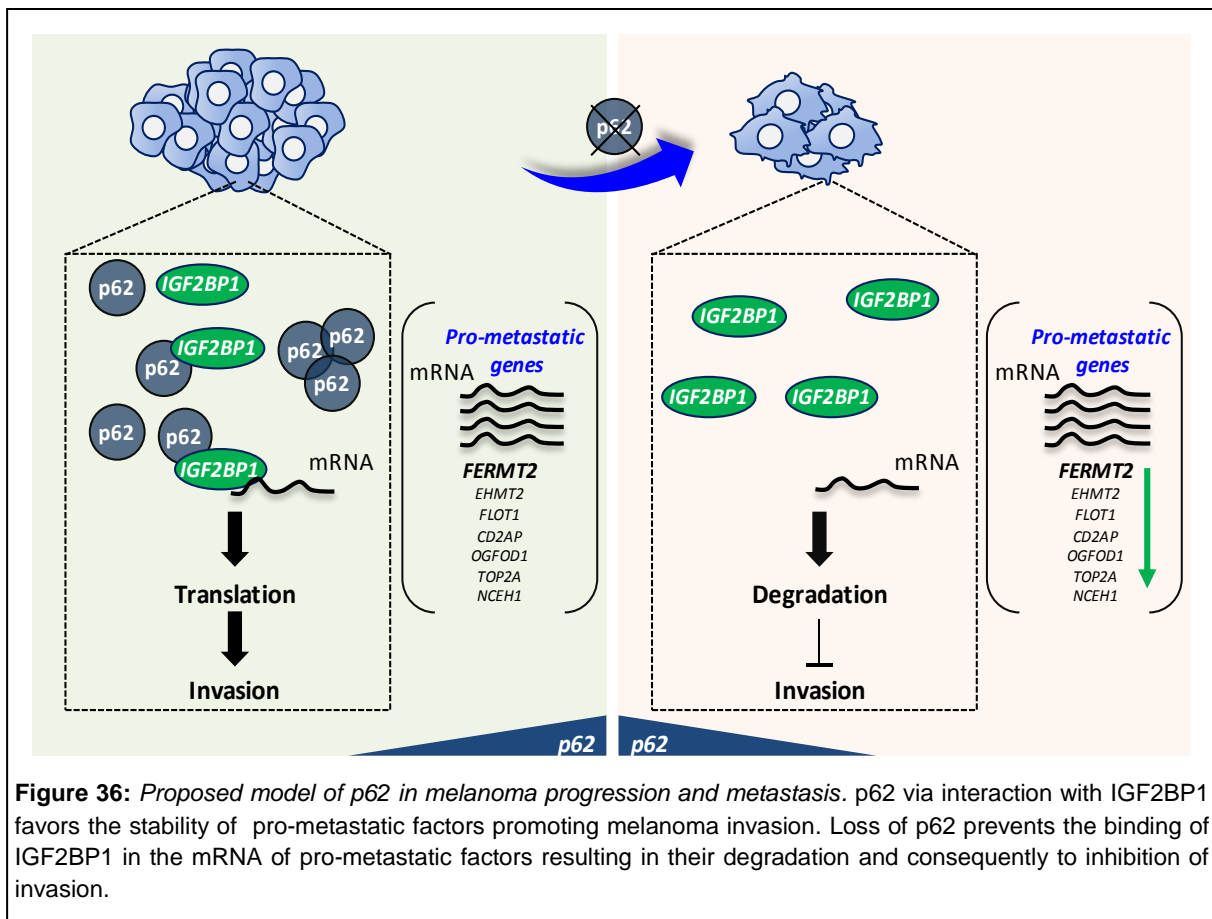
A relevant finding that stemmed from this PhD thesis was the identification of the interactors of p62 in melanoma which they were found to be distinct from other systems (BIOGRID) and they were specifically enriched in melanoma among other cancer cell lines (GSEA using as a reference the Cancer Cell Line Encyclopedia). This result comes in agreement with the above data that p62 is acting in a cell type specific manner controlling different signaling pathways. It is tempting to speculate that p62 adapts its activity depending on the cell type and the corresponding signals of the upstream regulators in order to act as a scaffold.

The most unanticipated finding of this study was the interaction of p62 with an increased number of RNA Binding Proteins (RBPs). The p62 interactors that corresponded to RBPs were almost 30% suggesting a new function of p62 as a hub for RBPs. Although, further studies need to be performed to address if the high number of RBPs are protein-protein interactions or p62 interacts with complexes of RBPs, these data imply possible roles of p62 in processes mediated through RBPs such as post-transcriptional gene regulation and RNA processing.

A fundamental role of RBPs (among others) is the regulation of mRNA stability<sup>391,392</sup>. The mRNAs are packaged into ribonucleoprotein particles (mRNPs). Thus, we investigated if any of the precipitated RBPs can directly regulate the stability of *FERMT2*. Our analyses indicated IGF2BP1 as the intermediate player acting in the p62-FERMT2 axis. Moreover, previous studies have shown the IGF2BP1 pro-metastatic roles in melanoma<sup>393,394</sup>. p62 via the interaction with IGF2BP1 stabilizes the mRNA of *FERMT2* resulting in protein translation. p62-mediated regulation linked to the inhibition of mRNA decay, offers therefore an additional strategy to sustain FERMT2 levels under situations of high demand for dynamic focal adhesions during invasive processes. Loss of p62 (i) prevents IGF2BP1 binding to *FERMT2*, (ii) destabilization and (iii) ultimately decreased invasive capacity of melanoma cells.

IGF2BP1 acts by preventing miRNA-mediated silencing, especially for the let-7 family<sup>395-399</sup>. It is possible that IGF2BP1 by counteracting miRNAs protects the degradation of *FERMT2* mRNA. Hence, through this mechanism *FERMT2* can favor the invasiveness of melanoma cells. This is an attractive scenario that needs to be investigated and more specifically it would be important to identify the miRNAs that can target *FERMT2* and also to characterize how *FERMT2* promotes invasion. Finally, it was observed that the p62-IGF2BP1 axis in mRNA decay is broader, as other pro-metastatic factors were regulated under similar settings as *FERMT2*. This implies that *FERMT2* and other pro-metastatic factors can positively promote invasion under the control of p62-IGF2BP1 axis (**Figure 36**).

Collectively, this PhD thesis underscores the relevance of p62 in melanoma progression and metastasis by unraveling a new mechanism of action, where p62 via interaction with RBPs can modulate the stability of pro-metastatic factors.



***VIII . CONCLUSIONS /  
CONCLUSIONES***

## Conclusions

---

In the light of the results presented in this PhD thesis we conclude the following:

1. Analyses of publicly available databases (TCGA and the CCLE) demonstrate that p62 is not a subject of heterozygous copy number loss in melanoma (as the case for ATG5). Instead, p62 was found to be overexpressed in human melanomas, especially at metastatic stages of the disease, a feature validated by histopathological analyses.
2. New Genetically Engineered Mouse Models (GEMM) revealed that p62 is dispensable for benign nevi, but it is required for the progression and the metastatic potential of malignant melanoma. These results distinguish melanoma from other tumor types where p62 exerts inhibitory roles via the stroma.
3. Targeted depletion of p62 compromises the proliferation and invasion capabilities of cultured melanoma cells, independently on the status of main melanoma-associated drivers (BRAF, NRAS, PTEN or p53).
4. Known roles of p62 in the modulation of mTOR, NF- $\kappa$ B, KEAP1-NRF2, MYC and mitochondrial respiration were not affected by targeted depletion or overexpression of p62 in melanoma cells (also different from other cancer types).
5. *In vitro* studies and newly generated GEMM revealed that p62 loss or ectopic expression does not affect autophagosome formation.
6. Transcriptome analyses and subsequent computational studies by GSEA identified melanoma-associated metastatic signatures significantly downregulated upon p62 downregulation.
7. A comprehensive transcriptomic/proteomic/interactomic approach identified downstream effectors of p62 implicated in metastasis. In particular, the scaffold protein FERMT2 was demonstrated to be a novel risk factor for poor prognosis in melanoma. Accordingly, p62 and FERMT2 were positively correlated in human melanoma biopsies.
8. Interactome analysis identified a large set of RNA Binding Proteins (RBPs) as new p62 binding partners. In particular, IGF2BP1 was validated as a p62-interacting factor that controls the mRNA half-life of *FERMT2*.

9. p62 was found to oppose mRNA decay of other pro-metastatic factors (i.e. EHMT2, CD2AP, TOP2A, FLOT1, OGFOD1, and NCEH1) through the interaction with IGF2BP1.

Collectively, the data presented in this PhD thesis underscore a novel mechanism of p62 in the stability of pro-metastatic factors via the interaction with RBPs.

## Conclusiones

---

A la luz de los resultados presentados en esta tesis doctoral, se presentan las siguientes conclusiones:

1. Un detallado análisis mediante bases de datos públicas (TCGA y CCLE) muestra que p62, a diferencia de ATG5, no está sujeto a una pérdida parcial del número de copias en melanoma. Por el contrario, se encuentra sobre-expresado especialmente en estadios metastásicos. Este dato se ha podido validar a través de estudios histopatológicos. .
2. Los experimentos con nuevos modelos de ratones modificados genéticamente revelan que p62 es prescindible en la formación de lesiones melanocíticas benignas (nevi), y sin embargo, es requerido en la iniciación y progresión del melanoma. Esto diferencia al melanoma de otros tumores, en los que p62 presenta un efecto inhibitorio a través del estroma.
3. La depleción de p62 *in vitro* compromete la capacidad proliferativa e invasiva de las células de melanoma en cultivo, con independencia del estado mutacional en los principales oncogenes como BRAF, NRAS, PTEN o p53.
4. Las funciones ya definidas de p62 en la modulación de factores como mTOR, NF- $\kappa$ B, KEAP1-NRF2, y MYC; o de procesos como la respiración mitocondrial, no se ven afectadas tras la supresión o expresión ectópica en células de melanoma. Esto remarca nuevamente el papel diferenciador de p62 en melanoma.
5. Tanto el silenciamiento como la sobreexpresión de p62 (*in vitro* o *in vivo*) carecen de efecto en la formación de autofagosomas.
6. Mediante análisis transcripcionales y estudios computacionales GSEA, se han podido identificar factores característicos asociados a la metástasis de melanoma cuya expresión disminuye al deplecionar p62.
7. Mediante un análisis global de la transcriptómica, proteómica e interactoma se han podido identificar proteínas efectoras de p62 implicadas en metástasis. En particular, hemos identificado la proteína de FERMT2 como un nuevo factor de riesgo y pronóstico desfavorable en pacientes de melanoma. Además, análisis histopatológicos de biopsias humanas confirman una correlación entre los niveles de p62 y FERMT2 .
8. El análisis del interactoma de p62 permitió identificar un grupo de proteínas de unión a RNA (RBPs) como nuevos factores de interacción. Entre ellos, se ha validado cómo

IGF2BP1 actúa como mediador en la regulación de la vida media del mRNA de FERMT2 por p62.

9. Además, la interacción de p62 con IGF2BP1 regula la estabilidad del mRNA de otros factores prometastáticos (EHMT2, CD2AP, TOP2A, FLOT1, OGFOD1, y NCEH1).

Todos los datos presentados en esta tesis confirman una nueva función de p62 como modulador de los niveles de factores pro-metastáticos a través de la interacción con RBPs.

## ***IX. REFERENCES***

1. Mort, R.L., Jackson, I.J. & Patton, E.E. The melanocyte lineage in development and disease. *Development* **142**, 620-632 (2015).
2. Maldonado, J.L., *et al.* Determinants of BRAF mutations in primary melanomas. *J Natl Cancer Inst* **95**, 1878-1890 (2003).
3. Long, G.V., *et al.* Prognostic and clinicopathologic associations of oncogenic BRAF in metastatic melanoma. *J Clin Oncol* **29**, 1239-1246 (2011).
4. Viros, A., *et al.* Improving melanoma classification by integrating genetic and morphologic features. *PLoS Med* **5**, e120 (2008).
5. Curtin, J.A., *et al.* Distinct sets of genetic alterations in melanoma. *N Engl J Med* **353**, 2135-2147 (2005).
6. Garbe, C., *et al.* Diagnosis and treatment of melanoma. European consensus-based interdisciplinary guideline--Update 2012. *Eur J Cancer* **48**, 2375-2390 (2012).
7. Coit, D.G., *et al.* Melanoma, version 2.2013: featured updates to the NCCN guidelines. *J Natl Compr Canc Netw* **11**, 395-407 (2013).
8. Miller, A.J. & Mihm, M.C., Jr. Melanoma. *N Engl J Med* **355**, 51-65 (2006).
9. Schadendorf, D., *et al.* Melanoma. *Nature Reviews Disease Primers*, 15055 (2015).
10. Scott, K.L., *et al.* Proinvasion metastasis drivers in early-stage melanoma are oncogenes. *Cancer Cell* **20**, 92-103 (2011).
11. Mayor, R. & Theveneau, E. The neural crest. *Development* **140**, 2247-2251 (2013).
12. Dupin, E. & Le Douarin, N.M. Development of melanocyte precursors from the vertebrate neural crest. *Oncogene* **22**, 3016-3023 (2003).
13. Zabierowski, S.E. & Herlyn, M. Embryonic stem cells as a model for studying melanocyte development. *Methods Mol Biol* **584**, 301-316 (2010).
14. Lin, J.Y. & Fisher, D.E. Melanocyte biology and skin pigmentation. *Nature* **445**, 843-850 (2007).
15. Kanitakis, J. Anatomy, histology and immunohistochemistry of normal human skin. *Eur J Dermatol* **12**, 390-399; quiz 400-391 (2002).
16. Jimbow, K., Roth, S.I., Fitzpatrick, T.B. & Szabo, G. Mitotic activity in non-neoplastic melanocytes in vivo as determined by histochemical, autoradiographic, and electron microscope studies. *J Cell Biol* **66**, 663-670 (1975).
17. Costin, G.E. & Hearing, V.J. Human skin pigmentation: melanocytes modulate skin color in response to stress. *FASEB J* **21**, 976-994 (2007).
18. Kaidbey, K.H., Agin, P.P., Sayre, R.M. & Kligman, A.M. Photoprotection by melanin--a comparison of black and Caucasian skin. *J Am Acad Dermatol* **1**, 249-260 (1979).
19. Cui, R., *et al.* Central role of p53 in the suntan response and pathologic hyperpigmentation. *Cell* **128**, 853-864 (2007).
20. Rodriguez, C.I. & Setaluri, V. Cyclic AMP (cAMP) signaling in melanocytes and melanoma. *Arch Biochem Biophys* **563**, 22-27 (2014).
21. Gaggioli, C., Busca, R., Abbe, P., Ortonne, J.P. & Ballotti, R. Microphthalmia-associated transcription factor (MITF) is required but is not sufficient to induce the expression of melanogenic genes. *Pigment Cell Res* **16**, 374-382 (2003).
22. Vetrini, F., *et al.* The microphthalmia transcription factor (Mitf) controls expression of the ocular albinism type 1 gene: link between melanin synthesis and melanosome biogenesis. *Mol Cell Biol* **24**, 6550-6559 (2004).
23. Hoek, K.S., *et al.* Novel MITF targets identified using a two-step DNA microarray strategy. *Pigment Cell Melanoma Res* **21**, 665-676 (2008).
24. Chiaverini, C., *et al.* Microphthalmia-associated transcription factor regulates RAB27A gene expression and controls melanosome transport. *J Biol Chem* **283**, 12635-12642 (2008).
25. Schouwey, K., *et al.* Notch1 and Notch2 receptors influence progressive hair graying in a dose-dependent manner. *Dev Dyn* **236**, 282-289 (2007).

26. Osawa, M., *et al.* Molecular characterization of melanocyte stem cells in their niche. *Development* **132**, 5589-5599 (2005).
27. Takeda, K., *et al.* Induction of melanocyte-specific microphthalmia-associated transcription factor by Wnt-3a. *J Biol Chem* **275**, 14013-14016 (2000).
28. Shibahara, S., *et al.* Regulation of pigment cell-specific gene expression by MITF. *Pigment Cell Res* **13 Suppl 8**, 98-102 (2000).
29. Moriyama, M., *et al.* Notch signaling via Hes1 transcription factor maintains survival of melanoblasts and melanocyte stem cells. *J Cell Biol* **173**, 333-339 (2006).
30. Lang, D., *et al.* Pax3 functions at a nodal point in melanocyte stem cell differentiation. *Nature* **433**, 884-887 (2005).
31. Aoki, Y., *et al.* Sox10 regulates the development of neural crest-derived melanocytes in Xenopus. *Dev Biol* **259**, 19-33 (2003).
32. Bastian, B.C. The molecular pathology of melanoma: an integrated taxonomy of melanocytic neoplasia. *Annu Rev Pathol* **9**, 239-271 (2014).
33. Harbour, J.W., *et al.* Recurrent mutations at codon 625 of the splicing factor SF3B1 in uveal melanoma. *Nat Genet* **45**, 133-135 (2013).
34. Van Raamsdonk, C.D., *et al.* Mutations in GNA11 in uveal melanoma. *N Engl J Med* **363**, 2191-2199 (2010).
35. Luke, J.J., Flaherty, K.T., Ribas, A. & Long, G.V. Targeted agents and immunotherapies: optimizing outcomes in melanoma. *Nat Rev Clin Oncol* (2017).
36. Zalaudek, I., *et al.* Frequency of dermoscopic nevus subtypes by age and body site: a cross-sectional study. *Arch Dermatol* **147**, 663-670 (2011).
37. Holly, E.A., Kelly, J.W., Shpall, S.N. & Chiu, S.H. Number of melanocytic nevi as a major risk factor for malignant melanoma. *J Am Acad Dermatol* **17**, 459-468 (1987).
38. English, J.S., *et al.* Site-specific melanocytic naevus counts as predictors of whole body naevi. *Br J Dermatol* **118**, 641-644 (1988).
39. Shain, A.H. & Bastian, B.C. From melanocytes to melanomas. *Nat Rev Cancer* **16**, 345-358 (2016).
40. Kincannon, J. & Boutzale, C. The physiology of pigmented nevi. *Pediatrics* **104**, 1042-1045 (1999).
41. Argenziano, G., Zalaudek, I., Ferrara, G., Hofmann-Wellenhof, R. & Soyer, H.P. Proposal of a new classification system for melanocytic naevi. *Br J Dermatol* **157**, 217-227 (2007).
42. Ichii-Nakato, N., *et al.* High frequency of BRAFV600E mutation in acquired nevi and small congenital nevi, but low frequency of mutation in medium-sized congenital nevi. *J Invest Dermatol* **126**, 2111-2118 (2006).
43. Bastian, B.C., LeBoit, P.E. & Pinkel, D. Mutations and copy number increase of HRAS in Spitz nevi with distinctive histopathological features. *Am J Pathol* **157**, 967-972 (2000).
44. Murali, R., McCarthy, S.W. & Scolyer, R.A. Blue nevi and related lesions: a review highlighting atypical and newly described variants, distinguishing features and diagnostic pitfalls. *Adv Anat Pathol* **16**, 365-382 (2009).
45. Shain, A.H., *et al.* The Genetic Evolution of Melanoma from Precursor Lesions. *N Engl J Med* **373**, 1926-1936 (2015).
46. Duffy, K. & Grossman, D. The dysplastic nevus: from historical perspective to management in the modern era: part I. Historical, histologic, and clinical aspects. *J Am Acad Dermatol* **67**, 1 e1-16; quiz 17-18 (2012).
47. Tucker, M.A., *et al.* Clinically recognized dysplastic nevi. A central risk factor for cutaneous melanoma. *JAMA* **277**, 1439-1444 (1997).
48. Shors, A.R., *et al.* Dysplastic naevi with moderate to severe histological dysplasia: a risk factor for melanoma. *Br J Dermatol* **155**, 988-993 (2006).
49. Tucker, M.A., *et al.* A natural history of melanomas and dysplastic nevi: an atlas of lesions in melanoma-prone families. *Cancer* **94**, 3192-3209 (2002).

50. Carr, J. & Mackie, R.M. Point mutations in the N-ras oncogene in malignant melanoma and congenital naevi. *Br J Dermatol* **131**, 72-77 (1994).
51. Pollock, P.M., *et al.* High frequency of BRAF mutations in nevi. *Nat Genet* **33**, 19-20 (2003).
52. Van Raamsdonk, C.D., *et al.* Frequent somatic mutations of GNAQ in uveal melanoma and blue naevi. *Nature* **457**, 599-602 (2009).
53. Michaloglou, C., *et al.* BRAFE600-associated senescence-like cell cycle arrest of human naevi. *Nature* **436**, 720-724 (2005).
54. Campisi, J. & d'Adda di Fagagna, F. Cellular senescence: when bad things happen to good cells. *Nat Rev Mol Cell Biol* **8**, 729-740 (2007).
55. Mancianti, M.L., *et al.* Growth and phenotypic characteristics of human nevus cells in culture. *J Invest Dermatol* **90**, 134-141 (1988).
56. Soo, J.K., *et al.* Malignancy without immortality? Cellular immortalization as a possible late event in melanoma progression. *Pigment Cell Melanoma Res* **24**, 490-503 (2011).
57. Tsao, H., Chin, L., Garraway, L.A. & Fisher, D.E. Melanoma: from mutations to medicine. *Genes Dev* **26**, 1131-1155 (2012).
58. Pacheco, I., Buzea, C. & Tron, V. Towards new therapeutic approaches for malignant melanoma. *Expert Rev Mol Med* **13**, e33 (2011).
59. Lo, J.A. & Fisher, D.E. The melanoma revolution: from UV carcinogenesis to a new era in therapeutics. *Science* **346**, 945-949 (2014).
60. Clark, W.H., Jr., From, L., Bernardino, E.A. & Mihm, M.C. The histogenesis and biologic behavior of primary human malignant melanomas of the skin. *Cancer Res* **29**, 705-727 (1969).
61. LeBoit, P.E. *Pathology and genetics of skin tumours*, (IARC, 2006).
62. Langley, R.G. & Sober, A.J. Clinical recognition of melanoma and its precursors. *Hematol Oncol Clin North Am* **12**, 699-715, v (1998).
63. Gilchrest, B.A., Eller, M.S., Geller, A.C. & Yaar, M. The pathogenesis of melanoma induced by ultraviolet radiation. *N Engl J Med* **340**, 1341-1348 (1999).
64. Liu, V. & Mihm, M.C. Pathology of malignant melanoma. *Surg Clin North Am* **83**, 31-60, v (2003).
65. Arrangoiz, R., *et al.* Melanoma Review: Epidemiology, Risk Factors, Diagnosis and Staging. *Journal of Cancer Treatment and Research* **4**, 1-15 (2016).
66. Plotnick, H., Rachmaninoff, N. & VandenBerg, H.J., Jr. Polypoid melanoma: a virulent variant of nodular melanoma. Report of three cases and literature review. *J Am Acad Dermatol* **23**, 880-884 (1990).
67. Coleman, W.P., 3rd, Loria, P.R., Reed, R.J. & Kremenz, E.T. Acral lentiginous melanoma. *Arch Dermatol* **116**, 773-776 (1980).
68. Cohen, L.M. Lentigo maligna and lentigo maligna melanoma. *J Am Acad Dermatol* **33**, 923-936; quiz 937-940 (1995).
69. Tannous, Z.S., Lerner, L.H., Duncan, L.M., Mihm, M.C., Jr. & Flotte, T.J. Progression to invasive melanoma from malignant melanoma in situ, lentigo maligna type. *Hum Pathol* **31**, 705-708 (2000).
70. Singh, A.D., Kalyani, P. & Topham, A. Estimating the risk of malignant transformation of a choroidal nevus. *Ophthalmology* **112**, 1784-1789 (2005).
71. Singh, A.D., Turell, M.E. & Topham, A.K. Uveal melanoma: trends in incidence, treatment, and survival. *Ophthalmology* **118**, 1881-1885 (2011).
72. Ballester Sanchez, R., de Unamuno Bustos, B., Navarro Mira, M. & Botella Estrada, R. Mucosal melanoma: an update. *Actas Dermosifiliogr* **106**, 96-103 (2015).
73. Hanahan, D. & Weinberg, R.A. Hallmarks of cancer: the next generation. *Cell* **144**, 646-674 (2011).
74. Elder, D.E. Pathology of melanoma. *Clin Cancer Res* **12**, 2308s-2311s (2006).

75. Clark, W.H., Jr., *et al.* A study of tumor progression: the precursor lesions of superficial spreading and nodular melanoma. *Hum Pathol* **15**, 1147-1165 (1984).
76. Braig, M. & Schmitt, C.A. Oncogene-induced senescence: putting the brakes on tumor development. *Cancer Res* **66**, 2881-2884 (2006).
77. Bauer, J., Curtin, J.A., Pinkel, D. & Bastian, B.C. Congenital melanocytic nevi frequently harbor NRAS mutations but no BRAF mutations. *J Invest Dermatol* **127**, 179-182 (2007).
78. Serrano, M., Lin, A.W., McCurrach, M.E., Beach, D. & Lowe, S.W. Oncogenic ras provokes premature cell senescence associated with accumulation of p53 and p16INK4a. *Cell* **88**, 593-602 (1997).
79. Kamijo, T., *et al.* Tumor suppression at the mouse INK4a locus mediated by the alternative reading frame product p19ARF. *Cell* **91**, 649-659 (1997).
80. Bianchi-Smiraglia, A. & Nikiforov, M.A. Controversial aspects of oncogene-induced senescence. *Cell Cycle* **11**, 4147-4151 (2012).
81. Cotter, M.A., Florell, S.R., Leachman, S.A. & Grossman, D. Absence of senescence-associated beta-galactosidase activity in human melanocytic nevi in vivo. *J Invest Dermatol* **127**, 2469-2471 (2007).
82. Gray-Schopfer, V.C., Soo, J.K. & Bennett, D.C. Comment on "Absence of senescence-associated beta-galactosidase activity in human melanocytic nevi in vivo". *J Invest Dermatol* **128**, 1581; author reply 1583-1584 (2008).
83. Michaloglou, C., Soengas, M.S., Mooi, W.J. & Peeper, D.S. Comment on "Absence of senescence-associated beta-galactosidase activity in human melanocytic nevi in vivo". *J Invest Dermatol* **128**, 1582-1583; author reply 1583-1584 (2008).
84. Tran, S.L., *et al.* Absence of distinguishing senescence traits in human melanocytic nevi. *J Invest Dermatol* **132**, 2226-2234 (2012).
85. Khodadoust, M.S., *et al.* Melanoma proliferation and chemoresistance controlled by the DEK oncogene. *Cancer Res* **69**, 6405-6413 (2009).
86. Zhuang, D., *et al.* C-MYC overexpression is required for continuous suppression of oncogene-induced senescence in melanoma cells. *Oncogene* **27**, 6623-6634 (2008).
87. Biroccio, A., Amodei, S., Antonelli, A., Benassi, B. & Zupi, G. Inhibition of c-Myc oncoprotein limits the growth of human melanoma cells by inducing cellular crisis. *J Biol Chem* **278**, 35693-35701 (2003).
88. Thompson, J.F., Scolyer, R.A. & Kefford, R.F. Cutaneous melanoma. *Lancet* **365**, 687-701 (2005).
89. Nobori, T., *et al.* Deletions of the cyclin-dependent kinase-4 inhibitor gene in multiple human cancers. *Nature* **368**, 753-756 (1994).
90. Kamb, A., *et al.* A cell cycle regulator potentially involved in genesis of many tumor types. *Science* **264**, 436-440 (1994).
91. Steck, P.A., *et al.* Identification of a candidate tumour suppressor gene, MMAC1, at chromosome 10q23.3 that is mutated in multiple advanced cancers. *Nat Genet* **15**, 356-362 (1997).
92. Li, J., *et al.* PTEN, a putative protein tyrosine phosphatase gene mutated in human brain, breast, and prostate cancer. *Science* **275**, 1943-1947 (1997).
93. Wu, H., Goel, V. & Haluska, F.G. PTEN signaling pathways in melanoma. *Oncogene* **22**, 3113-3122 (2003).
94. Gimotty, P.A., *et al.* Biologic and prognostic significance of dermal Ki67 expression, mitoses, and tumorigenicity in thin invasive cutaneous melanoma. *J Clin Oncol* **23**, 8048-8056 (2005).
95. Genomic Classification of Cutaneous Melanoma. *Cell* **161**, 1681-1696 (2015).
96. Menzies, A.M., *et al.* Distinguishing clinicopathologic features of patients with V600E and V600K BRAF-mutant metastatic melanoma. *Clin Cancer Res* **18**, 3242-3249 (2012).
97. Krauthammer, M., *et al.* Exome sequencing identifies recurrent mutations in NF1 and RASopathy genes in sun-exposed melanomas. *Nat Genet* **47**, 996-1002 (2015).

98. Shain, A.H., *et al.* Exome sequencing of desmoplastic melanoma identifies recurrent NFKBIE promoter mutations and diverse activating mutations in the MAPK pathway. *Nat Genet* **47**, 1194-1199 (2015).
99. Weinstock, M.A. & Sober, A.J. The risk of progression of lentigo maligna to lentigo maligna melanoma. *Br J Dermatol* **116**, 303-310 (1987).
100. Balch, C.M., *et al.* Final version of 2009 AJCC melanoma staging and classification. *J Clin Oncol* **27**, 6199-6206 (2009).
101. Bauer, J. & Bastian, B.C. Distinguishing melanocytic nevi from melanoma by DNA copy number changes: comparative genomic hybridization as a research and diagnostic tool. *Dermatol Ther* **19**, 40-49 (2006).
102. Bastian, B.C., LeBoit, P.E., Hamm, H., Brocker, E.B. & Pinkel, D. Chromosomal gains and losses in primary cutaneous melanomas detected by comparative genomic hybridization. *Cancer Res* **58**, 2170-2175 (1998).
103. van Kempen, L.C., van Muijen, G.N. & Ruiter, D.J. Melanoma progression in a changing environment. *Eur J Cell Biol* **86**, 65-67 (2007).
104. Brychtova, S., *et al.* *Stromal Microenvironment Alterations in Malignant Melanoma*, (INTECH Open Access Publisher, 2011).
105. Postow, M.A., Harding, J. & Wolchok, J.D. Targeting immune checkpoints: releasing the restraints on anti-tumor immunity for patients with melanoma. *Cancer J* **18**, 153-159 (2012).
106. Karagiannis, P., *et al.* IgG4 subclass antibodies impair antitumor immunity in melanoma. *J Clin Invest* **123**, 1457-1474 (2013).
107. Damsky, W.E., Rosenbaum, L.E. & Bosenberg, M. Decoding melanoma metastasis. *Cancers (Basel)* **3**, 126-163 (2010).
108. Morton, D.L., *et al.* Final trial report of sentinel-node biopsy versus nodal observation in melanoma. *N Engl J Med* **370**, 599-609 (2014).
109. Balch, C.M., *et al.* Efficacy of an elective regional lymph node dissection of 1 to 4 mm thick melanomas for patients 60 years of age and younger. *Ann Surg* **224**, 255-263; discussion 263-256 (1996).
110. Reid, A.L., *et al.* Markers of circulating tumour cells in the peripheral blood of patients with melanoma correlate with disease recurrence and progression. *Br J Dermatol* **168**, 85-92 (2013).
111. Ulmer, A., *et al.* Immunomagnetic enrichment, genomic characterization, and prognostic impact of circulating melanoma cells. *Clin Cancer Res* **10**, 531-537 (2004).
112. Sanborn, J.Z., *et al.* Phylogenetic analyses of melanoma reveal complex patterns of metastatic dissemination. *Proc Natl Acad Sci U S A* **112**, 10995-11000 (2015).
113. Wagle, N., *et al.* Dissecting therapeutic resistance to RAF inhibition in melanoma by tumor genomic profiling. *J Clin Oncol* **29**, 3085-3096 (2011).
114. Peinado, H., Lavotshkin, S. & Lyden, D. The secreted factors responsible for pre-metastatic niche formation: old sayings and new thoughts. *Semin Cancer Biol* **21**, 139-146 (2011).
115. Liu, Y. & Cao, X. Organotropic metastasis: role of tumor exosomes. *Cell Res* **26**, 149-150 (2016).
116. Hoshino, A., *et al.* Tumour exosome integrins determine organotropic metastasis. *Nature* **527**, 329-335 (2015).
117. Lazar, I., *et al.* Proteome characterization of melanoma exosomes reveals a specific signature for metastatic cell lines. *Pigment Cell Melanoma Res* **28**, 464-475 (2015).
118. Damsky, W.E., Theodosakis, N. & Bosenberg, M. Melanoma metastasis: new concepts and evolving paradigms. *Oncogene* **33**, 2413-2422 (2014).
119. Gruber, S.B., Barnhill, R.L., Stenn, K.S. & Roush, G.C. Nevomelanocytic proliferations in association with cutaneous malignant melanoma: a multivariate analysis. *J Am Acad Dermatol* **21**, 773-780 (1989).

120. Tsao, H., Bevona, C., Goggins, W. & Quinn, T. The transformation rate of moles (melanocytic nevi) into cutaneous melanoma: a population-based estimate. *Arch Dermatol* **139**, 282-288 (2003).
121. Morton, D.L., Davtyan, D.G., Wanek, L.A., Foshag, L.J. & Cochran, A.J. Multivariate analysis of the relationship between survival and the microstage of primary melanoma by Clark level and Breslow thickness. *Cancer* **71**, 3737-3743 (1993).
122. Dickson, P.V. & Gershenwald, J.E. Staging and prognosis of cutaneous melanoma. *Surg Oncol Clin N Am* **20**, 1-17 (2011).
123. Amin, M.B., *et al.* The Eighth Edition AJCC Cancer Staging Manual: Continuing to build a bridge from a population-based to a more "personalized" approach to cancer staging. *CA Cancer J Clin* **67**, 93-99 (2017).
124. Lawrence, M.S., *et al.* Mutational heterogeneity in cancer and the search for new cancer-associated genes. *Nature* **499**, 214-218 (2013).
125. Hodis, E., *et al.* A landscape of driver mutations in melanoma. *Cell* **150**, 251-263 (2012).
126. Rakosy, Z., *et al.* Integrative genomics identifies gene signature associated with melanoma ulceration. *PLoS One* **8**, e54958 (2013).
127. Mann, G.J., *et al.* BRAF mutation, NRAS mutation, and the absence of an immune-related expressed gene profile predict poor outcome in patients with stage III melanoma. *J Invest Dermatol* **133**, 509-517 (2013).
128. Miller, D.M. & Flaherty, K.T. Cyclin-dependent kinases as therapeutic targets in melanoma. *Pigment Cell Melanoma Res* **27**, 351-365 (2014).
129. Chin, L., *et al.* Cooperative effects of INK4a and ras in melanoma susceptibility in vivo. *Genes Dev* **11**, 2822-2834 (1997).
130. Sharpless, N.E., Kannan, K., Xu, J., Bosenberg, M.W. & Chin, L. Both products of the mouse Ink4a/Arf locus suppress melanoma formation in vivo. *Oncogene* **22**, 5055-5059 (2003).
131. Dovey, M., White, R.M. & Zon, L.I. Oncogenic NRAS cooperates with p53 loss to generate melanoma in zebrafish. *Zebrafish* **6**, 397-404 (2009).
132. Bardeesy, N., *et al.* Dual inactivation of RB and p53 pathways in RAS-induced melanomas. *Mol Cell Biol* **21**, 2144-2153 (2001).
133. Garraway, L.A. & Sellers, W.R. Lineage dependency and lineage-survival oncogenes in human cancer. *Nat Rev Cancer* **6**, 593-602 (2006).
134. Garraway, L.A., *et al.* Integrative genomic analyses identify MITF as a lineage survival oncogene amplified in malignant melanoma. *Nature* **436**, 117-122 (2005).
135. Levy, C., Khaled, M. & Fisher, D.E. MITF: master regulator of melanocyte development and melanoma oncogene. *Trends Mol Med* **12**, 406-414 (2006).
136. Du, J., *et al.* Critical role of CDK2 for melanoma growth linked to its melanocyte-specific transcriptional regulation by MITF. *Cancer Cell* **6**, 565-576 (2004).
137. Giuliano, S., *et al.* Microphthalmia-associated transcription factor controls the DNA damage response and a lineage-specific senescence program in melanomas. *Cancer Res* **70**, 3813-3822 (2010).
138. Carreira, S., *et al.* Mitf regulation of Dia1 controls melanoma proliferation and invasiveness. *Genes Dev* **20**, 3426-3439 (2006).
139. Cheli, Y., *et al.* Mitf is the key molecular switch between mouse or human melanoma initiating cells and their differentiated progeny. *Oncogene* **30**, 2307-2318 (2011).
140. Strub, T., *et al.* Essential role of microphthalmia transcription factor for DNA replication, mitosis and genomic stability in melanoma. *Oncogene* **30**, 2319-2332 (2011).
141. Goding, C.R. Commentary. A picture of Mitf in melanoma immortality. *Oncogene* **30**, 2304-2306 (2011).
142. Alonso-Curbelo, D., *et al.* RAB7 controls melanoma progression by exploiting a lineage-specific wiring of the endolysosomal pathway. *Cancer Cell* **26**, 61-76 (2014).

143. Solimini, N.L., Luo, J. & Elledge, S.J. Non-oncogene addiction and the stress phenotype of cancer cells. *Cell* **130**, 986-988 (2007).
144. Luo, J., Solimini, N.L. & Elledge, S.J. Principles of cancer therapy: oncogene and non-oncogene addiction. *Cell* **136**, 823-837 (2009).
145. Maiuri, M.C., Zalckvar, E., Kimchi, A. & Kroemer, G. Self-eating and self-killing: crosstalk between autophagy and apoptosis. *Nat Rev Mol Cell Biol* **8**, 741-752 (2007).
146. De Duve, C. & Wattiaux, R. Functions of lysosomes. *Annu Rev Physiol* **28**, 435-492 (1966).
147. Mizushima, N. & Komatsu, M. Autophagy: renovation of cells and tissues. *Cell* **147**, 728-741 (2011).
148. Sahu, R., *et al.* Microautophagy of cytosolic proteins by late endosomes. *Dev Cell* **20**, 131-139 (2011).
149. Cuervo, A.M. & Wong, E. Chaperone-mediated autophagy: roles in disease and aging. *Cell Res* **24**, 92-104 (2014).
150. Kissova, I., Deffieu, M., Manon, S. & Camougrand, N. Uth1p is involved in the autophagic degradation of mitochondria. *J Biol Chem* **279**, 39068-39074 (2004).
151. Lemasters, J.J. Selective mitochondrial autophagy, or mitophagy, as a targeted defense against oxidative stress, mitochondrial dysfunction, and aging. *Rejuvenation Res* **8**, 3-5 (2005).
152. Sakai, Y., Oku, M., van der Klei, I.J. & Kiel, J.A. Pexophagy: autophagic degradation of peroxisomes. *Biochim Biophys Acta* **1763**, 1767-1775 (2006).
153. Till, A., Lakhani, R., Burnett, S.F. & Subramani, S. Pexophagy: the selective degradation of peroxisomes. *Int J Cell Biol* **2012**, 512721 (2012).
154. Bernales, S., Schuck, S. & Walter, P. ER-phagy: selective autophagy of the endoplasmic reticulum. *Autophagy* **3**, 285-287 (2007).
155. Kraft, C., Deplazes, A., Sohrmann, M. & Peter, M. Mature ribosomes are selectively degraded upon starvation by an autophagy pathway requiring the Ubp3p/Bre5p ubiquitin protease. *Nat Cell Biol* **10**, 602-610 (2008).
156. Mah, L.Y. & Ryan, K.M. Autophagy and cancer. *Cold Spring Harb Perspect Biol* **4**, a008821 (2012).
157. Reggiori, F. & Klionsky, D.J. Autophagosomes: biogenesis from scratch? *Curr Opin Cell Biol* **17**, 415-422 (2005).
158. Rosenfeldt, M.T. & Ryan, K.M. The role of autophagy in tumour development and cancer therapy. *Expert Rev Mol Med* **11**, e36 (2009).
159. Kawamata, T., Kamada, Y., Kabeya, Y., Sekito, T. & Ohsumi, Y. Organization of the pre-autophagosomal structure responsible for autophagosome formation. *Mol Biol Cell* **19**, 2039-2050 (2008).
160. Inoki, K., Kim, J. & Guan, K.L. AMPK and mTOR in cellular energy homeostasis and drug targets. *Annu Rev Pharmacol Toxicol* **52**, 381-400 (2012).
161. Hosokawa, N., *et al.* Nutrient-dependent mTORC1 association with the ULK1-Atg13-FIP200 complex required for autophagy. *Mol Biol Cell* **20**, 1981-1991 (2009).
162. Weidberg, H., *et al.* LC3 and GATE-16/GABARAP subfamilies are both essential yet act differently in autophagosome biogenesis. *EMBO J* **29**, 1792-1802 (2010).
163. McEwan, D.G. & Dikic, I. The Three Musketeers of Autophagy: phosphorylation, ubiquitylation and acetylation. *Trends Cell Biol* **21**, 195-201 (2011).
164. Tanida, I., Ueno, T. & Kominami, E. LC3 conjugation system in mammalian autophagy. *Int J Biochem Cell Biol* **36**, 2503-2518 (2004).
165. Levine, B. & Klionsky, D.J. Development by self-digestion: molecular mechanisms and biological functions of autophagy. *Dev Cell* **6**, 463-477 (2004).
166. Yu, L., *et al.* Termination of autophagy and reformation of lysosomes regulated by mTOR. *Nature* **465**, 942-946 (2010).

167. Rosenfeldt, M.T. & Ryan, K.M. The multiple roles of autophagy in cancer. *Carcinogenesis* **32**, 955-963 (2011).
168. Axe, E.L., *et al.* Autophagosome formation from membrane compartments enriched in phosphatidylinositol 3-phosphate and dynamically connected to the endoplasmic reticulum. *J Cell Biol* **182**, 685-701 (2008).
169. Hayashi-Nishino, M., *et al.* A subdomain of the endoplasmic reticulum forms a cradle for autophagosome formation. *Nat Cell Biol* **11**, 1433-1437 (2009).
170. Yla-Anttila, P., Vihinen, H., Jokitalo, E. & Eskelinen, E.L. 3D tomography reveals connections between the phagophore and endoplasmic reticulum. *Autophagy* **5**, 1180-1185 (2009).
171. Hailey, D.W., *et al.* Mitochondria supply membranes for autophagosome biogenesis during starvation. *Cell* **141**, 656-667 (2010).
172. Morselli, E., *et al.* Oncosuppressive functions of autophagy. *Antioxid Redox Signal* **14**, 2251-2269 (2011).
173. Galluzzi, L., Bravo-San Pedro, J.M. & Kroemer, G. Autophagy Mediates Tumor Suppression via Cellular Senescence. *Trends Cell Biol* **26**, 1-3 (2016).
174. Kroemer, G., Marino, G. & Levine, B. Autophagy and the integrated stress response. *Mol Cell* **40**, 280-293 (2010).
175. Guo, J.Y., Xia, B. & White, E. Autophagy-mediated tumor promotion. *Cell* **155**, 1216-1219 (2013).
176. Galluzzi, L., *et al.* Autophagy in malignant transformation and cancer progression. *EMBO J* **34**, 856-880 (2015).
177. Lebovitz, C.B., *et al.* Cross-cancer profiling of molecular alterations within the human autophagy interaction network. *Autophagy* **11**, 1668-1687 (2015).
178. Amaravadi, R., Kimmelman, A.C. & White, E. Recent insights into the function of autophagy in cancer. *Genes Dev* **30**, 1913-1930 (2016).
179. Aita, V.M., *et al.* Cloning and genomic organization of beclin 1, a candidate tumor suppressor gene on chromosome 17q21. *Genomics* **59**, 59-65 (1999).
180. Liang, X.H., *et al.* Induction of autophagy and inhibition of tumorigenesis by beclin 1. *Nature* **402**, 672-676 (1999).
181. Qu, X., *et al.* Promotion of tumorigenesis by heterozygous disruption of the beclin 1 autophagy gene. *J Clin Invest* **112**, 1809-1820 (2003).
182. Yue, Z., Jin, S., Yang, C., Levine, A.J. & Heintz, N. Beclin 1, an autophagy gene essential for early embryonic development, is a haploinsufficient tumor suppressor. *Proc Natl Acad Sci U S A* **100**, 15077-15082 (2003).
183. Cianfanelli, V., *et al.* AMBRA1 links autophagy to cell proliferation and tumorigenesis by promoting c-Myc dephosphorylation and degradation. *Nat Cell Biol* **17**, 20-30 (2015).
184. Tang, H., *et al.* Decreased BECN1 mRNA Expression in Human Breast Cancer is Associated with Estrogen Receptor-Negative Subtypes and Poor Prognosis. *EBioMedicine* **2**, 255-263 (2015).
185. Laddha, S.V., Ganesan, S., Chan, C.S. & White, E. Mutational landscape of the essential autophagy gene BECN1 in human cancers. *Mol Cancer Res* **12**, 485-490 (2014).
186. Takamura, A., *et al.* Autophagy-deficient mice develop multiple liver tumors. *Genes Dev* **25**, 795-800 (2011).
187. Yang, S., *et al.* Pancreatic cancers require autophagy for tumor growth. *Genes Dev* **25**, 717-729 (2011).
188. Yang, A., *et al.* Autophagy is critical for pancreatic tumor growth and progression in tumors with p53 alterations. *Cancer Discov* **4**, 905-913 (2014).
189. Mathew, R., *et al.* Autophagy suppresses tumorigenesis through elimination of p62. *Cell* **137**, 1062-1075 (2009).
190. White, E. Deconvoluting the context-dependent role for autophagy in cancer. *Nat Rev Cancer* **12**, 401-410 (2012).

191. Strohecker, A.M., *et al.* Autophagy sustains mitochondrial glutamine metabolism and growth of BrafV600E-driven lung tumors. *Cancer Discov* **3**, 1272-1285 (2013).
192. Marino, G., *et al.* Tissue-specific autophagy alterations and increased tumorigenesis in mice deficient in Atg4C/autophagin-3. *J Biol Chem* **282**, 18573-18583 (2007).
193. Elgendy, M., Sheridan, C., Brumatti, G. & Martin, S.J. Oncogenic Ras-induced expression of Noxa and Beclin-1 promotes autophagic cell death and limits clonogenic survival. *Mol Cell* **42**, 23-35 (2011).
194. Dou, Z., *et al.* Autophagy mediates degradation of nuclear lamina. *Nature* **527**, 105-109 (2015).
195. Iannello, A., Thompson, T.W., Ardolino, M., Lowe, S.W. & Raulet, D.H. p53-dependent chemokine production by senescent tumor cells supports NKG2D-dependent tumor elimination by natural killer cells. *J Exp Med* **210**, 2057-2069 (2013).
196. Zhi, X. & Zhong, Q. Autophagy in cancer. *F1000Prime Rep* **7**, 18 (2015).
197. Karantza-Wadsworth, V., *et al.* Autophagy mitigates metabolic stress and genome damage in mammary tumorigenesis. *Genes Dev* **21**, 1621-1635 (2007).
198. Mathew, R., *et al.* Autophagy suppresses tumor progression by limiting chromosomal instability. *Genes Dev* **21**, 1367-1381 (2007).
199. Komatsu, M., *et al.* The selective autophagy substrate p62 activates the stress responsive transcription factor Nrf2 through inactivation of Keap1. *Nat Cell Biol* **12**, 213-223 (2010).
200. Guo, J.Y., *et al.* Activated Ras requires autophagy to maintain oxidative metabolism and tumorigenesis. *Genes Dev* **25**, 460-470 (2011).
201. Degenhardt, K., *et al.* Autophagy promotes tumor cell survival and restricts necrosis, inflammation, and tumorigenesis. *Cancer Cell* **10**, 51-64 (2006).
202. Guo, J.Y., *et al.* Autophagy suppresses progression of K-ras-induced lung tumors to oncocytomas and maintains lipid homeostasis. *Genes Dev* **27**, 1447-1461 (2013).
203. Viale, A., *et al.* Oncogene ablation-resistant pancreatic cancer cells depend on mitochondrial function. *Nature* **514**, 628-632 (2014).
204. Gong, C., *et al.* Beclin 1 and autophagy are required for the tumorigenicity of breast cancer stem-like/progenitor cells. *Oncogene* **32**, 2261-2272, 2272e 2261-2211 (2013).
205. Wolf, J., *et al.* A mammosphere formation RNAi screen reveals that ATG4A promotes a breast cancer stem-like phenotype. *Breast Cancer Res* **15**, R109 (2013).
206. Wei, H., *et al.* Suppression of autophagy by FIP200 deletion inhibits mammary tumorigenesis. *Genes Dev* **25**, 1510-1527 (2011).
207. Wei, H., Wang, C., Croce, C.M. & Guan, J.L. p62/SQSTM1 synergizes with autophagy for tumor growth in vivo. *Genes Dev* **28**, 1204-1216 (2014).
208. Yeo, S.K., Wen, J., Chen, S. & Guan, J.L. Autophagy Differentially Regulates Distinct Breast Cancer Stem-like Cells in Murine Models via EGFR/Stat3 and Tgfbeta/Smad Signaling. *Cancer Res* **76**, 3397-3410 (2016).
209. Gammoh, N., *et al.* Suppression of autophagy impedes glioblastoma development and induces senescence. *Autophagy* **12**, 1431-1439 (2016).
210. Thiery, J.P., Acloque, H., Huang, R.Y. & Nieto, M.A. Epithelial-mesenchymal transitions in development and disease. *Cell* **139**, 871-890 (2009).
211. Polyak, K. & Weinberg, R.A. Transitions between epithelial and mesenchymal states: acquisition of malignant and stem cell traits. *Nat Rev Cancer* **9**, 265-273 (2009).
212. Lazova, R., *et al.* Punctate LC3B expression is a common feature of solid tumors and associated with proliferation, metastasis, and poor outcome. *Clin Cancer Res* **18**, 370-379 (2012).
213. Avivar-Valderas, A., *et al.* Regulation of autophagy during ECM detachment is linked to a selective inhibition of mTORC1 by PERK. *Oncogene* **32**, 4932-4940 (2013).
214. Cai, Q., Yan, L. & Xu, Y. Anoikis resistance is a critical feature of highly aggressive ovarian cancer cells. *Oncogene* **34**, 3315-3324 (2015).

215. Avalos, Y., *et al.* Tumor suppression and promotion by autophagy. *Biomed Res Int* **2014**, 603980 (2014).
216. Ma, X.H., *et al.* Measurements of tumor cell autophagy predict invasiveness, resistance to chemotherapy, and survival in melanoma. *Clin Cancer Res* **17**, 3478-3489 (2011).
217. Xie, X., Koh, J.Y., Price, S., White, E. & Mehnert, J.M. Atg7 Overcomes Senescence and Promotes Growth of BrafV600E-Driven Melanoma. *Cancer Discov* **5**, 410-423 (2015).
218. Martin, S., *et al.* Concurrent MEK and autophagy inhibition is required to restore cell death associated danger-signalling in Vemurafenib-resistant melanoma cells. *Biochem Pharmacol* **93**, 290-304 (2015).
219. Liu, H., *et al.* Down-regulation of autophagy-related protein 5 (ATG5) contributes to the pathogenesis of early-stage cutaneous melanoma. *Sci Transl Med* **5**, 202ra123 (2013).
220. Garcia-Fernandez, M., *et al.* Metastatic risk and resistance to BRAF inhibitors in melanoma defined by selective allelic loss of ATG5. *Autophagy* **12**, 1776-1790 (2016).
221. Kirkin, V., McEwan, D.G., Novak, I. & Dikic, I. A role for ubiquitin in selective autophagy. *Mol Cell* **34**, 259-269 (2009).
222. Yang, Z. & Klionsky, D.J. Eaten alive: a history of macroautophagy. *Nat Cell Biol* **12**, 814-822 (2010).
223. Slobodkin, M.R. & Elazar, Z. The Atg8 family: multifunctional ubiquitin-like key regulators of autophagy. *Essays Biochem* **55**, 51-64 (2013).
224. Behrends, C., Sowa, M.E., Gygi, S.P. & Harper, J.W. Network organization of the human autophagy system. *Nature* **466**, 68-76 (2010).
225. Stolz, A., Ernst, A. & Dikic, I. Cargo recognition and trafficking in selective autophagy. *Nat Cell Biol* **16**, 495-501 (2014).
226. Narendra, D., Kane, L.A., Hauser, D.N., Fearnley, I.M. & Youle, R.J. p62/SQSTM1 is required for Parkin-induced mitochondrial clustering but not mitophagy; VDAC1 is dispensable for both. *Autophagy* **6**, 1090-1106 (2010).
227. Itakura, E. & Mizushima, N. p62 Targeting to the autophagosome formation site requires self-oligomerization but not LC3 binding. *J Cell Biol* **192**, 17-27 (2011).
228. Park, I., *et al.* Phosphotyrosine-independent binding of a 62-kDa protein to the src homology 2 (SH2) domain of p56lck and its regulation by phosphorylation of Ser-59 in the lck unique N-terminal region. *Proc Natl Acad Sci U S A* **92**, 12338-12342 (1995).
229. Puls, A., Schmidt, S., Grawe, F. & Stabel, S. Interaction of protein kinase C zeta with ZIP, a novel protein kinase C-binding protein. *Proc Natl Acad Sci U S A* **94**, 6191-6196 (1997).
230. Sanchez, P., De Carcer, G., Sandoval, I.V., Moscat, J. & Diaz-Meco, M.T. Localization of atypical protein kinase C isoforms into lysosome-targeted endosomes through interaction with p62. *Mol Cell Biol* **18**, 3069-3080 (1998).
231. Joung, I., Strominger, J.L. & Shin, J. Molecular cloning of a phosphotyrosine-independent ligand of the p56lck SH2 domain. *Proc Natl Acad Sci U S A* **93**, 5991-5995 (1996).
232. Pankiv, S., *et al.* Nucleocytoplasmic shuttling of p62/SQSTM1 and its role in recruitment of nuclear polyubiquitinated proteins to promyelocytic leukemia bodies. *J Biol Chem* **285**, 5941-5953 (2010).
233. Katsuragi, Y., Ichimura, Y. & Komatsu, M. p62/SQSTM1 functions as a signaling hub and an autophagy adaptor. *FEBS J* **282**, 4672-4678 (2015).
234. Lamark, T., *et al.* Interaction codes within the family of mammalian Phox and Bem1p domain-containing proteins. *J Biol Chem* **278**, 34568-34581 (2003).
235. Taguchi, K., Motohashi, H. & Yamamoto, M. Molecular mechanisms of the Keap1-Nrf2 pathway in stress response and cancer evolution. *Genes Cells* **16**, 123-140 (2011).
236. Johansen, T. & Lamark, T. Selective autophagy mediated by autophagic adapter proteins. *Autophagy* **7**, 279-296 (2011).
237. Long, J., *et al.* Ubiquitin recognition by the ubiquitin-associated domain of p62 involves a novel conformational switch. *J Biol Chem* **283**, 5427-5440 (2008).

238. Wooten, M.W., *et al.* Essential role of sequestosome 1/p62 in regulating accumulation of Lys63-ubiquitinated proteins. *J Biol Chem* **283**, 6783-6789 (2008).
239. Tan, J.M., *et al.* Lysine 63-linked ubiquitination promotes the formation and autophagic clearance of protein inclusions associated with neurodegenerative diseases. *Hum Mol Genet* **17**, 431-439 (2008).
240. Matsumoto, G., Wada, K., Okuno, M., Kurosawa, M. & Nukina, N. Serine 403 phosphorylation of p62/SQSTM1 regulates selective autophagic clearance of ubiquitinated proteins. *Mol Cell* **44**, 279-289 (2011).
241. Morissette, J., Laurin, N. & Brown, J.P. Sequestosome 1: mutation frequencies, haplotypes, and phenotypes in familial Paget's disease of bone. *J Bone Miner Res* **21 Suppl 2**, P38-44 (2006).
242. Michou, L., *et al.* Epidemiogenetic study of French families with Paget's disease of bone. *Joint Bone Spine* **79**, 393-398 (2012).
243. Pankiv, S., *et al.* p62/SQSTM1 binds directly to Atg8/LC3 to facilitate degradation of ubiquitinated protein aggregates by autophagy. *J Biol Chem* **282**, 24131-24145 (2007).
244. Ichimura, Y., *et al.* Structural basis for sorting mechanism of p62 in selective autophagy. *J Biol Chem* **283**, 22847-22857 (2008).
245. Jain, A., *et al.* p62/SQSTM1 is a target gene for transcription factor NRF2 and creates a positive feedback loop by inducing antioxidant response element-driven gene transcription. *J Biol Chem* **285**, 22576-22591 (2010).
246. Ishii, T., *et al.* Transcription factor Nrf2 coordinately regulates a group of oxidative stress-inducible genes in macrophages. *J Biol Chem* **275**, 16023-16029 (2000).
247. Taguchi, K., *et al.* Keap1 degradation by autophagy for the maintenance of redox homeostasis. *Proc Natl Acad Sci U S A* **109**, 13561-13566 (2012).
248. Cha-Molstad, H., *et al.* Amino-terminal arginylation targets endoplasmic reticulum chaperone BiP for autophagy through p62 binding. *Nat Cell Biol* **17**, 917-929 (2015).
249. Cha-Molstad, H., Kwon, Y.T. & Kim, B.Y. Amino-terminal arginylation as a degradation signal for selective autophagy. *BMB Rep* **48**, 487-488 (2015).
250. Duran, A., *et al.* The atypical PKC-interacting protein p62 is an important mediator of RANK-activated osteoclastogenesis. *Dev Cell* **6**, 303-309 (2004).
251. Rodriguez, A., *et al.* Mature-onset obesity and insulin resistance in mice deficient in the signaling adapter p62. *Cell Metab* **3**, 211-222 (2006).
252. Kirkin, V., *et al.* A role for NBR1 in autophagosomal degradation of ubiquitinated substrates. *Mol Cell* **33**, 505-516 (2009).
253. Duran, A., *et al.* The signaling adaptor p62 is an important NF-kappaB mediator in tumorigenesis. *Cancer Cell* **13**, 343-354 (2008).
254. Vadlamudi, R.K. & Shin, J. Genomic structure and promoter analysis of the p62 gene encoding a non-proteasomal multiubiquitin chain binding protein. *FEBS Lett* **435**, 138-142 (1998).
255. Puissant, A. & Auberger, P. AMPK- and p62/SQSTM1-dependent autophagy mediate resveratrol-induced cell death in chronic myelogenous leukemia. *Autophagy* **6**, 655-657 (2010).
256. Puissant, A., *et al.* Resveratrol promotes autophagic cell death in chronic myelogenous leukemia cells via JNK-mediated p62/SQSTM1 expression and AMPK activation. *Cancer Res* **70**, 1042-1052 (2010).
257. Lee, Y.H., Ko, J., Joung, I., Kim, J.H. & Shin, J. Immediate early response of the p62 gene encoding a non-proteasomal multiubiquitin chain binding protein. *FEBS Lett* **438**, 297-300 (1998).
258. Bao, L., *et al.* Impaired autophagy response in human hepatocellular carcinoma. *Exp Mol Pathol* **96**, 149-154 (2014).

259. Jin, G.Z., *et al.* A novel panel of biomarkers in distinction of small well-differentiated HCC from dysplastic nodules and outcome values. *BMC Cancer* **13**, 161 (2013).
260. Umemura, A., *et al.* p62, Upregulated during Preneoplasia, Induces Hepatocellular Carcinogenesis by Maintaining Survival of Stressed HCC-Initiating Cells. *Cancer Cell* **29**, 935-948 (2016).
261. Saito, T., *et al.* p62/Sqstm1 promotes malignancy of HCV-positive hepatocellular carcinoma through Nrf2-dependent metabolic reprogramming. *Nat Commun* **7**, 12030 (2016).
262. Hua, F., *et al.* TRB3 links insulin/IGF to tumour promotion by interacting with p62 and impeding autophagic/proteasomal degradations. *Nat Commun* **6**, 7951 (2015).
263. Inami, Y., *et al.* Persistent activation of Nrf2 through p62 in hepatocellular carcinoma cells. *J Cell Biol* **193**, 275-284 (2011).
264. Aishima, S., *et al.* p62+ Hyaline inclusions in intrahepatic cholangiocarcinoma associated with viral hepatitis or alcoholic liver disease. *Am J Clin Pathol* **134**, 457-465 (2010).
265. Mohamed, A., *et al.* P62/Ubiquitin IHC Expression Correlated with Clinicopathologic Parameters and Outcome in Gastrointestinal Carcinomas. *Front Oncol* **5**, 70 (2015).
266. Inoue, D., *et al.* Accumulation of p62/SQSTM1 is associated with poor prognosis in patients with lung adenocarcinoma. *Cancer Sci* **103**, 760-766 (2012).
267. Schlafli, A.M., *et al.* Prognostic value of the autophagy markers LC3 and p62/SQSTM1 in early-stage non-small cell lung cancer. *Oncotarget* **7**, 39544-39555 (2016).
268. Kuo, W.L., *et al.* p62/SQSTM1 accumulation in squamous cell carcinoma of head and neck predicts sensitivity to phosphatidylinositol 3-kinase pathway inhibitors. *PLoS One* **9**, e90171 (2014).
269. Inui, T., *et al.* Association of p62/SQSTM1 excess and oral carcinogenesis. *PLoS One* **8**, e74398 (2013).
270. Adams, O., *et al.* Prognostic relevance of autophagy markers LC3B and p62 in esophageal adenocarcinomas. *Oncotarget* **7**, 39241-39255 (2016).
271. Masuda, G.O., *et al.* Clinicopathological Correlations of Autophagy-related Proteins LC3, Beclin 1 and p62 in Gastric Cancer. *Anticancer Res* **36**, 129-136 (2016).
272. Park, J.M., Huang, S., Wu, T.T., Foster, N.R. & Sinicrope, F.A. Prognostic impact of Beclin 1, p62/sequestosome 1 and LC3 protein expression in colon carcinomas from patients receiving 5-fluorouracil as adjuvant chemotherapy. *Cancer Biol Ther* **14**, 100-107 (2013).
273. Thompson, H.G., Harris, J.W., Wold, B.J., Lin, F. & Brody, J.P. p62 overexpression in breast tumors and regulation by prostate-derived Ets factor in breast cancer cells. *Oncogene* **22**, 2322-2333 (2003).
274. Luo, R.Z., *et al.* Accumulation of p62 is associated with poor prognosis in patients with triple-negative breast cancer. *Onco Targets Ther* **6**, 883-888 (2013).
275. Rolland, P., *et al.* The ubiquitin-binding protein p62 is expressed in breast cancers showing features of aggressive disease. *Endocr Relat Cancer* **14**, 73-80 (2007).
276. Choi, J., Jung, W. & Koo, J.S. Expression of autophagy-related markers beclin-1, light chain 3A, light chain 3B and p62 according to the molecular subtype of breast cancer. *Histopathology* **62**, 275-286 (2013).
277. Xu, L.Z., *et al.* p62/SQSTM1 enhances breast cancer stem-like properties by stabilizing MYC mRNA. *Oncogene* **36**, 304-317 (2017).
278. Valencia, T., *et al.* Metabolic reprogramming of stromal fibroblasts through p62-mTORC1 signaling promotes inflammation and tumorigenesis. *Cancer Cell* **26**, 121-135 (2014).
279. Kitamura, H., *et al.* Cytosolic overexpression of p62 sequestosome 1 in neoplastic prostate tissue. *Histopathology* **48**, 157-161 (2006).
280. Giatromanolaki, A., Sivridis, E., Mendrinos, S., Koutsoopoulos, A.V. & Koukourakis, M.I. Autophagy proteins in prostate cancer: relation with anaerobic metabolism and Gleason score. *Urol Oncol* **32**, 39 e11-38 (2014).

281. Chang, M.A., *et al.* IL-1beta induces p62/SQSTM1 and represses androgen receptor expression in prostate cancer cells. *J Cell Biochem* **115**, 2188-2197 (2014).
282. Duran, A., *et al.* p62 is a key regulator of nutrient sensing in the mTORC1 pathway. *Mol Cell* **44**, 134-146 (2011).
283. Linares, J.F., *et al.* Amino Acid Activation of mTORC1 by a PB1-Domain-Driven Kinase Complex Cascade. *Cell Rep* **12**, 1339-1352 (2015).
284. Goodall, M.L., *et al.* The Autophagy Machinery Controls Cell Death Switching between Apoptosis and Necroptosis. *Dev Cell* **37**, 337-349 (2016).
285. Ellis, R.A., *et al.* Prognostic impact of p62 expression in cutaneous malignant melanoma. *J Invest Dermatol* **134**, 1476-1478 (2014).
286. Iwadate, R., *et al.* High Expression of p62 Protein Is Associated with Poor Prognosis and Aggressive Phenotypes in Endometrial Cancer. *Am J Pathol* **185**, 2523-2533 (2015).
287. Ju, L.L., Zhao, C.Y., Ye, K.F., Yang, H. & Zhang, J. Expression and clinical implication of Beclin1, HMGB1, p62, survivin, BRCA1 and ERCC1 in epithelial ovarian tumor tissues. *Eur Rev Med Pharmacol Sci* **20**, 1993-2003 (2016).
288. Galavotti, S., *et al.* The autophagy-associated factors DRAM1 and p62 regulate cell migration and invasion in glioblastoma stem cells. *Oncogene* **32**, 699-712 (2013).
289. Li, L., *et al.* SQSTM1 is a pathogenic target of 5q copy number gains in kidney cancer. *Cancer Cell* **24**, 738-750 (2013).
290. Zatloukal, K., *et al.* p62 Is a common component of cytoplasmic inclusions in protein aggregation diseases. *Am J Pathol* **160**, 255-263 (2002).
291. Denk, H., *et al.* Are the Mallory bodies and intracellular hyaline bodies in neoplastic and non-neoplastic hepatocytes related? *J Pathol* **208**, 653-661 (2006).
292. Fukuo, Y., *et al.* Abnormality of autophagic function and cathepsin expression in the liver from patients with non-alcoholic fatty liver disease. *Hepatol Res* **44**, 1026-1036 (2014).
293. Gonzalez-Rodriguez, A., *et al.* Impaired autophagic flux is associated with increased endoplasmic reticulum stress during the development of NAFLD. *Cell Death Dis* **5**, e1179 (2014).
294. Kirkin, V., Lamark, T., Johansen, T. & Dikic, I. NBR1 cooperates with p62 in selective autophagy of ubiquitinated targets. *Autophagy* **5**, 732-733 (2009).
295. Kim, P.K., Hailey, D.W., Mullen, R.T. & Lippincott-Schwartz, J. Ubiquitin signals autophagic degradation of cytosolic proteins and peroxisomes. *Proc Natl Acad Sci U S A* **105**, 20567-20574 (2008).
296. Moscat, J. & Diaz-Meco, M.T. p62 at the crossroads of autophagy, apoptosis, and cancer. *Cell* **137**, 1001-1004 (2009).
297. Rosenfeldt, M.T., *et al.* p53 status determines the role of autophagy in pancreatic tumour development. *Nature* **504**, 296-300 (2013).
298. Komatsu, M., *et al.* Homeostatic levels of p62 control cytoplasmic inclusion body formation in autophagy-deficient mice. *Cell* **131**, 1149-1163 (2007).
299. Qiang, L., *et al.* Regulation of cell proliferation and migration by p62 through stabilization of Twist1. *Proc Natl Acad Sci U S A* **111**, 9241-9246 (2014).
300. Watanabe, Y. & Tanaka, M. p62/SQSTM1 in autophagic clearance of a non-ubiquitylated substrate. *J Cell Sci* **124**, 2692-2701 (2011).
301. Rogov, V., Dotsch, V., Johansen, T. & Kirkin, V. Interactions between autophagy receptors and ubiquitin-like proteins form the molecular basis for selective autophagy. *Mol Cell* **53**, 167-178 (2014).
302. Antonucci, L., *et al.* Basal autophagy maintains pancreatic acinar cell homeostasis and protein synthesis and prevents ER stress. *Proc Natl Acad Sci U S A* **112**, E6166-6174 (2015).
303. Puissant, A., Fenouille, N. & Auberger, P. When autophagy meets cancer through p62/SQSTM1. *Am J Cancer Res* **2**, 397-413 (2012).

304. Ling, J., *et al.* KrasG12D-induced IKK2/beta/NF-kappaB activation by IL-1alpha and p62 feedforward loops is required for development of pancreatic ductal adenocarcinoma. *Cancer Cell* **21**, 105-120 (2012).
305. Li, N., *et al.* Loss of acinar cell IKKalpha triggers spontaneous pancreatitis in mice. *J Clin Invest* **123**, 2231-2243 (2013).
306. Lau, A., *et al.* A noncanonical mechanism of Nrf2 activation by autophagy deficiency: direct interaction between Keap1 and p62. *Mol Cell Biol* **30**, 3275-3285 (2010).
307. Moscat, J., Karin, M. & Diaz-Meco, M.T. p62 in Cancer: Signaling Adaptor Beyond Autophagy. *Cell* **167**, 606-609 (2016).
308. Duran, A., *et al.* p62/SQSTM1 by Binding to Vitamin D Receptor Inhibits Hepatic Stellate Cell Activity, Fibrosis, and Liver Cancer. *Cancer Cell* **30**, 595-609 (2016).
309. Linares, J.F., Amanchy, R., Greis, K., Diaz-Meco, M.T. & Moscat, J. Phosphorylation of p62 by cdk1 controls the timely transit of cells through mitosis and tumor cell proliferation. *Mol Cell Biol* **31**, 105-117 (2011).
310. Fernandez, Y., *et al.* Differential regulation of noxa in normal melanocytes and melanoma cells by proteasome inhibition: therapeutic implications. *Cancer Res* **65**, 6294-6304 (2005).
311. Denoyelle, C., *et al.* Anti-oncogenic role of the endoplasmic reticulum differentially activated by mutations in the MAPK pathway. *Nat Cell Biol* **8**, 1053-1063 (2006).
312. Ernoult, E., Gamelin, E. & Guette, C. Improved proteome coverage by using iTRAQ labelling and peptide OFFGEL fractionation. *Proteome Sci* **6**, 27 (2008).
313. Rappsilber, J., Ishihama, Y. & Mann, M. Stop and go extraction tips for matrix-assisted laser desorption/ionization, nanoelectrospray, and LC/MS sample pretreatment in proteomics. *Anal Chem* **75**, 663-670 (2003).
314. Olsen, J.V., *et al.* Parts per million mass accuracy on an Orbitrap mass spectrometer via lock mass injection into a C-trap. *Mol Cell Proteomics* **4**, 2010-2021 (2005).
315. Perkins, D.N., Pappin, D.J., Creasy, D.M. & Cottrell, J.S. Probability-based protein identification by searching sequence databases using mass spectrometry data. *Electrophoresis* **20**, 3551-3567 (1999).
316. Ho, J., *et al.* Novel breast cancer metastasis-associated proteins. *J Proteome Res* **8**, 583-594 (2009).
317. Gan, C.S., Chong, P.K., Pham, T.K. & Wright, P.C. Technical, experimental, and biological variations in isobaric tags for relative and absolute quantitation (iTRAQ). *J Proteome Res* **6**, 821-827 (2007).
318. Chen, Y., *et al.* Differential expression of novel tyrosine kinase substrates during breast cancer development. *Mol Cell Proteomics* **6**, 2072-2087 (2007).
319. Wisniewski, J.R., Zougman, A., Nagaraj, N. & Mann, M. Universal sample preparation method for proteome analysis. *Nat Methods* **6**, 359-362 (2009).
320. Franceschini, A., *et al.* STRING v9.1: protein-protein interaction networks, with increased coverage and integration. *Nucleic Acids Res* **41**, D808-815 (2013).
321. Cox, J. & Mann, M. MaxQuant enables high peptide identification rates, individualized p.p.b.-range mass accuracies and proteome-wide protein quantification. *Nat Biotechnol* **26**, 1367-1372 (2008).
322. Cox, J., *et al.* Andromeda: a peptide search engine integrated into the MaxQuant environment. *J Proteome Res* **10**, 1794-1805 (2011).
323. Alonso, S.R., *et al.* Progression in cutaneous malignant melanoma is associated with distinct expression profiles: a tissue microarray-based study. *Am J Pathol* **164**, 193-203 (2004).
324. Yajima, I., *et al.* Spatiotemporal gene control by the Cre-ERT2 system in melanocytes. *Genesis* **44**, 34-43 (2006).
325. Sugimoto, R., *et al.* Enhanced neointimal hyperplasia and carotid artery remodelling in sequestosome 1 deficient mice. *J Cell Mol Med* **14**, 1546-1554 (2010).

326. Hara, T., *et al.* Suppression of basal autophagy in neural cells causes neurodegenerative disease in mice. *Nature* **441**, 885-889 (2006).
327. Dankort, D., *et al.* Braf(V600E) cooperates with Pten loss to induce metastatic melanoma. *Nat Genet* **41**, 544-552 (2009).
328. Marino, S., *et al.* PTEN is essential for cell migration but not for fate determination and tumourigenesis in the cerebellum. *Development* **129**, 3513-3522 (2002).
329. Barretina, J., *et al.* The Cancer Cell Line Encyclopedia enables predictive modelling of anticancer drug sensitivity. *Nature* **483**, 603-607 (2012).
330. Szklarczyk, D., *et al.* STRING v10: protein-protein interaction networks, integrated over the tree of life. *Nucleic Acids Res* **43**, D447-452 (2015).
331. Oliveros, J. VENNY: An interactive tool for comparing lists with Venn diagrams., Vol. 2015 (2007-2015).
332. Bardou, P., Mariette, J., Escudie, F., Djemiel, C. & Klopp, C. jvenn: an interactive Venn diagram viewer. *BMC Bioinformatics* **15**, 293 (2014).
333. Gao, J., *et al.* Integrative analysis of complex cancer genomics and clinical profiles using the cBioPortal. *Sci Signal* **6**, pl1 (2013).
334. Riveiro, E.M. University of Complutense (2013).
335. Moscat, J. & Diaz-Meco, M.T. p62: a versatile multitasker takes on cancer. *Trends Biochem Sci* **37**, 230-236 (2012).
336. Alonso, S.R., *et al.* A high-throughput study in melanoma identifies epithelial-mesenchymal transition as a major determinant of metastasis. *Cancer Res* **67**, 3450-3460 (2007).
337. Kauffmann, A., *et al.* High expression of DNA repair pathways is associated with metastasis in melanoma patients. *Oncogene* **27**, 565-573 (2008).
338. Winnepeninckx, V. & Van den Oord, J.J. Gene expression profiling of primary cutaneous melanoma. *Verh K Acad Geneeskde Belg* **69**, 23-45 (2007).
339. Linares, J.F., *et al.* K63 polyubiquitination and activation of mTOR by the p62-TRAF6 complex in nutrient-activated cells. *Mol Cell* **51**, 283-296 (2013).
340. Muller, T.D., *et al.* p62 links beta-adrenergic input to mitochondrial function and thermogenesis. *J Clin Invest* **123**, 469-478 (2013).
341. Mathew, R., *et al.* Functional role of autophagy-mediated proteome remodeling in cell survival signaling and innate immunity. *Mol Cell* **55**, 916-930 (2014).
342. Calderwood, D.A., Campbell, I.D. & Critchley, D.R. Talins and kindlins: partners in integrin-mediated adhesion. *Nat Rev Mol Cell Biol* **14**, 503-517 (2013).
343. Zhan, J., *et al.* Kindlin-2 induced by TGF-beta signaling promotes pancreatic ductal adenocarcinoma progression through downregulation of transcriptional factor HOXB9. *Cancer Lett* **361**, 75-85 (2015).
344. Ge, Y.S., *et al.* Kindlin-2: a novel prognostic biomarker for patients with hepatocellular carcinoma. *Pathol Res Pract* **211**, 198-202 (2015).
345. Zhao, T., *et al.* Kindlin-2 promotes genome instability in breast cancer cells. *Cancer Lett* **330**, 208-216 (2013).
346. Chatr-Aryamontri, A., *et al.* The BioGRID interaction database: 2015 update. *Nucleic Acids Res* **43**, D470-478 (2015).
347. Hu, B., Yang, Y.T., Huang, Y., Zhu, Y. & Lu, Z.J. POSTAR: a platform for exploring post-transcriptional regulation coordinated by RNA-binding proteins. *Nucleic Acids Res* **45**, D104-D114 (2017).
348. Bell, J.L., *et al.* Insulin-like growth factor 2 mRNA-binding proteins (IGF2BPs): post-transcriptional drivers of cancer progression? *Cell Mol Life Sci* **70**, 2657-2675 (2013).
349. Degrauwe, N., Suva, M.L., Janiszewska, M., Riggi, N. & Stamenkovic, I. IMPs: an RNA-binding protein family that provides a link between stem cell maintenance in normal development and cancer. *Genes Dev* **30**, 2459-2474 (2016).

350. Fortis, S.P., *et al.* Potential Prognostic Molecular Signatures in a Preclinical Model of Melanoma. *Anticancer Res* **37**, 143-148 (2017).
351. Sheen, Y.S., *et al.* IMP-3 promotes migration and invasion of melanoma cells by modulating the expression of HMGA2 and predicts poor prognosis in melanoma. *J Invest Dermatol* **135**, 1065-1073 (2015).
352. Conway, A.E., *et al.* Enhanced CLIP Uncovers IMP Protein-RNA Targets in Human Pluripotent Stem Cells Important for Cell Adhesion and Survival. *Cell Rep* **15**, 666-679 (2016).
353. Hafner, M., *et al.* Transcriptome-wide identification of RNA-binding protein and microRNA target sites by PAR-CLIP. *Cell* **141**, 129-141 (2010).
354. Huang, H., Liu, J., Meng, Q. & Niu, G. Multidrug resistance protein and topoisomerase 2 alpha expression in non-small cell lung cancer are related with brain metastasis postoperatively. *Int J Clin Exp Pathol* **8**, 11537-11542 (2015).
355. Liu, S., *et al.* G9a is essential for EMT-mediated metastasis and maintenance of cancer stem cell-like characters in head and neck squamous cell carcinoma. *Oncotarget* **6**, 6887-6901 (2015).
356. Kwon, S.H., Oh, S., Nacke, M., Mostov, K.E. & Lipschutz, J.H. Adaptor Protein CD2AP and L-type Lectin LMAN2 Regulate Exosome Cargo Protein Trafficking through the Golgi Complex. *J Biol Chem* **291**, 25462-25475 (2016).
357. Cao, S., *et al.* Upregulation of flotillin-1 promotes invasion and metastasis by activating TGF-beta signaling in nasopharyngeal carcinoma. *Oncotarget* **7**, 4252-4264 (2016).
358. Rizvi, H., *et al.* Expression of the CD2AP adaptor molecule in normal, reactive and neoplastic human tissue. *Pathologica* **104**, 56-64 (2012).
359. Chang, J.W., Nomura, D.K. & Cravatt, B.F. A potent and selective inhibitor of KIAA1363/AADACL1 that impairs prostate cancer pathogenesis. *Chem Biol* **18**, 476-484 (2011).
360. Kim, J.H., *et al.* OGFOD1 is required for breast cancer cell proliferation and is associated with poor prognosis in breast cancer. *Oncotarget* **6**, 19528-19541 (2015).
361. Haqq, C., *et al.* The gene expression signatures of melanoma progression. *Proc Natl Acad Sci U S A* **102**, 6092-6097 (2005).
362. Hoek, K.S. DNA microarray analyses of melanoma gene expression: a decade in the mines. *Pigment Cell Res* **20**, 466-484 (2007).
363. Riker, A.I., *et al.* The gene expression profiles of primary and metastatic melanoma yields a transition point of tumor progression and metastasis. *BMC Med Genomics* **1**, 13 (2008).
364. Smith, A.P., Hoek, K. & Becker, D. Whole-genome expression profiling of the melanoma progression pathway reveals marked molecular differences between nevi/melanoma in situ and advanced-stage melanomas. *Cancer Biol Ther* **4**, 1018-1029 (2005).
365. Kraft, C., Peter, M. & Hofmann, K. Selective autophagy: ubiquitin-mediated recognition and beyond. *Nat Cell Biol* **12**, 836-841 (2010).
366. Birgisdottir, A.B., Lamark, T. & Johansen, T. The LIR motif - crucial for selective autophagy. *J Cell Sci* **126**, 3237-3247 (2013).
367. Jiang, T., *et al.* p62 links autophagy and Nrf2 signaling. *Free Radic Biol Med* **88**, 199-204 (2015).
368. Furfaro, A.L., *et al.* The Nrf2/HO-1 Axis in Cancer Cell Growth and Chemoresistance. *Oxid Med Cell Longev* **2016**, 1958174 (2016).
369. Xia, M., *et al.* p62/SQSTM1 is involved in cisplatin resistance in human ovarian cancer cells via the Keap1-Nrf2-ARE system. *Int J Oncol* **45**, 2341-2348 (2014).
370. Yang, C., *et al.* Gankyrin has an antioxidative role through the feedback regulation of Nrf2 in hepatocellular carcinoma. *J Exp Med* **213**, 859-875 (2016).
371. Itoh, K., *et al.* Keap1 represses nuclear activation of antioxidant responsive elements by Nrf2 through binding to the amino-terminal Neh2 domain. *Genes Dev* **13**, 76-86 (1999).

372. Karin, M. Nuclear factor-kappaB in cancer development and progression. *Nature* **441**, 431-436 (2006).
373. Zotti, T., *et al.* TRAF6-mediated ubiquitination of NEMO requires p62/sequestosome-1. *Mol Immunol* **58**, 27-31 (2014).
374. Starczynowski, D.T., *et al.* TRAF6 is an amplified oncogene bridging the RAS and NF-kappaB pathways in human lung cancer. *J Clin Invest* **121**, 4095-4105 (2011).
375. Okatsu, K., *et al.* p62/SQSTM1 cooperates with Parkin for perinuclear clustering of depolarized mitochondria. *Genes Cells* **15**, 887-900 (2010).
376. Liu, Z., *et al.* Ubiquitylation of autophagy receptor Optineurin by HACE1 activates selective autophagy for tumor suppression. *Cancer Cell* **26**, 106-120 (2014).
377. Shen, Z., *et al.* The novel focal adhesion gene kindlin-2 promotes the invasion of gastric cancer cells mediated by tumor-associated macrophages. *Oncol Rep* **29**, 791-797 (2013).
378. Yang, J.R., *et al.* Kindlin-2 promotes invasiveness of prostate cancer cells via NF-kappaB-dependent upregulation of matrix metalloproteinases. *Gene* **576**, 571-576 (2016).
379. Huang, Z., *et al.* The role of NEFL in cell growth and invasion in head and neck squamous cell carcinoma cell lines. *J Oral Pathol Med* **43**, 191-198 (2014).
380. Wang, Z.Y., *et al.* Up-Regulation of microRNA-183 Promotes Cell Proliferation and Invasion in Glioma By Directly Targeting NEFL. *Cell Mol Neurobiol* **36**, 1303-1310 (2016).
381. Dowling, J.J., Vreede, A.P., Kim, S., Golden, J. & Feldman, E.L. Kindlin-2 is required for myocyte elongation and is essential for myogenesis. *BMC Cell Biol* **9**, 36 (2008).
382. Dowling, J.J., *et al.* Kindlin-2 is an essential component of intercalated discs and is required for vertebrate cardiac structure and function. *Circ Res* **102**, 423-431 (2008).
383. Rognoni, E., Ruppert, R. & Fassler, R. The kindlin family: functions, signaling properties and implications for human disease. *J Cell Sci* **129**, 17-27 (2016).
384. Liu, Z., *et al.* Kindlin-2 phosphorylation by Src at Y193 enhances Src activity and is involved in Migfilin recruitment to the focal adhesions. *FEBS Lett* **589**, 2001-2010 (2015).
385. Qu, H., Tu, Y., Guan, J.L., Xiao, G. & Wu, C. Kindlin-2 tyrosine phosphorylation and interaction with Src serve as a regulatable switch in the integrin outside-in signaling circuit. *J Biol Chem* **289**, 31001-31013 (2014).
386. Theodosiou, M., *et al.* Kindlin-2 cooperates with talin to activate integrins and induces cell spreading by directly binding paxillin. *Elife* **5**, e10130 (2016).
387. Bledzka, K., *et al.* Kindlin-2 directly binds actin and regulates integrin outside-in signaling. *J Cell Biol* **213**, 97-108 (2016).
388. Zhan, J., *et al.* Opposite role of Kindlin-1 and Kindlin-2 in lung cancers. *PLoS One* **7**, e50313 (2012).
389. Yoshida, N., *et al.* Kindlin-2 in pancreatic stellate cells promotes the progression of pancreatic cancer. *Cancer Lett* **390**, 103-114 (2017).
390. Mahawithitwong, P., *et al.* Kindlin-2 expression in peritumoral stroma is associated with poor prognosis in pancreatic ductal adenocarcinoma. *Pancreas* **42**, 663-669 (2013).
391. Glisovic, T., Bachorik, J.L., Yong, J. & Dreyfuss, G. RNA-binding proteins and post-transcriptional gene regulation. *FEBS Lett* **582**, 1977-1986 (2008).
392. Muller-McNicoll, M. & Neugebauer, K.M. How cells get the message: dynamic assembly and function of mRNA-protein complexes. *Nat Rev Genet* **14**, 275-287 (2013).
393. Craig, E.A. & Spiegelman, V.S. Inhibition of coding region determinant binding protein sensitizes melanoma cells to chemotherapeutic agents. *Pigment Cell Melanoma Res* **25**, 83-87 (2012).
394. Craig, E.A., Weber, J.D. & Spiegelman, V.S. Involvement of the mRNA binding protein CRD-BP in the regulation of metastatic melanoma cell proliferation and invasion by hypoxia. *J Cell Sci* **125**, 5950-5954 (2012).

395. Bernstein, P.L., Herrick, D.J., Prokipcak, R.D. & Ross, J. Control of c-myc mRNA half-life in vitro by a protein capable of binding to a coding region stability determinant. *Genes Dev* **6**, 642-654 (1992).
396. Mongroo, P.S., *et al.* IMP-1 displays cross-talk with K-Ras and modulates colon cancer cell survival through the novel proapoptotic protein CYFIP2. *Cancer Res* **71**, 2172-2182 (2011).
397. Shyh-Chang, N., *et al.* Lin28 enhances tissue repair by reprogramming cellular metabolism. *Cell* **155**, 778-792 (2013).
398. Jonson, L., *et al.* IMP3 RNP safe houses prevent miRNA-directed HMGA2 mRNA decay in cancer and development. *Cell Rep* **7**, 539-551 (2014).
399. Busch, B., *et al.* The oncogenic triangle of HMGA2, LIN28B and IGF2BP1 antagonizes tumor-suppressive actions of the let-7 family. *Nucleic Acids Res* **44**, 3845-3864 (2016).
400. Boya, P., Reggiori, F. & Codogno, P. Emerging regulation and functions of autophagy. *Nat Cell Biol* **15**, 713-720 (2013).
401. Pan, J.A., *et al.* TRIM21 Ubiquitylates SQSTM1/p62 and Suppresses Protein Sequestration to Regulate Redox Homeostasis. *Mol Cell* **61**, 720-733 (2016).
402. Shimizu, T., *et al.* Accumulation of phosphorylated p62 is associated with NF-E2-related factor 2 activation in hepatocellular carcinoma. *J Hepatobiliary Pancreat Sci* **23**, 467-471 (2016).
403. Yang, S., Qiang, L., Sample, A., Shah, P. & He, Y.Y. NF-kappaB Signaling Activation Induced by Chloroquine Requires Autophagosome, p62 Protein, and c-Jun N-terminal Kinase (JNK) Signaling and Promotes Tumor Cell Resistance. *J Biol Chem* **292**, 3379-3388 (2017).
404. Ichimura, Y., *et al.* Phosphorylation of p62 activates the Keap1-Nrf2 pathway during selective autophagy. *Mol Cell* **51**, 618-631 (2013).

## ***X. APPENDIX***

## 10.1 Supplementary tables and figures

**Table S1:** Systemic therapies approved since 2011 for advanced-stage melanoma. Source: Ref.<sup>35</sup>

	Agent	Mechanism	FDA-approved indications
<b>Targeted therapies</b>	Vemurafenib	BRAF inhibitor	As monotherapy and in combination with cobimetinib for BRAF <sup>V600E/K</sup> -mutant disease
	Dabrafenib	BRAF inhibitor	As monotherapy and in combination with trametinib for BRAF <sup>V600E/K</sup> -mutant disease
	Trametinib	MEK inhibitor	As monotherapy and in combination with dabrafenib for BRAF <sup>V600E/K</sup> -mutant disease
	Cobimetinib	MEK inhibitor	In combination with vemurafenib for BRAF <sup>V600E/K</sup> -mutant melanoma
<b>Immunotherapies</b>	Ipilimumab	Anti-CTLA-4 antibody	As monotherapy and in combination with nivolumab
	Pembrolizumab	Anti-PD-1 antibody	As monotherapy
	Nivolumab	Anti-PD-1 antibody	In combination with ipilimumab, or as monotherapy
<b>Oncolytic viral therapy</b>	Talimogene laharparepvec	Modified oncolytic herpes virus	Local treatment of unresectable cutaneous, subcutaneous, and nodal lesions in patients with recurrent melanoma after surgery

**Table S2:** Prominent mechanisms of pathway alterations in BRAF, RAS, NF1 and Triple Wild-Type (WT) subtypes with potential predictive genetic alterations indicated (<sup>1,2,3,4,5,6</sup>). Source: Ref.<sup>95</sup>

Mutation Subtypes	BRAF	RAS	NF1	Triple Wild-Type
<sup>1</sup> MAPK pathway	<sup>1</sup> BRAFV600,K601	<sup>1</sup> (N/H/K)RASG12, G13,Q61	<sup>1</sup> NF1 LoF mut;(BRAF non-hot-spot mut)	<sup>1</sup> KITC OSMIC mut/amp, PDGFRa amp,KDR (VEGFR2)amp;rare COSMIC GNA11 mut, GNAQ mut
<sup>2</sup> Cell-cycle pathway	CDKN2A mut/del/h-meth (60%); <sup>2</sup> (CDK4 COSMIC mut)	CDKN2A mut/del/h-meth (70%);CCND1 amp (10%); <sup>2</sup> (CDK4 COSMIC mut)	CDKN2A mut/del/h-meth (70%);RB1 mut (10%)	CDKN2A mut/del/h-meth (40%);CCND1 amp (10%); <sup>2</sup> CDK4 amp (15%)
<sup>3</sup> DNA damage response and cell death pathways	TP53mut(10%); <sup>3</sup> (note:TP53 wild-type in 90% of BRAF subtype)	TP53mut(20%)	TP53 mut(30%)	<sup>3</sup> MDM2 amp(15%); <sup>3</sup> BCL2 upregulation
<sup>4</sup> PI3K/Akt pathway	<sup>4</sup> PTEN mut/del(20%); <sup>4</sup> (rare AKT1/3 and PIK3CA COSMIC mut)	<sup>4</sup> AKT3 overexpression (40%); <sup>4</sup> (rare AKT1/3 and PIK3CA COSMIC mut)	<sup>4</sup> AKT3 overexpression (30%)	<sup>4</sup> AKT3 overexpression (20%)
<sup>5</sup> Epigenetics	<sup>5</sup> IDH1 mut, <sup>5</sup> (rare EZH2 COSMIC mut); <sup>5</sup> ARID2 mut (15%)	<sup>5</sup> IDH1 mut, <sup>5</sup> (rare EZH2 COSMIC mut); <sup>5</sup> ARID2 mut(15%)	<sup>5</sup> IDH1 mut, <sup>5</sup> (EZH2 mut); <sup>5</sup> ARID2 mut(30%)	<sup>5</sup> IDH1 mut, <sup>5</sup> (rare EZH2 COSMIC mut)
Telomerase pathway	Promoter mut (75%)	Promoter mut(70%)	Promoter mut(85%)	Promoter mut(<10%); TERT amp(15%)
Other pathways	PD-L1 amp, MITF amp, PPP6C mut(10%)	PPP6C mut(15%)		
<sup>6</sup> High immune infiltration (pathology)	~30%	~25%	~25%	~40%

**Table S3:** Functions of AuTophagy (ATG) related proteins during autophagosome formation. Source:Ref.<sup>400</sup>

Protein	Yeast	High eukaryotes	Function
Atg1/ULKs	+	+	Protein kinase involved in the induction of autophagy and possibly in PAS/phagophore biogenesis
Atg2	+	+	Interacts with Atg18/WIP14; possibly involved in PAS/phagophore biogenesis
Atg3	+	+	E2-like enzyme for the ubiquitin-like conjugation system that catalyses Atg8/LC3's lipidation involved in phagophore expansion
Atg4	+	+	Cysteine protease processing and delipidating Atg8/LC3, thus involved in phagophore expansion
Atg5	+	+	Covalently linked to Atg12, generating the Atg12-Atg5 conjugate involved in phagophore expansion
Atg6/beclin 1	+	+	Component of various PI(3)K complexes, one of which is involved in induction of autophagy and PAS/phagophore biogenesis
Atg7	+	+	E1-like enzyme for the two ubiquitin-like conjugation systems, thus involved in phagophore expansion
Atg8/LC3s	+	+	Ubiquitin-like protein involved in phagophore expansion
Atg9	+	+	Transmembrane protein involved in the induction of autophagy and possibly in PAS/phagophore biogenesis
Atg10	+	+	E2-like enzyme for the ubiquitin-like conjugation system that mediates the formation of the Atg12-Atg5 conjugate involved in phagophore expansion
Atg12	+	+	Ubiquitin-like protein involved in phagophore expansion
Atg13	+	+	Binding partner and regulator of Atg1/ULKs, thus involved in the induction of autophagy and possibly PAS/phagophore biogenesis
Atg14	+	+	Component of the PI(3)K complex I involved in induction of autophagy and possibly PAS/phagophore biogenesis
Atg16	+	+	Associates with Atg12-Atg5 to form a large complex, which acts as an E3 ligase to direct LC3 lipidation on autophagosomal membranes, and thus involved in phagophore expansion
Atg17/FIP200	+	+	Binding partner and regulator of Atg1/ULKs, thus involved in the induction of autophagy and possibly PAS/phagophore biogenesis
Atg18/WIPs	+	+	PtsIns3P-binding proteins possibly involved in PAS/phagophore biogenesis
Atg23	+	-	Binding partner and regulator of Atg9, thus involved in the induction of autophagy and possibly in PAS/phagophore biogenesis
Atg27	+	-	Binding partner and regulator of Atg9, thus involved in the induction of autophagy and possibly in PAS/phagophore biogenesis
Atg29	+	-	Binding partner and regulator of Atg1, thus involved in the induction of autophagy and possibly in PAS/phagophore biogenesis
Atg31	+	-	Binding partner and regulator of Atg1, thus involved in the induction of autophagy and possibly in PAS/phagophore biogenesis
Atg101	-	+	Binding partner and regulator of ULKs, thus involved in the induction of autophagy and possibly in PAS/phagophore biogenesis
Ambra1	-	+	Regulator of the PI(3)K and Atg1/ULK complexes, and thus involved in the induction of autophagy
DFCP1	-	+	PtdIns3P-binding proteins concentrating at the omegasome, possibly involved in the induction of autophagy
VMP1	-	+	Transmembrane protein regulating autophagy induction
Vps15/p150	+	+	Kinase regulating Vps34/hVps34 activity; component of various PI(3)K complexes, one of which is involved in the induction of autophagy and PAS/phagophore biogenesis
Vps34/PtdIns3PKC3	+	+	Component of various PI(3)K complexes, one of which is involved in the induction of autophagy and PAS/phagophore biogenesis

**Table S4:** p62 main described functions in disease and in different cancer types.

system	Domain	interaction/Regulation	cancer/disease	Functions	reference
HeLa, CD4+ , Jurkat T	PB1	p56 <sup>lck</sup>	-	T cell activation	<a href="#">228</a>
COS	ZZ	PKC-ζ	-	scaffold	<a href="#">229</a>
HeLa/293	PB1	λ/ζ PKC	-	endolysosomal trafficking	<a href="#">230</a>
mouse brain	TB	CYLD	-	turnover of Lys63-polyubiquitinated proteins	<a href="#">238</a>
patients	UBA	-	Paget's disease	mutations in PDB patients	<a href="#">241</a>
HeLa/MEFs	LIR	LC3	-	degradation of polyubiquitinated proteins	<a href="#">243</a>
HeLa/MEFs/HEK293	KIR	KEAP1	-	activation of NRF2 target genes	<a href="#">245</a>
Atg7::Keap1-Alb double-mutant mice into p62- and Nrf2-null backgrounds	KIR	KEAP1	-	oxidative stress	<a href="#">247</a>

system	Domain	interaction/ Regulation	cancer/ disease	Functions	reference
HeLa, PC3 and HEK293. ATG5 and p62 KO cells	ZZ	R-BiP	-	ER-residing proteins degradation	<a href="#">248</a>
BMDMs from p62KO mice	PB1/TB	aPKCs, TRAF6	-	osteoclastogenesis	<a href="#">250</a>
p62 KO mice	-	ERK	-	obesity	<a href="#">251</a>
HeLa/p62 <sup>-/-</sup> , or Atg5 <sup>-/-</sup> MEFs. p62 <sup>-/-</sup> mice, and Atg7 <sup>-/-</sup> :Mx1:p62 <sup>-/-</sup> mice	PB1	NBR1	-	Autophagosomal Degradation of Ubiquitinated Substrates	<a href="#">252</a>
HeLa and HEK293/p62 KO MEFs	PB1	STAT5A_ΔE18	-	autophagic clearance of a non-ubiquitylated substrate	<a href="#">300</a>
BMK/TRIM21 KO mice	PRYSPRY	TRIM2	-	redox homeostasis	<a href="#">401</a>
Hela	-	PML bodies/ataxin/polyUb	prostate cancer	Recruitment of Nuclear Polyubiquitinated Proteins to PML bodies (Nucleocytoplasmic Shuttling)	<a href="#">232</a>
iBMK ATG5 KO and Beclin1 KO cell lines	-	defective autophagy	hepatocellular carcinomas	oxidative stress/ DNA damage/ NF-κB/ autophagy	<a href="#">189</a>
Tissue sections of patients with HCC	-	-	hepatocellular carcinomas	associated with HCC	<a href="#">258</a>
Tissue sections of patients with HCC	-	-	hepatocellular carcinomas	associated with HCC	<a href="#">259</a>
liver-specific ATG7-deficient mice	KIR	KEAP1	hepatocellular carcinomas	persistent activation of Nrf2	<a href="#">263</a>
Tissue sections of patients with HCC	-	-	hepatocellular carcinomas	In Japanese HCC, NRF2 activation is associated with phosphorylation of p62, but not with KEAP1 status	<a href="#">402</a>
HCC cell lines/Atg7 and NRF2 liver deficient mice. Human biopsies	KIR	KEAP1	hepatocellular carcinomas	Phosphorylation of p62 and metabolism	<a href="#">261</a>
Tissue sections of patients	-	-	cholangiocarcinoma with chronic liver	Hyaline Inclusions	<a href="#">264</a>
Tissue sections of patients	-	-	Gastrointestinal Carcinomas	p62 and ubiquitin are highly expressed in gastric, colonic, and pancreatic carcinomas	<a href="#">265</a>
Tissue sections of patients	-	-	lung adenocarcinoma	NRF2 and p62 are independent prognostic factors for NSCLC	<a href="#">266</a>
Tissue sections of patients	-	-	lung adenocarcinoma	LC3 and p62 are differentially expressed in NSCLC	<a href="#">267</a>
cell lines/tissue samples	-	-	Squamous Cell Carcinoma of Head and Neck	resistance to PI3Ki	<a href="#">268</a>
cell lines/tissue samples	-	-	oral squamous cell carcinomas	p62 accumulation and resistance to radiation or chemotherapy	<a href="#">269</a>
cell lines/tissue samples	-	-	Esophageal adenocarcinomas	Tumors with low LC3B and p62 expression show the most aggressive behavior	<a href="#">270</a>
Tissue sections of patients	-	-	gastric cancer	Autophagy determined by LC3, Beclin 1, and p62 significantly correlated with lymph node metastasis, vessel invasion, and hepatic metastasis	<a href="#">271</a>
Tissue sections of patients	-	-	colon cancer	p62 is overexpressed in 85% of the samples	<a href="#">272</a>
cell lines/Tissue sections of patients	-	-	breast cancer	PDEF stimulates the p62 promoter	<a href="#">273</a>
Tissue sections of patients	-	-	breast cancer (TNB)	p62 in TNBC is associated with a higher risk of distant metastases	<a href="#">274</a>
Tissue sections of patients	-	-	breast cancer	p62 expression correlated with grade and distant metastasis and EGFR, HER2, HER3 and HER4	<a href="#">275</a>
cell lines/Tissue sections of patients	-	-	prostate cancer	high-grade prostatic intraepithelial neoplasia	<a href="#">279</a>
Tissue sections of patients	-	-	prostate cancer	p62 expression was related with LC3A and B reactivity and also with extraprostatic invasion	<a href="#">280</a>
Tissue sections of patients	-	-	melanoma	p62 expression was related with melanoma progression	<a href="#">285</a>
cell lines/Tissue sections of patients	-	-	endometrial cancer	High expression of cytoplasmic p62 correlates with endometrial cancer	<a href="#">286</a>
Tissue sections of patients	-	-	ovarian cancer	p62 expression epithelial ovarian cancer and platinum resistance during chemotherapy	<a href="#">287</a>
A498, A704, Caki-2, HK-2, RCC4, 769-P, 786-O, UMRC-2, UMRC-6, and UOK101	-	NRF2, NF-κB and mTOR	kidney cancer	selection pressure to amplify 5q in ccRCC is driven, at least partly, by p62	<a href="#">289</a>
Tissue sections of patients	-	-	hepatocellular carcinomas	p62 in Mallory bodies (MBs) and intracellular hyaline bodies (IHBs)	<a href="#">291</a>
Tissue sections of patients	-	-	non-alcoholic fatty liver disease	suppression of autophagic proteolysis by hepatic steatosis is involved in the pathogenesis of NAFLD	<a href="#">292</a>
Tissue sections of patients/mouse models	-	increased ER stress	non-alcoholic fatty liver disease	autophagic flux is impaired in NAFLD human mouse NAFLD due to elevated ER stress leading to apoptosis	<a href="#">293</a>
Human GSC	-	-	glioblastoma	DRAM1 and p62 regulate cell motility and invasion	<a href="#">288</a>

system	Domain	interaction/Regulation	cancer/disease	Functions	reference
			multiforme	in GSCs	
Pca	-	-	prostate cancer	IL-1 $\beta$ can drive Pca progression in an inflammatory microenvironment through AR repression and p62 induction to promote the development and survival of androgen independent Pca	<a href="#">281</a>
Tissue sections of patients/mice xenografts	-	raptor	prostate cancer	critical mediator for mTOR activation	<a href="#">282</a>
Tissue sections of patients/mouse models	LIR/UBA	TRB3	HCC, colon cancer and lung cancer	TRB3 interacts with p62, which causes p62 deposition and suppresses autophagic/ proteasomal degradation	<a href="#">262</a>
mouse prostate epithelial cells floxed or Cre-deleted Map3k7	-	-	prostate cancer	p62 Regulates the Switch between Apoptotic and Necroptotic Cell Death	<a href="#">284</a>
cell lines/p62 KO, PTEN <sup>+/+</sup> , and TRAMP <sup>+</sup>	-	mTORC1/c-Myc	prostate and breast cancer	p62 levels were reduced in the stroma of several tumors and that its loss in the tumor microenvironment or stromal fibroblasts resulted in increased tumorigenesis of epithelial prostate cancer cells	<a href="#">260</a>
HEK 293T/Liver-specific TRAF6 KO mice	TB	TRAF6	-	TRAF6, through its interaction with p62 and activation of mTORC1, modulates autophagy and is an important mediator in cancer cell proliferation	<a href="#">339</a>
cell lines and PTEN <sup>+/+</sup> and PTEN <sup>fl/fl</sup> -PBcre mice	PB1	MEKK3	prostate cancer	p62 is phosphorylated via a cascade that includes MEK3/6 and p38 $\delta$ and is driven by the PB1-containing kinase MEKK3	<a href="#">283</a>
cell lines/lkka <sup>Δpan</sup>	-	-	pancreatitis	p62 accumulation through IKK $\alpha$ and ATG12L2	<a href="#">305</a>
Atg5,Atg3,Atg7,Atg9,Atg12,Atg14,p62 KO MEFs, HaCaT,HEK-293T,A431,A375.	UBA	Twist1	MEFs/melanoma cells	p62 promotes loss of Ecadherin, cell proliferation and migration in vitro, and tumor growth and metastasis in vivo through stabilizing Twist1 (EMT modulation)	<a href="#">299</a>
Mel624,A375,A431,p62 KO MEFs	-	-	squamous cell carcinoma cells/melanoma cells	CQ induced NF- $\kappa$ B activation and the expression of its target genes HIF-1 $\alpha$ , IL-8, Bcl-2 and Bcl-XL through the accumulation of autophagosomes, p62, and JNK signaling.	<a href="#">403</a>
COS-7 and HeLa cells	-	-	-	Mammalian cells use a common pathway involving ubiquitin and p62 for targeting diverse types of substrates for autophagy	<a href="#">295</a>
Atg7 <sup>F/F</sup> :Mx1:GFP-LC3 mice Atg7 <sup>F/F</sup> :Mx1:p62 <sup>-/-</sup> , Atg7 <sup>F/F</sup> :Mx1:p62 <sup>-/-</sup> :GFP-LC3, and Atg7 <sup>F/F</sup> :Nes:p62 <sup>-/-</sup> mice	LIR	LC3	liver injury and neurodegeneration	role of homeostatic level of p62, which is regulated by autophagy, in controlling intracellular inclusion body formation	<a href="#">298</a>
FIP200f;MMTV-PyMT and p62 KO mice/HEK293, MEFs, and MDA-MB-231 cells	-	-	mammary tumor cells	p62 synergizes with autophagy for tumor growth in vivo	<a href="#">207</a>
Flp-in Neuro2a/Atg5-KO mice and MEF cells	-	-	meFs	phosphorylation of p62 at S403 regulates autophagic clearance of ubiquitinated proteins and protein aggregates that are poorly degraded by proteasomes	<a href="#">240</a>
Rpt2f;Alb-Cre mice/ p62 KO MEFs	KIR	KEAP1	hepatocellular carcinomas	p62 phosphorylation induces expression of cytoprotective Nrf2 targets through interaction with KEAP1	<a href="#">404</a>
PDAC mouse models based on KRAS <sup>G12D</sup>	-	-	Pancreatic Ductal Adenocarcinoma	Dual feed forward loops of IL-1 $\alpha$ /p62 through which IKK2/ $\beta$ /NF- $\kappa$ B is activated by Kras <sup>G12D</sup> in PDAC	<a href="#">304</a>
p62KO, CCSP-rtTA, and KRASG12D mice/ p62KO MEFs	-	-	lung adenocarcinoma	p62 is induced by Ras, activates IKK through TRAF6 polyubiquitination, is overexpressed in human tumors, and is necessary for survival of human lung adenocarcinoma cells	<a href="#">253</a>
Atg7 <sup>F/F</sup> :Mx1:Nrf2 <sup>-/-</sup> / Keap1 <sup>F/F</sup> :Atg7 <sup>F/F</sup> :Alb mice	KIR	KEAP1	MEFs	p62 accumulation results in hyperactivation of Nrf2 and delineates unexpected roles of selective autophagy in controlling the transcription of cellular defence enzyme genes	<a href="#">199</a>
HEK293/A549/p62 KO MEFs	-	-	MEFs K-Ras <sup>V12</sup>	lack of p62 phosphorylation by cdk1 leads to enhanced cell proliferation and tumorigenesis in Ras-transformed cells.	<a href="#">309</a>
DA-MB-231, BT-549, MCF-7 and SKBR-3	-	-	breast cancer stem cells	p62 promotes MYC mRNA stabilization at the post-transcriptional level in breast cancer cells	<a href="#">277</a>
p62 KO mice/ hepatic stellate cells	several domains	VDR:RXR $\alpha$ dimer		Loss of p62 in hepatic stellate cells results in increased fibrosis, inflammation, and HCC	<a href="#">308</a>

**Table S5:** Common enriched pathways from GSEA ( using KEGG and Reactome) upon p62 knockdown in two melanoma cell lines (SK-Mel-103 and UACC-62) and two different time points (day 3 and day 6).

CELLULAR PATHWAYS	SK-Mel-103		UACC-62		
	day 3	day 6	day 3	day 6	
	FDR-q value	FDR-q value	FDR-q value	FDR-q value	
REACTOME__EGFR DOWNREGULATION	0.0049	0.0408	0.0438	0.0749	trafficking
REACTOME__MEMBRANE TRAFFICKING	0.0565	0.0605	0.2141	0.0870	
KEGG__ENDOCYTOSIS	0.0124	0.0817	0.0608	0.0633	
REACTOME__CELL CYCLE, MITOTIC	<0.0001	<0.0001	0.0706	<0.0001	Cell cycle
REACTOME__G2_M CHECKPOINTS	<0.0001	<0.0001	0.0639	<0.0001	
REACTOME__G1_S TRANSITION	<0.0001	<0.0001	0.0685	<0.0001	
REACTOME__CELL CYCLE CHECKPOINTS	<0.0001	<0.0001	0.0567	<0.0001	
REACTOME__E2F MEDIATED REGULATION OF DNA REPLICATION	<0.0001	<0.0001	0.0704	<0.0001	
REACTOME__M_G1 TRANSITION	0.0003	<0.0001	0.0621	0.0001	
REACTOME__CYCLIN E ASSOCIATED EVENTS DURING G1_S TRANSITION	0.0134	0.0009	0.0842	0.0492	
REACTOME__DNA REPAIR	0.0036	0.0040	0.2150	0.0012	DNA damage
REACTOME__ACTIVATION OF ATR IN RESPONSE TO REPLICATION STRESS	<0.0001	<0.0001	0.0603	<0.0001	
KEGG__DNA REPLICATION	<0.0001	0.0044	0.1642	<0.0001	DNA replication
REACTOME__ACTIVATION OF THE PRE-REPLICATIVE COMPLEX	<0.0001	<0.0001	0.0962	<0.0001	
REACTOME__DNA REPLICATION	<0.0001	<0.0001	0.0691	<0.0001	
REACTOME__DNA REPLICATION PRE-INITIATION	<0.0001	<0.0001	0.0626	<0.0001	
REACTOME__ASSEMBLY OF THE PRE-REPLICATIVE COMPLEX	0.0004	<0.0001	0.0649	0.0002	
REACTOME__CHOLESTEROL BIOSYNTHESIS	0.0029	<0.0001	0.0475	0.0029	Metabolism
REACTOME__METABOLISM OF CARBOHYDRATES	0.0118	0.0039	0.0768	0.0017	
REACTOME__ORNITHINE METABOLISM	0.0331	0.0084	0.0495	0.1479	
REACTOME__GLUCONEOGENESIS	0.1432	0.0139	0.1369	0.0109	
REACTOME__CITRIC ACID CYCLE (TCA CYCLE)	0.1627	0.0093	0.1833	0.0064	
KEGG__STEROID BIOSYNTHESIS	0.0123	0.0511	0.1142	0.0653	
KEGG__PENTOSE PHOSPHATE PATHWAY	0.0227	0.0589	0.1087	0.0115	
KEGG__CARBON METABOLISM	0.0481	0.0456	0.0877	0.0063	
KEGG__BIOSYNTHESIS OF AMINO ACIDS	0.0830	0.0653	0.1419	0.0320	
KEGG__CITRATE CYCLE (TCA CYCLE)	0.2296	0.0408	0.1633	0.0012	
KEGG__BIOSYNTHESIS OF UNSATURATED FATTY ACIDS	0.2362	0.0679	0.2280	0.0854	

\*Red indicates upregulation and green downregulation, respectively. Intensity of colours indicates the degree of significance (*dark: FDR < 0.01; light: 0.01 < FDR < 0.25*)

**Table S6:** Upregulated proteins detected by iTRAQ analysis upon p62 knockdown in melanoma cell lines.

SK-Mel-103					
UPREGULATED PROTEINS					
Accession	Gene name	log <sub>2</sub> FC (shp62/shcon)	Accession	Gene name	log <sub>2</sub> FC (shp62/shcon)
P52926	HMGA2	2.380	Q9Y277	VDAC3	1.383
Q99856	ARID3A	1.907	Q5U3C3	TMEM164	1.382
Q8WUH1	CHURC1	1.831	P55786	NPPS	1.381
P00414	MT-CO3	1.810	Q9BWS9	CHID1	1.380
A6NKG5	RTL1	1.771	O15156	ZBTB7B	1.380
Q9HCG8	CWC22	1.745	Q9C0H2	TTYH3	1.377
Q14643	ITPR1	1.739	P09486	SPARC	1.376
P15954	COX7C	1.704	P27540	ARNT	1.372
P33947	KDEL2	1.700	Q5BJD5	TMEM41B	1.370
Q9NPH3	IL1RAP	1.668	Q5NDL2	EOGT	1.369
O75909	CCNK	1.657	Q9NRX4	PHPT1	1.368
O00622	CYR61	1.627	Q8N5L8	RPP25L	1.364
P43355	MAGEA1	1.624	Q9NW08	POLR3B	1.364
Q9NUD5	ZCCHC3	1.616	Q8WWI5	SLC44A1	1.363
P09669	COX6C	1.612	P48060	GLIPR1	1.361

SK-Mel-103					
UPREGULATED PROTEINS					
Accession	Gene name	log <sub>2</sub> FC (shp62/shcon)	Accession	Gene name	log <sub>2</sub> FC (shp62/shcon)
O75152	ZC3H11A	1.610	Q86TP1	PRUNE	1.359
P52823	STC1	1.604	P35555	FBN1	1.359
Q14978	NOLC1	1.596	Q9Y6B6	SAR1B	1.359
P11047	LAMC1	1.583	Q9BSV6	TSEN34	1.355
Q92521	PIGB	1.576	O14817	TSPAN4	1.355
Q96DC9	OTUB2	1.573	Q9UPT9	USP22	1.354
O14686	MLL2	1.567	P15923	TCF3	1.354
O60331	PIP5K1C	1.567	Q5T9L3	WLS	1.349
Q9NWT6	HIF1AN	1.557	Q17RY0	CB4	1.349
Q13542	EIF4EBP2	1.527	O14802	POLR3A	1.349
P98153	DGCR2	1.513	P49356	FNTB	1.348
P24311	COX7B	1.512	O75340	PDCD6	1.347
Q9H7F0	ATP13A3	1.511	O94887	FARP2	1.347
P35908	KRT2	1.511	P43251	BTD	1.347
Q9UI42	CPA4	1.503	O00592	PODXL	1.347
Q15047	SETDB1	1.501	Q8NDZ6	TMEM161B	1.346
P05120	SERPINB2	1.485	Q3YEC7	RABL6	1.345
Q9UBU8	MORF4L1	1.469	Q00534	CDK6	1.345
P19021	PAM	1.465	O75143	ATG13	1.344
O95470	SGPL1	1.464	A6NLU0	RFPL4A	1.342
Q9BPZ3	PAIP2	1.450	P51161	FABP6	1.340
Q9UPY3	DICER1	1.449	Q7LBR1	CHMP1B	1.338
O00507	USP9Y	1.447	P32121	ARRB2	1.338
P04264	KRT1	1.439	P05496	ATP5G1	1.337
Q7Z3C6	ATG9A	1.437	P10606	COX5B	1.331
Q5XKK7	FAM219B	1.431	Q9Y2K7	KDM2A	1.331
Q13277	STX3	1.430	P01583	IL1A	1.330
O75794	CDC123	1.430	Q9Y2V2	CARHSP1	1.328
Q8WU17	RNF139	1.428	Q9UMX5	NENF	1.328
Q9BW60	ELOVL1	1.427	Q9NUM3	SLC39A9	1.327
O95182	NDUFA7	1.425	Q9H300	PARL	1.327
Q9BY49	CR	1.421	O95857	TSPAN13	1.323
O14672	ADAM10	1.420	P20933	AGA	1.323
P00403	MT-CO2	1.418	O96011	X11B	1.321
P60520	GABARAPL2	1.416	P17612	PRKACA	1.321
O95168	NDUFB4	1.411	O14880	MGST3	1.319
O95835	LATS1	1.405	Q14696	MESDC2	1.316
P15407	FOSL1	1.405	Q3SXM5	HSDL1	1.315
Q14980	NUMA1	1.402	Q9H3K6	BOLA2	1.313
A5PLL7	TMEM189	1.398	Q8N954	CCDC75	1.310
Q9ULU4	ZMYND8	1.394	P11171	EPB41	1.309
Q99985	SEMA3C	1.393	Q9H5X1	FAM96A	1.306
Q5TCZ1	SH3PXD2A	1.392	Q92833	JARID2	1.306
Q8IVP5	FUNDC1	1.391	Q01432	AMPD3	1.304
O43731	KDEL3	1.388	Q9NRR4	DROSHA	1.303
Q5HY18	RABL3	1.384	P13645	KRT10	1.301
P20674	COX5A	1.384	Q96AQ6	PBXIP1	1.300

UACC-62					
UPREGULATED PROTEINS					
Accession	Gene name	log <sub>2</sub> FC (shp62/shcon)	Accession	Gene name	log <sub>2</sub> FC (shp62/shcon)
O60315	ZEB2	4.375	Q9NYB0	TERF2IP	1.425
P30508	HLA-C	3.020	Q6NXE6	ARMC6	1.424
Q9NUM3	SLC39A9	2.902	Q9UKN8	GTF3C4	1.422
Q6N063	OGFOD2	2.708	Q9NVV4	MTPAP	1.422
O14646	CHD1	2.699	Q86XA9	HEATR5A	1.420
P35908	KRT2	2.662	Q2TAL8	QRICH1	1.408
Q9H9Q2	COPS7B	2.635	P19022	CDH2	1.407
P00533	EGFR	2.348	O14734	ACOT8	1.407
P61244	MAX	2.327	Q6PKG0	LARP1	1.406
Q7Z5J4	RAI1	2.222	Q69YN2	CWF19L1	1.406
P04264	KRT1	2.186	Q7Z3J2	C16orf62	1.403
Q9UII2	ATPIF1	2.163	Q15004	PAF	1.403
P14136	GFAP	2.147	P05026	ATP1B1	1.400
P11908	PRPS2	1.943	O14521	SDHD	1.397
Q7Z569	BRAP	1.917	Q14738	PPP2R5D	1.385

SK-Mel-103					
UPREGULATED PROTEINS					
Accession	Gene name	log <sub>2</sub> FC (shp62/shcon)	Accession	Gene name	log <sub>2</sub> FC (shp62/shcon)
Q13131	PRKAA1	1.889	Q16890	TPD52L1	1.383
Q9Y3D8	TAF9	1.813	O15259	NPHP1	1.381
Q7Z4Q2	HEATR3	1.801	P23497	SP100	1.379
Q8NEB9	PIK3C3	1.734	Q9C0C9	UBE2O	1.373
Q9BRS2	RIOK1	1.723	Q96ME7	ZNF512	1.372
P52926	HMGA2	1.700	Q8WVJ2	NUDCD2	1.371
P13645	KRT10	1.698	Q9UNX4	WDR3	1.366
Q9H5K3	SGK196	1.687	P40937	RFC5	1.366
Q9BTZ2	DHRS4	1.663	Q96QU8	XPO6	1.366
P08651	NFIC	1.656	Q92922	SMARCC1	1.359
P53667	LIMK1	1.637	O75030	MITF	1.359
Q9NR12	PDLIM7	1.618	Q9Y3A6	TMED5	1.358
Q9UKJ3	GPATCH8	1.617	P35227	PCGF2	1.358
Q12933	TRAF2	1.614	Q5T9L3	WLS	1.358
O00141	SGK1	1.607	Q9NZ32	ACTR10	1.349
O43264	ZW10	1.597	Q00653	NFKB2	1.348
O75506	HSBP1	1.596	P49356	FNTB	1.348
Q6DKK2	TTC19	1.596	Q9Y294	ASF1A	1.348
Q8NEZ5	FBXO22	1.593	Q15003	NCAPH	1.347
Q9H074	PAIP1	1.590	Q9NRF9	POLE3	1.345
Q12986	NFX1	1.580	Q15334	LLGL1	1.345
P31323	PRKAR2B	1.562	Q9BT09	CNPY3	1.345
Q9HCG8	CWC22	1.558	Q9UQN3	CHMP2B	1.345
Q9UJY4	GGA2	1.556	Q5NDL2	EOGT	1.342
Q9BWE0	REPIN1	1.550	Q04721	NOTCH2	1.342
Q6ZT12	UBR3	1.537	O75122	CLASP2	1.341
P57076	C21orf59	1.535	Q9NR50	EIF2B3	1.338
Q14653	IRF3	1.519	P61421	ATP6V0D1	1.337
Q9NPH3	IL1RAP	1.513	Q8TAE8	GADD45GIP1	1.335
P07992	ERCC1	1.512	O00139	KIF2A	1.332
Q86WA6	BPHL	1.506	O14545	TRAFD1	1.329
Q9NPH0	ACP6	1.498	Q9BUL8	PDCD10	1.328
Q7Z4S6	KIF21A	1.489	P15927	RPA2	1.328
O75439	PMPCB	1.484	P19387	POLR2C	1.325
Q9Y3T9	NOC2L	1.484	Q15796	SMAD2	1.322
Q9Y383	LUC7L2	1.482	Q86UU1	PHLDB1	1.321
Q6BCY4	CYB5R2	1.481	P05121	SERPINE1	1.319
P49366	DHPS	1.481	Q8TBQ9	TMEM167A	1.319
Q15843	NEDD8	1.473	Q6ZNE5	ATG14	1.318
Q5MNZ6	WDR45L	1.471	Q96GC9	VMP1	1.317
Q6WCQ1	MPRIIP	1.469	P62714	PPP2CB	1.312
Q96AX1	VPS33A	1.466	Q9ULV0	MYO5B	1.309
Q96GQ7	DDX27	1.464	Q6ZSR9	1 SV	1.309
P51116	FXR2	1.464	Q92878	RAD50	1.305
O00499	BIN1	1.464	Q9UKM9	RALY	1.305
Q8WW12	PCNP	1.455	Q9P253	VPS18	1.304
P14923	JUP	1.455	Q8N128	FAM177A1	1.303
P78362	SRPK2	1.452	Q9UHQ4	BCAP29	1.303
O14976	GAK	1.452	O43765	SGTA	1.303
O14524	TMEM194A	1.445	O75152	ZC3H11A	1.302

**Table S7:** Downregulated proteins detected by iTRAQ analysis upon p62 knockdown in melanoma cell lines.

SK-Mel-103					
DOWNREGULATED PROTEINS					
Accession	Gene name	log <sub>2</sub> FC (shp62/shcon)	Accession	Gene name	log <sub>2</sub> FC (shp62/shcon)
Q9P2R3	ANKFY1	0.767	Q13287	NMI	0.693
Q9BQE5	APOL2	0.767	Q9UPN7	PPP6R1	0.689
Q6ZTR7	FAM92B	0.766	Q9HC78	ZBTB20	0.687
O43741	PRKAB2	0.766	Q00587	CDC42EP1	0.687
Q7Z7A4	PXK	0.766	Q9Y3Z3	SAMHD1	0.686
Q8N8A2	ANKRD44	0.766	Q8IWA0	WDR75	0.685
P43121	MCAM	0.766	Q14592	ZNF460	0.683
O94919	ENDOD1	0.766	Q06787	FMR1	0.683
Q96RT1	ERBB2IP	0.765	Q9UIQ6	LNP	0.682
Q15050	RRS1	0.764	Q96KB5	PBK	0.682

SK-Mel-103					
DOWNREGULATED PROTEINS					
Accession	Gene name	log <sub>2</sub> FC (shp62/shcon)	Accession	Gene name	log <sub>2</sub> FC (shp62/shcon)
Q31612	HLA-B	0.764	Q9Y2H2	INPP5F	0.682
Q86VI3	IQGAP3	0.763	Q9NUQ6	SPATS2L	0.681
Q14534	SQLE	0.763	Q5SSJ5	HP1BP3	0.680
Q15345	LRRRC41	0.762	P23381	WARS	0.680
Q9Y2U8	LEMD3	0.761	P16298	PPP3CB	0.679
Q01082	SPTBN1	0.761	P06280	GLA	0.677
Q9BV79	MECR	0.761	O14519	CDK2AP1	0.677
Q13393	PLD1	0.760	O95864	FADS2	0.673
Q8N6L1	KRTCAP2	0.760	P51788	CLCN2	0.673
Q96IV0	NGLY1	0.759	Q6ICB0	DESI1	0.672
Q63HN8	RNF213	0.759	P49247	RPIA	0.669
Q9BRJ6	C7orf50	0.759	Q8IYM9	TRIM22	0.667
Q99598	TSNAX	0.759	O00562	PITPNM1	0.665
Q9BXS9	SLC26A6	0.759	Q6PIJ6	FBXO38	0.661
P12931	SRC	0.759	Q92736	RYR2	0.660
P07196	NEFL	0.759	P0CW20	LIMS3L	0.658
A3KMH1	VWA8	0.758	Q9Y653	GPR56	0.658
Q8TCS8	PNPT1	0.758	P80217	IFI35	0.653
Q8IWS0	PHF6	0.758	Q53GL7	PARP10	0.653
Q96EU7	C1GALT1C1	0.758	Q9Y5Q0	FADS3	0.652
Q9UKL6	PCTP	0.757	O95249	GOSR1	0.651
Q15025	TNIP1	0.757	Q14202	ZMYM3	0.651
Q12929	EPS8	0.756	O15554	KCNN4	0.650
Q12765	SCRN1	0.756	O43493	TGOLN2	0.649
Q8N543	OGFOD1	0.756	O60307	MAST3	0.648
O00442	RTCA	0.756	Q5D862	FLG2	0.647
Q14693	LPIN1	0.756	Q8NHU6	TDRD7	0.645
Q92743	HTRA1	0.755	Q9NYZ1	FAM18B1	0.643
P06396	GSN	0.755	Q13438	OS9	0.643
P43360	MAGEA6	0.755	P30281	CCND3	0.642
Q9ULT8	HECTD1	0.755	Q9Y5A7	NUB1	0.640
P46976	GYG1	0.754	P40306	PSMB10	0.640
P07996	THBS1	0.754	Q9NUG6	PDRG1	0.640
Q16666	IFI16	0.754	P19474	TRIM21	0.638
Q8TEL6	TRPC4AP	0.753	P36954	POLR2I	0.634
P53985	SLC16A1	0.752	Q9H5Z1	DHX35	0.634
O15234	CASC3	0.751	Q15417	CNN3	0.632
Q5T3I0	GPATCH4	0.751	P19525	EIF2AK2	0.631
A0AVT1	UBA6	0.751	Q16222	UAP1	0.630
Q68D91	MBLAC2	0.751	P32004	L1CAM	0.629
Q05193	DNM1	0.750	Q5K651	SAMD9	0.628
Q99538	LGMN	0.749	P11137	MAP2	0.628
Q9UBV2	SEL1L	0.749	Q9Y3R5	DOY2	0.628
P51884	LUM	0.748	Q9UBT7	CTNNAL1	0.625
O00767	SCD	0.747	Q9Y6K5	OAS3	0.625
Q9BRP1	PDCD2L	0.746	Q9BRQ6	CHCHD6	0.622
Q9H7E9	C8orf33	0.746	Q96AC1	FERMT2	0.618
Q03135	CAV1	0.744	Q92624	APPBP2	0.617
P60602	ROMO1	0.743	P05121	SERPINE1	0.613
P30460	HLA-B	0.740	O75955	FLOT1	0.610
Q9BSU1	C16orf70	0.739	Q9Y2Z2	MTO1	0.607
Q9BTE7	DCUN1D5	0.738	Q9C0D9	EPT1	0.604
Q8TB03	CXorf38	0.737	Q8IXQ6	PARP9	0.604
Q8NBM8	PCYOX1L	0.737	Q460N5	PARP14	0.601
Q9H814	PHAX	0.737	O00418	EEF2K	0.598
Q9NWS0	PIH1D1	0.735	O75886	STAM2	0.596
O43592	XPOT	0.735	Q9NQ25	SLAMF7	0.594
P69905	HBA1	0.734	Q9NY97	B3GNT2	0.589
Q9NZR1	TMOD2	0.733	Q96EN8	MOCOS	0.588
A1X283	SH3PXD2B	0.733	P06899	HIST1H2BJ	0.587
Q9H6X4	TMEM134	0.733	Q8TDB6	DTX3L	0.582
O00472	ELL2	0.732	P08138	NGFR	0.582
Q8NC69	KCTD6	0.732	Q15800	MSMO1	0.578
Q15631	TSN	0.730	Q99541	PLIN2	0.578
Q9Y5K6	CD2AP	0.729	O60814	HIST1H2BK	0.576
P09455	RBP1	0.729	Q9HCJ6	VAT1L	0.575
P28838	LAP3	0.729	P30508	HLA-C	0.569
Q96S19	C16orf13	0.728	Q14699	RFTN1	0.562

SK-Mel-103					
DOWNREGULATED PROTEINS					
Accession	Gene name	log <sub>2</sub> FC (shp62/shcon)	Accession	Gene name	log <sub>2</sub> FC (shp62/shcon)
Q96EP0	RNF31	0.728	P42574	CASP3	0.562
P38159	RBMX	0.728	Q81YT2	FTSJD1	0.560
Q96D46	NMD3	0.728	Q8N9M5	TMEM102	0.560
Q9H6R7	C2orf44	0.725	P48723	HSPA13	0.559
Q8WVB7	C1orf85	0.724	Q6PIU2	NCEH1	0.551
Q96BN2	TADA1	0.723	Q9BYK8	PRIC285	0.541
A0JNW5	UHRF1BP1L	0.721	Q9UMR5	PPT2	0.541
O14763	TNFRSF10B	0.721	Q9Y2V0	C15orf41	0.535
Q49A26	GLYR1	0.719	Q9NUL5	C19orf66	0.531
Q7L5N7	LPCAT2	0.719	Q13501	SQSTM1	0.525
Q9P0R6	GSKIP	0.719	O94856	NFASC	0.521
Q6P996	PDXDC1	0.719	O95786	DDX58	0.519
P55265	ADAR	0.717	O14933	UBE2L6	0.519
P23229	ITGA6	0.716	P61960	UFM1	0.506
Q03518	TAP1	0.716	Q5QJ74	TBCEL	0.501
Q9UDT6	CLIP2	0.716	P42224	STAT1	0.492
Q13938	CAPS	0.714	P05161	ISG15	0.486
Q8N2F6	ARMC10	0.713	P41226	UBA7	0.485
O95365	ZBTB7A	0.713	Q9BPU6	DPYSL5	0.481
Q96JQ2	CLMN	0.711	P52630	STAT2	0.474
O00635	TRIM38	0.710	P35610	SOAT1	0.474
Q9H330	TMEM245	0.710	Q7Z417	NUFIP2	0.463
Q15785	TOMM34	0.708	Q9P2E3	ZNFX1	0.460
Q2VPB7	AP5B1	0.708	P32455	GBP1	0.456
Q08AF3	SLFN5	0.706	Q13325	IFIT5	0.446
Q9H0P0	NT5C3	0.705	P62805	HIST1H4A	0.424
Q96JG6	CCDC132	0.704	Q8TCB0	IFI44	0.383
Q9Y3C0	CCDC53	0.704	Q8N4J0	C9orf41	0.382
Q96MU7	YTHDC1	0.702	P61587	RND3	0.374
P00750	PLAT	0.701	O15162	PLSCR1	0.318
P61769	B2M	0.700	O14879	IFIT3	0.267
O95210	STBD1	0.700	Q9NQC7	CYLD	0.258
Q9BZQ8	FAM129A	0.698	P09914	IFIT1	0.217
Q9BTE3	MCMBP	0.697	Q86UL8	MAGI2	0.210
P16190	HLA-A	0.696	P09913	IFIT2	0.118
P09884	POLA1	0.694			

UACC-62					
DOWNREGULATED PROTEINS					
Accession	Gene name	log <sub>2</sub> FC (shp62/shcon)	Accession	Gene name	log <sub>2</sub> FC (shp62/shcon)
Q86U38	NOP9	0.768	P82914	MRPS15	0.714
P53634	CTSC	0.767	Q7Z417	NUFIP2	0.712
P04271	S100B	0.767	O43592	XPOT	0.712
P33897	ABCD1	0.767	Q9Y653	GPR56	0.710
P01011	SERPINA3	0.765	Q43719	HTATSF1	0.709
O15541	RNF113A	0.764	P27338	MAOB	0.709
P61604	HS1	0.764	P37840	SNCA	0.703
Q8NHU6	TDRD7	0.764	P16403	HIST1H1C	0.703
Q9BX68	HINT2	0.764	Q9UBD5	ORC3	0.701
P05556	ITGB1	0.763	Q15050	RRS1	0.700
P34059	GALNS	0.763	P20338	RAB4A	0.699
Q9UBB9	TFIP11	0.762	Q96RF0	SNX18	0.699
Q8N511	TMEM199	0.762	Q8WTV0	SCARB1	0.697
Q9NZJ4	SACS	0.761	Q9Y250	LZTS1	0.691
O95070	YIF1A	0.761	O95249	GOSR1	0.691
Q9Y5U9	IER3IP1	0.761	O00762	UBE2C	0.689
Q969X5	ERGIC1	0.759	Q9H2J7	SLC6A15	0.686
P57088	TMEM33	0.759	Q03154	ACY1	0.683
P41240	CSK	0.757	Q9BW72	HIGD2A	0.683
O95149	SNUPN	0.757	Q6PIU2	NCEH1	0.683
Q9UJW0	DCTN4	0.757	Q96PU8	QKI	0.681
Q8WUA2	PPIL4	0.756	Q9NVR2	INTS10	0.681
Q9NW82	WDR70	0.756	P53675	CLTCL1	0.679
Q8WW59	SPRYD4	0.755	P46976	GYG1	0.677
Q7Z333	SETX	0.755	Q9Y6W5	WASF2	0.675
Q96D46	NMD3	0.754	P23229	ITGA6	0.672
Q96J42	TXNDC15	0.754	Q99538	LGGMN	0.670

UACC-62					
DOWNREGULATED PROTEINS					
Accession	Gene name	log <sub>2</sub> FC (shp62/shcon)	Accession	Gene name	log <sub>2</sub> FC (shp62/shcon)
Q9Y606	PUS1	0.754	Q14146	URB2	0.663
Q15005	SPCS2	0.753	Q6P996	PDXDC1	0.663
Q969E4	TCEAL3	0.753	O60443	DFNA5	0.661
O14773	TPP1	0.753	Q9Y5B9	SUPT16H	0.655
Q86WB0	ZC3HC1	0.752	Q9BV36	MLPH	0.654
Q6RW13	AGTRAP	0.751	Q6P2C8	MED27	0.650
P61513	RPL37A	0.750	Q9H4A3	WNK1	0.649
Q15785	TOMM34	0.749	Q9UBM4	OPTC	0.644
Q7Z739	YTHDF3	0.749	Q9C0D9	EPT1	0.641
O43847	NRD1	0.747	Q9NRL2	BAZ1A	0.641
Q92743	HTRA1	0.747	Q9NVN8	GNL3L	0.640
Q9BY43	CHMP4A	0.747	Q16222	UAP1	0.636
Q15631	TSN	0.746	Q6ICB0	DESI1	0.631
Q86VU5	COMTD1	0.746	P55795	HNRNPH2	0.630
Q6L8Q7	PDE12	0.745	P49247	RPIA	0.630
Q9H6W3	NO66	0.743	Q9H0W9	C11orf54	0.629
Q8N131	TMEM123	0.742	Q9H814	PHAX	0.627
Q9Y3A2	UTP11L	0.742	Q8WU79	SMAP2	0.623
P15586	GNS	0.741	P49711	CTCF	0.623
O43776	NARS	0.740	Q96AC1	FERMT2	0.616
P62341	SELT	0.740	P11388	TOP2A	0.615
Q8N6V9	TEX9	0.739	Q96E52	OMA1	0.610
O14497	ARID1A	0.737	Q8NB46	ANKRD52	0.603
Q12765	SCRN1	0.736	P27694	RPA1	0.594
Q9P2Q2	FRMD4A	0.735	P33552	CKS2	0.592
P43360	MAGEA6	0.729	Q9BUP3	HTATIP2	0.588
Q9P1U0	ZNRD1	0.727	Q9UDW1	UQCR10	0.585
Q96SZ5	ADO	0.726	Q96KQ7	EHMT2	0.583
Q96GQ5	C16orf58	0.726	P51692	STAT5B	0.583
Q9BRX2	LO	0.726	Q5TAQ9	DCAF8	0.567
P53367	ARFIP1	0.726	Q330K2	NDUFAF6	0.563
Q5J8M3	EMC4	0.725	Q9UNN8	PROCR	0.555
O60518	RANBP6	0.725	Q9Y5Q0	FADS3	0.527
Q99598	TSNAX	0.724	Q14739	LBR	0.519
Q9BU61	NDUFAF3	0.723	P42574	CASP3	0.498
O60671	RAD1	0.723	Q13510	ASAH1	0.492
Q9H8Y8	GORASP2	0.723	Q8N2G6	ZCCHC24	0.476
P61163	ACTR1A	0.722	P48426	PIP4K2A	0.470
Q86YV9	HPS6	0.720	Q8TDX7	NEK7	0.459
O43172	PRPF4	0.719	P48723	HSPA13	0.456
P02794	FTH1	0.718	Q8N4J0	C9orf41	0.451
Q9Y6Y0	IVNS1ABP	0.717	P24043	LAMA2	0.450
P82675	MRPS5	0.717	Q6GQQ9	OTUD7B	0.424
Q5VWP3	MLIP	0.717	P50443	SLC26A2	0.397
P51608	MECP2	0.714	Q13501	SQSTM1	0.284

**Table S8:** Upregulated proteins detected by iTRAQ analysis upon ATG5 knockdown in melanoma cell lines.

SK-Mel-103					
UPREGULATED PROTEINS					
Accession	Gene name	log <sub>2</sub> FC (siATG5/shcon)	Accession	Gene name	log <sub>2</sub> FC (siATG5/shcon)
Q92581-3	SLC9A6	3.006	H3BPR7	TYRO3	1.410
Q8TD22	SFXN5	2.028	A6NM62	LRRC53	1.407
G3V0H6	NARG2	2.003	B4DGV4	RYR2	1.403
Q6ZTA4-2	TRIM67	1.996	Q8NI37	PPTC7	1.397
Q9UBN7-2	HDAC6	1.901	O15504	NUPL2	1.390
A8MZ59	LEUTX	1.859	O00429-4	DNM1L	1.382
Q9BV19	C1orf50	1.745	B4E3L6	D2HGDH	1.381
Q92871	PMM1	1.693	Q9NUH8-2	TMEM14B	1.374
P35527	KRT9	1.689	P53675-2	CLTCL1	1.371
Q8WXG9-3	GPR98	1.651	C9JZR9	SLC30A6	1.370
Q8NBPO-2	TTC13	1.641	P02533	KRT14	1.367
F8WEM9	ZNF655	1.592	Q9Y248	GINS2	1.364
D6RJA4	AMOTL2	1.586	P60660	MYL6	1.364
Q9NZ71-5	RTEL1	1.584	E9PPF2	TYK2	1.363
F8W036	2	1.583	P20749	BCL3	1.361

SK-Mel-103					
UPREGULATED PROTEINS					
Accession	Gene name	log <sub>2</sub> FC (siATG5/shcon)	Accession	Gene name	log <sub>2</sub> FC (siATG5/shcon)
Q9H2H9	SLC38A1	1.570	Q9Y3Y2-4	CHTOP	1.361
Q68DH5	LMBRD2	1.541	Q9BYC5-3	FUT8	1.354
Q9BWW5	SSDP4	1.528	P10412	HIST1H1E	1.350
C9J9V6	NME6	1.501	H3BTL1	MAP1LC3B	1.348
Q8WWB7-2	C1orf85	1.498	Q96BR1-2	SGK3	1.347
Q9NS91	RAD18	1.493	Q9NVN3-3	RIC8B	1.342
Q16384	SSX1	1.491	E7ET89	DTX2	1.341
P33552	CKS2	1.488	Q8NB46	ANKRD52	1.336
O15069	NACAD	1.488	B4DJJ3	TAPT1	1.334
D3DWC4	TMEM23	1.488	Q05D32-2	CTDSPL2	1.331
Q71DI3	HIST2H3A	1.487	O43854-2	EDIL3	1.331
A6NDU8	C5orf51	1.480	Q9NSY1	BMP2K	1.324
Q7L0J3-2	SV2A	1.474	Q9BZM4	ULBP3	1.324
Q86SX6	GLRX5	1.460	Q9Y233	PDE10A	1.322
A8MUN2	APOB	1.439	Q9NZD2	GLTP	1.321
P07585	DCN	1.438	Q96HY7	DHTKD1	1.316
Q9NQG6	SMCR7L	1.433	E9PP15	LRP8	1.312
C9JEZ4	CDC42EP3	1.433	O60725	ICMT	1.311
C9J5B3	KCTD20	1.432	Q9NP73-2	ALG13	1.311
Q8IWT0	ZBTB8OS	1.427	H3BVI5	RHOT2	1.311
Q96IV0-3	NGLY1	1.425	Q9NR31	SAR1A	1.308
H7COU0	PARL	1.423	Q12913	PTPRJ	1.306
P12259	F5	1.419	Q9BV23	ABHD6	1.304
Q96S97	MYADM	1.414	Q96DX7	TRIM44	1.302
Q86UT6-2	NLRX1	1.411	P62745	RHOB	1.300

UACC-62					
UPREGULATED PROTEINS					
Accession	Gene name	log <sub>2</sub> FC (siATG5/shcon)	Accession	Gene name	log <sub>2</sub> FC (siATG5/shcon)
P35527	KRT9	5.091	P51397	DAP	1.403
Q9UQL6	HDAC5	2.742	P51512	MMP16	1.402
P02533	KRT14	2.333	P08582-2	MF12	1.398
P14859-3	POU2F1	2.283	F8VUA5	RAB5B	1.397
Q15366-6	PCBP2	2.001	H0YL93	FMN1	1.392
Q95IE3	HLA-DRB1	1.922	E9PPF2	TYK2	1.391
P59542	TAS2R19	1.915	P16402	HIST1H1D	1.385
P04264	KRT1	1.895	A5A3E0	POTEF	1.380
Q4G0P3-2	HYDIN	1.838	Q9HCE3	ZNF532	1.375
B1AZU4	HLA-F	1.815	Q08AT0	SGCZ	1.372
E7ENQ1	MAP4K4	1.805	Q9BWW5	SSDP4	1.370
Q4VC05	BCL7A	1.794	Q12769-3	NUP160	1.368
O14893-2	GEMIN2	1.787	Q9NQS3	PVRL3	1.367
Q76176	SSH2	1.744	A8MXF6	RABL2B	1.360
Q9BQQ3	GORASP1	1.690	Q9NRF2-2	SH2B1	1.359
Q13015	MLLT11	1.655	H7C1Q1	2	1.357
Q9Y248	GINS2	1.650	P17535	JUND	1.354
Q9UPN3	MACF1	1.631	P25440	BRD2	1.341
F8WEM9	ZNF655	1.614	P17066	HSPA6	1.339
K7EJS5	MFS12	1.564	Q9UMN6	WBP7	1.337
P61601	NCALD	1.549	E9PDF6	MYO1B	1.336
Q6T4R5-4	NHS	1.547	Q9NTU7	CBLN4	1.333
O00329	PIK3CD	1.542	Q7L7V1-2	DHX32	1.332
P13284	IFI30	1.536	Q8TD30	GPT2	1.329
D6RGY8	YIPF3	1.524	H0Y853	WDR52	1.327
H7C4F8	CD86	1.518	Q9BVS4-2	RIOK2	1.325
C4AMC7	WASH3P	1.492	O43854-2	EDIL3	1.324
O76061	STC2	1.468	Q6NTF9	RHBDD2	1.322
MOQX48	EPHX3	1.464	E9PSI1	TM9SF1	1.313
Q9Y2S2-2	CRYL1	1.451	P12074	COX6A1	1.312
Q9HCJ6	VAT1L	1.448	Q9NVH2-4	INTS7	1.311
C9J9D7	SIAH2	1.445	O60218	AKR1B10	1.308
Q2MD36	MBD4	1.442	P17028	ZNF24	1.307
P58107	EPPK1	1.437	Q7Z7G8-2	VPS13B	1.303
G3V217	CCDC63	1.405	Q9UGU5	HMGXB4	1.302

**Table S9:** Downregulated proteins detected by iTRAQ analysis upon ATG5 knockdown in melanoma cell lines.

SK-Mel-103					
DOWNREGULATED PROTEINS					
Accession	Gene name	log <sub>2</sub> FC (siATG5/shcon)	Accession	Gene name	log <sub>2</sub> FC (siATG5/shcon)
Q5JQ6	CTNNAL1	0.457	E9PSH3	TSPAN4	0.703
B4EQJ7	RRN3	0.466	O43194	GPR39	0.714
C9J473	MPV17	0.485	Q8TBN0-2	RAB3IL1	0.714
E5RFF3	TRPS1	0.525	O14556	GAPDHS	0.717
E7ER97	ASMTL	0.537	Q96AC1	FERMT2	0.717
Q9H1Y0-2	ATG5	0.554	Q9NZJ4	SACS	0.718
Q13495-4	MAMLD1	0.565	P05120	SERPINB2	0.720
B7ZKP8	UBXN2A	0.568	Q14676-3	MDC1	0.720
O94817	ATG12	0.577	Q16739	UGCG	0.722
E7ENQ1	MAP4K4	0.579	H0Y9R9	IDUA	0.723
Q9H469	FBXL15	0.594	E7EMN6	PPP1R2	0.728
Q8N3X1	FNBP4	0.607	P15104	GLUL	0.728
Q8IYT2	FTSDJ1	0.608	Q9P0S9	TMEM14C	0.729
Q8IYQ7	THNSL1	0.609	D3DR31	IFIT1	0.731
Q58FG1	HSP90AA4P	0.623	E5RG63	PSEN2	0.735
Q15173-2	PPP2R5B	0.628	P12532	CKMT1A	0.736
Q8TCZ2-3	CD99L2	0.632	Q9Y2I1	NISCH	0.737
Q8NHU2-4	C20orf26	0.635	Q15366-6	PCBP2	0.740
P09913	IFIT2	0.637	Q5SW96	LDLRAP1	0.740
Q99675	CGRRF1	0.639	Q5T0D9	TPRG1L	0.743
O14578-3	CIT	0.640	P53985	SLC16A1	0.743
P12074	COX6A1	0.641	C9J0J0	CCDC126	0.748
P38432	COIL	0.641	Q9H7E2-2	TDRD3	0.749
A8MX49	PPM1F	0.641	B3KRF7	ZKSCAN1	0.749
O95785	WIZ	0.642	P58511	SMIM11	0.749
I3L196	ARL16	0.644	D6RC69	CEP120	0.749
Q01518-2	CAP1	0.645	Q9BYT5	KRTAP2-2	0.750
E9PCV0	GUSB	0.649	O75600	GCAT	0.750
J3KN27	FBRSL1	0.650	H7C2M2	POLM	0.750
B4E2D5	SUPT20H	0.652	P25445-6	FAS	0.750
Q9UI10-3	EIF2B4	0.653	Q9UPS8-2	ANKRD26	0.750
P58107	EPPK1	0.653	Q9UNW1	MINPP1	0.751
Q9UJU3-2	ZNF112	0.654	B8ZZR0	CLK1	0.753
F5GYA1	CAPRIN2	0.658	P02790	HPX	0.754
Q96SI9-2	STRBP	0.661	K7EIN1	WBP2	0.754
K7ERE1	4	0.662	Q8IYM9-2	TRIM22	0.755
Q9P1Y5	CAMSAP3	0.667	Q3MIP1	ITPRIPL2	0.755
Q58FF3	HSP90B2P	0.669	Q6UWH4-3	FAM198B	0.755
H3BRL3	UBFD1	0.670	Q02156	PRKCE	0.758
Q08345	DDR1	0.672	O60502	MGEA5	0.759
Q676U5-3	ATG16L1	0.675	C9JKF1	SAMD9	0.759
F5H4R4	DCP1B	0.677	G3V1U5	GOLT1B	0.759
Q8WWQ0	PHIP	0.679	C9JMQ9	KLHL24	0.759
Q8N1W1-4	ARHGEF28	0.679	B4DN24	FANCL	0.760
Q8NDV7-2	TNRC6A	0.679	Q6GYQ0-4	RALGAPA1	0.760
K7EJS5	MFSD12	0.680	Q12959-4	DLG1	0.760
P43356	MAGEA2	0.681	O14933	UBE2L6	0.760
G3V1V8	MYL2	0.681	Q9NQL2	RRAGD	0.760
H7BXR5	SNX29	0.681	Q9Y2F5	KIAA0947	0.762
Q8IVT1	PGPEP1	0.685	Q9NR16-2	CD163L1	0.764
Q9Y6V0-2	PCLO	0.688	Q9H2G4	TSPYL2	0.764
Q5EBL4-2	RILPL1	0.688	P82909	MRPS36	0.764
P54646	PRKAA2	0.694	Q15434	RBMS2	0.764
Q15651	HMGN3	0.694	Q9Y3Q8	TSC22D4	0.765
Q9Y6R7	FCGBP	0.696	Q6P1X5	TAF2	0.766
Q9Y289	SLC5A6	0.700	Q96EH3	MALSU1	0.769
Q96DX8	RTP4	0.702			

UACC-62					
DOWNREGULATED PROTEINS					
Accession	Gene name	log <sub>2</sub> FC (siATG5/shcon)	Accession	Gene name	log <sub>2</sub> FC (siATG5/shcon)
Q330K2-2	NDUF6AF6	0.413	Q9Y3R5-2	DOPEY2	0.715
E9PBG7	CAMK2D	0.415	Q9NQN1	OR2S2	0.715
Q0VDD8-3	DNAH14	0.433	Q9NQA3	WASH6P	0.718
C9J9V6	NME6	0.475	Q8N1W1-4	ARHGEF28	0.719

UACC-62					
DOWNREGULATED PROTEINS					
Accession	Gene name	log <sub>2</sub> FC (siATG5/shcon)	Accession	Gene name	log <sub>2</sub> FC (siATG5/shcon)
O94817	ATG12	0.496	F5H5W6	DDX58	0.720
Q8TD22	SFXN5	0.497	Q9H4E5-2	RHOJ	0.721
Q13495-4	MAMLD1	0.532	Q5XG87	PAPD7	0.724
Q9UGJ0-2	PRKAG2	0.535	O14578-3	CIT	0.724
K7EQ93	UNK	0.540	A8MU44	HOOK1	0.725
K7ES52	TK1	0.596	P57088	TMEM33	0.725
Q5T0D9	TPRG1L	0.599	P07108	DBI	0.727
Q9ULP9-2	TBC1D24	0.615	Q9Y5N5-2	N6AMT1	0.728
Q9H1Y0-2	ATG5	0.615	Q14676-3	MDC1	0.729
Q676U5-3	ATG16L1	0.616	D6RD42	MLIP	0.730
B3KU92	LOC90826	0.617	P78358-2	CTAG1A	0.731
Q8N9M5	TMEM102	0.626	Q08345	DDR1	0.731
Q9Y289	SLC5A6	0.627	Q9UBX3	SLC25A10	0.731
K7EIN1	WBP2	0.631	Q9NY84-3	VNN3	0.732
P07602-2	PSAP	0.639	O43194	GPR39	0.737
Q6N069	NAA16	0.640	Q8NHU2-4	C20orf26	0.739
Q13424	SNTA1	0.648	Q6N075	MFSD5	0.740
Q6EEV4-2	POLR2M	0.654	Q8IYQ7	THNSL1	0.741
A0JNW5	UHRF1BP1L	0.656	Q9H334-2	FOXP1	0.743
Q8IYT2	FTSJD1	0.658	Q07020	RPL18	0.743
H0Y7G7	HLA-DPB1	0.660	O75487	GPC4	0.745
Q13433	SLC39A6	0.664	Q9P086	MED11	0.746
Q86V85	GPR180	0.670	Q9UIL1-3	SCOC	0.748
Q9NPG3-2	UBN1	0.679	A6NN40	SHROOM1	0.750
Q96SI9-2	STRBP	0.685	H0YLN8	TRPM7	0.750
Q92994	BRF1	0.686	F5H050	DYNC111	0.752
K7ENR6	PSMG2	0.689	Q96T88	UHRF1	0.754
Q9BZG9-3	LYNX1	0.689	B4DWK3	TFAP2C	0.758
Q9NQ34	TMEM9B	0.692	K7ENE2	GID4	0.758
O14879	IFIT3	0.695	F5H5D4	PAAF1	0.758
Q8N2Y8	RUSC2	0.696	B1AHG3	PRR5	0.759
Q69YL0	4	0.698	Q9H617	TMEM164	0.759
Q9ULX9-2	MAFF	0.700	J3KST3	GLTPD1	0.760
H3BRL3	UBFD1	0.701	F8W036	2	0.760
Q9H0F6-2	SHARPIN	0.703	E7EMN6	PPP1R2	0.761
B7ZKP8	UBXN2A	0.704	D3DWC4	TMEM23	0.762
Q99808	SLC29A1	0.708	Q86X10-2	RALGAPB	0.763
E9PB91	TIMM23	0.709	B4DXS1	NMT2	0.763
Q8NDV7-2	TNRC6A	0.709	C9JSE3	FANCG	0.764
Q6PID8-2	KLHDC10	0.710	K7EK07	H3F3B	0.764
J3KPS2	FAM83H	0.710	K7ERE1	4	0.767
Q96HN2-3	AHCYL2	0.712	Q9Y385	UBE2J1	0.768
E9PCV0	GUSB	0.713	P05161	ISG15	0.769
F6RY50	SIPA1	0.713	H3BPT0	CMC2	0.769
P53794	SLC5A3	0.714			

**Table S10.** Quantification of FERMT2 immunostaining in tissue microarrays of melanocytic tumors.

Melanocytic tumors	FERMT2 negative n (%)	FERMT2 low n (%)	FERMT2 high n (%)	Total n
Dermal nevi	28 (82.4%)	5 (14.7%)	1 (2.9%)	34
VGP melanomas	20 (24.4%)	24 (29.3%)	31 (37.8%)	82
Cutaneous metastases	9 (27.3%)	8 (24.2%)	16 (48.5%)	33
Lymph node metastases	7 (25.0%)	14 (50.0%)	7 (25.0%)	28
Visceral metastases	4 (18.2%)	13 (59.1%)	5 (22.7%)	22
<b>Total</b>	<b>68 (34.2%)</b>	<b>64 (32.2%)</b>	<b>60 (30.2%)</b>	<b>199</b>

**Table S11.** Clinical and histological data of melanoma cases included in the study of FERMT2 immunostaining (total n=82).

<b>Age (years)</b>	25–89 (mean 58.88)
<b>Gender</b>	<b>n (%)</b>
Female	43 (52.44%)
Male	39 (47.56%)
<b>Region of primary melanoma</b>	<b>n (%)</b>
Trunk	24 (29.27%)
Limbs	27 (32.93 %)
Hands and feet	16 (19.51%)
Head and neck	12 (14.63%)
NA	3 (3.66%)
<b>Histological type of melanoma</b>	<b>n (%)</b>
Superficial spreading	40 (48.78%)
Nodular	17 (20.73%)
Acral	19 (23.17%)
Lentigo maligna	4 (4.88%)
NA	2 (2.44%)
<b>Breslow thickness (mm)</b>	0.4–19 (mean 3.68)
<b>Clark level</b>	<b>n (%)</b>
I	0 (0%)
II	3 (3.66%)
III	32 (39.02%)
IV	33 (40.24%)
V	10 (12.20%)
NA	4 (4.88%)
<b>Ulceration status</b>	<b>n (%)</b>
Not ulcerated	44 (53.66%)
Ulcerated	37 (45.12%)
NA	1 (1.22%)

(Abbreviation; NA=not available)

**Table S12.** Univariate and multivariate survival analyses using the Cox proportional hazards model in patients with melanoma according to FERMT2 immunostaining.

Characteristics	Univariate analysis			Multivariate analysis		
	HR	95% CI	p value	HR	95% CI	p-value
<b>Disease free survival</b>						
FERMT2 high expression	1.945	1.107-3.417	0.021*	1.845	1.040-3.272	0.036*
Breslow	-	-	-	1.085	0.992-1.187	0.073
<b>Distant metastasis free survival</b>						
FERMT2 high expression	2.541	1.260-5.126	0.009*	2.357	1.163-4.774	0.017*
Breslow	-	-	-	1.102	0.981-1.238	0.100
<b>Overall survival</b>						
FERMT2 high expression	1.882	0.986-3.593	0.055	1.716	0.895-3.288	0.104
Breslow	-	-	-	1.157	1.043-1.283	0.006*

(HR, hazard ratio. CI, confidence interval. \*Significantly different)

**Table S13:** p62 interactors with the corresponding number of peptides identified by co-IP followed by Mass spectrometry in melanoma cell lines.

Gene Name	p62_CytoREP_01	p62_CytoREP_02	p62_CytoREP_03	p62_NucREP_01	p62_NucREP_02	p62_NucREP_03
<b>SQSTM1</b>	<b>175</b>	<b>176</b>	<b>169</b>	<b>45</b>	<b>52</b>	<b>46</b>
DARS2	175	171	157	63	58	63
UTRN	84	80	79			
ZC3H4	76	65	67	19	18	20
AZI1	73	70	67			
RBM12B	62	58	59	53	50	54
ATAD3A	62	58	57	42	40	38
ARHGEF18	57	60	48			
BCKDK	52	49	45	4	3	5
TUBB	50	55	50	8	6	4
GBAS	45	48	45	1	2	2
TUBB4B	43	42	42	6	4	3
RAPGEF2	42	41	39			
TAOK1	41	45	41			
NIPSNAP1	40	35	39			
FN1	39	47	42	12	11	10
TUBB2A	38	41	39	6	5	4
CEP350	34	29	29			
AHNAK	33	36	34	18	21	22
ATAD3B	32	31	31	22	22	19
PCNT	30	23	29			
TUBA1B	30	34	30	4	5	3
HADHB	26	28	26	3	4	3
SOD3	25	26	24	1		
TUBA1C	25	31	29	4	5	3
CDK5RAP2	24	21	30			
SLC25A4	24	28	25	57	59	57
GOLGB1	22	19	20			
ROBO1	22	26	27			
MYO1B	22	24	27	23	26	25
WDR82	20	22	19	10	9	12
SMG1	18	12	15			
RAI14	18	11	17	1		1
TNC	16	19	19			1
GAPVD1	15	12	14			
PRRC2A	15	12	14			
OFD1	15	18	12			
SLC25A3	15	17	15	30	29	29
TJP1	14	16	11		1	1
RRBP1	14	20	15	24	18	20
HNRNPUL1	14	10	11	12	14	15
MIB1	14	14	16			
MYO5A	13	14	12			
PRKCI	12	12	11			
MTDH	12	15	12	18	15	15
FGFR1OP	12	10	12			
CD44	12	10	9			
AIFM1	12	13	12	14	16	16
PIBF1	12	11	12			
POLRMT	11	7	10			
SPATA20	11	11	10			
PGAM5	11	9	12	6	6	6
CEP290	11	10	12			
CCDC77	11	14	15			
SNTB1	10	10	10			
GLG1	10	8	10			
CHCHD3	10	8	9	2	3	3
ATP5B	10	11	7	22	16	16
PARD3	9	7	9			
MOGS	9	10	8	7	7	6
EPDR1	9	9	10			
CNST	9	9	9			
IQGAP1	8	9	7	1		1
MAGI1	8	8	6			
CTHRC1	8	8	7			
ATP5A1	8	8	8	26	24	22
SNTB2	7	7	6			

Gene Name	p62_CytoREP_01	p62_CytoREP_02	p62_CytoREP_03	p62_NucREP_01	p62_NucREP_02	p62_NucREP_03
IGF2BP3	7	4	7			
LLGL1	7	6	6			
MPRIIP	7	7	5	1	1	2
OSBPL8	7	6	7			
FRYL	7	6	8			
IQSEC1	6	3	3			
TPX2	6	4	3	7	8	7
CKAP4	6	6	6	20	13	11
RPS16	6	5	5	10	10	9
RPS24	6	6	5	7	5	5
GDF15	6	5	6	1	2	1
EIF5B	5	3	5	1	1	1
SERPINE2	5	5	6			
RPS5	5	6	5	12	11	11
EPRS	5	4	5			
CT45A2	5	6	5	11	12	13
RPS15	5	3	3	5	5	6
ACTR1A	5	4	6			
CCDC61	5	5	3			
SLC25A11	5	4	5	17	21	19
ITIH5	5	6	5			
SLC25A1	5	6	6	16	15	15
KEAP1	4	4	4			
SMG8	4	4	4			
PRPF38A	4	2	4	1	2	
CEP170	4	4	4			
PAFAH1B1	4	2	3			
PPP2R1A	4	4	4	1		
MRPS28	4	2	4			
CNP	4	5	5	12	10	15
GNB1	4	5	3			
CD59	4	4	5			
SMU1	3	1	1	13	12	11
TAOK2	3	3	2			
AP2B1	3	4	2	2	1	
MRPS22	3	3	4			
ERAL1	3	3	3			
MRPS26	3	4	2			
SRPR	3	4	3	3	3	2
MRPS18B	3	4	3			
UQCRH	3	2	2	3	4	4
HSD17B12	3	2	2			
CEP250	3	4	3			
GNAI2	3	7	3			
NBR1	2	6	3			
DYNC1LI2	2	3	3			
IGF2BP1	2	2	4			
DAP3	2	2	3			
MRPS34	2	2	3			
SRPK2	2	4	5			
DYNC1LI1	2	2	4			
MRPS9	2	3	3			
HS2ST1	2	2	2			
BICD1	2	2	2			
FARP1	2	2	3			
MTX2	2	3	3		1	
GOLGA2	2	2	4			
SNAP23	2	3	3			
TBC1D31	2	4	4			
IK	1			7	6	4
SRP14	1	2	1	2	2	2
CETN2	1	2	2	2	2	2
EIF4B				2	3	2
NOL8				6	10	8
NOL9				6	8	4
CHAMP1				5	3	3
PWP1				4	4	3
SMPD4				4	2	4
AP2A2				3	3	3
UTP23				3	4	2

Gene Name	p62_CytoREP_01	p62_CytoREP_02	p62_CytoREP_03	p62_NucREP_01	p62_NucREP_02	p62_NucREP_03
RFC4				2	2	4
NFIX				2	2	3
DHX33				2	3	2
SCO1				3	2	3
ZNF384				2	2	2
ATP5H				2	2	2
SMARCD1				2	2	2
CAPZA2				2	2	2
SLC25A10				2	2	2
S100A9				4	4	4
SSR3				2	2	2
CSTF3				2	2	2
PTRH2				4	4	2
FKBP11				2	2	2
ACSL3				4	3	4
PNKP				4	4	3

## 10.2 Publications

---

- ✓ **p62 sustains a protumorigenic gene signature in melanoma opposing mRNA-dependent decay** (manuscript in preparation)  
**P. Karras**, E. Riveiro-Falkenbach, E. Cañón, T. G. Calvo, R. Martinez, E. Pérez-Guijarro, C. Tejado, M. Cifdaloz, P. Ximenez-Embun, J. Muñoz, D. Megías, P. Ortiz-Romero, JL. Rodríguez-Peralto and María S. Soengas.
- ✓ **Cross-tumor differences in the landscape of RNA binding proteins identify a protumorigenic regulon controlled by CELF1 in melanoma** (under revision)  
M. Cifdaloz, L. Osterloh, O. Graña, E. Riverio-Falkenbach, J. Muñoz, T. G. Calvo, **P. Karras**, D. Olmeda, B. Miñana. G. Gómez-López, E. Perez-Guijarro, E. Cañón, E. Eyra, P L. Ortiz-Romero, J L. Rodríguez-Peralto, J. Valcárcel, and MS. Soengas
- ✓ **Lineage-specific control of melanoma cell proliferation by the cytoplasmic polydenylation factor CPEB4.** **Nature Communications**, 2016  
E. Pérez-Guijarro, **P. Karras**, M. Cifdaloz, R. Martínez-Herranz, E. Cañón, O. Graña, C. Horcajada, D. Alonso Curbelo, T. G. Calvo, G. Gomez, N. Bellora, E. Riveiro-Falkenbach, P. Ortiz-Romero, JL. Rodríguez-Peralto, L. Maestre, G. Roncador, JC. Agustín Asensio, C. Goding, D. Megías, E. Eyra, R. Méndez and María S. Soengas.
- ✓ **Metastatic risk and resistance to BRAF inhibitors in melanoma defined by selective allelic loss of ATG5.** **Autophagy**, 2016  
M. García-Fernández, **P. Karras**, A. Checinska, E. Cañón, G. Gómez-López, T. Guadalupe Calvo, G. Gomez-Lopez, M. Cifdaloz, A. Colmenar, L. Espinosa, D. Olmeda and M. Soengas.
- ✓ **Vascular endothelial cadherin downregulation as a feature of endothelial transdifferentiation in monocrotaline- induced pulmonary hypertension.** **A.J.P.-Lung**, 2016  
Nikitopoulou I, Orfanos SE, Kotanidou A, Maltabe V, Manitsopoulos N, **Karras P**, Kouklis P, Armaganidis A, Maniatis NA.
- ✓ **RAB7 counteracts PI3K-driven macropinocytosis activated at early stages of melanoma development.** **Oncotarget**, 2015  
Alonso-Curbelo D, Osterloh L, Cañón E, Calvo TG, Martínez-Herranz R, **Karras P**, Martínez S, Riveiro-Falkenbach E, Romero PO, Rodríguez-Peralto JL, Pastor J, Soengas MS
- ✓ **RAB7 controls melanoma progression by exploiting a lineage-specific wiring of the endolysosomal pathway.** **Cancer Cell**, 2014  
D. Alonso-Curbelo, E. Riveiro-Falkenbach, E. Perez-Guijarro, M. Cifdaloz, **P. Karras**, L. Osterloh, D. Megías, E. Cañón, TG. Calvo, D. Olmeda, G. Gómez-Lopez, O. Graña, VJ. Sánchez-Arévalo, DG. Pisano, H-W. Wang, P. Ortiz-Romero, D. Tormo, K. Hoeck, JL. Rodríguez-Peralto, JA. Joyce, MS. Soengas.

## 10.3 Presentations

---

### Oral

- ✓ **Hallmarks of Cancer**  
**Title:** *Fine tuning of pro-metastatic factors by RNA complexes controlled by p62/Sequestosome-1 in melanoma*  
Ghent, Belgium, December 2016
- ✓ **CNIO Lab day**  
**Title:** *p62/SQSTM-1, more than a scavenger in melanoma progression and metastasis*  
Madrid, Spain, December 2015

## Posters

- ✓ **13th International Congress of the Society for Melanoma Research** Boston, Massachusetts  
P. Karras, E. Riveiro-Falkenbach, D. Megias, J. Muñoz, P.Ortiz-Romero, JL. Rodríguez-Peralto and Maria S. Soengas.  
*Fine tuning of pro-metastatic factors by RNA complexes controlled by p62/Sequestosome-1 in melanoma* 06-09/11/2016
- ✓ **12th International Congress of the Society for Melanoma Research** San Francisco, California  
P. Karras, E. Riveiro-Falkenbach, D. Megias, J. Muñoz, P.Ortiz-Romero, JL. Rodríguez-Peralto and M.S. Soengas.  
*Global control of the melanoma transcriptome by the p62/Sequestosome-1 autophagy modulator.* 8-21/11/2015
- ✓ **6<sup>th</sup> European Melanoma Workshop** Las Palmas, Canary islands,Spain  
P. Karras, E. Riveiro Falkenbach, J. Munoz, P. Embun, I. Ruppen, O. Grana; P. Ortiz Romero; JL. Rodríguez-Peralto, M. Soengas.  
*p62/Sequestosome-1, more than a scavenger protein in melanoma progression.* 27-29/06/2014
- ✓ **10<sup>th</sup> International Meeting of the Society for Melanoma Research** Philadelphia, Pennsylvania  
P.Karras, E. Riveiro-Falkenbach, P. Ximénez-Embún, I.I Ruppen, P. Ortiz-Romero, JL. Rodríguez-Peralto and M.S. Soengas.  
*p62/Sequestosome-1, more than a scavenger protein in melanoma progression.* 17-20/11/2013

## 10.4 Fellowships/Awards

---

- ✓ Travel Award, Hallmarks of Cancer Ghent, Belgium, December 2016
- ✓ Best poster at CNIO Lab day Madrid, Spain, December 2013
- ✓ Best poster at 10<sup>th</sup> International Meeting of the Society for Melanoma Research Philadelphia, November 2013
- ✓ La Caixa"/CNIO International PhD Programme Scholarship Nov. 2011 – Nov. 2015

## 10.5 Certificates

---

- ✓ **Course of Flow Cytometry** Spanish National Cancer Research Center (CNIO) , 2013
- ✓ **Course of Laboratory Animal Sciences for Researchers: Categories B and C**  
 Spanish National Cancer Research Center (CNIO) and Animalaria, Formación y Gestion S.L.,  
 Madrid, Spain, 2013
- ✓ **Course on "Functional Analysis of gene Expression Experiments"**  
 Spanish National Cancer Research Center (CNIO). Madrid, Spain. 2012